Proceedings of the International Conference on Innovations in Energy Engineering & Cleaner Production

21–22 July 2022

Oxford, United Kingdom

Preface

Renewable energy is the fastest-growing energy source since the beginning of the century and the demand growth with the fast development in industrial and transportation sectors. Renewable energy will continue to grab market share from fossil fuels in 2022. Indeed, renewables were the only energy source for which demand increased in 2020 despite the pandemic, while consumption of all other fuels declined. Will renewable energy source uptake therefore expand more quickly as the global economy recovers from the crisis ?

The International Conference on Innovations in Energy Engineering & Cleaner Production (IEE^{CP}'22) aims to investigate innovation applications and last researches in the areas of energy production, alternative and renewable energy supply, energy savings analysis, cleaner production, optimization of energy processes and the environmental impacts. The volume contains the proceedings of the international conference on Innovations in Energy Engineering & Cleaner Production (IEE^{CP}'22). The IEE^{CP}'22 conference is a scientific event which gathered leading researchers and practitioners who will present ideas to more than 50 attendees. Authors have provided high quality contributions reviewed by a program committee featuring renowned international experts on a broad range of knowledge management topics. More than 150 papers were submitted to the IEE^{CP}'22 conference from authors of many countries and continents. Two or three reviewers were assigned to each paper and according to these reviews, 25 papers were accepted which makes acceptance rate of 17%.

We are grateful to the Chairs, Program Committee, External Reviewers, Organizing Committee and the keynote speakers for their wonderful work and efforts. Finally, we would like to thank all the participants and sponsors hoping to meet them soon for other collaboration in scientific events.

Sincerely yours,

IEE^{CP}'22 Chair

Program Committee IEE^{CP}'22

International Advisory Board

- Dr. Baozhen Li, Institute of Advanced Grinding and Precision Machining, School of Mechanical, Electronic and Control Engineering, Beijing Jiaotong University, China
- Dr. Silvio Cristiano, Università Ca' Foscari Venezia, Research Institute for Complexity, Venice, Italy
- Dr. P.S.Shivakumar Gouda, SDM College of Engg. and Technology, Dharwad, India
- Dr. Sin Jin Chung, Department of Petrochemical Engineering, Faculty of Engineering and Green Technology, Universiti Tunku Abdul Rahman, Malaysia
- Dr. Tanmaya Badapanda, Department of Physics, C.V. Raman Global University, India
- Dr. Hwai Chyuan Ong, University of Technology Sydney, UTS, Australia
- Dr.M.Sujith, IFET College of Engineering, Villupuram, India
- Prof. Werner J.F., Christian-Albrechts-University, Germany
- Dr. Jae-Jin Shim, School of Chemical Engineering, Gyeongsan-si, South Korea
- Dr. Jei-Pil Wang, Pukyong National University, South Korea
- Pr. Vaidotas Kažukauskas, Institute of Photonics and Nanotechnology, Vilnius University, Lithuania
- Dr. Ishwar Chandra Yadav, Tokyo University of Agriculture and Technology (TUAT), Japan
- Dr. Farhad Shahnia, Murdoch University, Australia
- Dr. Bimal Kumar Ghimire, College of Sanghuh Life Science, Konkuk University, Seoul, Korea
- Prof. Hui Li, College of Transportation at Tongji University, Shanghai, China
- Dr. Javier Velázquez Saornil, Universidad Católica de Ávila, Spain
- Dr. Hugo Morais, GECAD, Polytechnic Institute of Porto (IPP) Porto, Portugal
- Dr. Arun Kishor Johar, Department of Electronics and Communication Engineering, Malaviya National Institute of Technology Jaipur, India.
- Dr. Jan Bocianowski, Dept. of Mathematical and Statistical Methods, Poznan University, Poland
- Dr. Jania Betania Silva, Universidade Federal da Bahia, Brazil
- Dr. Jesus David Coral Medina, Mariana University, Federal of Paraná University, Colombia
- Dr. Jaime Andrés Pérez Taborda, Universidad de los Andes, Colombia
- Dr. Isam H. Aljundi, King Fahd University of Petroleum and Minerals, Dhahran, Saudi Arabia

International Chairman Board

- Pr. Joao Fernando Gomes, Chemical Engineering Department, ISEL - Instituto Superior de Engenharia de Lisboa, Portugal
- Dr. Fusheng Yang, Department of Process Equipment and Control Engineering, Xi'an Jiaotong Universitym China

- Dr. G. Jaffino, Department of SENSE (School of Electronics Engineering), VIT University, Vellore, India
- Dr. Mallikarjunaswamy M S, Department of Electronics & Instrumentation , Sri Jayachamarajendra College of Engineering, J.S.S. Science & Technology University, India.
- Dr. Silvio Cristiano, Università Ca' Foscari Venezia, Research Institute for Complexity, Venice, Italy
- Dr. Arun Kishor Johar, Department of Electronics and Communication Engineering, Malaviya National Institute of Technology Jaipur, India.
- Dr. Baha I. Elzaki, Chemical Engineering Department., Karary University.
- Dr. Agata Egea, University of Cadiz, Puerto Real, Cádiz, Spain

Technical Program Committee

- Prof. Bo Jin, College of Materials Science and Engineering, Jilin University, China
- Prof. Jun Li, Kansas State University, Department of Chemistry, Manhattan, USA
- Dr. Junbo Zhao, Mississippi State University, USA
- Prof. Eddie YK NG, College of Engineering, Nanyang, Technological University, Singapore
- Dr. Guohai Chen, CNT-Application Research Center, AIST, Japan
- Prof. Fei Wang, Qingdao University of Science & Technology, China
- Dr. Hongwei WU, School of Physics, University of Hertfordshire, UK
- Dr. Eike Marie Thaysen, School of Geosciences, University of Edinburgh, UK
- Prof. Guimin Chen, School of Mechanical Engineering, Xi'an Jiaotong University, China
- Dr. Feng Lin, Natural Resources Canada
- Dr. Eliseu Leandro de Magalhães Monteiro, University of Coimbra, Portugal
- Dr. Esmaeil Zarei, Memorial University, St. John's, NL, Canada
- Dr. Francesca Deganello, CNR-ISMN Palermo, Via Ugo La Malfa, Italy
- Dr. Géremi Gilson Dranka, Department of Production and Systems Campus Azurem, Portugal
- Dr. Hock Jin QUAH, INOR, Universiti Sains Malaysia
- Dr. Hao Yi, College of Mechanical Engineering, Chongqing University, China
- Dr. Mesfin Kebede, Energy centre, CSIR – South Africa
- Dr. Gaetano LISI, e-Campus University, Department of Economics, Novedrate (CO), Italy
- Dr. Grzegorz Woroniak, Bialystok University of Technology, Poland
- Dr. Fiseha TESFAYE, Faculty of Science and Engineering, Åbo Akademi University, Finland
- Prof. Haitham M. S. Lababidi, College of Engineering, Petroleum, Kuwait University, Kuwait
- Dr. Guohua Xie, Department of Chemistry, Wuhan University, China
- Dr. Ellen Cristine Giese, Centro de Tecnologia Mineral (CETEM), Brazil
- Dr. Hassan Abdulmouti, Sharjah Men's College, Sharjah, UAE
- Prof. Edimilson Costa Lucas, Federal Univesity of Sao Paulo (EPPEN-UNIFESP), Brazil
- Dr. Liu Hongfei, Institute of Materials Research and Engineering (IMRE), Singapore
- Dr. Daniel Assumpção Bertuol, Universidade Federal de Santa Maria, Brazil

- Dr. Chun Kai Leung, Fairbank Center for Chinese Studies, Harvard University, USA
- Dr. Ketut Suastika, Department of Naval Architecture, Faculty of Marine Technology, Indonesia
- Dr. G. Jaffino, Department of SENSE (School of Electronics Engineering), VIT University, Vellore, India
- Dr. Haidong SHAO, College of Mechanical and Vehicle Engineering, Hunan University, China
- Dr. Aseem K, Electrical Engg. Dept., LBS College of Engineering, India
- Dr. B.Amutha, SRM Institute of Science and Technology, India
- Dr. Lucas Massaro Sousa, Postdoctoral Researcher at IFP Energies Nouvelles, France
- Dr. Aref Wazwaz, Chemical Engineering Department, College of Engineering, Dhofar University, Sultanate Of Oman
- Dr. Mourad Boutahir, Advanced Materials and Applications Laboratory (LEM2A), University Moulay Ismail, Morocco
- Dr. Mostafa Behtouei, National Institute for Nuclear Physics-National Laboratory of Frascati
- (INFN-LNF), Italy
- Dr.T. Jemima Jebaseeli, Karunya Institute of Technology and Sciences, India
- Dr. A.Anita Margret, Department of Biotechnology, Bishop Heber College, Tiruchirappalli -India
- Dr. Ping Xiang, Central South University, China
- Dr. Anum Tanveer, Mirpur University of Science and Technology (MUST), Pakistan
- Pr. M. Benlattar, Faculty of Sciences Ben M'sik University Hassan II, Casablanca, Morocco
- Dr. R. Velmurugan, Department of Aerospace Engineering, Indian Institute of Technology Madras, India
- Dr. Gujjala Raghavendra, Department of Mechanical Engineering, National Institute of Technology Warangal, India
- Dr. Mallikarjunaswamy M S, Department of Electronics & Instrumentation , Sri Jayachamarajendra College of Engineering, J.S.S. Science & Technology University, India
- Dr. Rahul, CNSNT, Panjab University, Chandigarh, India
- Dr. Oscar Cigarroa-Mayorga, Advanced technologies department, Energy academy, National Polytechnic Institute-UPIITA, Mexico city
- Dr F. T. Thema, Botswana University of Agriculture and Natural Resources (BUAN), Botswana
- Dr. Sarjiya, Department of Electrical and Information Engineering, Faculty of Engineering, Gadjah Mada University, Indonesia
- Dr.V.Santhanam, Department of Mechatronics Engineering, Rajalakshmi Engineering College (Autonomous), India
- Dr. Simona Rada, National Institute for Research and Development of Isotopic and Molecular Technologies, Cluj-Napoca, Romania
- Prof. Nkosikhona Hlabangana, Director, Research and Internationalisation Office, National University of Science & Technology (NUST), Zimbabwe
- Dr. Nitika Dahiya, Department of Physics, SRM University, B247Delhi-NCR, India
- Dr. Nicholas Munu, Department of Mechanical Engineering, Ndejje University, Uganda

Table of Contents

Article 007 (ID: 214) Environmental Effects of dust deposition on solar PV panels in the surface Mining Industry.
Ganti Praful Kumar, Hrushikesh Naik and Kanungo Barada Mohanty.

Article 008 (ID: 216) Energy and environmental impact of banning the sale of traditional fossil fuel vehicles.
Shouheng Sun, Qi Wu and Dafei Yang.

Article 009 (ID: 218) Whole-body Vibration Exposure of Opencast HEMM Operators –Development of a Conceptual Structural Equation Model.
D.R. Grahacharya , Falguni Sarkar and H.K. Naik.

Article 010 (ID: 221) Bioelectricity generation in microbial fuel cell by a membrane electrode assemble: Startup assessment.
Ana Carla Sorgato, Thamires Custódio Jeremias, Fernanda Leite Lobo, Flávio Rubens Lapolli.

Article 011 (ID: 228) Cr and Polycrystalline Diamond Coatings for Accident Tolerant Nuclear Fuel Tubes.
Irena Kratochvilova, Lucie Celbova and Radek Skoda.

Article 012 (ID: 233) A methodology for assessment of deep decarbonisation pathways for manufacturing industries in Ireland.
Kirestena saeed, John Cosgrove and Frank Doyle.

Article 013 (ID: 237) Production of synthesis gas obtained via alkaline water electrolysis and added biomass.
Gomes J., Puna J. and Santos T..

Article 014 (ID: 239) Multi-scale landscape visual impact assessment for onshore wind farms in rural area of China.
Jinjin Guan, Beining Li, Yinan Lin.

Article 015 (ID: 241) An efficient model for induction motor fault detection using deep transfer learning network.
Alasmer Ibrahim, Fatih Anayi, Michael Packianather.

Article 016 (ID: 234) Strategy for institutional cook stoves promotion in the context of a behavioral change-A case study of Opoku Ware School and ST. Paul's Seminary, Accra, as the control in the research in Ghana.
Michael Kweku Commeh, Christlove Opoku-Appiah, Joseph Okine, James Hawkins Ephraim.

Article 017 (ID: 253) Blackcurrant pomace as a biodegradable filler for rigid polyurethane foam.
Patrycja Trestka, Beata Zygmunt-Kowalska, Monika Kuźnia, Mariusz Oleksy.

Article 018 (ID: 259) Theoretical performance study of Cs2AgBi(I(1-x)Brx)6: a promising lead-free perovskite for photovoltaic technology.
Fatima Elfatouaki, Omar Farkad, Rabi Takassa, Sanae Hassine, Ouamaima Choukri, El Alami Ibnouelghazi, Driss Abouelaoualim, Abdelkader Aoutzourhit.

Article 019 (ID: 264) Removal of pollutants in wastewater treatment plants.
Julita Šarko, Aušra Mažeikienė.

On the development of a novel energy-cascading system for quad-generation

Chua Kian Jon
Department of Mechanical Engineering; National University of Singapore
mpeckje@nus.edu.sg

Plenary Abstract

Quad-generation encompasses the features of a multiple utility plant, with combined electricity, heat, cooling and potable water but in addition includes the recovery of thermal energy from the exhaust gas with minimum wastage of energy. Key benefits (1) potential for low or zero carbon emissions to produce multiple utilities; (2) reduced operational costs versus separate purchase of electricity, heat, cooling and potable water; (3) maximize the use of all potential resources from gas utilisation to produce useful outputs; and (4) Improved reliability for sustainable utilities production. This presentation focuses on the development of a unique smart quad-generation plant, whereby all four key resources are generated simultaneously using a single, integrated system in an energy efficient manner, through maximizing the recovery of its generated waste energy. Specifically tailored for tropical countries, the plant can contribute to greater energy and cost savings, and is also more space-efficient. It employs a smart temperature cascading method to maximum the utilization of waste heat. More importantly, it can significantly reduce energy consumption by 30 per cent or more and potentially trim the amount of carbon dioxide emitted to the environment by 2 to 4 per cent for countries at business-as-usual levels while meeting varying needs of electricity, potable water, cooling and heating. Such a novel system is particularly suited to countries whereby cooling and water production are essential utilities**.**

Short biography

Dr Chua Kian Jon is currently an Associate Professor with the Department of Mechanical Engineering, National University of Singapore. He has been conducting research on air-conditioning, refrigeration, and heat recovery systems since 1997. He has conducted both modelling and experimental works for specific thermal energy systems. These include dehumidification, cooling, heat pumping, compact heat exchangers and refined temperature/humidity control. He is highly skilled in designing; fabricating; commissioning and testing many sustainable energy systems to provide for heating, cooling and humidity control for both small and large scale applications. He has more than 200 international peer-reviewed journal publications, 6 book chapters and two recent monographs on advances in air conditioning (https://www.springer.com/gp/book/9789811584763 and https://www.springer.com/gp/book/9783030808426). He was highlighted among the top 1% of scientists in the world by the Universal Scientific Education and Research Network and top 0.5% in the Stanford list of energy researchers. His works has garnered more than 10,900 over citations with a current h-index of 55. Further, he owns more than 10 patents related to several innovative cooling and dehumidification systems. He is the Principal Investigator of several multi-million competitive research grants. Additionally, he has been awarded multiple local, regional, and international awards for his breakthrough research endeavours.

IEECP'22, July 21-22, 2022, Oxford, United Kingdom

Energy-environment-economy(3E) assessment of a novel low-carbon emission process integrating coal-to-methanol with green hydrogen

Han Yang, Min Dai, Fusheng Yang*, Zhen Wu, Yunsong Yu, Zaoxiao Zhang
School of Chemical Engineering and Technology
Xi'an Jiaotong University
Xi'an, China
yang.fs@mail.xjtu.edu.cn

Abstract

Methanol is an alternative fuel that offers convenient storage, transport and utilization, hence has attracted many attentions recently. Coal-to-methanol (CTM) is a mature, inexpensive industrial process for methanol production, yet accompanied with large CO2 emissions and low C conversion rate due to the mismatch of H/C ratio between feedstock and product. In this study, a novel low carbon process of the CTM coupled with green hydrogen is proposed, in which the water gas shift (WGS) sector is replaced by water electrolysis based on solar power for adjusting the hydrogen carbon ratio. Additional methanol production could be achieved from the hydrogenation of CO2 absorbed by rectisol, hence further increasing the C conversion rate and decreasing CO2 emissions. Sensitivity analysis is conducted with regard to the key parameters such as synthetic pressure and temperature, and the comprehensive performance of the new process system is compared with the conventional CTM from the perspective of energy-environment-economy (3E), using exergy efficiency, total annual cost (TAC) and equivalent CO2 emissions as evaluation indicators. In addition, a quantitative sustainability evaluation method is introduced, in which a dynamic econometric model considering volatility of product/raw material price, electricity price and carbon tax is established. The results reveal that the system is operated successfully under the optimum settings, increasing methanol output with lower carbon emission. The goal of green and efficient production is achieved economically, showing the perspective of CTM integration with renewable energy sources.

Keywords: *Coal-to-methanol, green hydrogen, 3E assessment, economic uncertainty*

Short biography

Dr.Yang works as a faculty staff at Xi'an Jiaotong University since he got the PhD degree from the University on 2010. He once conducted studies abroad at the University of Queensland (2009.1-2010.1) and Tokyo University of Science, Noda (2011.6-2012.6). He is now the head of Department of Process Equipment and Control Engineering, Xi'an Jiaotong University. His present research interests include efficient storage and utilization of hydrogen energy, industrial energy saving technology, process modeling and optimization based on historical data. He has published tens of peer-reviewed journal papers in the field of energy and chemical engineering, and was granted multiple Chinese patents. Some representative publications are listed below.

IEECP'22, July 21-22, 2022, Oxford, United Kingdom

On the limitations of Machine Learning (ML) methodologies in predicting the wake characteristics of wind turbines

Ng Yin Kwee
School of Mechanical and Aerospace Engineering,
College of Engineering, Nanyang Technological University, Singapore
MYKNG@ntu.edu.sg

Abstract

Machine Learning (ML) algorithms have been more prevalent in recent years, and they are being used to tackle complicated issues across a broad range of fields. Wind energy is not an exception, as ML has recently been applied to wind turbine blade design, wake velocity and wake turbulence intensity prediction, and even wind farm optimization. The immense learning ability of ML models enables them to be trained to predict and regress a complex relationship with a high degree of accuracy. However, data for testing ML models often originate from the same rotor simulation used for training, with just slight variations in operating conditions. This research aims to investigate the generalizability of ML-based wake prediction models, i.e., whether ML can correctly predict wake properties using data from a different wind turbine that was not taken for training. This investigation's observation shows that a generalized ML wake model requires training data from multiple turbines with a wide range of operating conditions. In addition, advanced regularization, complex loss functions, and ML methods that focus on capturing the physics (such as Physics Informed Artificial Neural Networks (PINN) and symbolic regression) can be utilized.

Keywords: *Wake velocity, turbulence intensity, Support Vector Regression (SVR), Artificial Neural Networks (ANN), eXtreme Gradient Boosting (XGBoost).*

Short biography

Prof. Eddie is elected as:

Academician for European Academy of Sciences and Arts (EASA, EU);
Fellow of the American Society of Mechanical Engineers (FASME, USA);
Fellow of Institute of Engineering and Technology (FIET, United Kingdom);
Fellow of International Engineering and Technology Institute (FIETI, Hong Kong),
Distinguished Fellow for Institute of Data Science and Artificial Intelligence, (DFIDSAI, China), and, Academician for Academy of Pedagogy and Learning, (USA).
He has published numerous papers in SCI-IF int. journal (430); int. conf. proceedings (130), textbook chapters (>105) and others (32) over the 29 years. Co-edited 14 books in STEM areas.
He is the:
Lead Editor-in-Chief for the ISI Journal of Mechanics in Medicine and Biology for dissemination of original research in all fields of mechanics in medicine and biology since 2000;
Founding Editor-in-Chief for the ISI indexed Journal of Medical Imaging and Health Informatics;
Associate editor or EAB of various referred international journals such as Applied Intelligence, BioMedical Engineering OnLine, Computers in Biology & Medicine, and, Journal of Advanced Thermal Science Research..

IEECP'22, July 21-22, 2022, Oxford, United Kingdom

Hydrogen for Greening Production in Heavy-Emitter Industries

Kamiel Gabriel
Faculty of Engineering and Applied Sceince, Ontario Tech University
Oshawa, ON, Canada
Kamiel.Gabriel@ontariotechu.ca

Plenary Abstract

Today, hydrogen is enjoying a strong momentum worldwide as the fuel of the future, and is expected to have a considerable role to play in securing a clean energy future. Nations of the world have been adopting national roadmaps to employ hydrogen for their transition plans to low-carbon future. However, it remains a challenge to find clean energy sources to drive the hydrogen production process and divest it from the fossil-based production technologies. Currently, demand of hydrogen is dominated by heavy industries including oil and gas, steel, cement, glass and fertilizers manufacturing, among other heavy emitters of CO2. This demand is met by reforming or gasification of carbon-based fuels (e.g., methane, coal, and biomass). In this talk, innovative thermochemical Copper-Chlorine (Cu-Cl) hydrogen production technology, developed at Ontario Tech University, is introduced as a reliable and scalable technology for clean Hydrogen production. The Cu-Cl hydrogen cycle can operate on recovered waste-heat (approximately 500°C) from industrial processes. In this talk, Prof. Gabriel will highlight the potential integration of this innovative technology in steel and cement industries in Canada and elsewhere in Europe, China and the Middle East. This process which utilizes waste/process heat has the potential to significantly cut of CO2 emissions from such polluting industries. A case study on coupling this technology with a cement plant in Ontario will be presented.

Keywords: *Hydrogen, thermochemical Cu-Cl cycle, energy recovery, cement, steel*

Short biography

Dr. Gabriel is an elected member of the Canadian Academy of Engineering and the former A/Deputy Minister of Research at the Ontario Ministry of Research and Innovation. In 1990, Dr. Gabriel attended the prestigious, MIT-founded, International Space University and received a diploma in Space Sciences. For over 14 years, Dr. Gabriel led an international team in the research efforts spearheaded by NASA to design, test and operate a thermal management system for the International Space Station (ISS). In 2004, Dr. Gabriel was invited to lead the development of the research and innovation ecosystem in a newly established university. He assumed the position of the founding AVP research and graduate programs at Ontario Tech University (formerly the University of Ontario Institute of Technology) in Ontario, Canada. Under his leadership, Ontario Tech University was ranked as one of the top Canadian higher learning institutions in the categories of innovation and leaders of tomorrow.

IEECP'22, July 21-22, 2022, Oxford, United Kingdom

Breakthrough Heating and Cooling Technologies Using Novel Solid State Functional Materials

Victor Koledov
Laboratory of magnetic phenomena
Kotel'nikov Institute of Radioengineering and Electronics Russian Academy of Sciences
Moscow Russia
victor_koledov@mail.ru

Abstract

In recent decades, there have been a number of remarkable breakthroughs in energy conservation, one of which is related to the development of new types of solid-state light sources. The discovery of new semiconductor materials, in particular GaN and heterostructures based on them, made it possible to create blue and white LEDs and lasers, which have orders of magnitude greater efficiency and service life than incandescent lamps. This outstanding achievement was awarded the 2014 Nobel Prize. Thus, the energy consumption of all mankind for lighting has decreased by an order of magnitude. The search for these materials took serval decades of hard work of physicists and materials scientists. An even more ambitious project is aimed at reducing energy consumption for cooling and heating by at least an order of magnitude. The fundamental possibility of such a revolution is opened by Carnot's theorem, which allows using not direct energy consumption for heating, but pumping heat using a device called Thomson's heat pump. The efficiency of a heat pump is determined by the efficiency of the process, (COP), which is always more than 1, but less than T1/Δ T, where Δ T = (T1-T0) is the temperature difference between the temperature T1 of a room that is heated and T0 an external environment temperature, from where we take heat, according to Carnot's theorem. At the moment, the liquid materials - freons - are mainly used as a working fluid in Thomson's heat pump. However, the use of freons for pumping heat has practically exhausted itself, at the COP level of the order of 300-400%, and do not grow further. In addition, the use of freons is considered dangerous for the destruction of the Earth's ozone layer. So to reach the predicted level of 1000% is the realistic purpose of the emerging field of solid state heating/cooling. Therefore, the number of scientific works, patents and innovations on the creation of solid-state functional materials for cooling and heating is exponentially growing all over the world. The effects of changes in temperature and heat content that arise in these materials under the influence of external fields are known as multicaloric effects, including the magnetocaloric effect, elastocaloric effect, and electrocaloric effect etc. The maximum value of the caloric effects is achieved near the phase transition point, for example, near the boiling point of freon, or near the Curie point of a magnet or ferroelectric. Therefore, all over the world there is a search for the new solid-state multi-caloric materials, especially with phase transitions. The values of various caloric effects of the order of several tens of Kelvins of temperature changes or several tens of kJ/kg of heat consumption have already been achieved. Also, the devices are being developed that, in principle, in terms of COP could approach the limit of Carnot's theorem. The present report highlights the state of the art record achievements in the study of the properties of solid-state materials for cooling and heating, and record values of COP of multicaloric solid state refrigerators and heat pumps and original results of authors. we describe the formatting guidelines for the conference keynote abstract. We ask that authors follow some simple guidelines. In essence, we ask you to make your abstract look exactly like this document. The easiest way to do this is simply to replace the content with your own material. Please use a 9-point Times Roman font, or other Roman font with serifs, as close as possible in appearance to Times Roman in which these guidelines have been set. The goal is to have a 9-point text, as you see here. Please use sans-serif or non-proportional fonts only for special purposes, such as distinguishing source code text. If Times Roman is not available, try the font named Computer Modern Roman. On a Macintosh, use the font named Times. Right margins should be justified, not ragged.

Keywords: *multicaloric effects, magnetocaloric effect, elastocaloric effect, and electrocaloric effect, solid stste refrigeration*

Hightlight

1. *New solid-state semiconductor materials have already revolutionized lighting technologies for residential and open spaces, reducing the required energy costs by an order of magnitude.*
2. *The fundamental laws of thermodynamics allow for a reduction of at least an order of magnitude a needed energy as well as the cost of home and industrial heating.*
3. *There is an active search all over the world for new solid-state caloric materials that could bring the efficiency of new machines for cooling and heating closer to the ideal Carnot machine.*
4. *The report highlights both the world's best achievements in recent years and the challenges facing the development of advanced solid-state heating and cooling technologies.*

IEECP'22, July 21-22, 2022, Oxford, United Kingdom

Short biography

Brief biography of Dr. PhD Victor Koledov

Dr. Dr. Sci. Koledov Victor was born 20 of April 1955 in city Rostov am Don. From 1972 till 1978 he studied in Study of Moscow Institute of Physics and Technology (MIPT) (Technical University) and finished this University 1978 with Dipl. Eng. in Physics and Electronics. In 1986 he has got PhD (Solid State Physics). In 2008 he has done work for Doctor Habilitation of Sciences with the thesis: "Phase transition and giant deformation in Heusler alloys in external fields. " (Kotelnikov' IRE RAS). Since 1982 till now he is working Institute of Radio Engineering and Electronics Russian Academy of Sciences (IRE RAS). Now he is Leading scientist in this IRE RAS. His research areas are experimental studies of magnetic properties, magnetooptics, ferromagnetic domains, semiconductor lasers, fiber optics, ferromagnetic shape memory alloys, functional materials, medical applications of functional materials, multiferroics, strong magnetic fields, giant magnetocaloric effect, micromechanics, nanomechanics, nanomanipulation system based on record small nano-tweezers, mechanical bottom up nano-assembling, superconducting magnetic levitation, photonics, nano-optics.

He has got awards / Prizes / Honours at 2009 Start2grow competition of Businessplan Germany for Nano-tools, 2010 Start2grow competition of Businessplan Germany for MST-technology of Nano-tools. And after this since 2010 he is founder and director of German innovative Innowledgement GmbH.

He is leader of more the 25 national and international projects. Victor Koledov is author and coauthor of more then 180 scientific paper in referred journals and more, then 160 presentations at national and international presentation, among then more than 25 Invited and Keynote speaker. He was invited Professor in – Spain, Italy, Romania, Portugal, China, India, Brazil, South Africa.

He participates in organization of conferences 1. Conference on Manipulation, Automation and Robotics at Small Scales (MARSS). 2. Conference 3 M nano International Conference on Manipulation, Manufacturing and Measurement on the Nanoscale, 3. METANANO 2019,

4. RAMAN OPTRONICS WEBINAR SERIES (ROWS-2021). Conference Organizing Committee Yaseen Academy http://www.yaseen.org.cnhttp://www.yaseen.org.cn

Victor Koledov is supervisor of more than 20 students, and about 10 PhD.

2014, 2018 Nano 3 M Award for invited report, 2018 3M Nano Award as Keynote speaker. Honorary Professor, Changchun University of Science and Technology (CUST) China

Teaching – Victor Koledov is invited Professor in Changchun University of Science and Technology (CUST) China, World-class scientific and educational centers Nanophys IRE RAS, Sirius University Sochi, Russia. University of Oviedo, Spain.

Calibration of anaerobic digestion BioModel by using multi-objective optimization and full-scale biogas plant data

Tina Kegl
Faculty of Chemistry and Chemical Engineering
University of Maribor
Maribor, Slovenia
tina.kegl@um.si

Abstract

Waste management and energy crisis are some of the greatest issues that the world is facing today. This problem can be mitigated by anaerobic digestion (AD), where microorganisms in the absence of oxygen produce biogas from organic waste. A useful tool for AD process understanding and optimization is numerical simulation by using mechanistically inspired mathematical models. In this paper attention is focused on modeling of the AD process of a full-scale biogas plant. Special attention is focused on calibration of 178 model parameters belonging to the BioModel, developed in-house; this is done by using an active set optimization procedure. The agreement of the obtained results of numerical simulation in a single CSTR and the measured AD performance over a period of one year, confirms the efficiently of the used BioModel when considering the presence of the Kemira BDP-840 additive to reduce H_2S content of the produced biogas. The obtained results show that the active set optimization procedure, coupled by a gradient based optimizer to calibrate the model parameters, performs very well. The procedure is numerically efficient, especially if the computation of design derivatives is parallelized. The used BioModel can easily be coupled with the procedure of AD performance optimization.

Keywords: Model parameters, calibration, additives, gradient-based optimization, active set optimization procedure

I. INTRODUCTION

A useful tool for anaerobic digestion (AD) process understanding and optimization is numerical simulation by using mechanistically inspired mathematical models. Till today, various mechanistically inspired AD models, ADM1 [1-6] and BioModel [7-13] based models, were developed containing various number of unknown or hardly determined AD model parameters, such are biochemical, kinetic, physicochemical, and stoichiometric model parameters. As the number of model parameters increases by expanding mathematical models, the efficiency and reliability of the calibration procedure typically decreases. Therefore, various procedures to reduce the number of the model parameters, which has to be calibrated, were proposed. In general, these procedures are based on adequate sensitivity analysis or similar approaches to calibrate various number of model parameters [13-21]. For example, Ahmed & Rodríguez [22] proposed the combined correlation-based parameter estimation with a sensitivity-based hierarchical and sequential single parameter optimization for sulfate reduction process by using the ADM1 model, while Kegl & Kovač Kralj [12] used an active set optimization (ASO) procedure combined with a gradient-based optimization algorithm in order to calibrate 113 model parameters of a BioModel.

In this paper attention is focused on the modeling of the AD process of a full-scale biogas plant by using a BioModel. More preciselly, the focus is on the calibration of its 178 unknown design parameters by engaging the ASO procedure. A comparison of the daily dynamics of the predicted and measured AD performance as well as statistical indicators show that all 178 AD parameters (13 feedstock and 165 model parameters) can be successfully and efficiently calibrated by the engaged ASO procedure.

II. BIOGAS PLANT EXPERIMENTAL DATA

The operation data used for AD simulation input and model calibration were obtained from a full-scale biogas plant Draženci (Slovenia). This plant consists of two equal mesophilic continuously mixed reactors (CSTRs). Both single-stage CSTRs have a hold up of 2500 m^3 with one common gas storage facility of 2500 m^3. The daily variation of total loading rate of the complex substrate (F-CS), temperature, and pH value in the CSTRs for a total period of two years are presented in Figure 1. The AD process with a retention time of approximately 33 days takes place at a constant pressure of 1.006 bar. The F-CS consists of poultry manure (PM), corn silage (CS), corn meal (CM), fat matter (FM), food waste (FW), and added water (W). The daily variations of fractions of CM, FM, FW, PM, CS, and W in the F-CS are shown for a total period of two years in Figure 2 and Figure 3. The composition of each substrate of F-CS containing TS-total solid, OM-organic matter, ch-carbohydrates, pr-proteins, li-lipids, C_{io}, N_{io}, S_{io}, K_{io}, and P_{io} - inorganic carbon, nitrogen, sulfur, potassium, and phosphorus, and other elements and compounds, Table 1, was determined by the usage of methods prescribed in the corresponding standards.

IEECP'22, July 21-22, 2022, Oxford, United Kingdom

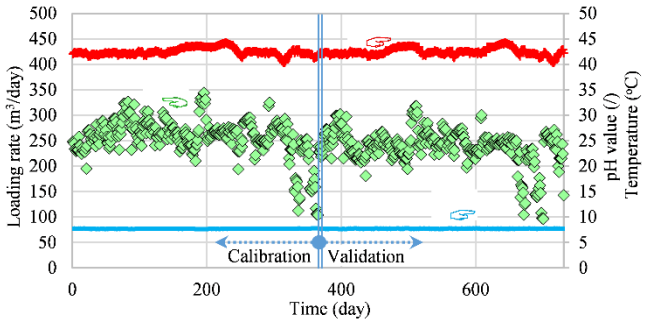

Figure 1. Measured loading rate of F-CS and AD conditions.

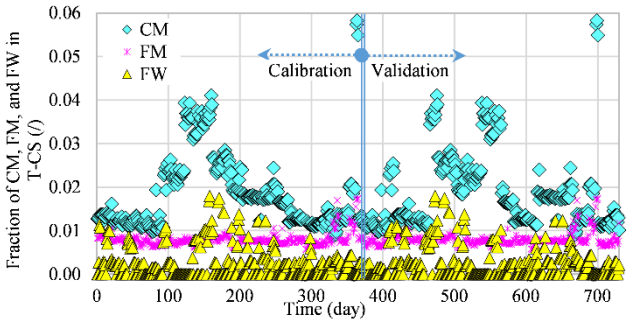

Figure 2. Measured fractions of CM, FM, and FW in F-CS.

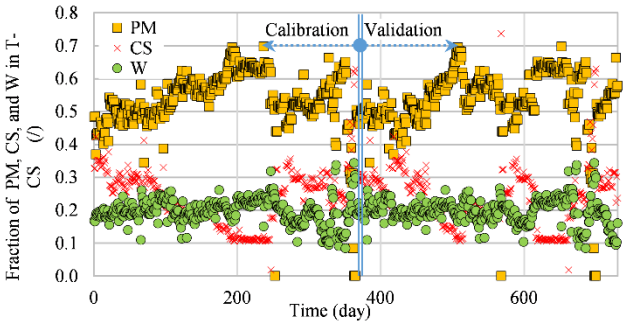

Figure 3. Measured fractions of PM, CS, and W in F-CS.

Table 1. Composition of substrates in F-CS

F-CS	PM	CS	CM	FM	FW
TS (%)	75.73	47.68	65.85	34.12	91.99
OM (% TS)	84.76	96.58	98.35	98.00	98.08
ch (gL^{-1})	10.735	6.488	6.438	4.309	31.707
pr (gL^{-1})	45.936	33.022	56.970	74.723	66.220
li (gL^{-1})	3.555	3.226	19.750	236.312	26.970
C_{io} (gL^{-1})	3.57499	2.14185	0.71529	0.13711	42.80220
N_{io} (gL^{-1})	1.55322	0.62786	1.08176	1.30420	1.15234
S_{io} (gL^{-1})	3.57599	0.06147	0.37446	0.00100	0.98493
K_{io} (gL^{-1})	3.23805	1.10575	1.13509	0.04708	2.51013
P_{io} (gL^{-1})	2.61164	1.01155	3.54957	0.90058	6.63018
Ca (gL^{-1})	3.61388	0.18493	0.02899	1.56674	18.09087
Cr (gL^{-1})	0.00346	0.00026	0.00083	0.00250	0.00111
Cu (gL^{-1})	0.00991	0.00035	0.00083	0.00238	0.01258
Fe (gL^{-1})	0.11026	0.00542	0.01380	0.20543	0.27517
Mg (gL^{-1})	0.81457	0.10843	0.30957	0.06587	0.88034
Na (gL^{-1})	0.38816	0.00055	0.00746	0.06184	0.50550
NO_2 (gL^{-1})	0.00871	0.00025	0.00175	0.00003	0.00048
Ni (gL^{-1})	0.00052	0.00026	0.00083	0.00110	0.00111
Pb (gL^{-1})	0.00028	0.00026	0.00083	0.00067	0.00111
Zn (gL^{-1})	0.05228	0.00026	0.00535	0.02188	0.13295

To reduce the production of H_2S during the AD process, the Kemira BDP-840 additive, containing the $FeCl_2$, in the amount of 100 L/day is added daily to the F-CS.

The total measured unrefined biogas volume is 4720983 m^3 in the first year, and 4364544 m^3 in the second year. This biogas contains approximately 54% CH_4, 45% CO_2, 60 ppm of H_2, 200 ppm of H_2S, and 800 ppm of NH_3. For the two years of observation, the measured daily produced biogas and CH_4 flow rates are presented in Figure 4, while H_2 and H_2S flow rates are given in Figure 5.

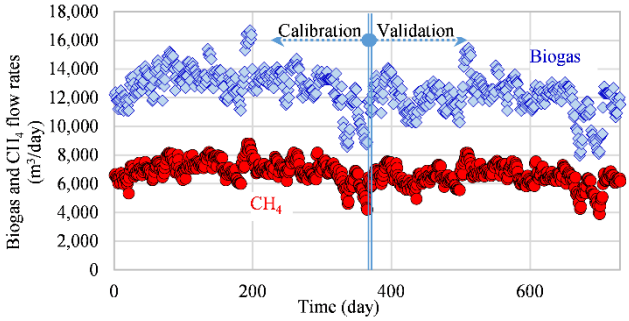

Figure 4. Measured biogas and CH_4 flow rates in the biogas plant.

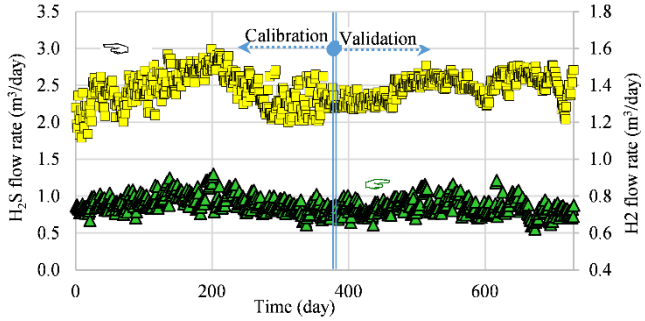

Figure 5. Measured H_2 and H_2S flow rates in the biogas plant.

The daily variations of the shown data, measured at the plant during the first 365 days period, were used to calibrate the feedstock and model parameters of the proposed BioModel, while the measured data of the second year were used for BioModel validation.

III. BIOMODEL PARAMETERS CALIBRATION

In order to calibrate a large number of design parameters (feedstock and model parameters) belonging to the BioModel, the ASO procedure is used in this work. In general, the employed ASO procedure involves the BioModel for numerical simulation of the AD process, a sensitivity analysis for determination of the active design variables from the set of all included design parameters, and an optimal design procedure.

A. BioModel

The used mathematical model in this paper is of a BioModel-type [12], where biochemical and physicochemical processes during AD, considering the degradation of carbohydrates, proteins, and lipids into CH_4 and many other by-products, are described by the system of 75 ordinary differential equations (ODEs) and 53 algebraic equations (AEs). Physicochemical processes are related to (i) liquid-gas mass transfer for the set of biogas compounds $I_{gas} = \{CH_4, CO_2, H_2, H_2S, NH_3\}$ and to (ii) liquid-solid mass transfers for the set of precipitates $I_{prec} = \{CaCO_3, MgCO_3, FeCO_3, NiCO_3, CuCO_3, PbCO_3, ZnCO_3, FeS, CuS, NiS, PbS, ZnS, Ca_3(PO_4)_2, Fe_3(PO_4)_2, Ni_3(PO_4)_2, MgNH_4PO_4, KMgPO_4\}$. The BioModel includes a set of 178 design parameters as follows: (i) initial

concentrations of 13 bacteria types from the set of I_{bac}; acidogenic degraders of sugar, amino acids, glycerol, and oleic acid (X_{Asu}, X_{Aaa}, X_{Agly}, and X_{Aoa}), acetogenic degraders of propionic acid, butyric acid, and valeric acid (X_{Apro}, X_{Abu}, X_{Ava}), methanogenic degraders of acetate and hydrogen (X_{Mac} and X_{Mhyd}) sulfate reducing bacteria involving in reduction of sulfates (X_{Ss}), and competing for propionate, acetate, and hydrogen (X_{Spro}, (X_{Sac}, and X_{Shyd}; (ii) 3 hydrolysis rate constant: for carbohydrates, proteins, and lipids ($k_{\text{hyd,ch}}$, $k_{\text{hyd,pr}}$, $k_{\text{hyd,li}}$); (iii) 26 inhibition constants; VFA inhibition of hydrolysis process ($K_{\text{i,VFA}}$) and inhibitions of various compounds and metals ions on various bacteria growth ($K_{\text{i,H}_2\text{,Agly}}$, $K_{\text{i,H}_2\text{,Aoa}}$, $K_{\text{i,H}_2\text{,Apro}}$, $K_{\text{i,H}_2\text{S,Apro}}$, $K_{\text{i,H}_2\text{,Abu}}$, $K_{\text{i,H}_2\text{S,Abu}}$, $K_{\text{i,H}_2\text{,Ava}}$, $K_{\text{i,H}_2\text{S,Ava}}$, $K_{\text{i,H}_2\text{S,Mac}}$, $K_{\text{i,NH}_3\text{,Mac}}$, $K_{\text{i,Cu}^{2+}\text{,Abu}}$, $K_{\text{i,Zn}^{2+}\text{,Abu}}$, $K_{\text{i,Cr}^{2+}\text{,Abu}}$, $K_{\text{i,Pb}^{2+}\text{,Abu}}$, $K_{\text{i,Ni}^{2+}\text{,Abu}}$, $K_{\text{i,Cu}^{2+}\text{,Mac}}$, $K_{\text{i,Zn}^{2+}\text{,Mac}}$, $K_{\text{i,Cr}^{2+}\text{,Mac}}$, $K_{\text{i,Pb}^{2+}\text{,Mac}}$, $K_{\text{i,Ni}^{2+}\text{,Mac}}$, $K_{\text{i,H}_2\text{S,Mhyd}}$, $K_{\text{i,H}_2\text{S,Ss}}$, $K_{\text{i,H}_2\text{S,Spro}}$, $K_{\text{i,H}_2\text{S,Sac}}$, and $K_{\text{i,H}_2\text{S,Shyd}}$); (iv) 2 limitation factors of inorganic nitrogen and inorganic phosphorus ($K_{\text{M,N}_{\text{io}}}$ and $K_{\text{M,P}_{\text{io}}}$) to all microbial growth rates and 16 Monod saturation constants including various substrates and bacteria ($k_{\text{M,suAsu}}$, $k_{\text{M,aaAaa}}$, $k_{\text{M,glyAgly}}$, $k_{\text{M,oaAoa}}$, $k_{\text{M,proApro}}$, $k_{\text{M,buAbu}}$, $k_{\text{M,vaAva}}$, $k_{\text{M,H}_2\text{Mhyd}}$, $k_{\text{M,acMac}}$, $k_{\text{M,Sio,atSs}}$, $k_{\text{M,proSpro}}$, $k_{\text{M,Sio,atSpro}}$, $k_{\text{M,acSac}}$, $k_{\text{M,Sio,atSac}}$, $k_{\text{M,H}_2\text{Shyd}}$, $k_{\text{M,Sio,atShyd}}$), (v) maximal microbial grow rates at optimal temperature for each of the 13 bacteria types $\mu_{i,\max,T_{\text{opt}}}, i \in I_{\text{bac}}$, microbial decays as a percentage of maximal microbial growth rates for each of 13 bacteria types $b_{i,\text{dec}}, i \in I_{\text{bac}}$, (vi) 10 parameters of mass transfer rates from liquid to gas phase, $(K_{\text{L}}a)_{j,\text{a}}$ and $(K_{\text{L}}a)_{j,\text{b}}, j \in I_{\text{gas}}$; (vii) 17 precipitation rate constants $k_{\text{cryst},k}, k \in I_{\text{prec}}$; (viii) 65 parameters related to the determination of the bacteria growth rate of various microbial groups; pK_i^{lo}, pK_i^{up}, α_i, $T_{i,\text{opt}}$, and $T_{i,\max}$, $i \in I_{\text{bac}}$. These parameters are treated as design parameters and are assembled into the vector $\mathbf{x}$.

B. Sensitivity analysis

In the scope of the sensitivity analysis, a set $S_{\mathbf{x}}$ of random AD model designs $\mathbf{x_j}, j = 1, \dots N_S$ (each design $\mathbf{x}_j$ is a complete set of design parameters) is generated. Here, a set of $N_S = 5 \times 178 = 890$ random designs was used, since numerical experience has shown that such a sample was statistically representative enough. For each design $\mathbf{x}_j$ from the set $S_{\mathbf{x}}$ the derivatives $\frac{\partial g_0}{\partial x_i}$ of the objective function are computed. The objective function g_0, Eq. (1), was used for this purpose since it was defined as a high-quality measure of deviation between numerical simulation (NS) and actual measured biogas plant data.

$$
\begin{aligned}
g_0 = {} & \psi_{0,1} \int_{t_{\text{stab}}}^{t_{\text{total}}} \left(\frac{Q_{\text{biogas}}(t) - Q_{\text{biogas,exp}}(t)}{\bar{Q}_{\text{biogas,exp}}} \right)^2 dt + \\
& \psi_{0,2} \int_{t_{\text{stab}}}^{t_{\text{total}}} \left(\frac{Q_{\text{g,CH}_4}(t) - Q_{\text{g,CH}_4\text{,exp}}(t)}{\bar{Q}_{\text{g,CH}_4\text{,exp}}} \right)^2 dt + \\
& \psi_{0,3} \int_{t_{\text{stab}}}^{t_{\text{total}}} \left(\frac{Q_{\text{g,H}_2}(t) - Q_{\text{g,H}_2\text{,exp}}(t)}{\bar{Q}_{\text{g,H}_2\text{,exp}}} \right)^2 dt + \\
& \psi_{0,4} \int_{t_{\text{stab}}}^{t_{\text{total}}} \left(\frac{Q_{\text{g,H}_2\text{S}}(t) - Q_{\text{g,H}_2\text{S,exp}}(t)}{\bar{Q}_{\text{g,H}_2\text{S,exp}}} \right)^2 dt + \\
& \psi_{0,5} \int_{t_{\text{stab}}}^{t_{\text{total}}} \left(\frac{\text{pH}(t) - \text{pH}_{\text{exp}}(t)}{\overline{\text{pH}}_{\text{exp}}} \right)^2 dt
\end{aligned} \tag{1}
$$

where $\psi_{0,1}$, $\psi_{0,2}$, $\psi_{0,3}$, $\psi_{0,4}$, and $\psi_{0,5}$ are normalized weighting factors used to scale the relative importance of individual deviations, while $Q_{\text{biogas}}(t)$, $Q_{\text{g,CH}_4}(t)$, $Q_{\text{g,H}_2}(t)$, $Q_{\text{g,H}_2\text{S}}(t)$, $Q_{\text{biogas,exp}}(t)$, $Q_{\text{g,CH}_4\text{,exp}}(t)$, $Q_{\text{g,H}_2\text{,exp}}(t)$, $Q_{\text{g,H}_2\text{S,exp}}(t)$, $\bar{Q}_{\text{biogas,exp}}$, $\bar{Q}_{\text{g,CH}_4\text{,exp}}$, $\bar{Q}_{\text{g,H}_2\text{,exp}}$, $\bar{Q}_{\text{g,H}_2\text{S,exp}}$ are time dependent predicted, time dependent measured, and average values of the measured biogas, CH_4, H_2, and H_2S flow rates, respectively. Meanwhile, $\text{pH}(t)$, $\text{pH}_{\text{exp}}(t)$, and $\overline{\text{pH}}_{\text{exp}}$ denote time dependent predicted, time dependent measured, and the average values of the measured pH value.

The obtained results of sensitivity analysis are normalized so that $\max_i \left(\left| \frac{\partial g_0}{\partial x_i} \right| \right) = 1$ for each $\mathbf{x}_j$. For each design parameter x_i the average absolute value $f_{\text{AA},i}$ and variance $f_{\text{VA},i}$ of the normalized $\frac{\partial g_0}{\partial x_i}$ with respect to the whole set $S_{\mathbf{x}}$ are computed. The normalized values of $f_{\text{AA},i}$ and $f_{\text{VA},i}$ are used to define the importance factor $f_{\text{IM},i} = \frac{1}{2} f_{\text{VA},i} + \frac{1}{2} f_{\text{AA},i}$ of the design parameter x_i.

C. Optimal design procedure

The multi-objective optimization problem is reformulated into a single-objective function g_0 by summing all considered deviations, multiplied by adequate weighting factors, Eq. (1).

The optimal design problem can be defined by Eq. (2)-(4).

$$\max g_0(\mathbf{x}, \mathbf{q}) \tag{2}$$

subject to constraints

$$g_i(\mathbf{x}, \mathbf{q}) \leq 0, \quad i = 1, \dots, k^* \tag{3}$$

and the response equation

$$h(\mathbf{x}, \mathbf{q}, \dot{\mathbf{q}}, t) = 0 \tag{4}$$

where the vector $\mathbf{x} \in R^{n^*}$ of design variables represents the set of all AD parameters of the BioModel. The vector $\mathbf{q} \in R^{m^*}$ assembles the response variables describing the response of the AD system and $\dot{\mathbf{q}} \in R^{m^*}$ are their first time derivatives. The response equation, Eq. (4), establishes the dependency of $\mathbf{q}$ on t and $\mathbf{x}$ and is given by the BioModel described in [12]. The scalar functions g_0 and g_i are termed the objective and constraint functions, respectively. The objective function is related to the quality of AD performance, while the constraints reflect the imposed limitations. The constraint functions in the standard form, Eq. (3), are related to the maximal allowed initial concentration of all bacteria group and to the allowed range of the differences between measured and predicted values of the observed AD performance [12]. The symbol n^* denotes the number of design variables, k^* is the number of constraints and m^* is the number of response variables.

D. ASO procedure

The ASO procedure used to calibrate the values of a large number of design parameters is described in detail in [12]. In short, it consists of following two steps.

1) Identification and initialization of design variables

In [12], the following 113 parameters are considered: the initial concentrations of the 13 types of bacteria in the F-CS, 3 hydrolysis rate constants, 26 inhibition constants, 2 limitation factors, 16 Monod saturation constants, maximal microbial grow rates at optimal temperature for each of the 13 bacteria types, microbial decays as a percentage of maximal microbial growth rates for each of 13 bacteria types, 10 parameters of mass transfer rates from liquid to gas phase, and 17 precipitation rate constants. In this paper, another 65 parameters, influencing the growth rate of 13 microbial groups $\mu_j, j \in I_{\text{bac}}$ (parameters pK_i^{lo}, pK_i^{up}, α_i, $T_{i,\text{opt}}$, and $T_{i,\max}$, $i \in I_{\text{bac}}$) are included. The normalized design variables are defined as: $x_i = \frac{(x_{\text{P},i} - x_{\text{P},i}^{\min})}{(x_{\text{P},i}^{\max} - x_{\text{P},i}^{\min})} \in [0,1]$, $i = 1 \dots n^*$, where $x_{\text{P},i}$ is the i^{th} AD feedstock/model parameter, $x_{\text{P},i}^{\min}$ and $x_{\text{P},i}^{\max}$ are its lower an upper limits, and $n^* = 178$. The initial values of all design variables are set to the recommended values obtained from the literature.

2) Gradual optimization of design variables

This step is performed in several cycles. Within each cycle, an adequate activation threshold value f_T is chosen to select the active

design variables x_i^* for which it holds $f_{\mathrm{IM},i} \geq f_T$; all other design variables are designated as passive in the current cycle. After that, the optimal design problem, Eqs. (2)-(4), is solved in order to optimize the active design variables; for this purpose, a gradient-based algorithm with adaptive approximation scheme is engaged. This completes the current cycle. After that a new cycle with a lower activation threshold value is started. This procedure is continued until all design variables are active and optimized (calibrated).

IV. RESULTS AND DISCUSSION

The proposed AD model and the whole optimization procedure were coded in-house in the C# language. The system of ODEs was solved by the Runge-Kutta method with an option to resort to the Euler method in case of (very rare) numerical instabilities. The engaged optimization algorithm is based on an approximation method [23-24] which sequentially generates approximate, strictly convex, and separable nonlinear programming problems and solves them to generate a sequence of converging approximate solutions. The algorithm uses the history of design derivatives of the objective and constraint functions to gradually improve the quality of the approximation. In this work numerical differentiation by using simple forward differences was used to get the needed design derivatives. Since there are 178 design variables, such derivatives computation is rather CPU intensive. To improve numerical performance, the computation of design derivatives was parallelized; this accelerated the computation by a factor practically equal to the number of CPU cores. In this scenario, one full optimization cycle (with all 178 design variables being active) took about 1 minute of CPU time on an 8-core i7 CPU desktop computer. The number of optimization cycles, needed to obtain optimum parameters, ranged usually up to 100.

In the following, the results of BioModel calibration are given as well as the results of the calibrated BioModel validation.

A. BioModel calibration

During optimization the values of 178 design parameters (13 feedstock and 165 model parameters) were allowed to vary between lower and upper limits. Wherever possible, these limits were obtained by taking the smallest and largest values of those parameters as reported in the literature [3, 6, 12, 13, 15, 25-29]; the lower and upper limit values, $\mathrm{x}_{\mathrm{P},i}^{\min}$ and $\mathrm{x}_{\mathrm{P},i}^{\max}$, $i = 1 \ldots n^*$, actually used in this work, are collected in Table 2.

In numerical simulation, the first 135 simulation days have been considered as a transient response or stabilization period, t_{stab}, needed to reach steady state conditions for the input data corresponding to measured biogas plant data at day one. Therefore, in case of BioModel calibration, the comparison of the simulated and measured results was done only for the period of 365 days which follows the stabilization period of 135 days.

At the beginning, the value of 0.5 is used for the initial values of all normalized design variables x_i. During gradual optimization, the threshold values f_T were sequentially chosen as 0.2 (Set1 1), 0.01 (Set 2), and 0.001 (Set 3). The corresponding number of active design variables x_i^* increased from 7 (Set 1), through 24 (Set 2), up to 178 (Set 3). The optimized values of 7 active design variables, obtained in the optimization of Set 1, were kept as initial values of these variables for the optimization of the next set and so on. In Set 3 all design variables were included as the active design variables x_i^* and the optimized values of all feedstock and model parameters are presented in Table 2.

The value of the objective function g_0 was gradually minimized from 9.685 (initial design) to 0.08575 (optimal design of Set 1 after 19 iterations), 0.0194 (optimal design of Set 2 after 31 iterations) to 0.0191 (optimal design of Set 3 after 60 iterations).

Table 2. Feedstock and model parameters: lower, upper and optimized data.

i	Parameter	$\mathrm{x}_{\mathrm{P},i}^{\min}$	$\mathrm{x}_{\mathrm{P},i}^{\max}$	Optimal value
1	X_{Asu} ($\mathrm{gL^{-1}}$)	0.1	0.5	0.29131
2	X_{Aaa} ($\mathrm{gL^{-1}}$)	0.1	0.5	0.29092
3	X_{Agly} ($\mathrm{gL^{-1}}$)	0.1	0.5	0.29108
4	X_{Aoa} ($\mathrm{gL^{-1}}$)	0.1	0.5	0.29144
5	X_{Apro} ($\mathrm{gL^{-1}}$)	0.1	0.5	0.30138
6	X_{Abu} ($\mathrm{gL^{-1}}$)	0.1	0.5	0.30078
7	X_{Ava} ($\mathrm{gL^{-1}}$)	0.1	0.5	0.29793
8	X_{Mac} ($\mathrm{gL^{-1}}$)	0.1	0.5	0.30778
9	X_{Mhyd} ($\mathrm{gL^{-1}}$)	0.1	0.5	0.10299
10	X_{Spro} ($\mathrm{gL^{-1}}$)	0.1	0.5	0.28040
11	X_{Sac} ($\mathrm{gL^{-1}}$)	0.1	0.5	0.29094
12	X_{Ss} ($\mathrm{gL^{-1}}$)	0.1	0.5	0.29112
13	X_{Shyd} ($\mathrm{gL^{-1}}$)	0.1	0.5	0.28475
14	$k_{\mathrm{hyd,ch}}$ ($\mathrm{day^{-1}}$)	1.0	10.0	5.44266
15	$k_{\mathrm{hyd,pr}}$ ($\mathrm{day^{-1}}$)	1.0	10.0	4.95942
16	$k_{\mathrm{hyd,li}}$ ($\mathrm{day^{-1}}$)	1.0	10.0	5.01598
17	$K_{\mathrm{i,VFA}}$ ($\mathrm{gL^{-1}}$)	0.1	0.6	0.22880
18	$K_{\mathrm{i,H_2,Agly}}$ ($\mathrm{gL^{-1}}$)	0.01	0.1	0.05280
19	$K_{\mathrm{i,H_2,Aoa}}$ ($\mathrm{gL^{-1}}$)	0.01	0.1	0.05280
20	$K_{\mathrm{i,H_2,Apro}}$ ($\mathrm{gL^{-1}}$)	0.01	0.1	0.05284
21	$K_{\mathrm{i,H_2,Abu}}$ ($\mathrm{gL^{-1}}$)	0.01	0.1	0.05280
22	$K_{\mathrm{i,H_2,Ava}}$ ($\mathrm{gL^{-1}}$)	0.01	0.1	0.05279
23	$K_{\mathrm{i,H_2S,Apro}}$ ($\mathrm{gL^{-1}}$)	0.1	0.9	0.48386
24	$K_{\mathrm{i,H_2S,Abu}}$ ($\mathrm{gL^{-1}}$)	0.1	0.9	0.47729
25	$K_{\mathrm{i,H_2S,Ava}}$ ($\mathrm{gL^{-1}}$)	0.1	0.9	0.47697
26	$K_{\mathrm{i,H_2S,Mac}}$ ($\mathrm{gL^{-1}}$)	0.1	0.9	0.50035
27	$K_{\mathrm{i,H_2S,Mhyd}}$ ($\mathrm{gL^{-1}}$)	0.1	0.9	0.46746
28	$K_{\mathrm{i,H_2S,Ss}}$ ($\mathrm{gL^{-1}}$)	0.1	0.9	0.48012
29	$K_{\mathrm{i,H_2S,Spro}}$ ($\mathrm{gL^{-1}}$)	0.1	0.9	0.48043
30	$K_{\mathrm{i,H_2S,Sac}}$ ($\mathrm{gL^{-1}}$)	0.1	0.9	0.48051
31	$K_{\mathrm{i,H_2S,Shyd}}$ ($\mathrm{gL^{-1}}$)	0.1	0.9	0.48081
32	$K_{\mathrm{i,NH_3,Mac}}$ ($\mathrm{gL^{-1}}$)	0.1	0.3	0.22095
33	$K_{\mathrm{i,Cu^{2+},Abu}}$ ($\mathrm{gL^{-1}}$)	0.1	0.9	0.48041
34	$K_{\mathrm{i,Zn^{2+},Abu}}$ ($\mathrm{gL^{-1}}$)	0.1	0.9	0.48038
35	$K_{\mathrm{i,Cr^{2+},Abu}}$ ($\mathrm{gL^{-1}}$)	0.1	0.9	0.48008
36	$K_{\mathrm{i,Pb^{2+},Abu}}$ ($\mathrm{gL^{-1}}$)	0.1	0.9	0.48041
37	$K_{\mathrm{i,Ni^{2+},Abu}}$ ($\mathrm{gL^{-1}}$)	0.1	0.9	0.48041
38	$K_{\mathrm{i,Cu^{2+},Mac}}$ ($\mathrm{gL^{-1}}$)	0.1	0.9	0.48044
39	$K_{\mathrm{i,Zn^{2+},Mac}}$ ($\mathrm{gL^{-1}}$)	0.1	0.9	0.48052
40	$K_{\mathrm{i,Cr^{2+},Mac}}$ ($\mathrm{gL^{-1}}$)	0.1	0.9	0.47892
41	$K_{\mathrm{i,Pb^{2+},Mac}}$ ($\mathrm{gL^{-1}}$)	0.1	0.9	0.48042
42	$K_{\mathrm{i,Ni^{2+},Mac}}$ ($\mathrm{gL^{-1}}$)	0.1	0.9	0.48042
43	$K_{\mathrm{M,N_{io}}}$ ($\mathrm{gL^{-1}}$)	0.001	0.01	0.00528
44	$K_{\mathrm{M,P_{io}}}$ ($\mathrm{gL^{-1}}$)	0.001	0.01	0.00527
45	$k_{\mathrm{M,suAsu}}$ ($\mathrm{gL^{-1}}$)	0.1	0.9	0.47809
46	$k_{\mathrm{M,aaAaa}}$ ($\mathrm{gL^{-1}}$)	0.1	0.9	0.47919
47	$k_{\mathrm{M,glyAgly}}$ ($\mathrm{gL^{-1}}$)	0.1	0.9	0.47978
48	$k_{\mathrm{M,oaAoa}}$ ($\mathrm{gL^{-1}}$)	0.1	0.9	0.47888
49	$k_{\mathrm{M,proApro}}$ ($\mathrm{gL^{-1}}$)	0.01	0.1	0.04837
50	$k_{\mathrm{M,buAbu}}$ ($\mathrm{gL^{-1}}$)	0.01	0.1	0.05169
51	$k_{\mathrm{M,vaAva}}$ ($\mathrm{gL^{-1}}$)	0.01	0.1	0.05266
52	$k_{\mathrm{M,H_2Mhyd}}$ ($\mathrm{gL^{-1}}$)	0.01	0.1	0.03533
53	$k_{\mathrm{M,acMac}}$ ($\mathrm{gL^{-1}}$)	0.1	0.5	0.10038
54	$k_{\mathrm{M,Sio,atSs}}$ ($\mathrm{gL^{-1}}$)	0.1	0.5	0.28649

55	$k_{M,proSpro}$ (gL^{-1})	0.1	0.5	0.29016
56	$k_{M,Sio,atSpro}$ (gL^{-1})	0.1	0.5	0.29016
57	$k_{M,acSac}$ (gL^{-1})	0.1	0.5	0.28999
58	$k_{M,Sio,atSac}$ (gL^{-1})	0.1	0.5	0.28999
59	k_{M,H_2Shyd} (gL^{-1})	0.01	0.1	0.05147
60	$k_{M,Sio,atShyd}$ (gL^{-1})	0.01	0.1	0.05041
61	$\mu_{Asu,max,T_{opt}}$ (day^{-1})	1.0	10.0	5.29994
62	$\mu_{Aaa,max,T_{opt}}$ (day^{-1})	1.0	10.0	5.30838
63	$\mu_{Agly,max,T_{opt}}$ (day^{-1})	1.0	10.0	5.28801
64	$\mu_{Aoa,max,T_{opt}}$ (day^{-1})	1.0	10.0	5.30106
65	$\mu_{Apro,max,T_{opt}}$ (day^{-1})	1.0	12.0	6.49033
66	$\mu_{Abu,max,T_{opt}}$ (day^{-1})	1.0	10.0	5.22845
67	$\mu_{Ava,max,T_{opt}}$ (day^{-1})	1.0	10.0	5.24772
68	$\mu_{Mac,max,T_{opt}}$ (day^{-1})	1.0	20.0	10.86708
69	$\mu_{Mhyd,max,T_{opt}}$ (day^{-1})	1.0	10.0	5.40755
70	$\mu_{Ss,max,T_{opt}}$ (day^{-1})	1.0	10.0	5.26495
71	$\mu_{Spro,max,T_{opt}}$ (day^{-1})	1.0	10.0	5.28305
72	$\mu_{Sac,max,T_{opt}}$ (day^{-1})	1.0	10.0	5.28666
73	$\mu_{Shyd,max,T_{opt}}$ (day^{-1})	1.0	10.0	5.28801
74	$b_{dec,Asu}$ (/)	0.01	0.05	0.02899
75	$b_{dec,Aaa}$ (/)	0.01	0.05	0.02907
76	$b_{dec,Agly}$ (/)	0.01	0.05	0.02902
77	$b_{dec,Aoa}$ (/)	0.01	0.05	0.02903
78	$b_{dec,Apro}$ (/)	0.01	0.05	0.02783
79	$b_{dec,Abu}$ (/)	0.01	0.05	0.02827
80	$b_{dec,Ava}$ (/)	0.01	0.05	0.02880
81	$b_{dec,Mac}$ (/)	0.01	0.05	0.01001
82	$b_{dec,Mhyd}$ (/)	0.01	0.05	0.01253
83	$b_{dec,Ss}$ (/)	0.01	0.05	0.02914
84	$b_{dec,Spro}$ (/)	0.01	0.05	0.02903
85	$b_{dec,Sac}$ (/)	0.01	0.05	0.02902
86	$b_{dec,Shyd}$ (/)	0.01	0.05	0.02808
87	$(K_La)_{CO_2,a}$ ($^oC^{-1}day^{-1}$)	1.0	5.0	2.89764
88	$(K_La)_{CO_2,b}$ (day^{-1})	10.0	20.0	14.75347
89	$(K_La)_{CH_4,a}$ ($^oC^{-1}day^{-1}$)	1.0	5.0	2.90732
90	$(K_La)_{CH_4,b}$ (day^{-1})	10.0	20.0	14.75598
91	$(K_La)_{H_2,a}$ ($^oC^{-1}day^{-1}$)	0.0001	0.001	0.00034
92	$(K_La)_{H_2,b}$ (day^{-1})	0.001	0.01	0.00510
93	$(K_La)_{H_2S,a}$ ($^oC^{-1}day^{-1}$)	0.0001	0.001	0.00010
94	$(K_La)_{H_2S,b}$ (day^{-1})	0.001	0.01	0.00281
95	$(K_La)_{NH_3,a}$ ($^oC^{-1}day^{-1}$)	0.0001	0.001	0.00053
96	$(K_La)_{NH_3,b}$ (day^{-1})	0.001	0.01	0.00528
97	$k_{cryst,CaCO_3}$ (day^{-1})	5.0	10.0	7.42617
98	$k_{cryst,MgCO_3}$ (day^{-1})	5.0	10.0	7.37970
99	$k_{cryst,FeCO_3}$ (day^{-1})	5.0	10.0	7.42335
100	$k_{cryst,NiCO_3}$ (day^{-1})	5.0	10.0	7.37760
101	$k_{cryst,CuCO_3}$ (day^{-1})	5.0	10.0	7.37770
102	$k_{cryst,PbCO_3}$ (day^{-1})	5.0	10.0	7.37759
103	$k_{cryst,ZnCO_3}$ (day^{-1})	5.0	10.0	7.37813
104	$k_{cryst,FeS}$ (day^{-1})	50.0	100.0	73.74520
105	$k_{cryst,NiS}$ (day^{-1})	50.0	100.0	73.77575
106	$k_{cryst,CuS}$ (day^{-1})	50.0	100.0	73.77565
107	$k_{cryst,PbS}$ (day^{-1})	50.0	100.0	73.77575
108	$k_{cryst,ZnS}$ (day^{-1})	50.0	100.0	73.77525
109	$k_{cryst,Ca_3(PO_4)_2}$ (day^{-1})	50.0	100.0	73.79385
110	$k_{cryst,Fe_3(PO_4)_2}$ (day^{-1})	50.0	100.0	73.76085
111	$k_{cryst,Ni_3(PO_4)_2}$ (day^{-1})	50.0	100.0	73.77580
112	$k_{cryst,MgNH_4PO_4}$ (day^{-1})	100.0	200.0	147.87560
113	$k_{cryst,K\ MgPO_4}$ (day^{-1})	50.0	100.0	73.84320
114	pK_{Asu}^{lo} (/)	4.5	5.5	4.97564
115	pK_{Asu}^{up} (/)	7.5	8.5	7.97649
116	pK_{Aaa}^{lo} (/)	4.5	5.5	4.97558
117	pK_{Aaa}^{up} (/)	7.5	8.5	7.97601
118	pK_{Agly}^{lo} (/)	4.5	5.5	4.97555
119	pK_{Agly}^{up} (/)	7.5	8.5	7.97580
120	pK_{Aoa}^{lo} (/)	4.5	5.5	4.97560
121	pK_{Aoa}^{up} (/)	7.5	8.5	7.97621
122	pK_{Apro}^{lo} (/)	5.5	6.5	5.97771
123	pK_{Apro}^{up} (/)	8.0	9.0	8.48162
124	pK_{Abu}^{lo} (/)	5.5	6.5	5.97646
125	pK_{Abu}^{up} (/)	8.0	9.0	8.48030
126	pK_{Ava}^{lo} (/)	5.5	6.5	5.97590
127	pK_{Ava}^{up} (/)	8.0	9.0	8.47841
128	pK_{Mac}^{lo} (/)	5.5	6.5	5.97397
129	pK_{Mac}^{up} (/)	8.0	9.0	8.49239
130	pK_{Mhyd}^{lo} (/)	5.5	6.5	5.97724
131	pK_{Mhyd}^{up} (/)	8.0	9.0	8.47170
132	pK_{Ss}^{lo} (/)	5.5	6.5	5.97527
133	pK_{Ss}^{up} (/)	7.5	8.5	7.97432
134	pK_{Spro}^{lo} (/)	5.5	6.5	5.97553
135	pK_{Spro}^{up} (/)	7.5	8.5	7.97556
136	pK_{Sac}^{lo} (/)	5.5	6.5	5.97558
137	pK_{Sac}^{up} (/)	7.5	8.5	7.97567
138	pK_{Shyd}^{lo} (/)	5.5	6.5	5.97586
139	pK_{Shyd}^{up} (/)	7.5	8.5	7.97696
140	α_{Asu} ($K^{-1}day^{-1}$)	0.00015	0.00019	0.00017
141	α_{Aaa} ($K^{-1}day^{-1}$)	0.00015	0.00019	0.00017
142	α_{Agly} ($K^{-1}day^{-1}$)	0.00015	0.00019	0.00017
143	α_{Aoa} ($K^{-1}day^{-1}$)	0.00015	0.00019	0.00017
144	α_{Apro} ($K^{-1}day^{-1}$)	0.00015	0.00019	0.00017
145	α_{Abu} ($K^{-1}day^{-1}$)	0.00016	0.00020	0.00018
146	α_{Ava} ($K^{-1}day^{-1}$)	0.00016	0.00020	0.00018
147	α_{Mac} ($K^{-1}day^{-1}$)	0.00015	0.00019	0.00017
148	α_{Mhyd} ($K^{-1}day^{-1}$)	0.00015	0.00019	0.00017
149	α_{Ss} ($K^{-1}day^{-1}$)	0.00016	0.00020	0.00018
150	α_{Spro} ($K^{-1}day^{-1}$)	0.00016	0.00020	0.00018
151	α_{Sac} ($K^{-1}day^{-1}$)	0.00016	0.00020	0.00018
152	α_{Shyd} ($K^{-1}day^{-1}$)	0.00016	0.00020	0.00018
153	$T_{Asu,opt}$ (^oC)	50	60	54.75515
154	$T_{Asu,max}$ (^oC)	60	70	64.75515
155	$T_{Asa,opt}$ (^oC)	50	60	54.75515
156	$T_{Aaa,max}$ (^oC)	60	70	64.75515
157	$T_{Agly,opt}$ (^oC)	50	60	54.75515
158	$T_{Agly,max}$ (^oC)	60	70	64.75515
159	$T_{Aoa,opt}$ (^oC)	50	60	54.75515
160	$T_{Aoa,max}$ (^oC)	60	70	64.75515
161	$T_{Apro,opt}$ (^oC)	50	60	54.75513
162	$T_{Apro,max}$ (^oC)	60	70	64.75515
163	$T_{Abu,opt}$ (^oC)	55	65	59.75517
164	$T_{Abu,max}$ (^oC)	65	75	69.75515
165	$T_{Ava,opt}$ (^oC)	55	65	59.75516
166	$T_{Ava,max}$ (^oC)	65	75	69.75515

167	$T_{Mac,opt}$ (°C)	50	60	54.75522
168	$T_{Mac,max}$ (°C)	60	70	64.75515
169	$T_{Mhyd,opt}$ (°C)	50	60	54.75515
170	$T_{Mhyd,max}$ (°C)	60	70	64.75515
171	$T_{Ss,opt}$ (°C)	30	40	34.75274
172	$T_{Ss,max}$ (°C)	60	70	64.75389
173	$T_{Spro,opt}$ (°C)	30	40	34.75592
174	$T_{Spro,max}$ (°C)	60	70	64.75487
175	$T_{Sac,opt}$ (°C)	30	40	34.75672
176	$T_{Sac,max}$ (°C)	60	70	64.75518
177	$T_{Shyd,opt}$ (°C)	30	40	34.75631
178	$T_{Shyd,max}$ (°C)	60	70	64.75447

The biogas flow rates, obtained by simulation with the initial and various optimal values of design parameters (computed with active design variables from Sets 1 to Set 3 – optimal design), are compared to the measured data in Figure 6. The mean biogas flow rate, obtained with initial values of design parameters, differs on average from the measured values by around 6.5 % (average absolute daily difference divided by average daily measurement). By far the largest improvement of these results is reached by optimizing the active design variables of Set 1. Further optimization of the Set 2 and Set 3 gradually also improves the result but the improvements are becoming progressively small. It is clearly evident that the biogas flow rate obtained with the optimal (calibrated) values of all 178 design parameters, presented in Table 2, are the closest to the measured biogas rates. The simulated data of biogas flow rate agree very well with the measured values; the average difference is less than 0.1%. The total biogas volume, delivered by the biogas plant within 365 days, is by about 7% higher than the one computed with the initial values of design parameters. After optimization, this difference becomes practically negligible (less than 0.5%).

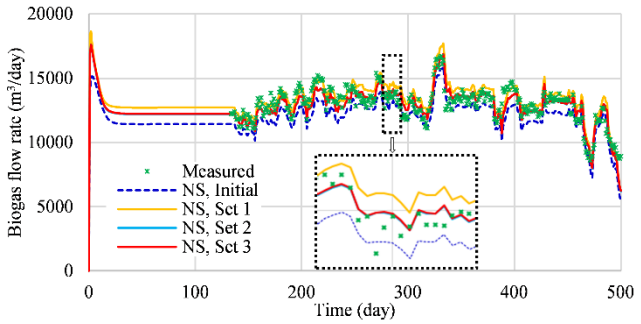

Figure 6. Dynamics of biogas flow rate, BioModel calibration.

The CH_4 flow rates, obtained numerically with the initial and the optimal values of design parameters from various sets, are compared to the measured data in Figure 7. Initially, the simulated CH_4 flow rate differs from the measured one by 9.4% on average. By optimizing the active design variables of Set 1, this difference is decreased substantially, while further improvements obtained by optimizing the design parameters from Set 2 and Set 3 are rather small, resulting in the final difference of approximately 1.2%. The total produced CH_4 volume, delivered by the plant within 365 days, is around 10% higher than the one computed with the initial values of design parameters. After the optimization, this difference is below 0.3%.

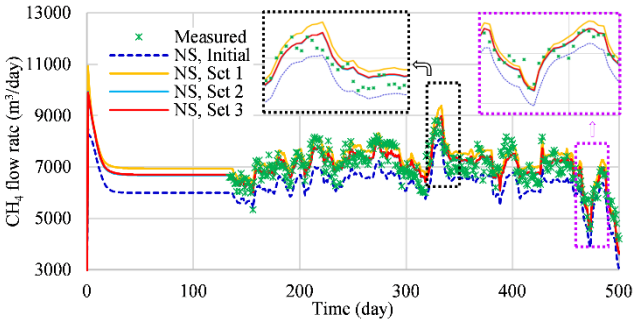

Figure 7. Dynamics of CH_4 flow rate, BioModel calibration.

The numerically obtained H_2 flow rate history is compared to measured data in Figure 8. It can be observed that the substantial difference between measured and simulation (initial design) decreased drastically after optimizing Set 1. Further optimization including more design parameters improves gradually the result. The average difference, which was initially approximately 138%, fell after optimizing Set 1 to about 8.6% and after optimizing Set 3 to 1%. With fully optimized design parameters, the computed total H_2 volume differs by around 0.1% from the measured data; initially this difference was around 138%.

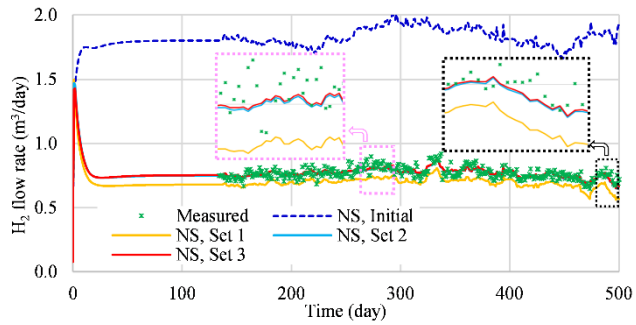

Figure 8. Dynamics of H_2 flow rate, BioModel calibration.

Figure 9 shows the comparison of dynamics of H_2S flow rate, obtained by simulation and experiment. Similar to H_2 flow rate, it can be observed that the difference between measured and initial design is substantially. These differences are reduced significantly after optimizing the Set 1; however, little further progress can be observed after optimizing Set 2 and Set 3. Low values of H_2S flow rate can be obtained by considering the Kemira BDP-840 additive, which contains $FeCl_2$ to reduce H_2S content in the produced biogas. The average difference, which was initially approximately 535%, fell after optimizing the design variables of Set 3 to a negligible value. With fully optimized design parameters (Set 3), the computed total H_2S volume differs by less than 0.1% from the measured data; initially this difference was over 539%.

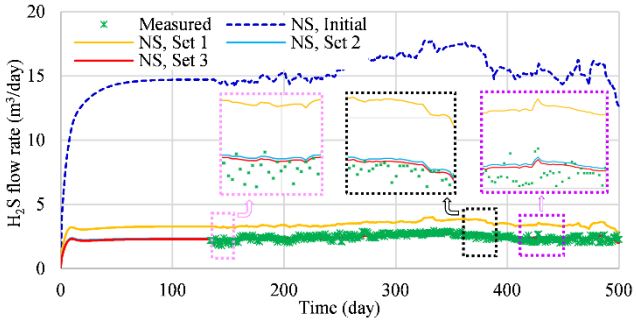

Figure 9. Dynamics of H_2S flow rate, BioModel calibration.

The numerically obtained dynamics of pH values are compared to experimental data in Figure 10. It can be seen that after the

stabilization period of 135 days, the optimal values of design parameters deliver a rather constant pH value very close to pH 7.7, which is the mean measured value. The average difference, which was initially approximately 4.5%, fell after optimizing the design variables of Set 3 to less than 0.3%.

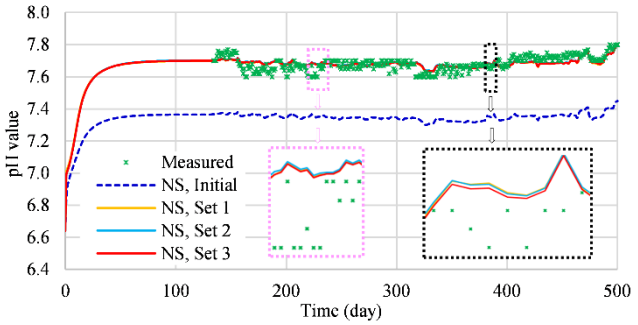

Figure 10. Dynamics of pH *value, BioModel calibration.*

According to the presented results, one can say that the optimization of the most important parameters (Set 2) yields relatively good results. For the fine tuning, however, the activation of all design parameters (Set 3, Optimal) may be worth a consideration.

B. BioModel validation

The calibrated values of all 178 design parameters were validated by using another set of measured data from the same biogas plant. The comparison between measured and predicted values of pH value, biogas and CH_4 flow rates are given in Figure 11.

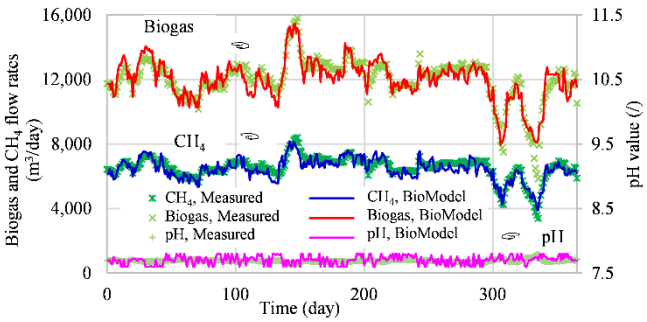

Figure 11. Dynamics of biogas and CH_4 *flow rates and* pH *value, BioModel validation.*

Figure 12 shows the dynamics of H_2 and H_2S flow rates, obtained by measurements and simulation.

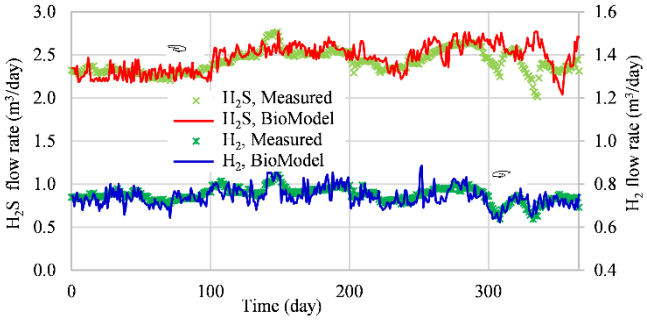

Figure 12. Dynamics of H_2 *and* H_2S *flow rates, BioModel validation.*

From Figure 11 and Figure 12 it can be seen, that the dynamics of the predicted AD performances follow very well the dynamics of the measured AD performance through the 365 days. The agreement between all measured and predicted AD performances is quite good; therefore, it can be concluded that the calibrated values of all 178 design parameters by using the proposed ASO procedure enable satisfactory prediction of the AD process.

C. Evaluation of the ASO procedure

For the evaluation of the proposed ASO procedure, the measured and predicted AD performances are estimated by two statistical indicators (SI): coefficient of determination (R^2), Eq. (5), and the relative index of agreement $I_{A,rel}$, Eq. (6) [12, 30].

$$R^2 = \left(\frac{\sum_{i=1}^{n} |y_{exp,i} - \bar{y}_{exp}| \, |y_{NS,i} - \bar{y}_{NS}|}{\sqrt{\sum_{i=1}^{n} (y_{exp,i} - \bar{y}_{exp})^2} \sqrt{\sum_{i=1}^{n} (y_{NS,i} - \bar{y}_{NS})^2}} \right)^2 \quad (5)$$

$$I_{A,rel} = 1 - \frac{\sum_{i=1}^{n} \left(\frac{y_{exp,i} - y_{NS,i}}{\bar{y}_{exp}} \right)^2}{\sum_{i=1}^{n} \left(\frac{|y_{NS,i} - \bar{y}_{exp}| + |y_{exp,i} - \bar{y}_{exp}|}{\bar{y}_{exp}} \right)^2} \quad (6)$$

where n is the number of comparison points, $y_{exp,i}$ and $y_{NS,i}$ relate to the measured and predicted values of AD performance at i^{th} day of the AD process, respectively, while $\bar{y}_{exp}$ and $\bar{y}_{NS}$ are average values of the measured and predicted AD performance of the complete AD process, respectively.

The coefficient of determination R^2 and relative index of agreement $I_{A,rel}$ in case of BioModel calibration and BioModel validation are given in Table 3.

Table 3. Statistical indicators for ASO procedure

SI	Mode	Design	Q_{CH_4}	Q_{H_2}	Q_{H_2S}	Q_{biogas}
R^2	Calibration	Initial	0.8215	0.4389	0.6073	0.8314
		Optimal	0.8310	0.6459	0.5985	0.8324
	Validation		0.8299	0.6130	0.6226	0.8616
$I_{A,rel}$	Calibration	Initial	0.7569	0.0663	0.0317	0.8514
		Optimal	0.9350	0.8048	0.7582	0.9406
	Validation		0.9352	0.7823	0.7455	0.9535

The obtained values of the statistical indicators confirm that the presented ASO procedure based on the included BioModel are reliable and efficient. It is clearly evident, that the optimization of all 178 parameters results in the improvement of the accuracy of simulation when compared with the BioModel containing only 113 design parameters [12].

V. CONCLUSIONS

The agreement of the obtained results by numerical simulation of the AD process in a single CSTR of a full-scale biogas plant and the measured AD performance through the observed two years, confirms the efficiency of the used AD BioModel which takes into account the Kemira BDP-840 additive to reduce H_2S content in the produced biogas. Furthermore, it is evident that the active set optimization procedure and the engaged gradient-based optimizer to calibrate all 178 feedstock and model parameters is reliable and efficient, especially, if the computation of design derivatives is parallelized.

VI. ACKNOWLEDGMENTS

The author is grateful for the financial support of the Slovenian Research Agency (PhD research fellowship contract No. 1000-18-0552 and core research funding No. P2-0032). The author highly appreciates the collaboration with Biogas Plant Draženci for providing the necessary experimental data.

VII. REFERENCES

[1] D. J. Batstone, J. Keller, I. Angelidaki, S. V. Kalyuzhnyi, S. G. Pavlostathis, A.Rozzi, W. T. M. Sanders, H. Siegrist, V. A. Vavilin, Anaerobic Digestion Model No. 1 (ADM1). London: IWA Publishing, 2002.

[2] A. Donoso-Bravo, D. Olivares, Y. Lesty, H. V. Bossche, "Explotation of the ADM1 in a XXI century wastewater resource recovery facility (WRRF): The case of codigestion and thermal hydrolysis." Water Research vol. 175, no. 115654, 2020.

[3] X. Flores-Alsina, K. Solon, C. K. Mbamba, S. Tait, K. V. Gernaey, U. Jeppsson, D. J. Batstone, "Modelling phosphorus (P), sulfur (S) and iron (Fe) interactions for dynamic simulations of anaerobic digestion processes," Water Research, vol. 95, pp. 370-382., 2016.

[4] L. Frunzo, F. G. Fermoso, V. Luongo, M. R. Mattei, G. Esposito, "ADM1-based mechanistic model for the role of trace elements in anaerobic digestion processes," Journal of Environmental Management, vol. 241, pp. 587-602, 2019.

[5] B. C. Maharaj, M. R. Mattei, L. Frunzo, E.D. van Hullebusch, G. Esposito, "ADM1 based mathematical model of trace element precipitation/dissolution in anaerobic digestion processes," Bioresource Technology, vol. 267, pp. 666-676, 2018.

[6] H. Sun, Z. Yang, Q. Zhao, M. Kurbonova, R. Zhang, G. Liu, W. Wang,, "Modification and extension of anaerobic digestion model No.1 (ADM1) for syngas biomethanation simulation: From lab-scale to pilot-scale," Chemical Engineering Journal, vol. 403, no. 126177, 2021.

[7] I. Angelidaki, L. Ellegaard, B. K. Ahring, "A mathematical model for dynamic simulation of anaerobic digestion of complex substrates: Focusing on ammonia inhibition," Biotechnology and Bioengineering vol. 42, pp. 159-166, 1993.

[8] I. Angelidaki, L. Ellegaard, B. K. Ahring, "A comprehensive model of anaerobic bioconversion of complex substrates to biogas," Biotechnology and Bioengineering , vol. 63(3), pp. 363-372, 1999.

[9] T. Fitamo, A. Boldrin, G. Dorini, K. Boe, I. Angelidaki, C. Scheutz, "Optimising the anaerobic co-digestion of urban organic waste using dynamic bioconversion mathematical modelling, " Water Research, vol. 106, pp. 283-294, 2016.

[10] T. Kegl, A. Kovač Kralj, "Multi-objective optimization of anaerobic digestion process using a gradient-based algorithm," Energy Conversion and Management, vol. 226, no. 113560, 2020.

[11] T. Kegl, T., A. Kovač Kralj, "Optimization of biogas production from cattle manure by anaerobic digestion using a gradient-based algorithm," Computer Aided Chemical Engineering, vol. 50, pp. 1909-1915, 2021.

[12] T. Kegl, A. Kovač Kralj, "An enhanced anaerobic digestion BioModel calibrated by parameters optimization based on measured biogas plant data," Fuel, vol. 322, no. 122984, 2022.

[13] A. Kovalovszki, M. Alvarado-Morales, I. A. Fotidis, I. Angelidaki, "A systematic methodology to extend the applicability of a bioconversion model for the simulation of various co-digestion scenarios," Bioresource Technology, vol. 235, pp. 157-166, 2017.

[14] K. Bułkowska, I. Białobrzewski, Z. Mariusz Gusiatin, E. Klimiuk, T. Pokoj, "ADM1-based modeling of anaerobic codigestion of maize silage and cattle manure – calibration of parameters and model verification (part II)," Archives of Environmental Protection, vol. 41, pp. 20-27, 2015.

[15] Z. Fatolahi, G. Arab, V. Razaviarani, "Calibration of the Anaerobic Digestion Model No. 1 for anaerobic digestion of organic fraction of municipal solid waste under mesophilic condition," Biomass and Bioenergy, vol. 139, no. 105661, 2020.

[16] A. Kovalovszki, L. Treu, L. Ellegaard, G. Luo, I. Angelidaki, "Modeling temperature response in bioenergy production: Novel solution to a common challenge of anaerobic digestion," Applied Energy, vol. 263, no. 114646, 2020.

[17] F. A. Neba, H. M. Tornyeviadzi, S. W. Østerhus, R. Seidu, "Self-optimizing attainable regions of the anaerobic treatment process: Modeling performance targets under kinetic uncertainty," Water Research, vol. 171, no. 115377, 2020.

[18] H. Ozgun, "Anaerobic Digestion Model No. 1 (ADM1) for mathematical modeling of full-scale sludge digester performance in a municipal wastewater treatment plant," Biodegradation, vol. 30, pp. 27-36, 2019.

[19] D. Poggio, M. Walker, W. Nimmo, L. Ma, M. Pourkashanian, "Modelling the anaerobic digestion of solid organic waste – Substrate characterisation method for ADM1 using a combined biochemical and kinetic parameter estimation approach," Waste Management, vol. 53, pp. 40-54, 2016.

[20] K. Postawa, J. Szczygiel, M. Kułażyński, "Heuristic methods in optimization of selected parameters of Two-Phase Anaerobic Digestion (TPAD) model," Fuel, vol. 281, no. 118257, 2020.

[21] D. P. Van, T. Fujiwara, B. L. Tho, P. P. S. Toan, G. H. Minh, "A review of anaerobic digestion systems for biodegradable waste: Configurations, operating parameters, and current trends," Environmental Engineering Research, vol. 25(1), pp. 1-17, 2020.

[22] W. Ahmed, J. Rodríguez, "Generalized parameter estimation and calibration for biokinetic models using correlation and single variable optimisations: Application to sulfate reduction modelling in anaerobic digestion," Water Research, vol. 122, pp. 407-418, 2017.

[23] M. Kegl, B. J. Butinar, B. Kegl, "An efficient gradient-based optimization algorithm for mechanical systems," Communications in Numerical Methods in Engineering, vol. 18, pp. 363-371, 2002.

[24] M. Kegl, M. M. Oblak, "Optimization of mechanical systems: on non-linear first-order approximation with an additive convex term," Communications in Numerical Methods in Engineering, vol. 13, pp. 13-20, 1997.

[25] D. J. Batstone, Y. Amerlinck, G. Ekam, R. Goel, P. Grau, B. Johnson, I. Kaya, J. P. Steyer, S. Tait, I. Takács, A. Vanrolleghem, C. J. Brouckaert, E. Volcke, "Towards a generalized physicochemical framework," Water Science & Technology , vol. 66(6), pp. 1147-1161, 2012.

[26] S. Jabłoński, M. Łukaszewicz, "Mathematical modelling of methanogenic reactor start-up: Importance of volatile fatty acids degrading population," Bioresource Technology, vol. 174, pp. 74-80, 2014.

[27] C. Kazadi Mbamba, D. J. Batstone, X. Flores-Alsina, "A generalised chemical precipitation modelling approach in wastewater treatment applied to calcite," Water Research, vol. 68, pp. 342-353, 2015.

[28] C. Kazadi Mbamba, S. Tait, X. Flores-Alsina, D. J. Batstone, "A systematic study of multiple minerals precipitation modelling in wastewater treatment," Water Research, vol. 85, pp. 359-370, 2015.

[29] A. Keshtkar, H. Ghaforian, G. Abolhamd, B. Meyssami, "Dynamic simulation of cyclic batch anaerobic digestion of cattle manure," Bioresource Technology, vol. 80, pp. 9-17., 2001.https://doi.org/10.1016/S0960-8524(01)00071-2

[30] V. Phogat, M. A. Skewes, J. Simunek, "Statistical assessment of a numerical model simulating agro hydrochemical processes in soil under drip fertigated mandarin tree," Irrigation & Drainage Systems Engineering, vol. 5, no.155, 2016.

The Social Assimilation of a New Architectural Proposal for Comfort

Esperanza García López, and Christopher Heard
Universidad Autónoma Metropolitana-Unidad Cuajimalpa
Departamento de Teoría y Procesos del Diseño, DCCD, Mexico City, Mexico
egarcialopez@dccd.mx

Abstract

The case history is of a community called "La Cañada" which is found in the municipality of Huixquilucan, Estado de México, Mexico. It is a village not far from the eastern edge of Mexico City and thus subject to strong social and transcultural pressures. A covering based on textile fibres was proposed for an experimental building in the aforementioned village. The design of the covering took into account relevant climatic factors such as temperature, humidity and rainfall. A double roof was proposed which would attenuate extreme low temperatures and at the same time be impervious. The whole proposal was made considering the villagers, especially their average income (to assure economic feasibility). Statistics for the population were consulted: age distribution, gender, religion etc. with a view to grounding the proposal in their local needs. However, during the development of the proposal, a question arose: are we really designing for this population or are we assuming that they will appropriate the suggested materials and will they identify with our objectives of lower energy use and greater sustainability? This was the objective of the research herein presented.

Initially a comparison was made between the official Environmental Education in Mexico and that with which the population has been imbued. Following this a traditional characterisation of the place and how it was changing in relation to what the inhabitants considered to be their 'ideal' in terms of spaces and forms, or what architectural elements occur in their dreams of the future. The work is based on the results of statistical analysis of questionnaires. Two types of questionnaires were developed which correspond to two different objectives. Focus groups were organized to allow a result close to reality to be obtained.

The first questionnaire was multiple choice which allowed a fast application. This was oriented to find out what was the ideal architecture that the subjects would want some day, and to map what for them was Environmental Educaction and if they had a commitment and awareness with regard to Ecology, Energy and Sustainability. This questionnaire was applied at the 10% level (52 questionnaires) in the same proportion as the distribution of age and gender that the National Institute for Statistics and Geography (INEGI) reports for the village (discarding children under ten years of age, considering that they don't yet have a structured reply to this type of questionnaire).

A second questionnaire consisted of questions that concerned the feeling and perception of an architecture of the type proposed and whether the subjects would adopt the proposed roof design. To achieve this couples and families were invited to stay in the prototype dwelling during two days. A total of five families accepted the invitation, amounting to thirteen villagers corresponding to 2.5% of the population. The second questionnaire was applied to these subjects.

The necessary data was obtained and analysed to reach a conclusion. The conclusion was surprising and saddening in that it was realized that Environmental Education and architectural proposals with energy efficiency were not part of their everyday language. In reality they didn't consider them a priority and some didn't know their meaning although they had heard of them mentioned "on the telly". For them their status relative to there peers in the community was more important than to live comfortably, including indoor temperatures and humidity. Upon enquiring if they would reproduce the proposal in their own homes they clearly responded that only if all the community knew and that they could then 'teach' it. The most notable conclusion reached from this research was that in addition to proposing solar housing that is energy efficient and sustainable, the duty of researchers is to communicate not only to professional peers but also bring this knowledge to the Mexican population in general so that they can appropriate these proposals such that they are assimilated into everyday customs and behaviours.

This research has taught that very little has been achieved in public awareness of energy use in villages, nor has work been carried out in a coordinated manner to accomplish it (except for a few communities where organized groups have worked in them). In addition to the techniques and technologies, social work is needed to promote environmental education and "solar culture" such that it becomes an inherent part of the majority of social groups.

IEECP'22, July 21-22, 2022, Oxford, United Kingdom

Assessing the Overall Feasibility of a Commercial Scale Food Irradiation Facility in Manila, Philippines

Chua, Justin
Student
International School Manila
Manila, Philippines
chuaju@ismanila.org

Abstract

Food irradiation is a novel, up and coming technology that preserves and extends the lifespan of food. The Philippines (more specifically, its capital city of Manila) is yet to capitalize on this effective technique, which has the potential to mitigate many of its pervasive issues such as hunger and food insecurity, unnecessary food wastage, and air pollution. Many of the Philippines' neighboring countries in the Asia-Pacific region (such as China, Japan and India) have had major success implementing food irradiation facilities. In fact, the Philippines already has a semi- commercial irradiation facility in Intramuros, Manila; however, it's relatively small and its impacts are negligible. Currently, there is a dearth of research on the feasibility of utilizing this technology on a larger scale in the Philippines, but the potential benefits a larger facility could bring to the country are too significant to ignore. Thus, this paper will conduct a cost-benefit analysis to assess the feasibility of the Philippines constructing a commercial scale gamma irradiation facility with a capacity of 1 millicurie (MCi)—comparable to those found in the aforementioned neighboring countries and 12 times larger than the current facility in Intramuros. A variation of Bateman et al.'s SEER framework ("Social, Economic and Environmental Assessment for Land Use Decision Making" model)—which evaluates a project from its environmental, economic, and social impacts—will be utilized to guide the cost- benefit analysis, in conjunction with the 5-point Likert assessment framework. Overall, the results deemed that a larger scale facility had a cost-benefit ratio of 1:5 and would be highly advantageous for the Philippines.

Keywords: cost-benefit analysis, economic, environmental, food irradiation, social

I. Introduction

Food irradiation is a versatile technique that helps solve various issues such as hunger and food waste through the preservation of food. The food irradiation process exposes products to a source of ionizing radiation for a predetermined time to sterilize the product. There are three types of radiation based processes approved for use on foods: Gamma rays, X-rays and Electron beams, however this paper will focus on the utilization of gamma rays. Gamma rays irradiate products by emitting sources of radiation from the elements Cobalt 60 or Cesium 137, these rays then kill disease-causing microorganisms in the food which increases the shelf life of perishable products. Other benefits of this process are, the reduction of the risk of food borne illnesses, prevention of invasive pests and delaying or even eliminating sprouting or ripening. In order to utilize this technique, a radiation facility must be built. Currently there are 180 large-scale gamma irradiation facilities in 42 countries which irradiate approximately 500,000 MT of food products worldwide each year, in particular, herbs and spices are among top irradiated foods [9]. However, in Manila and the Philippines, there are no commercial scale facilities. Other countries have had major success with this technology and even the semi-commercial facility in Manila has shown the potential of food irradiation. So this begs the question, would a commercial scale facility be beneficial to Manila? To start, the Philippines is filled with significant issues such as hunger, food waste and the production of methane emissions, which on the base level, food irradiation on a larger scale would tackle. It also creates the opportunity to make profit through more efficient exports and renting the facility. Thus, a cost benefit analysis will be conducted to determine a conclusion.

II. Method

In this paper, a cost-benefit analysis will be conducted to determine whether a commercial scale radiation facility would be beneficial in Manila and the Philippines. This will be done through the evaluation of a theoretical gamma ray facility which will have a capacity of 1 MCi—12 times larger than the existing facility in Intramuros. The cost-benefit analysis will be guided by Bateman et al.'s SEER framework [17]—which analyzes the social, economic and environmental impacts of the project—and various assessment schemes or indicators will be used within each individual category. For the environmental pillar, the benefits of reduced food waste, methane emissions, and the increase in the food's lifespan will be compared to the cost of energy consumption. For the economic pillar, the benefits in local and international revenue will be juxtaposed against the financial costs of conducting the radiation and costs to build the facility. Lastly, for the social pillar, the benefits of reduced hunger and increased job opportunities will be compared to the cost of exposing employees to radiation and the radiation hazards to the surrounding environment. From there, each individual indicator within the cost-benefit analysis will be evaluated using the Likert framework, which ranks the performances on a scale of 1 to 5, with 1 being the poorest score and 5 being the highest [10]. This will allow us to attain a cost-benefit ratio (benefits divided by cost). If the average ratio is greater than 1, the benefits outweigh the costs and the facility can be deemed overall beneficial.

IEECP'22, July 21-22, 2022, Oxford, United Kingdom

III. Results

A. Environmental Impacts

I. Benefits

The first environmental benefit is the reduction of food waste. Using food irradiation will prolong the lifespan of food, reducing food waste. According to World Wildlife Fund-Philippines, an estimated 439,350 tons of food scraps

in Metro Manila alone are thrown in the garbage annually [13]. Using data from the Intramuros facility (Cobalt-60 Multipurpose Irradiation Facility or MIF) on tons irradiated per year, an exponential trend of $y = 3.76 \times 10^{-34} e^{0.0413x}$. Using this equation, the tons of food this plant will irradiate in 2020 is estimated to be 641 tons. Since the capacity of the theoretical facility is 12 times larger than MIF, the tons irradiated annually at the 1 MCi facility would be 7,719 tons. Equation 1 will calculate the food waste reduction index (F.W.R.I.), where 0 represents an ineffective project and 1 denotes a perfectly effective project.

$$\textit{Equation 1: } F.W.R.I = \frac{food\ waste\ saved\ from\ project}{food\ waste\ of\ Metro\ Manila} = \frac{7{,}719}{439{,}350} = 0.01756913622 \approx 0.018$$

The value of this index may seem low and insufficient, but considering other food waste reduction methods into consideration, reducing 1.8% of the entire food waste of Metro Manila with just one factory is remarkable. Furthermore, the increased efficiency that comes with larger scale facilities that the Philippines is yet to experience suggests high potential in this new technology. Thus, it is determined that the environmental benefit of the reduction of food waste scores a **4**.

The reduction of food waste has a domino effect as it also reduces methane emissions from landfills, another major problem in the Philippines. Currently, Metro Manila has three major landfills that cumulatively produce 11.71 million tons of methane gas annually due to food decomposition [12]. According to Biocycle, 1 dry ton of food waste produces approximately 65 kg of methane [5]. Thus, the 1 MCi facility would decrease methane emissions from food waste by 1,501,735 tons. To put this into perspective, Equation 2 will calculate the methane emissions reduction index (M.E.R.I.), where 0 represents an ineffective project and 1 denotes a perfectly effective project.

$$\textit{Equation 2: } M.E.R.I = \frac{methane\ emissions\ saved\ from\ project}{methane\ emissions\ from\ Metro\ Manila} = \frac{1501735}{11710000} = 0.1283534188 \approx 0.13$$

13% of Metro Manila's methane emissions is an extremely significant reduction considering this positive impact is just from a single irradiation facility alone. Furthermore, this value is even more impressive due to the fact that the irradiation facility's primary purpose is to prolong the lifespan of food and not reduce methane emissions. This is a huge added environmental benefit, hence it is determined that the environmental benefit of reduction of methane emissions is a **5** on the Likert scale.

The third benefit is the increase in the food's lifespan without changing its nutrients through the irradiation. The United States' credible Food and Drug Administration has spent more than 30 years assessing the safety of irradiated food and has concluded the process to be safe and beneficial [4]. To illustrate, Table 1 displays the impact of irradiation for various foods.

Table 1: Impact of Irradiation on Various Food Products

Food Products	Impact	Results
Garlic, onion, potatoes, yams	Prevents sprouts	Reduces food spoilage
Pork	Kills trichinella spiralis worms	Reduces food borne diseases
Fruits and vegetables	Kills insects Delays ripening	Increases food safety Prolongs shelf life
Meat, poultry, fish, seafood	Inactives pathogens and microorganisms	Prolongs shelf life, and preserves food for export

Moreover, irradiating fruits benefits the exporting process as it allows the fruit to be exported without quarantine processing. The two top exported fruits of the Philippines are mangoes and bananas, and according to an experiment done by Bangladeshi scientists, when a banana was treated with <1 kGy, the banana's shelf life was extended by 20 days [19]. The International Atomic Energy Agency also released an article stating, "low dose gamma irradiation of mangoes in the dose range 10 to 200 krad alone or in combination with other physical and chemical treatments (i.e. hot water dipping and skin coating with 9 percent emulsion of acetylated monoglyceride) show that physiological, pathological and entomological factors can be controlled to extend the shelf-life of mangoes by one to two weeks." [18] Food irradiation may not be the cheapest option to extend a product's lifespan, however its ability to not interfere with the product's nutritional value is highly beneficial. Alternative methods to increase the lifespan of food, such as canning, bottling and pasteurization, either chemically alter the nutrients or don't fully eliminate all microorganisms. Thus, it is determined that the environmental benefit of increasing the food's lifespan without changing any nutrients is ranked a **3**.

To encapsulate, Equation 3 will calculate the average score of the environmental benefits for the cost-benefit ratio.

$$\textit{Equation 3: } Average\ Score\ of\ Environmental\ Benefits = \frac{Benefit\ 1\ Rating\ +\ Benefit\ 2\ Rating\ldots}{Number\ of\ Benefits} = \frac{4\ +\ 5\ +\ 3}{3} = 4$$

This average rating of 4 is very high.

II. Costs

The first cost is energy consumption, the use of a gamma ray facility requires a lot of energy. A 60-kW Cobalt-60 facility operating for 6,000 hours in one year uses 2.7 × 1012 joules/year [7]. Using this as a reference point, the 1 MCi facility can be estimated to need 4.5 × 1013 joules/year, which is a good amount of energy. However, with every method comes energy usage in one way or another so this cost can be deemed insignificant. On top of this, the benefits brought at the cost of this energy for a facility makes this a good investment. Thus, it is determined that the environmental cost of energy consumption is a **2**.

$$Equation\ 4: Average\ Score\ of\ Environmental\ Costs = \frac{Cost\ 1\ Rating\ +\ Cost\ 2\ Rating\ldots}{Number\ of\ Costs} = \frac{2}{1} = 2$$

This average rating is 2.

III. Cost-Benefit Ratio

Using our determined ratings, we can deduce a cost-benefit ratio for the environmental pillar using Equation 5.

$$Equation\ 5: Environmental\ Benefit\ Cost\ Ratio = \frac{Average\ Rating\ of\ Environmental\ Benefits}{Average\ Rating\ of\ Environmental\ Costs} = \frac{4}{2} = 2$$

To interpret this value, Table 2 can be consulted.

Table 2: Interpretation of Cost-Benefit Ratio

Benefit/Cost Ratio	Interpretation
> 1	Beneficial
= 1	Neutral
< 1	Costly

Thus, with a cost to benefit ratio significantly greater than 1, the environmental impacts of the 1 MCi irradiation facility have a net positive effect and would be overall beneficial to the country.

B. Economic Impacts

Recognizing the lack of an economic framework that fully encompasses the unique components of food security infrastructure and technology, we have developed a new system. We identified that the major economic factors that contribute to projects such as these are generally 1) profits from the local market, 2) profits from the international export market, 3) costs of technology, 4) cost incurred from the facility. As these are the four major economic factors regarding these projects, we can bring these together to determine the net economic impact.

I. Benefits

The first economic benefit is the local revenue generated from using the facility. In 2015, the Philippines Nuclear Research Institute (PNRI) produced revenues of ₱7 million from the 500 tons of food irradiated at MIF. Using this rate, the local revenue of the 1 MCi facility is estimated to be ₱108,006,000. To standardize this statistic, the 63.3 MW Calatagan Solar Farm (one of the Philippines government's most successful projects) will be used as a benchmark. Equation 6 will calculate the percentage yield of the annual local revenue for the irradiation facility in comparison to the Calatagan Solar Farm.

$$Equation\ 6: Percentage\ Yield = \frac{local\ revenue\ of\ the\ 1\ MCi\ irradiation\ facility}{local\ revenue\ of\ the\ Calatagan\ Solar\ Farm} = \frac{108066000}{101077440} =$$

$$1.06914065097 \approx 107\%$$

A 107% yield is phenomenal. With the value being greater than 100% , it indicates the estimated local revenue of the facility is greater than the income of a very successful government project. Additionally, the irradiation facility project is much cheaper to execute than the solar farm, costing ₱249.4 million and ₱5.7 billion respectively [3], a difference of ₱5,450,578,300. This data demonstrates the potential of an irradiation facility, it can cost 1/25 less than a solar farm and still generate more revenue. The MIF provided services for 80 clients, with a bigger facility there will be more room for clients or significantly larger orders. Therefore, it is determined that the economic benefit of local revenue generated receives a **5** on the Likert scale.

Not only will the irradiation facility generate local revenue, it can also produce International revenue through exports. The Philippines Department of Agriculture had plans to develop a commercial scale irradiation facility to serve the purpose to irradiate the country's top food product exports like mango, pineapple, and banana, however these plans haven't followed through yet. Food irradiation specifically of fruit can be beneficial for the exporting process as it speeds up the quarantining process of the products as it arrives in the US or other country. According to Oxford Business Group, in 2013, the Philippines exported 4.42 billion kg of fruits and vegetables worth a combined total of 1.97 billion USD or ₱98.7 billion [14]. Using this data, if 20% of the tons irradiated at the facility (1543.8 tons) are dedicated for exports, the estimated gross profit of the exported goods would be ₱34,314,582. In order to determine the net profit of the exported goods, the cost of the irradiation must be calculated, which can be quantified through Table 3.

Table 3: Dosage and Cost of Irradiation on Various Food Products

Food Products	Dosage (kGy)	Cost of Irradiation (PHP/kg)
Meat	3	25
Seafood	3	25
Rice	1	10
Fruits (Banana, Pineapple & Mango)	1	10
Vegetables (Onions, Garlic & Potatoes)	0.1	7

If the 20% of tons irradiated is separated into 15% fruit and 5% vegetables, the cost of irradiation would be ₱14,280,150. Therefore, the net profit of exported goods from the irradiation facility would be ₱20,212,987. Furthermore, the goods exported are often sold at a price higher than the expected value. For example, in 2018, the Philippines banana exports for all purchasing countries surged to 1.5 billion USD from 1.4 billion USD [16]. Thus, it is determined that the economic benefit of international revenue scores a **4** on the Likert scale.

To summarize, Equation 7 will calculate the average score of the economic benefits for the cost-benefit ratio.

$$Equation\ 7: Average\ Score\ of\ Economic\ Benefits = \frac{Benefit\ 1\ Rating + Benefit\ 2\ Rating\ \ldots}{Number\ of\ Benefits} = \frac{5\ +\ 4}{2} = 4.5$$

This average rating of 4.5 is extremely high.

II. Costs

The first economic cost is the cost of the technology. In order to irradiate food products, radiation must be utilized, which can be quite expensive. Using Table 3 and the estimate that fruits,

vegetables, meat and seafood, and rice make up 70%, 20%, 5%, 5% of the food irradiated respectively, the total dosage needed to irradiate all the food for one year would be 7,101,400 kGy. The cost of this radiation would be ₱78,348,000, a hefty amount of money. Currently, there is no way to lower this price without changing the dosage of radiation, however modifying the measurements would affect the irradiation process and may take away the benefits of this technology. The only way to justify this expense is through the benefits brought by this process or that every alternative method would still cost money to implement. In the end, despite all the benefits, it cannot be denied that food irradiation is on the more expensive end of food preserving techniques costing millions. Thus, it is determined that the economic cost of the price of resources earns a **4** out of 5.

In order to even perform food irradiation, a gamma ray facility must be built. According to the University of Wisconsin, a typical commercial processing plant, specifically a gamma irradiation facility involves a capex of around 5 million USD as per estimates [11]. Converting that to PHP would make the cost to build a 1 MCi facility ₱249,421,700, a large capital investment. This may sound like a lot of money, however this is within the price range of plants for other technologies. For example, a moderately-sized, ultra-high temperature plant for sterilizing liquids costs about 2 million USD or ₱100.4 million [11]. Another example is a small vapor-heat treatment plant for disinfecting fruits, which costs about 1 million USD or ₱50.2 million [11]. Besides this, the ₱249,421,700 would be a onetime expense, once the facility is built, it just needs to be maintained which would not cost as much. Also as shown in the economic benefits section, the facility can earn back the invested money very quickly after a few years through its local and international revenue. Thus, it is determined that the economic cost of building a gamma irradiation facility is a 3 on the Likert scale.

Equation 8 will calculate the average score of the economic costs for the cost-benefit ratio.

$$\textit{Equation } 8\text{: } \textit{Average Score of Economic Costs} = \frac{\textit{Cost 1 Rating} + \textit{Cost 2 Rating}\ldots}{\textit{Number of Costs}} = \frac{4 + 3}{2} = 3.5$$

III. Cost-Benefit Ratio

Using our determined ratings, we can deduce a cost-benefit ratio for the economic pillar using Equation 9 and interpret the results using Table 2.

$$\textit{Equation } 9\text{: } \textit{Economic Benefit Cost Ratio} = \frac{\textit{Average Rating of Economic Benefits}}{\textit{Average Rating of Economic Costs}} = \frac{4.5}{3.5} = 1.285714\ldots \approx 1.3$$

With a cost to benefit ratio greater than 1, the economic impacts of the 1 MCi irradiation facility have a net positive effect on the country's economy.

C. Social Impacts

I. Benefits

The first social benefit is the reduction of hunger. With food irradiation, the lifespan of food increases, reducing waste since people won't need to buy as much food. This means that there is more food for the hungry to eat. In 2019 the Food and Agriculture Organization (FAO) revealed that 690 million people went hungry that year [2]. Using the average weight of an Filipino adult, it can be estimated that one Filipino eats about 1290 pounds of food or 0.585 metric tons [1]. This means that the 1 MCi facility has the potential to save food of an amount capable of feeding 13,191 people. This is not the largest decrease however this is a passive benefit, thus any difference is positive. Hence, it is determined that the social benefit of reducing hunger is a 3.

The second social benefit is creating job opportunities. We can take a conservative estimate that about 70 job opportunities are created from this facility. Not just inside the facility but also on the outside such as drivers and farmers. As society moves towards a more digital lifestyle, it is important to still have physical job opportunities that allow for people to make money and create a living which won't get replaced by AI. The only downside to this benefit is that 70 jobs isn't very many job opportunities for the amount of people. Thus, it is determined that the social benefit of creating job opportunities is a 2.

Equation 10 calculates the average score for the social benefits.

$$\textit{Equation } 10\text{: } \textit{Average Score of Social Benefits} = \frac{\textit{Benefit 1 Rating} + \textit{Benefit 2 Rating}\ldots}{\textit{Number of Benefits}} = \frac{3 + 2}{2} = 2.5$$

II. Costs

The first social cost is the negative impacts of prolonged exposure to radiation. A lot of risks may occur while working with radiation which may be a danger for workers in the facility. At very high radiation exposures, death will occur within several months or less. At moderate levels, radiation exposure increases the chance that an individual will develop cancer [15]. At low levels, the cancer risk decreases but still is a concern [15]. On top of this, gamma rays have extremely high penetrating power which can pass completely through the human body [8]. If it does pass through a human, it may damage tissue and DNA [8]. In the end, these costs all come with working with radiation, and if the facility is made correctly and run properly, this shouldn't be much of an issue. Thus, it is determined that the social cost of prolonged exposure to radiation is a 2.

Additionally, another social cost is the hazard of radiation to a gamma ray facility's surrounding environment. If a facility is poorly constructed, it could lead to devastating consequences to its surrounding areas. When working with a gamma ray facility, there is always the hazard of radiation, if the facility is made poorly, it could lead to devastating consequences on the area surrounding it. According to an employee from Symec Engineers (India), an irradiation plant manufacturer, "While constructing and maintaining an irradiation facility is expensive in itself, but what is harder is to ensure that the surrounding environment is free from any kind of contamination and this can get costly as well." [6] Ensuring the gamma ray facility is built well should be a priority. Manila is packed with 368 people per km2, a fair amount living in clumped slums. So one mistake handling the radiation would put millions of lives at risk. But as long as the facility is built properly and maintained, this shouldn't be the biggest concern. Many other projects pursued that use some form of radiation have been done before and there have been close to 0 freak accidents with these facilities. Theoretically, if there were to be a tragedy and an area in Manila does get contaminated by radiation then it can be expected that many people may get infected, this scenario a major factor in the scoring for this cost. But to combat this issue, the facility can either be built far away from civilization or living areas. Again, as long as the facility is built correctly and maintained properly, this cost can be disregarded. Thus, it is determined that the environmental cost of working with radiation is a 2.

Equation 11 calculates the average score for the social costs.

$$\textit{Equation 11: Average Score of Social Costs} = \frac{\textit{Cost 1 Rating} + \textit{Cost 2 Rating}\ldots}{\textit{Number of Costs}} = \frac{2 + 2}{2} = 2$$

III. Cost-Benefit Ratio

Using our determined ratings, we can deduce a cost-benefit ratio for the social pillar using Equation 12 and interpret the results using Table 2.

$$\textit{Equation 12: Social Benefit Cost Ratio} = \frac{\textit{Average Rating of Social Benefits}}{\textit{Average Rating of Social Costs}} = \frac{2.5}{2} = 1.25$$

With a cost to benefit ratio greater than 1, the social impacts of the 1 MCi irradiation facility have a net positive social effect.

IV. Conclusion

$$\textit{Equation 13: Benefit Cost Ratio} = \frac{\textit{Environmental Benefit Cost Ratio} + \textit{Economic Benefit Cost Ratio} + \textit{Social Benefit Cost Ratio}}{\textit{Number of Pillars}} = \frac{2 + 1.3 + 1.25}{3} = 1.51666666667 \approx 1.5$$

Using Table 2 to intercept the results, the benefit cost ratio of 1.5 displays how a commercial scale irradiation facility will be beneficial to the Philippines. For this project, improvements can still be made on the economic and social pillars, something which can be changed with the size of the facility and time. The earlier a facility is built, the quicker it can earn the invested money back. Ultimately, this research has proven that food irradiation would be an overall success and a worthwhile endeavor to invest in. The lessons learned from this project should be considered when planning future food irradiation plants.

V. References

1. Aubrey, Allison. "The Average American Ate (Literally) a Ton This Year." *NPR*, NPR, 31 Dec. 2011, https://www.npr.org/sections/thesalt/2011/12/31/144478009/the-average-american-ate-literally-a-ton-this-year.
2. BusinessMirror. "Millions of Filipinos Are Going Hungry." *BusinessMirror*, 20 Apr. 2021, https://businessmirror.com.ph/2021/04/21/millions-of-filipinos-are-going-hungry/.
3. "Calatagan Solar Farm." *Wikipedia*, Wikimedia Foundation, 14 May 2020, https://en.wikipedia.org/wiki/Calatagan_Solar_Farm.
4. Center for Food Safety and Applied Nutrition. "Food Irradiation: What You Need to Know." *U.S. Food and Drug Administration*, FDA, https://www.fda.gov/food/buy-store-serve-safe-food/food-irradiation-what-you-need-know.
5. "Connection: Climate Calculations." *BioCycle*, 19 June 2013, https://www.biocycle.net/connection-climate-calculations/#:~:text=For%20this%20approximation%2C%20we%20can,kg%20of%20methane%20(CH4).
6. dharm_anki. "Food Irradiation Advantages and Disadvantages." *Symec Engineers*, 28 Sept. 2019, https://www.symecengineers.com/food-irradiation-advantages-and-disadvantages/.
7. ENERGY AND FOOD IRRADIATION. https://apps.dtic.mil/sti/pdfs/ADA058502.pdf
8. *EPA*, Environmental Protection Agency, https://www.epa.gov/radiation/radiation-basics.
9. *Global Status and Commercial Applications of Food Irradiation*. http://www.foodirradiation.org/Global%20Status%20of%20Food%20irradiation.pdf.
10. Mcleod], [Saul. "[Likert Scale Definition, Examples and Analysis]." *Simply Psychology*, 1 Jan. 1970, https://www.simplypsychology.org/likert-scale.html.
11. *A Mobile Food Irradiation Facility - Trace.tennessee.edu*. https://trace.tennessee.edu/cgi/viewcontent.cgi?article=2264&context=utk_chanhonoproj.
12. Neil. "A Solution to Metro Manila's Garbage Problem." *BusinessWorld Online*, 30 June 2019, https://www.bworldonline.com/a-solution-to-metro-manilas-garbage-problem/.
13. Neil. "Collective Action to Combat Food Waste." *BusinessWorld Online*, 25 Jan. 2021, https://www.bworldonline.com/collective-action-to-combat-food-waste/.
14. "Production Volumes and Exports of Philippine Fruit and Vegetables Continue to Rise." *Oxford Business Group*, 8 Sept. 2015, https://oxfordbusinessgroup.com/analysis/fruitful-business-production-volumes-and-exports-fruit-and-vegetables-continue-rise.
15. *Radiation Damage and Its Study*, https://www2.lbl.gov/abc/wallchart/chapters/15/1.html.
16. Santiago, Danny. "Philippines Bananas Exports by Country." *Philippines Around the World*, 13 Apr. 2021, https://www.philippinesaroundtheworld.com/philippines-bananas-exports-by-country/.
17. "Social, Economic and Environmental Research Project." *Social, Economic and Environmental Research Project | Land, Environment, Economics and Policy Institute | University of Exeter*, https://www.exeter.ac.uk/research/leep/research/projects/socialeconomic/.
18. Thomas, Paul, and S.R. Padwal Desai. "Improvement of Shelf-Life and Quality of Mangoes by Gamma Irradiation." *Indian Food Packer*, 1 Jan. 1976, https://inis.iaea.org/search/search.aspx?orig_q=RN%3A8347055.
19. Zaman, W, et al. "Shelf Life Extension of Banana (*Musa Sapientum*) by Gamma Radiation." *Journal of Bio-Science*, https://www.banglajol.info/index.php/JBS/article/view/2202.

Black-out diesel engine operation modelling for the CHPP start-up

Dušan Strušnik
Energetika Ljubljana d.o.o.,
TE-TOL Unit, Toplarniška ulica 19
SI-1000 Ljubljana, Slovenia
dusan.strusnik@gmail.com
https://orcid.org/0000-0003-2531-3081

Marko Agrež
Energetika Ljubljana d.o.o.,
TE-TOL Unit, Toplarniška ulica 19
SI-1000 Ljubljana, Slovenia
marko.agrez@energetika.si

Jurij Avsec
University of Maribor
Faculty of Energy Technology
Hočevarjev trg 1
SI-8270 Krško, Slovenia
urij.avsec@um.si

Abstract

Modelling power plants using real process data is crucial in determining the cost-effectiveness and flexibility of systems. The quality of the elaborated model is determined with the validation of the model, which can also give results for the operating regimes of the plant, which are not often used in practice. In this way, also the operation and responsiveness of power plants outside the range of planned operation are determined. The model simulates the operation of a diesel engine (DE) required to start a combined heat & power plant (CHPP) from a black-out or loss of the electrical power network supply. The model is made on the basis of data provided by the manufacturer and the measured DE data. The results of the model enable detailed insight into the characteristics of the DE behaviour at different operating regimes. The economic and ecological rationale ranges of operation of the DE can be determined from the characteristics of operation. The results of the model show that the DE operates with a 41.72% average efficiency, consumes from 0.114 kg/s of diesel fuel for its operation and up to 3.68 kg/s of air, the air ratio ranges from 2.2 to 2.5. DE develops shaft power up to 2170 kW.

Keywords: Air-Fuel Equivalence Ratio, Black-Out, Diesel Engine, Thermal Efficiency, Shaft Power

I. INTRODUCTION

Optimization of thermal power systems and ecological awareness is a key development strategy of larger thermal power facilities. Despite the fact that the production of electricity with low-carbon or non-carbon technology is on the rise, it will not be possible to completely avoid the production of electricity by burning fossil fuels. One of the most efficient methods to convert fossil resources or chemically bound energy of gaseous and liquid fuels into electricity is the use of gas turbines.

IEECP'22, July 21-22, 2022, Oxford, United Kingdom

The production of electricity using a gas turbine and an electric generator can be ensured in the open cycle [1], where hot flue gases after expansion are released through the chimney directly into the atmosphere. The disadvantage of this process is the relatively low efficiency of the plant, which in practice ranges from 30% to 40%. If we want to improve the efficiency, the open cycle is upgraded with a boiler, heat recovery steam generator [2] and a steam turbine that takes the generated steam from the said boiler and drives its electric generator. The really useful efficiencies achieved in this process range from 50% to 60%. Such a process is called a combined cycle gas turbine [3]. If we have the option of heat extraction, the total energy efficiency of the plant can exceed 85%. The operation of such an energy system is also called combined heat & power [4].

In addition to achieving high energy efficiency, the combined cycle gas turbine process is also characterized by its universality. Simultaneously with the production of heat and electricity, both generators powered by gas and steam turbines can be included in the system of balancing the production and consumption of electricity. The said balancing is performed by the operators who operate the transmission high-voltage system. The entire Slovenian electricity system is included in the European interconnection system or the European Network of Transmission System Operators for Electricity [5]. Individual networks, connected to the interconnection by means of the interaction of synchronous generators and system regulations of electric frequency, ensure the quality of operation of power systems. This means that the power hubs, where the dividing line between the transmission and distribution of electricity begins, are constantly supplied. In practice, however, this balancing means that electricity must be produced practically at the same time as the random consumer connects to the power supply.

The combined cycle gas turbine installation is very efficient in providing regulation or ancillary services for the needs of working or operation of the electricity transmission system. Its fast response and gradient of increasing the electric power of the generator connected to the gas turbine, allows a very fast adjustment of electricity production to its consumption. The system is designed in such a way that it also enables the quick start of cold units. The advantage of fast start-up of a combined cycle gas turbine is especially pronounced when starting from a voltage-free state of the power system, since the combined cycle gas turbine is able to ensure electricity production in a very short time and thus to maintain the frequency of the power grid in a smaller island, which expands by adding the resources.

In the event of a power system breakdown resulting in a black-out, the combined cycle gas turbine needs an energy source to start the auxiliary devices needed to start the system. Most often, these auxiliary devices are internal combustion engines that drive a starting electric generator. In practice, DEs have proven to be reliable resources. The task of the DE is therefore to provide, in the case of black-out, the electricity needed to start the combined cycle gas turbine.

The paper is designed in such a way that the characteristic data and components of the DE are presented first. Then the presentation of the simulation model of the DE operation follows, followed by the presentation of the results of the simulation model. Finally, a summary with the most important findings is presented.

II. DA CHARACTERISTICS AND COMPONENTS

The DE for CHPP start-up at black-out is turbocharged, aftercooled and four-stroke engine and operates with a constant revolution frequency of 1500 min-1, which is required to drive the generator. The basic characteristic data of the DE are shown in Table 1.

Table 1. The basic characteristic data of DE, industrial engine with constant speed [5]

Manufacturer	Mitsubishi
Model	S16R2-PTAW
Engine type	four-stroke, diesel
Cylinder configuration	16 / 60 °V
Maximum output power	2167 kW
Engine speed	1500 min^{-1}
Aspiration and cooling	Turbocharged and aftercooled
Total displacement	79.90 litters
Bore and stroke	170 mm x 220 mm
Compression ratio	14:1
Fuel consumption at full load	0.114 kg/s
Cooling system	Water-cooled
Combustion system	Direct injection
Fuel injection system	Pump – line - nozzle

Figures 1 and 2 were taken during the first phase of the DE tests. Figure 1 shows the right side of the body of 60° V16 DE. Each side of DE therefore has 8 cylinders.

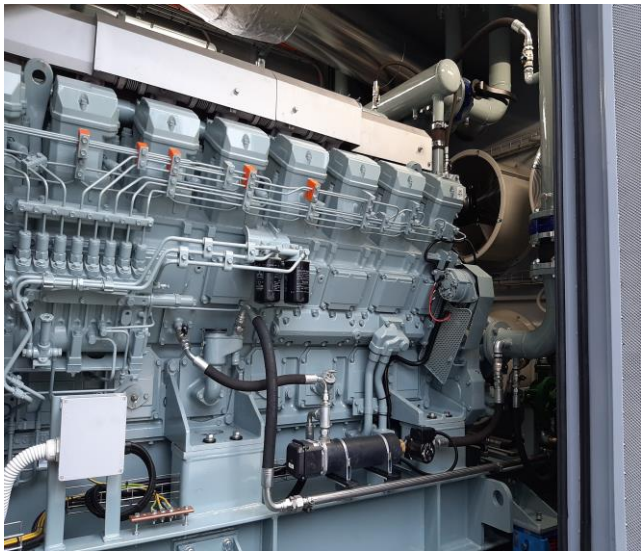

Figure 1. The right side of the body of 60° V16 DE.

Figure 2 shows the first trial run. The left DE is operating and the right DE is in the phase of the first start-up trial run.

Figure 2. DE first start-up trial run.

Figure 3 shows the DE view from the left side with the basic components marked. Table 2 presents the basic components of DE from Figure 2.

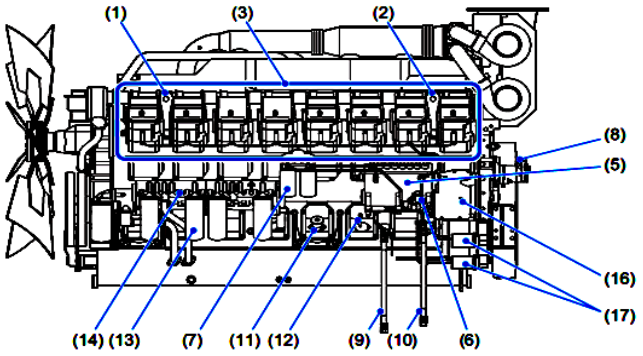

Figure 3. View of the DE from the left side with components [7].

Table 2. The basic characteristic data of the DE, industrial engine with constant speed [7]

	No.	Name		No.	Name
Engine body	(1)	Front hanger	Lubrication system	(11)	Oil filler
	(2)	Rear hanger		(12)	Oil level gauge
	(3)	Cylinder head		(13)	Oil filter
	(4)	Manual turning gear		(14)	Oil cooler
Fuel system	(5)	Fuel injection pump	Cooling system	(15)	Coolant inlet
	(6)	Priming pump		(16)	Coolant drain cock
	(7)	Fuel filter	Starting system	(17)	Starter
	(8)	Fuel control link	Electrical system	(18)	Alternator
	(9)	Fuel inlet			
	(11)	Fuel return port			

The left side of Figure 4 shows the view of the DE from the front with the basic components marked. The right of Figure 4 shows the view of the DE from the back, where the basic components are also marked, and Table 3 presents the basic components of the DE from Figure 3.

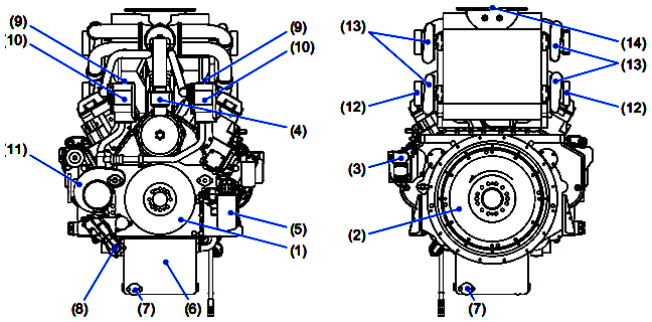

Figure 4. DE front view and DE rear view [7].

Table 3. The basic characteristic data of the DE, industrial engine with constant speed [7]

	No.	Name		No.	Name
Engine body	(1)	Damper	Cooling system	(9)	Coolant outlet
	(2)	Flywheel		(10)	Thermostat case
Fuel system	(3)	Governor actuator		(11)	Water pump
Lubrication system	(4)	Breather	Inlet and exhaust systems	(12)	Intake port
	(5)	Bypass oil filter		(13)	Turbocharger
	(6)	Oil pan		(14)	Exhaust outlet
	(7)	Engine oil drain port			
	(8)	Oil pump			

The remaining necessary DE data required for the production of a quality model are shown in Table 4.

Table 4. The remaining DE data, industrial engine with constant speed [7]

ENGINE	
Number of cylinders	16
Bore	170 mm
Stroke	220 mm
Displacement	79.9 litres
Brake power without fan	2209 kW
Brake mean effective pressure	21.1 bar
Mean piston speed	11 m/s
Maximum regenerative power	152 kW
PERFORMANCE DATA	
Steady state speed stability band at any constant load - electric governor	± 0.25 %
Maximum overspeed capacity	1750 rpm
Moment of inertia of rotating components	33.22 kg*m^2
Cyclic speed variation with flywheel at 1500 rpm	1/182
AIR INLET SYSTEM	
Maximum Intake Air Restriction	0.064 bar
EXHAUST SYSTEM	
Maximum Allowable Back Pressure	0.059 bar
LUBRICATION SYSTEM	
Oil Pressure	5 bar
Maximum oil temperature	105 °C
Oil capacity of standard pan	240 litres
COOLING SYSTEM	
Coolant capacity of jacket	157 litres
Coolant capacity of air cooler	33 litres
Maximum external friction head at engine outlet	0.34 bar
Standard thermostat (modulating) range of jacket	71 °C ~ 85 °C
Standard thermostat (modulating) range of air cooler	42 °C ~ 55 °C
Maximum coolant temperature at engine inlet	75 °C
Maximum coolant temperature at engine outlet	83 °C
Minimum coolant expansion space	10 %
Maximum coolant temperature at air cooler inlet	45 °C
FUEL SYSTEM	
Fuel Injector	Mitsubishi PS8 Type × 2
Maximum suction head of feed pump	0.1 bar
Maximum static head of return & leak pipe	0.2 bar
STARTING SYSTEM	
Battery charging alternator	24 V, 35 Ah
Starting motor capacity	24 V, 7.5x2 kW

III. DE OPERATE SIMULATION MODEL

The DE operate simulation model consists of three units: the DE input data unit, the DE calculation unit and the results report unit. A schematic representation of the architecture of the simulation model is shown in Figure 5.

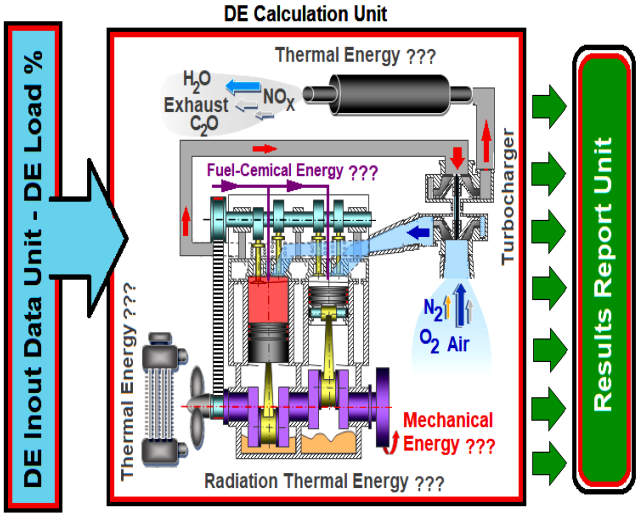

Figure 5. Schematic representation of the simulation model.

Using input data of the DE loads, the DE calculation unit calculates: the diesel fuel consumption, the combustion air volume, the air ratio, the exhaust gas quantity, the cooling water quantity, etc. In addition to the stated values, the DE calculation unit also calculates the following values: the mechanical power of the engine shaft, the thermal power of exhaust gases, the thermal power of cooling water, the radiated heat released into the environment and the thermal power of the oil cooler. The DE calculation unit calculates the stated values using the thermodynamic equations and equations that were generated with the help of realistically

measured data of the working of DE in dependence on load. The mass flow of diesel fuel in dependence on the load is calculated by the DE calculation unit using equation [8]:

$$\dot{m}_{fuel} = \frac{m \cdot N_{cysm} \cdot n_e}{60 \cdot N_{nst}} \quad (1)$$

where $\dot{m}_{fuel}$ is the mass flow of diesel fuel for the working of DE, m is the cycle fuel injection quantity, N_{cysm} is the number of cylinders, n_e is the engine speed, N_{nst} and is the number of engine strokes. The mass flow of exhaust gases in dependence on the load is calculated by the DE calculation unit using a polynomial equation of the second degree, which was generated using the measured data:

$$\dot{m}_{ex} = \frac{(0.01522 \cdot DE_{load}{}^2 + 2.545 \cdot DE_{load} + 91.72) \cdot 0.457}{60} \quad (2)$$

where $\dot{m}_{ex}$ is the mass flow of exhaust gases from the DE and DE_{load} is the load of the DE. The mass flow of air required for the working of the DE is the difference between the mass flow of exhaust gases and the mass flow of diesel fuel and is calculated by the DE calculation unit using equation [9]:

$$\dot{m}_{air} = \dot{m}_{ex} - \dot{m}_{fuel} \quad (3)$$

where $\dot{m}_{air}$ is the mass flow of air for the working of the DE. However, now that the actual mass flows of air and fuels required for the working of the DE are known, the calculation unit can calculate the air-fuel equivalence ratio (ʎ) [10]:

$$\lambda = \frac{AFR_{actual}}{AFR_{stoich}} = \frac{AFR_{actual}}{14.7} \quad (4)$$

where ʎ is the air-fuel equivalence ratio, AFR_{actual} is the air-fuel ratio at actual conditions and AFR_{stoich} is the air-fuel ratio at stoichiometry conditions. The power of the shaft developed by the DE is calculated by the calculation unit using the measured value of the electric power of the generator and using the efficiency of the generator [11]:

$$P_{shaft} = P_{gen} \cdot \eta_{gen} \quad (5)$$

where P_{shaft} is the power of the shaft of DE and η_{gen} is the efficiency of the generator of DE. The thermal power of the exhaust gases is calculated by the DE calculation unit using equation [12]:

$$P_{ex} = \dot{m}_{ex} \cdot c_{p-ex} \cdot T_{ex} \quad (6)$$

where P_{ex} is the thermal power of the exhaust gases from the DE, c_{p-ex} is the specific heat of the exhaust gases and T_{ex} is the exhaust gas temperature obtained from the measurements made. In a similar way, with the help of the measured data, the calculation unit also calculates the thermal power discharged from the DE by means of cooling water and oil cooler [13]:

$$P_{cool} = \dot{m}_{cool} \cdot c_{p-cool} \cdot (T_{cool-out} - T_{cool-in}) \quad (7)$$

$$P_{oil} = \dot{m}_{oil} \cdot c_{p-oil} \cdot (T_{oil-out} - T_{oil-in}) \quad (8)$$

where P_{cool} is the thermal power of cooling water discharged from the DE, $\dot{m}_{cool}$ is measured mass flow of cooling water trough the DE, c_{p-cool} is the specific heat of the cooling water, $T_{cool-out}$ is the measured temperature of cooling water from the DE, $T_{cool-in}$ is the measured temperature of cooling water into the DE, P_{oil} is the thermal power of oil cooler discharged from the DE, $\dot{m}_{oil}$ is the mass flow of oil trough the DE, $T_{oil-out}$ is the temperature of oil from the DE and T_{oil-in} is the temperature of oil into DE. The heat released from the DE into the environment in the form of radiation is calculated by the calculation unit using the polynomial equation of the second degree generated by the data provided by the manufacturer of DE [6]:

$$P_{rad} = 0.002888 \cdot DE_{load}{}^2 + 1.192 \cdot DE_{load} + 17.03 \quad (9)$$

where P_{rad} is the radiative heat of the DE. The efficiency of the DE is calculated by the calculation unit using the equation [14]:

$$\eta = \frac{\sum P_{use}}{P_{fuel}} \cdot 100\% = \frac{\sum P_{use}}{\dot{m}_{fuel} \cdot se_{fuel} \cdot 3600} \cdot 100\% \quad (10)$$

where η is the efficiency of the DE, $\sum P_{use}$ is the sum of all the usefully consumed power of the DE, P_{fuel} is the power supplied by the fuel and se_{fuel} is the specific energy of diesel fuel.

IV. SIMULATION MODEL RESULTS

The results of the model are shown at a constant revolution frequency of the DE, which is 1500 min^{-1}, since the DE is used to drive a generator that always operates at a constant rpm. The results of the model are designed so that the flow characteristics of air, fuel, exhaust gases and the distribution of the generated power of the DE in depending on the DE load are presented first. This is followed by a display of the generated power of the DE shaft, the diesel fuel combustion temperature and the air-fuel ratio (AFR) in dependence on the DE load. Then, the air and exhaust gas temperatures are shown, and finally the generator useful efficiencies and the DE useful efficiencies in dependence on the DE load are shown.

From Figure 6 (a), it is evident that the mass flow of the diesel fuel for driving the DE ranges from 0.035 kg/s at 30% load of the DE and up to 0.114 kg/s at 100% load of the DE. The mass flow of air entering DE ranges from 1.35 kg/s at 30% DE load up to 3.68 kg/s at 100% DE load. The mass flow of exhaust gases is the sum of the mass flow of fuel and the mass flow of air entering DE. The air-fuel equivalence ratio or ʎ decreases with increasing of the DE load and ranges from 2.2 to 2.5. This means that DE works from 120% to 150% of excess air, which has a positive ecological impact as it reduces the sootiness of exhaust gases.

Figure 6 (b) shows the power supplied by diesel fuel and the distribution of generating power of the DE in dependence on the load. The supplied power of diesel fuel amounts from

1550 kW to 4880 kW and increases in dependence on the DE load. Also, as the DE load increases, the power of the engine shaft increases and ranges from 480 kW to 2170 kW. The power of exhaust gases of the DE ranges from 730 kW to 1820 kW. The cooling water power of the DE ranges from 250 kW to 640 kW. Radiation through the DE housing ranges from 55 kW to 165 kW depending on the DE load. The heat dissipated from the oil cooler to the surroundings also increases with increasing the DE load and ranges from 30 kW up to 84 kW.

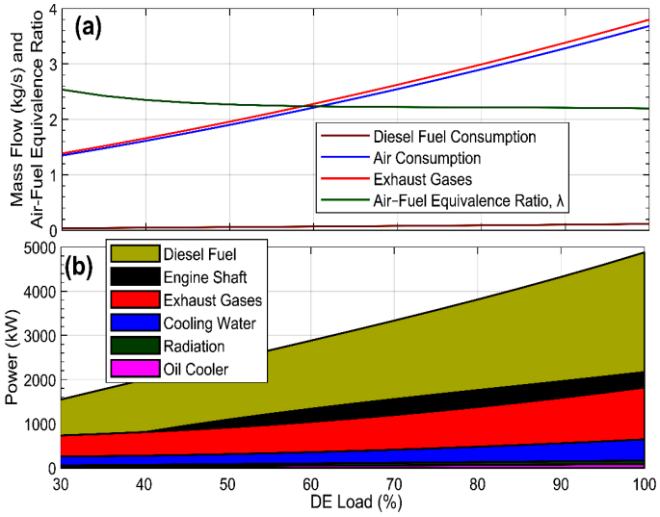

Figure 6. (a) the flow characteristics of air, fuel, exhaust gases and air-fuel equivalence ratio or ʎ of the DE; (b) the power supplied by the diesel fuel and the distribution of the power generated by the DE.

Figure 7 (a) shows the power of the DE shaft and the combustion temperatures in dependence on the DE load. At 30% of the DE load, the generated power of the DE shaft is 475 kW and as the DE load increases, the generated power of the DE shaft also increases. At 100% of the DE load, the power of the DE shaft amounts to 2164 kW. The combustion temperature increases up to 60% of the DE load, where it amounts to 1755 °C, and with increasing the DE load, it starts to decrease and at 100% of the DE load it is 1521 °C. At 30% of the DE load, the combustion temperature is 1650 °C.

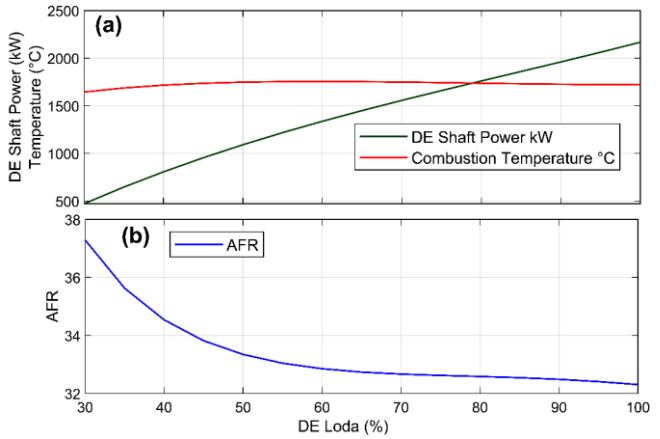

Figure 7. (a) power of the DE shaft and combustion temperature in dependence on the DE load; (b) AFR in dependence on the DE load.

However, from the diagram in Figure 7 (b) it is evident that the AFR depends on the DE load. At 30% of the DE load, the AFR value is at its maximum of 37 and decreases with increasing the DE load. At 100% of the DE load, the ARF decreases to the value of 32. The ratios of AFR and ʎ indicate that the DE is working with a high excess of air. The working of the DE with excess air has positive effects on the environment in terms of minimizing the generation of soot particles in exhaust gases or reducing sootiness.

The DE therefore work in the range with a high air excess, and the DE power is regulated by the amount of injected fuel. When increasing the DE load, the more fuel is injected and vice versa. As fuel injection increases, however, the mixture of air and fuel becomes richer, making it increasingly difficult to mix fuel and air in the combustion chamber. Due to the increasing difficulty of mixing fuel and air, the efficiency of combustion begins to decrease, but not the power of the DE. There is an upper limit at which the reduction in combustion efficiency can no longer be compensated by the addition of fuel. In this way, the optimal AFR which is in the range between poor and rich mixture is determined. The efficiency of the combustion in DE in dependence on ʎ is shown in Figure 8.

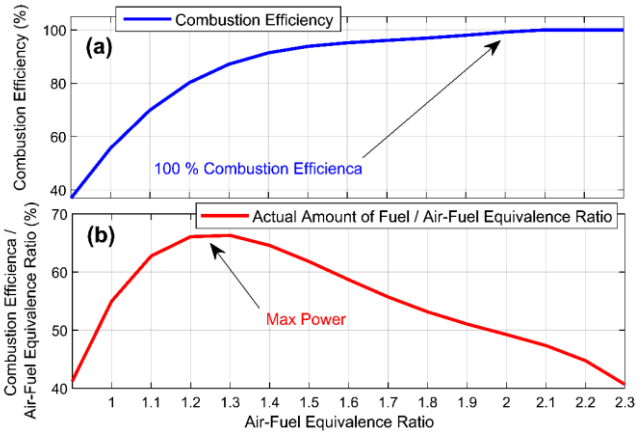

Figure 8. (a) The efficiency of the combustion in DE in dependence on the air-fuel equivalence ratio, or ʎ; (b) the ratio of "combustion efficiency / air-fuel equivalence ratio" in dependence on the air-fuel equivalence ratio, or ʎ.

It is evident from Figure 8 (a) that the efficiency of combustion in DE is achieved only at the air-fuel equivalence ratio, or ʎ = 2, which means that efficient combustion in DE is achieved when ʎ > 2. However, increasing ʎ decreases the power of the DE. DE develops maximum power ʎ = 1.25, which can be seen from the diagram in Figure 8 (b). The ratio of "combustion efficiency / air-fuel equivalence ratio" in Figure 8 (b) represents the actual amount of fuel consumed by the DE. Due to the generation of a huge amount of soot, the ʎ = 1.25 is used in DM only in a racial context. Serial production DE work for normal use ʎ > 1.65 [15].

The results of the model also give the results of the air-exhaust gases temperature profile in dependence on the DE load. It is evident from Figure 9 that the air temperature after the intercooler ranges from 70 °C to 98 °C. The maximum air

temperature after the intercooler is reached at 45% of the DE load, and then begins to decrease. At 100% of the DE load, the air temperature after the intercooler is the lowest and amounts to 70 °C. The lower air temperature after the intercooler has a positive effect on the work done by the DE, as the air density increases with decreasing temperature, which means that a larger mass of air can be brought to the same constant volume.

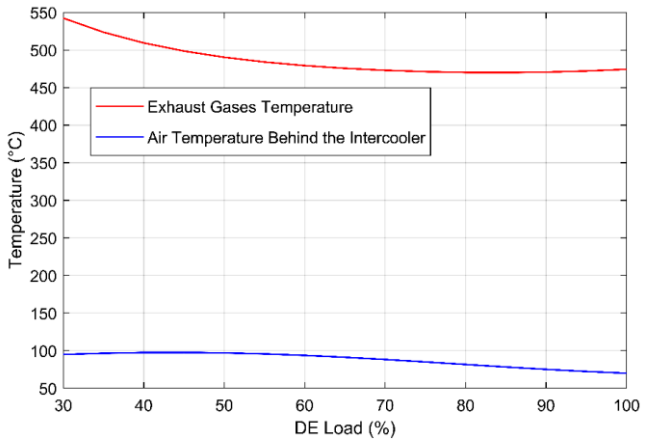

Figure 9. The air-exhaust gas temperature profile in dependence on the DE load.

The change in exhaust gas temperature in dependence on the DE load is also evident in Figure 9. Exhaust gas temperature ranges from 470 °C to 545 °C. The lowest exhaust gas temperature is reached at 80% of the DE load and the highest exhaust gas temperature is reached at the minimal DE loads.

Figure 10 shows the efficiency of the generator and the efficiency of the DE at different loads. From Figure 10 (a), it is evident the efficiency of the generator, which ranges from 94% of the minimal DE load to 96% at 70% of the DE load, then the generator efficiency starts to decrease and at 100% of the DE load it is 95.7%. The efficiency of DE ranges from 28% at minimal load to 45% at 60% of the load. Then the efficiency of DE starts to decrease and at 100% of load it is 42.5%.

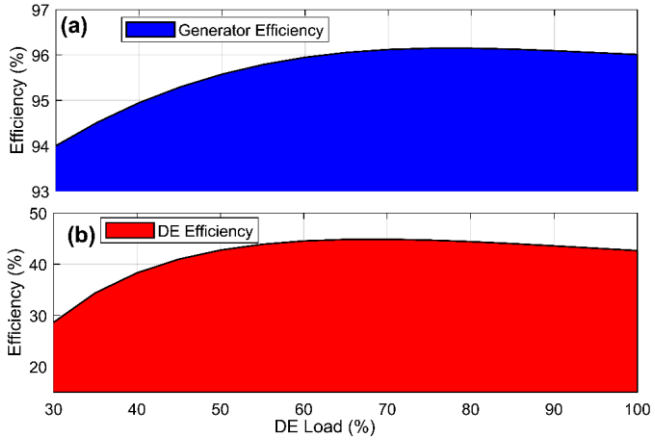

Figure 10. (a) generator efficiency in dependency of the DE load; (b) DE efficiency in dependency on load.

V. CONCLUSIONS

In this paper, the model and modelling results of the DE for the CHPP start-up at black-out are presented. The model consists of several sub-models, each sub-model has its own task. The most important sub-model is the calculation unit in which the mathematical equations are written, which are needed to accurately and precisely present the results. The quality of the model, however, depends on the quality of the set of measured data from the operating system, as this data is a key link that serves in generating mathematical expressions written in the calculation unit. The results of the model show that the DE works with a large excess of air $\lambda = 2.2$, which is mainly attributed to ecological aspects, namely the reduction of soot in exhaust gases Particular attention should also be paid to the efficiency of the DE, as the heat of the exhaust gases, as well as the heat of the cooling water, is discharged into the environment. Therefore, the efficiency varies depending on the DE load, ranging from 20% of the minimal DE load to 45% at 60% of the DE load. By using the heat of the exhaust gases and the heat of the cooling water of the DE, cogeneration operation for the production of heat and electricity, the efficiency of the DE can be greatly improved. In the case of the use of exhaust gas heat and cooling water, the DE could operate not only in the event of an electric eclipse, but also in cases of high electricity needs of the electricity system, since the price of electricity is high at that time.

VI. REFERENCES

[1] L. Chen, B. Yang, H. Feng, Y. Ge, S. Xia, "Performance optimization of an open simple-cycle gas turbine combined cooling, heating and power plant driven by basic oxygen furnace gas in China's steelmaking plants," Energy, 2020; 203, p. 117791. https://doi.org/10.1016/j.energy.2020.117791.

[2] M. A. Elhosseini M. A, A. Ahmed shams El-din, H. A. Hesham Arafat Ali, A. Abraham, "Heat recovery steam generator (HRSG) three-element drum level control utilizing Fractional order PID and fuzzy controllers," ISA Transactions, 2021. https://doi.org/10.1016/j.isatra.2021.04.035.

[3] A. Aya, A. Barakat, H. Jad, j. H. Diab, N. S. Badawi, W. S. B. Nader, C. J. Mansour, "Combined cycle gas turbine system optimization for extended range electric vehicles," Energy Conversion and Management, 2020; 226, p. 113538. https://doi.org/10.1016/j.enconman.2020.113538.

[4] G. Hou, L. Gong, B. Hu, T. Huang, H. Su, C. Huang, G. Zhou, S. Wang, "Flexibility oriented adaptive modeling of combined heat and power plant under various heat-power coupling conditions," Energy, 2021; p. 122529. https://doi.org/10.1016/j.energy.2021.122529.

[5] European Network of Transmission System Operators for Electricity, https://www.entsoe.eu/.

[6] Mitsubishi heavy industries, Mitsubishi diesel engine S16R2-PTAW, powerful and reliable, https://engine-genset.mhi.com.

[7] C. Maraffi, M. Turchiarelli, L. Sepe L, "Black start diesel generator. Operation & maintenance manual," Mitshubishi diesel engine S16R, 2018, No. 29001-00120.

[8] T. Ouyanga, Z. Su, B. Gao, M. Pan, N. Chen, H. Huang, "Design and modeling of marine diesel engine multistage waste heat recovery system integrated with flue-gas desulfurization," Energy Conversion and Management, 2019; 196, pp. 1353–1368. https://doi.org/10.1016/j.enconman.2019.06.065.

[9] D. Strušnik, "Integration of machine learning to increase steam turbine condenser vacuum and efficiency through gasket resealing and higher heat extraction into the atmosphere," International Journal of Energy Research, 2021. https://doi.org/10.1002/er.7375.

[10] I. Arsie, R. Di Leo, C. Pianese, M. De Cesare, "Estimation of in-cylinder mass and AFR by cylinder pressure measurement in automotive Diesel engines," Proceedings of the 19th World Congress, The International Federation of Automatic Control, 2014; pp. 24-29.

https://doi.org/10.3182/20140824-6-ZA-1003.01602.

[11] . J. D. Forero, "Energy, exergy and environmental assessment of partial fuel substitution with hydroxy powered by a thermoelectric generator in low displacement diesel engines," Cleaner Engineering and Technology, 2021; 3, p. 100086.
https://doi.org/10.1016/j.clet.2021.100086.

[12] H. Li, Y. Li, P. Zhao, J. Wang, G. Zhang, X. Qin, J. Chen, "Optimization research on the off-design characteristics of partial heating supercritical carbon dioxide power cycle in the landfill gas exhaust heat utilization system," Applied Thermal Engineering, 2021; 199, p. 117585.
https://doi.org/10.1016/j.applthermaleng.2021.117585.

[13] Y. Cao, W. W. L. Mihardjo, M. Dahari, A. M. Mohamed, H. Ghaebi, T. Parikhani, "Assessment of a novel system utilizing gases exhausted from a ship's engine for power, cooling, and desalinated water generation," Applied Thermal Engineering, 2021; 184, p. 116177.
https://doi.org/10.1016/j.applthermaleng.2020.116177.

[14] M. Oikawa, Y. Kojiya, R. Sato, K. Goma, Y. Takagi, Y. Mihara, "Effect of supercharging on improving thermal efficiency and modifying combustion characteristics in lean-burn direct-injection near-zero-emission hydrogen engines," International Journal of Hydrogen Energy, 2021.
https://doi.org/10.1016/j.ijhydene.2021.10.061.

[15] H. H. Schrekn, L. B. Berger, "Composition of Diesel Engine Exhaust Gas," American Journal of Pblic Health, 1941.

Effect of energy renovation on indoor air quality of a French school building

Najwa Kanama
LOCIE UMR 5271
USMB, CNRS
73376 Le Bourget-du-Lac, France
najwa.kanama@univ-smb.fr

Michel Ondarts
LOCIE UMR 5271
michel.ondarts@univ-smb.fr

Guyot Gaëlle
Cerema Centre-Est
Ministry of Ecological Transition
38081 L'Isle d'Abeau, France
Gaelle.Guyot@cerema.fr

Jonathan Outin
LOCIE UMR 5271
jonathan.outin@univ-smb.fr

Benjamin Golly
LOCIE UMR 5271
benjamin.golly@univ-smb.fr

Evelyne Gonze
LOCIE UMR 5271
evelyne.gonze@univ-smb.fr

Abstract

Indoor air quality (IAQ) and thermal comfort issues in schools are of particular public concern because children represent a vulnerable population group to air pollution. In fact, their respiratory and immune systems are still developing and a long-term exposure to indoor air pollutants might have a significant impact on their health and scholarly. This study focuses on the effect of the energy renovation of two classrooms which consists of the implementation of a dual flow ventilation system with high efficiency filters (F7). The classrooms are located in an alpine valley (France) known for its high level of atmospheric pollution. To do this, carbon dioxide (CO_2), temperature (T), relative humidity (RH) and $PM_{2.5}$ were monitored continuously over twice two-month periods before and after the renovation in winter 2018 and 2020, respectively. In addition, the ventilation airflows were measured and a daily questionnaire that report the information on general condition in the classroom were recorded day-to-day. The results of these campaigns indicate that before the renovation, the two rooms were confined, estimated by IAQ index such as ICONE index which are equal to 2. The CO_2 concentration reached to 4790 ppmv due to a very low air exchange rate 0.05 h^{-1}. During the high $PM_{2.5}$ levels episodes observed in outdoor air, the low air exchange rate limited the transport of $PM_{2.5}$ from the outside to the inside of the classrooms. As a result, the percentages of concentration exceedance compared to WHO recommendations were 23% and 17%, in class 1 and class 2 respectively, while it reached 68% in outdoor air.

After the renovation, the ventilation airflow was higher than before renovation and reached to 2.46 h^{-1}. As consequence, a drastic reduction of the confinement was measured with ICONE index of class 2 reaching to 0. The CO_2 concentrations are remained low with a maximum value of 1150 ppmv. Rather the high air renewal generates a significant inflow of outdoor particulate pollution which the indoor $PM_{2.5}$ concentrations range were 20-80 $\mu g.m^{-3}$ during the outdoor air pollution episodes. However, the indoor concentrations were all the time lower than those observed outside with indoor/outdoor concentration ratio about 0.5. It can be assumed that the filtration of the supply air allowed to limit the entrance of the particles. However, this figure should be taken with caution because of the complex physic associated with particle behaviours (e.g. sedimentation, resuspension, etc). In addition, it is interesting to note that a dysfunction of the ventilation system led to a situation close to that before renovation, both with regard to the rate of ventilation airflow, as well as the concentrations of CO_2 and $PM_{2.5}$.

Keywords: *Indoor air quality, energy renovation, school, ventilation, filtration, thermal comfort, $PM_{2.5}$, ventilation airflow*

IEECP'22, July 21-22, 2022, Oxford, United Kingdom

Improving the energy efficiency of microsystems with solar PV sources for individual power supply of residential buildings (feasibility study for the regions of Azerbaijan)

Nariman Rahmanov
Modeling, Analysis and Control of Power System with Integrated VRS
Azerbaijan Research Institute of Energetic & Energy Design
Baku, Azerbaijan
nariman@cpee.az

Aynur Mahmudova
Modeling, Analysis and Control of Power System with Integrated VRS
Azerbaijan Research Institute of Energetic & Energy Design
Baku, Azerbaijan
aynur.mahmudova25@gmail.com

Abstract

In recent years, small, isolated power supply systems have been widely developed, in which the main share of electricity generation is produced based on low-power renewable sources (solar PV converters, wind turbines and other types of RS). At present, schemes of mini and micro-systems of power supply with different composition of renewable sources, differing in parameters depending on geographic and weather conditions of their locations. While there are no universal approaches to choosing the optimal combination used in such systems of renewable sources and traditional sources (diesel generator, batteries) used. This article provides a practical method for the technical feasibility study for the construction of a Stand-Alone Photovoltaic (SAPV) system in Karabakh region of Azerbaijan Republic. Based on the current growing role of the subject region, its energy security and economic development the aim is to build the most efficient and optimal cleaner energy production facilities in this area. Considering the lack of methodology for the measurement of renewable energy potential in Karabakh region, we employed evaluation methods based on mapping techniques, simulation software for solar stand-alone unit and the analytical tools offered by PVSyst Software. Solar module, battery, DC/AC pure sine wave power inverter, and the charge controller are the main components of the suggested PV system design. Choosing optimal capacity and arrangement increase the plant's efficiency and reduces the overall system costs. In this method, according to the geographical location the number of solar modules and their optimal angles are defined. PVSyst software is used for the system analysis, and the simulation results show the performance of the designed system on an individual residential building located in Zangilan city of Karabakh region. The main novelty of this study is related to the integration of the renewable energy potential maps combined with a density of population, are good predictors of locations for the development of renewable energy source-based facilities. The contribution of the proposed method is the provision of technical calculation and feasibility check for remote areas where making local measurements of RES potential is a constrain. The study concludes with recommendations towards the optimal size of stand-alone solar system and its components and use of renewable energy potential to achieve more balanced regional development and clean energy production.

Keywords: stand-alone, clean energy, solar photovoltaic, PV system, PVsyst

IEECP'22, July 21-22, 2022, Oxford, United Kingdom

I. INTRODUCTION

The world-wide demand for solar electric power systems has grown steadily over the last 20 years. The need for reliable and low-cost electric power in rural areas of the world is the primary force driving the world-wide photovoltaic (PV) industry today. For a large number of applications, PV technology is simply the least-cost option.

Typical applications of PV in use today include stand-alone power systems for cottages and remote residences, remote telecommunication sites for utilities and the military, water pumping for farmers, and emergency call boxes for highways and college campuses, to name just a few [1, 2, 3]

Significant growth in demand for PV systems is expected to occur in developing countries to help meet the basic electrical needs of the 2 billion people without access to conventional electricity grids. PV modules are integrated into systems designed for specific applications. The components added to the module constitute the

"balance of system" or BOS. Balance of system components can be classified into three categories:

• Batteries - store electricity to provide energy on demand at night or on overcast days;

• Inverters - required to convert the DC power produced by the PV module into AC power;

• Controllers - manage the energy storage to the battery and deliver power to the load

Not all systems will require all these components. For example, in systems where no AC loads present an inverter is not required. For on-grid systems, the utility grid acts as the storage medium and batteries are not required [4, 5].

Some stand-alone systems, for example, include a fossil fuel generator that provides electricity when the batteries become depleted; and water pumping systems require a DC or AC pump. This article suggests an off-grid solar power system, for a typical home at Zangilan, Azerbaijan. To computing the off-grid solar system components, as it was requested the design was done for the shortest day of the year which is 21st of December. The solar data is obtained from NASA web site and PVSyst software.

In the Figure 1,2, 3 and 4 it is shown the photovoltaic power potential of the study area for one day, monthly averages and yearly data.

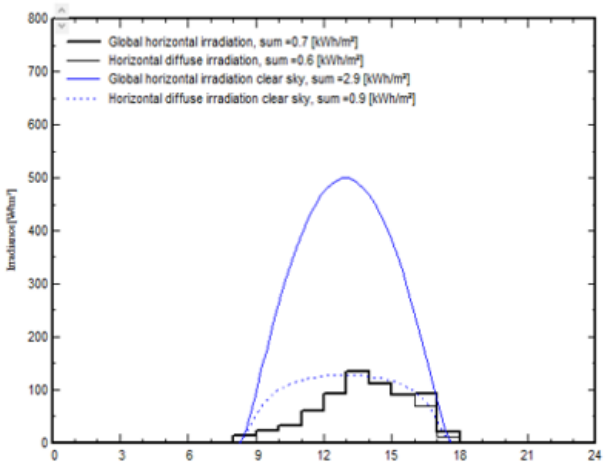

Figure 1. Daily photovoltaic power potential

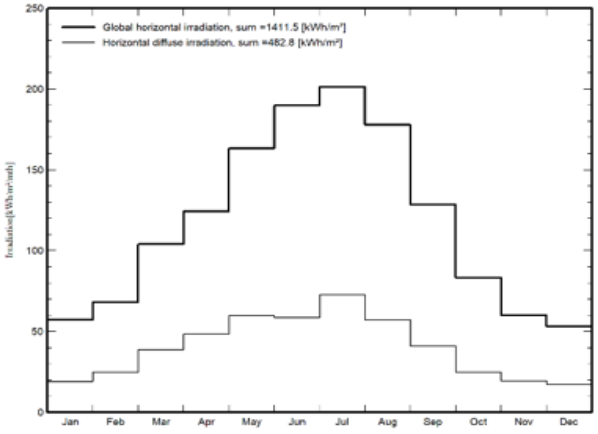

Figure 2. Monthly photovoltaic power potential

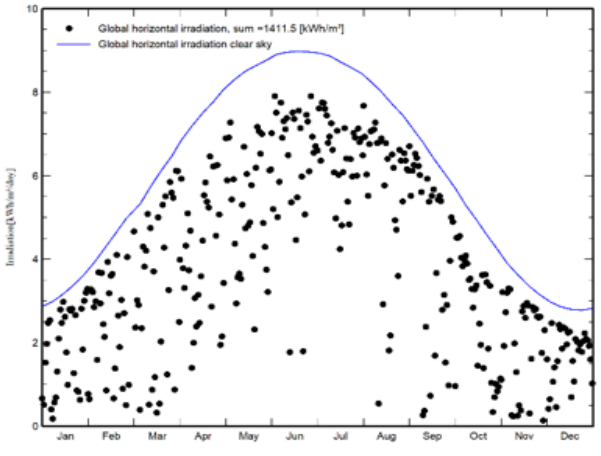

Figure 3. Daily photovoltaic power potential for one year

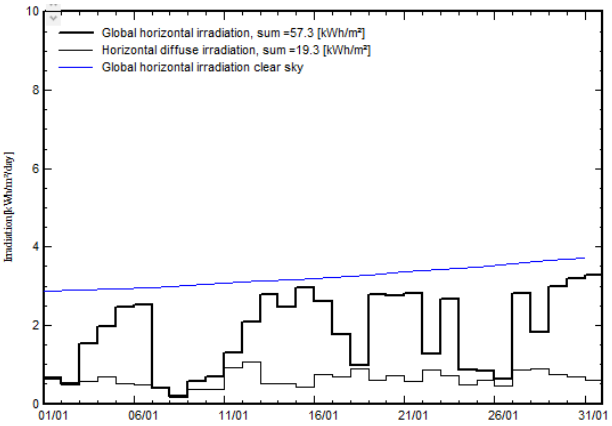

Figure 4. Daily photovoltaic power potential for one month

Obtained results are compared with the data extracted from SolarGIS web software and NASA available data. The data from NASA collected from Surface meteorology and Solar Energy (SSE) Release 6.0 Data Set (Jan 2008), 22-year Monthly & Annual Average (July 1983 - June 2005) and shown on Table 1.

Table 1. Average monthly values and annual amount of Solar radiation

Month	SolarGIS GHI kWh/m²/month	Pvsyst GHI kWh/m²/month	PVSyst kWh/m²/day	NASA kWh/m²/day
Jan	64.0	57.3	1.85	20.3
Feb	79.4	68.3	2.44	2.75
Mar	110.7	104.1	3.36	3.61
Apr	124.5	124.5	4.15	4.44
May	151.7	163.3	5.27	5.37
Jun	179.3	189.8	6.33	6.34
Jul	187.7	201.3	6.49	6.33
Aug	172.8	177.8	5.74	5.59
Sep	121.0	128.5	4.28	4.64
Oct	92.9	83.3	2.69	3.38
Nov	68.2	60.1	2.00	2.27
Dec	57.2	53.3	1.72	1.70
Yearly	1409.4	1411.5	3.87	4.04

There is minor difference between the data, and this considered applicable as the data are collected via satellite. In previous studies

it has been identified that the Zangilan city has more solar power potential than the other cities of Karabakh region, Azerbaijan.

II. LOAD MODELING

A typical home is a 120 square meter house located in Zangilan, Azerbaijan, location: latitude: 39.30N, longitude: 46.590E.

A typical home loads are described in Table 2. Hourly distribution and the daily consumption are presented in Figure 5.

Table 2. Household characteristics and energy demand

Loads	Power (watt)	Qty	Hours	Total power (watt)	Energy (Watt.h)
Lamps	10	12	5	120	600
TV/PC/Mobile	100	2	5	200	1000
Domestic Appliances	500	1	4	500	2000
Fridge	33.292	1	24	33.292	799.008
Washing Machine	1000	1	2	1000	2000
Heater (Hot water)	100	1	24	100	2400
Air Conditioning	1000	1	3	1000	3000
Stand-by consumers	6	1	24	6	144
Total Power of Loads	2959.292				
Total Energy Demand	11943.008				

While creating load parameters seasonal demand is considered and identified higher demand during summer season due to air connditioning system. Table 2 shows the summer season load characteristics during June-August.

The calculation is based on the energy demand which is in our case is 11943Wh≈ 12kWh.

It has been identified that the maximum demand of the house is during summer season due to air conditioning unit. Considering the daily household consumers and seasonal modulation, the avarage 12kWh is used for calculation.

III. TYPICAL LAYOUT

Stand-alone systems are always organized around a battery storage:

- A PV Array charges the battery or directly delivers its power to the user

- The user's needs should be well defined, with its daily profile

Figure 6 describes the typical layout of standalone system:

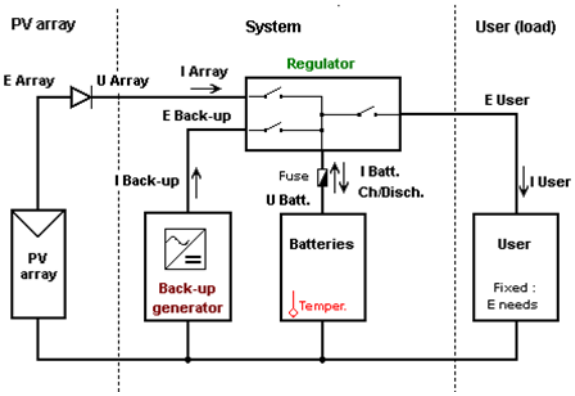

Figure 6. Typical layout of Stand-alone system.

The system performs a balance between the PV production (depending on irradiance) and the users' needs. The difference should be derived in the battery, either Positively(charge) or negatively (discharge) [6, 7, 8].

The energy balance is controlled by the charger controller. The role of the controller is to handle the energy flow, mainly for the protection of the battery:

- When the battery is full, the PV array should be disconnected
- When the battery is empty, the user should be disconnected

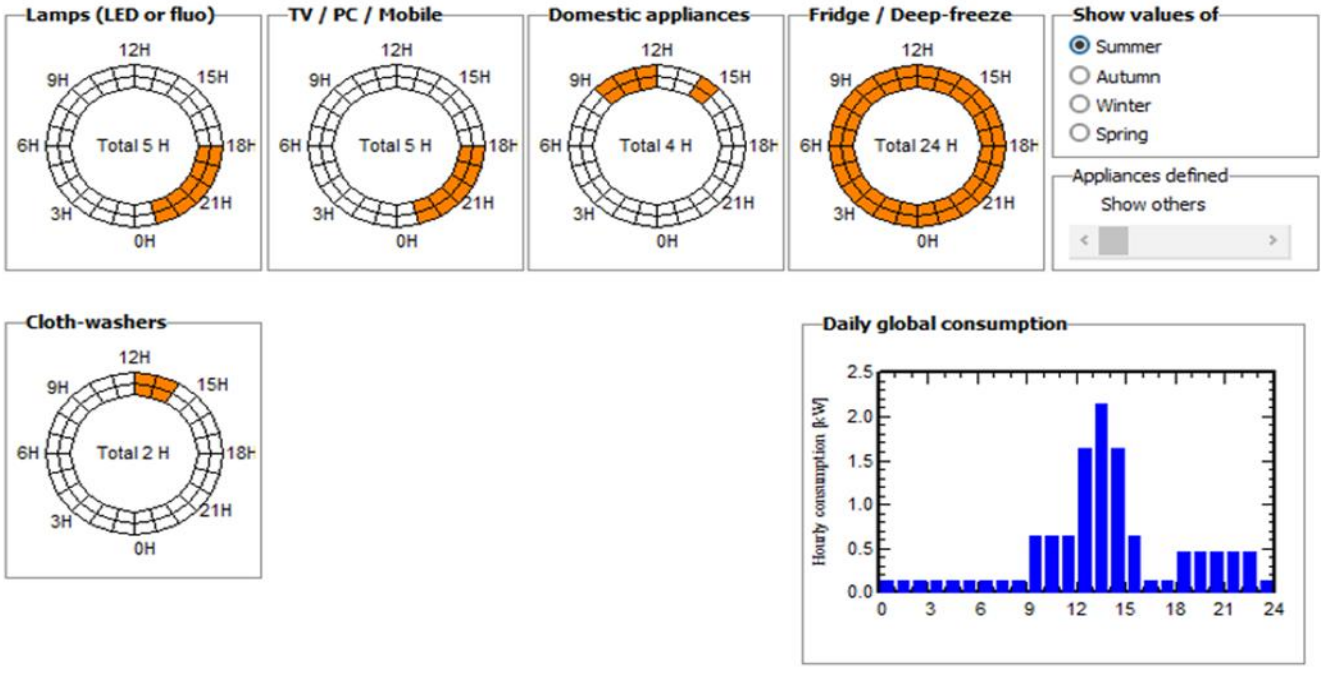

Figure 5. Households' hourly distribution

Moreover, the controller may manage the starting of an eventual back-up generator, when the battery is empty, and the solar gain is not sufficient. However, back-up generator is optional and is not considered in this article [9, 10].

IV. CALCULATION OF SYSTEM COMPONENTS FOR AUTONOMOUS STAND-ALONE POWER SUPPLY OF INIDIVIDUAL RESIDENTIAL HOUSE FIGURES/CAPTIONS

The calculation is starting with defining of declination, elevation and tilt angles based on the selected area coordinates (latitude and longitude). This is required to define the peak sun hours which is the main parameters in correct selection of PV panels [11, 12].

Declination angle determined by using below formula and it is the angle between the universe axis and the earth axis:

$$\delta = 23.5 \sin\left[\frac{360}{365}(284 + d)\right]$$

Where δ – is declination angle, d – is the day number of the year.

Elevation angle is the angle between the sun rays and the horizontal plane and determined as below formula:

$$\alpha = 90 - \emptyset + \delta$$

Here, α – is elevation angle, ∅- is the latitude of the selected area.

The tilt angle is an angle between the solar panel and the horizontal plane. It is defined as per below formula:

$$\beta = 90 - \alpha$$

Where, β- is a tilt angle, α – is an elevation angle.
The calculation is done for each month of the year.

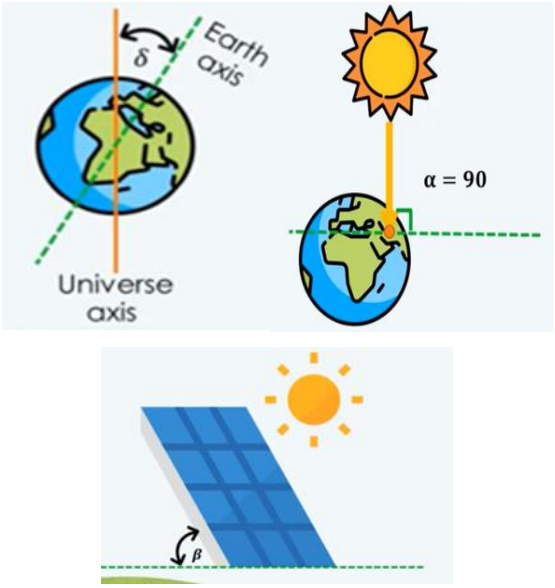

Figure 7. Declination, elevation and tilt angles

Ones the required angles are calculated, the peak sun hours can be defined by using below formula:

$$S_m = \frac{S_H \times \sin(\alpha+\beta)}{sin\alpha}$$

Where, S_m – is peak sun hour, α and β elevation and declination angles, accordingly.

The results obtained from calculations are presented in Table 3.

Based on the calculated peak sun hour and energy demand the number of required PV panels can be calculated as following:

$$Number\ of\ panels = \frac{P_{in}}{power\ of\ single\ panel}$$

$$P_{in} = \frac{Energy}{\eta \times S_m}$$

Where the P_{in} – is an input power of PV panel, η- is an efficiency of panel. While selecting PV panel NOCT-Nominal operating cell temperature, TCP-Temperature coefficient of panel, efficiency and open circuit voltage are collected from the panel datasheets.

To choose batteries below calculation is done:

$$Total\ Ah = \frac{Energy \times AD}{\eta \times V_{bus} \times DOD}$$

Where the AD – autonomy days, considered to compensate sun absence, DOD – Depth of discharge, V_{bus} – total system voltage, η – battery efficiency.

By taking in to account the inverter nominal voltage, the bus voltage is identified. Thus, the number of parallel branch of batteries are calculated.

$$N.of\ batteries\ in\ each\ branch = \frac{V_{bus}}{V_{battery}}$$

$$V_{bus} = V_{inverter}$$

$$AH\ for\ single\ branch = single\ battery\ AH \times N.of\ bat\ in\ each\ branch$$

$$N.of\ parallel\ branch = \frac{Total\ AH}{AH\ for\ single\ branch}$$

Charger Controller is calculated and selected based on its rated minimum current.

$$I_{charger\ min.} = \frac{N.of\ panel \times P_{single}}{V_{bus}}$$

Table 3. Angles and peak sun hour calculation results

Parameters	Jan	Feb	March	Apr	May	Jun	Jul	Aug	Sep	Oct	Nov	Dec
S_H	2.03	2.75	3.61	4.44	5.37	6.34	6.33	5.59	4.64	3.38	2.27	1.7
Latitude	39.04	39.04	39.04	39.04	39.04	39.04	39.04	39.04	39.04	39.04	39.04	39.04
Longitude	46.61	46.61	46.61	46.61	46.61	46.61	46.61	46.61	46.61	46.60	46.61	46.61
Day Number	21	52	80	111	141	172	202	233	264	294	325	355
Declination	-20.155	-11.2	-0.3452	11.66	20.27	23.5	20.47	11.77	-0.291	-11.861	-20.53	-23.50
Elevation	30.804	39.76	50.614	62.62	71.18	74.46	71.40	62.67	50.68	39.10	30.43	27.46
Beta(calc.)	62.54	62.54	62.55	62.54	62.5	62.54	62.56	62.54	62.55	62.54	62.55	62.55
Beta(design)	60	60	60	60	60	60	60	60	60	60	60	60
Sm	3.97	4.24	4.38	4.22	4.277	4.70	5.015	5.302	5.617	5.30	4.484	3.685
Sm(min)	**3.684557**											
Sm(max)	**5.61689907**											
P.S.H	**4.597850573**											

Inverter selection is implemented based on the below formula:

$$P_{inverter} = \frac{P_{load} \times Safety\ Factor}{PF}$$

Where, $Safety\ Factor$ – consider the sudden increase of the loads power, PF – is the power factor.

Ones the panels are selected required area calculation can be done. During this calculation the actual dimensions of each panel and spacing between the panels are considered

V. RESULTS & DISCUSSION

Based on the calculation, the optimal tilt angle of PV panels shall be 60 degrees. At this degree the PV panel calculated is Generic STP-415S-A78-Vfh, Si-Mono type 8 of panels with 415Wp nominal power and 38A open circuit current. The suitable battery is Li-Ion battery, 180Ah, 26V batteries. The calculated inverter power is 5kW. Obtained results are simulated via PVSyst software.

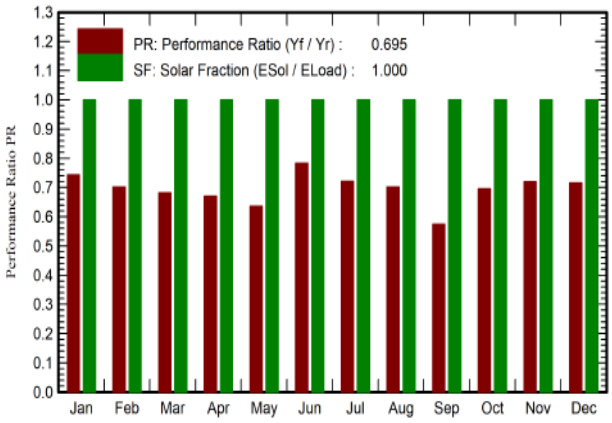

Figure 8. Performance Ratio

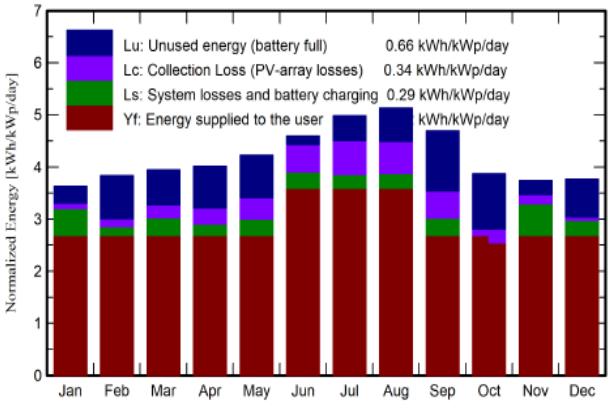

Figure 9. Normalized production (per installed kWp)

Table 4. Balances and Main result

Month	GlibHor kWh/m2	E_Avail kWh/m^2	E_User kWh	E-Load kWh
Jan	57.3	345.2	277.2	277.2
Feb	68.3	328.7	250.4	250.4
Mar	104.1	363.1	277.2	277.2
Apr	124.5	354.9	268.3	268.3
May	163.3	378.3	277.2	277.2
Jun	189.8	385.0	358.3	358.3
Jul	201.3	427.1	370.2	370.2
Aug	177.8	444.8	370.2	370.2
Sep	128.5	399.7	268.3	268.3
Oct	83.3	357.8	277.2	277.2
Nov	60.1	338.0	268.3	268.3
Dec	53.3	367.1	277.2	277.2
Yearly	1411.5	4489.7	3540.3	3540.3

Legend:
GlobHor- Global horizontal Irradiation
E_Avail- Available Solar Energy
E_User- Energy Supplied to the user
E_load - Energy Need of the user

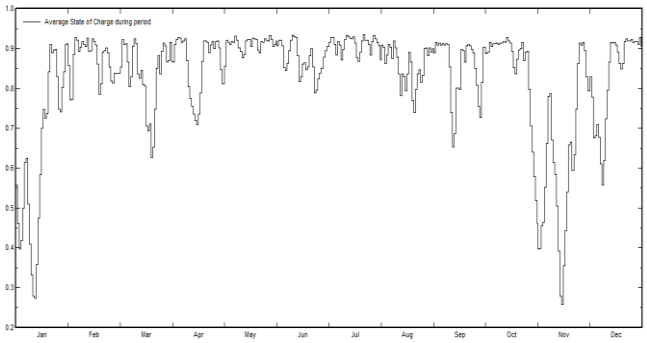

Figure 10. Battery State of Charge Daily Distribution

VI. CONCLUSION

The simulation results are shown for the system that includes 8 of 415Wp PV panels connected in 4 Strings and 2 in series. The NOCT of panel is 450. The selected battery is Li-Ion 26V, 180Ah battery connected 8 in parallel x 2 in series. The nominal capacity of the battery is 1140Ah (C10). The universal type of controller is selected for the simulation.

The Table 4 and Figure 8 and 9 reported by PvSyst software, shows that by using the selected panel the user demand can be fully covered by solar energy. The solar fraction is equal to 1.0 which means that the required energy is provided by solar panel. The performance ratio is almost 70% by taking in to account the system loses. As per Figure 10 the batteries maximum DOD is 0.28 during January and November for only 2-3 days. In all other cases battery DOD remains close to 0.5, which is an effective value for its lifecycle. The dimensions of the panel are taken from the technical datasheet and identified 18m2 location space is required to install the PV panels. The panels are considered to be free mounted type with air circulation for cooling system.

Provision of residential buildings with the individual PV systems will significantly affect the life of the residents, where they can independently regulate their energy demand and usage, learn RES based innovative technologies from operation and maintenance wise and improve their social life.

VII. REFERENCES

[1] N.R. Rahmanov, N.M. Tabatabaei, R.E. Kerimov, A.Z.Mahmudova "Fundamentals of Hybrid Distributed Generation Systems Construction with renwable energy sources for remote consumers power supply" IJTPE Conference Proceedings, pp 44-55, October 2021, Istanbul, Turkey

[2] Morteza Khatami, Hashem Mortozavi "Designing an off-grid PV system: For a residential consumer in Mashhad-Iran", Conference Paper · September 2013

[3] Nallapaneni Manoj Kumar, M.Rohit Kumar, P.Ruth Rejoice, Mabi Mathew "Performance analysis of 100kWp grid connected Si-Poly photovoltaic system", 1st ICCON, March 2017, VIT University, Chennai Campus

[4] Cyris Mehdipour, Fazel Mohammedi "Design and Analysis of a Stand-Alone Photovoltaic System for Footbridge Lighting" 2019 Published by University of Tehran Press.

[5] N.R. Rahmanov, O.Z. Kerimov, S.T. Ahmadova, Z.A. Mammadov, K.M. Dursun "Practical Implementation of AC / DC Microgrid with Renewable sources for Isolated area". 12th International Conference on Technical and Physical Problems of Electrical Engineering, University of Basque country, N. 16., ICTPE, pp. 84-89, Bilbao Spain. 2016.

[6] Ayaz A.Khamisani "Design Methodology of Off-Grid PV Solar Powered System (A Case Study of Solar Powered Bus Shelter)".

[7] Benedek, J., Sebastian, T.T., Bartok, "Evaluation of Renewable energy sources in peripheral areas and renewable energy-based rural development", Renew. Sustain. Energy Rev. 90, 516-535, 2018

[8] Hashimov A.M., Mammadov Z.A., Tabatabaei N.M., Rahmanov N.R. "Optimal combination of the renewable energy sources for remote distributed system in Proceedings ICTPE-2020. The International Conference on Technical and Physical Problems of Engineering ", 12-13 October 2020, Istanbul Rumelia University, Istanbul, Turnery.

[9] IEA, International Energy Association, World Energy outlook 20019.

[10] M. Jianpera, B. Domenech, L. Ferrer-Marti, A. Garzon, R. Pastor. "Renewable-based electrification for remote locations. Does short-term success endure over time ". A case study in Peru journal Renewable and Sustainable Energy Reviews, Volume 146, August 2021, 111177

[11] Kerimov R.E., Kerimov O.Z., Rahmanov N.R., "Estimation of Renewable Energy potential for Solar RV System located on the water, Surface of small lakes and Reservoirs". IS. "Technical and Physical Problems of Engineering". 2021, vol. 13. pp. 107-111.

[12] The Complete 2022 PV Solar Energy w/ PVsyst, Excel & AutoCAD, Udemy, Online Learning platform

Environmental Effects of Dust Deposition on Solar PV Panels in the Surface Mining Industry

Ganti Praful Kumar
Research Scholar, Department of Mining Engineering
National Institute of Technology, Rourkela.
Odisha, India.
Email address: 518mn1002@nitrkl.ac.in

Dr. Hrushikesh. Naik
Associate Professor, Department of Mining Engineering
National Institute of Technology, Rourkela.
Odisha, India.
Email address: hknaik@nitrkl.ac.in

Dr. Kanungo Barada Mohanty
Professor, Department of Electrical Engineering
National Institute of Technology, Rourkela.
Odisha, India.
Email address:kbmohanty@nitrkl.ac.in

Abstract

This paper highlights a study of Solar Photo-Voltaic (PV) energy system from the environmental impact analysis and its effects point of view and the enhancement factors affecting the Solar Photovoltaic (PV) module by the tilt angles variation on power output of MPPT and dust accumulation on solar PV panel. The Efficiency of solar PV energy system from the environmental impacts in Mining Industry and also a Laboratory study is also conducted and a specific investigation on dust deposition effect on the solar photovoltaic (PV) panel, its power loss and overall efficiency of the solar panel are made. The Scanning Electron Microscope (SEM) analysis carried out for the collected dust samples, and obtained images are also analyzed. A specific investigation on dust samples like Iron ore, Coal, Limestone, Sandstone of different weights, and three different irradiation levels of 500,700,900W/m^2 is done and the following data collected. In this study, measuring of voltage current, power in the solar photovoltaic (PV) panel is also done. According to the accumulation of dust particles on the solar panel the minimum power of the solar panel is observed for deposition of Coal dust on the solar PV panel and the maximum power of the solar PV panel is observed for deposition of Iron ore dust on the solar PV module.

Keywords: *Scanning Electron Microscope, dust deposition, irradiation levels voltage, current, power*

I. INTRODUCTION

Now a days, most of the electrical energy has been generated by using conventional energy sources like coal, nuclear, gas, petrol, and diesel. This affects the environmental conditions and depletion of traditional energy sources. So, this has led to research on some alternative energy sources like solar, wind, tidal, biomass, and geothermal [1]. These are natural sources, which are refilled over some time, and the power generated from these sources is called renewable energy sources.

Generating electrical energy from renewable power sources has many advantages like [2] pollution free, reliable, inexhaustible, lower maintenance, and availability everywhere[3]. Nonconventional power sources are also called renewable energy sources. The solar photovoltaic (PV) cells comes under renewable energy sources, it converts the solar energy into electrical energy. Therefore, electrical power is produced by PV cells with the help of sun light is called solar energy[4]. The most used material in the PV cell is silicon. In PV cell, the sun light falls on the surface of the cell, which results in exciting the electrons in the cell and generation of an electric voltage and current. The performance of the solar panel greatly influenced by environmental factors like available radiation from sun, temperature, Mining dust, Relative humidity, direction of wind speed [5]. Because of airborne dust particles on the surface of the PV module, blocking of solar irradiation is happened.

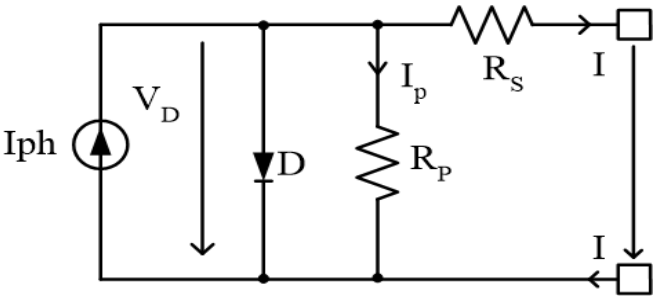

Figure 1: Single diode equivalent circuit of Photovoltaic cell

- I_{ph} = Photo or light generated current (A),
- V_d = Voltage through diode (A),
- R_S = Series resistance (Ω).
- R_p = Parallel resistance (Ω),
- D = Diode,
- I =Current.

2.Photovoltaic cell

The term "photo" means light, and "voltaic" means electricity. Thus, a PV cell is a device which directly converts light into power. At present, there are broadly two types of PV cell materials, such as crystalline PV cells and thin-film PV cells. Crystalline PV cells are of three kinds: mono-crystalline PV cells (Mono-Si), polycrystalline PV cells (p-Si), and Gallium Arsenide (GaAs) PV cells. Similarly, thin-film PV cells of different types, such as amorphous silicon PV cells (a-Si), Cadmium Telluride PV cells (CdTe), Copper Indium Gallium Selenide PV cells (CIS/CIGS) and organic PV cells (OPC) [14].

IEECP'22, July 21-22, 2022, Oxford, United Kingdom

Photovoltaic cells generate heat by converting sunlight to electricity. The electric current produced depends on solar irradiation. A PV cell can make around 0.5 to 0.8V. Because of the tiny PV cells change, solar PV panels contain distinct Photovoltaic cells connected in series and parallel.

3. Impact of Environment on the Photovoltaic System

3.1 Temperature effect on the photovoltaic system

In the photovoltaic system, usually, the solar cell is the best at low temperatures. In high heat, semiconductor properties change resulting in increased current, and significant decrease in the voltage too. Impact of temperature on PV cell efficiency can be traced to influence on Current (I), and Voltage (V) as maximum power given by [11]

$$P_m=V_mI_m(FF)V_{oc}I_{sc} \quad (1)$$

where FF is called Fill factor, V_{oc} is called open circuit voltage, I_{sc} is called short circuit current, V_m= maximum voltage, I_m is called maximum current.

3.2 Impact of humidity on the photovoltaic system:

In this impact of moisture on the Solar panel system, [12]which obstructs extreme variation in the power generated system, indirectly in the photovoltaic system,[6] it makes the device work less efficiently than it could have without it. Humidity can decelerate efficiency in two ways:

- In this first efficiency way, tiny water droplet like beads of sweat reflects sunlight away from solar cells. This process reduces the amount of the sun hitting the solar panel to produce electricity.
- In this second efficiency way, in consistent hot, humidity climatic weather, degrade the solar panels lifetime. It is for a combination of both thin-film modules cells and crystalline silicon cells, in case cadmium telluride (thin film) of the PV cell it can perform in the tropical climatic condition [13].

3.3 Impact of dust on the photovoltaic system

In the process of mining, the large amount of dust comes from the process of mining at mineral mines site from following mining activities like Heavy Earthmoving Machinery [HEMM], drilling, blasting, etc. In this process, a large number of tiny dust particles will generate from the mining process. This type of dust Pm_{10} is also called a particulate matter. This type of dust is produced by HEMM when the soil got disturbed, and the wind blows from over bare ground and stockpiles in the mine area [6]. Dust accumulation is one of the significant factors affecting the solar panel efficiency. Especially in remote mining areas where weather conditions are going to effect, the solar panels performance.

4. Description of the Experiment:

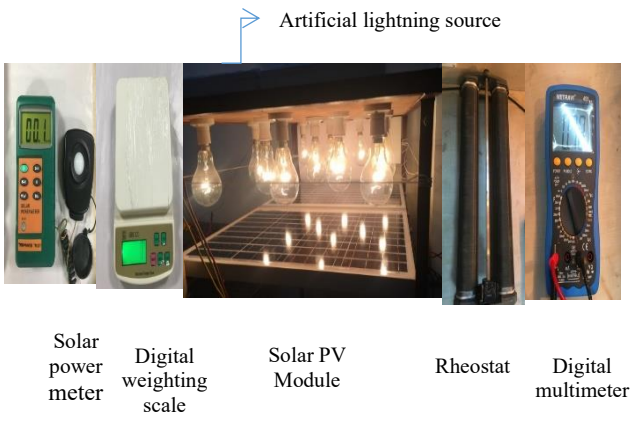

Figure 2: Experimental setup used in the present study

4.1 Description of the present study

In this Investigation, four mine dust samples are collected from the surface mining where solar panels are installed in the mine. For this experiment, 40W Polycrystalline photovoltaic panel is mounted on a stand to carry out an experimental study various equipment required for the study are: 1) 40W Polycrystalline PV module (Make: LUMINOUS), number of cells= 36, the material used in the PV technology is Aluminum. This is placed under artificial light representing sunlight. For artificial lighting, 16 number of electrical bulbs each (200W) are used. This acts as artificial lighting. 2) Digital Multimeter (Make: METRAVI-451) is used to find the voltage, current, temperature for this experiment and load Resistance of 100(ohms). 3) Solar power meter (Make: TENMARS TM-207). 4) Cooling fan (230V), 5) Banana type connecting pins as per requirement (2A Capacity). 6) Dust samples: a) Iron ore b) Coal c) Limestone d) Sandstone. 7) Digital weighing machine (Make: SRS-120) used for the dust samples' weight. With the help of a flour mesh with the sieve size approx. (15-20mm) dust samples were spread uniformly on the Polycrystalline photovoltaic panel under artificial lighting source. After evenly spreading the dust samples of different weight, at different irradiation levels 500,700,900W/m^2, the results are collected.

5. I-V and P-V characteristics of series and parallel connected PV modules by variation of radiation and temperature for series and parallel connected PV modules.

Photo voltaic panels can be connected in either series or parallel combinations to increase the voltage or current capacity of solar array. However, the solar panels are connected, the upper hand corner will always be the maximum power point (MPP) of the array. From this we can find fill factor and efficiency of solar panels.

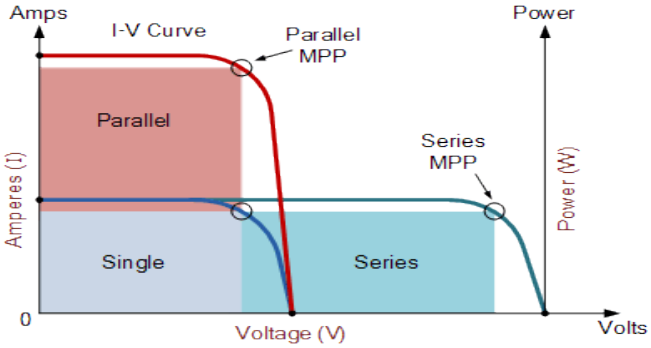

Figure 3: I-V Characteristics of series and parallel connected PV module

By the variation of radiation and temperature for series and parallel connected PV Modules we observed in the Figure 4 and 5 the I-V Characteristics of parallel and P-V Characteristics of parallel are both connected PV modules with constant temperature of 30°C and different irradiance levels of 1002 W/m^2 and 508 W/m^2.

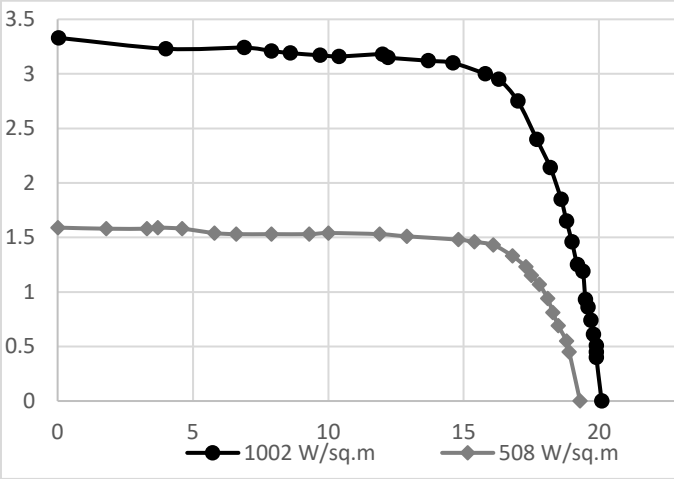

Figure 4: I-V Characteristics of parallel connected PV Modules with constant temperature of 30°C and irradiance of 1002 W/m^2 and 508 W/m^2

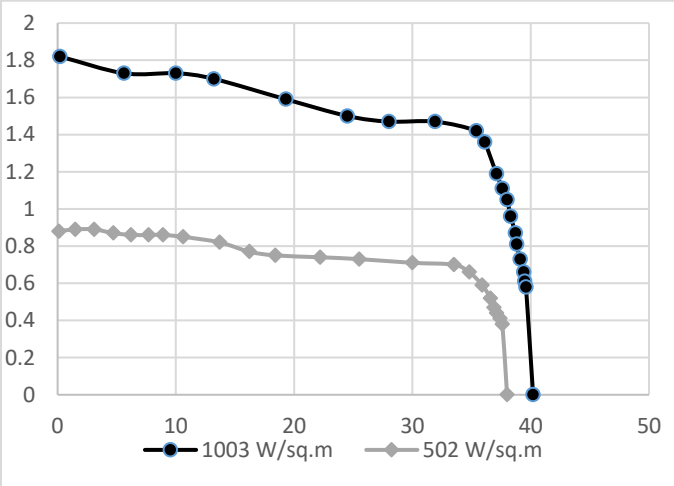

Figure 5: I-V Characteristics of series connected PV Modules with constant temperature of 29°C and irradiance of 1003 W/m^2 and 502 W/m^2

Figure 6: Solar PV Modules Installed at Mine

6. Solar Power Generation at Mine

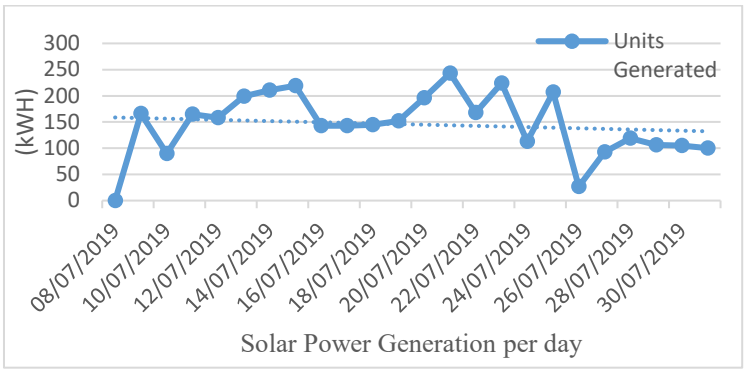

Figure 7: Solar Power Generated per day

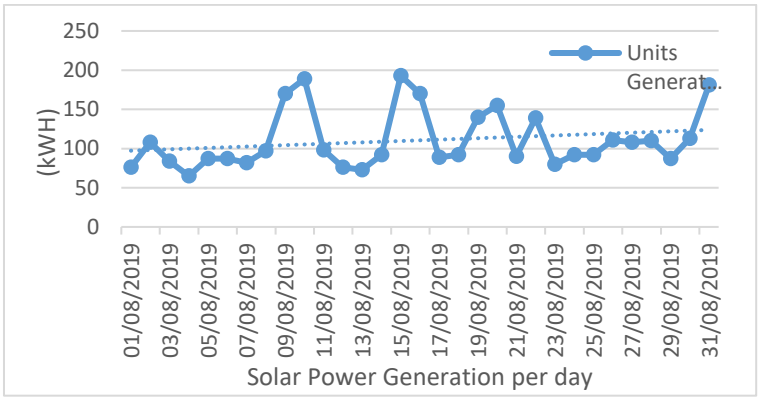

Figure 8: Solar Power Generated per day

6.1 Monthly Load Profile of Solar Power Generation

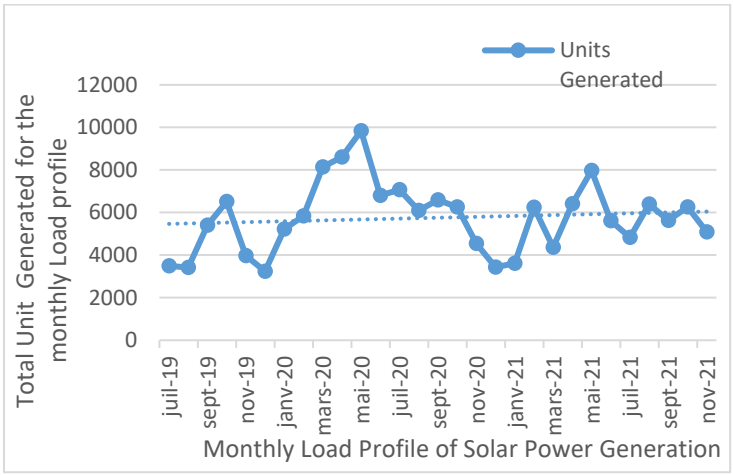

Figure 9: Monthly Load Profile of Solar Power Generation in Mines

Based on the Solar power generation in mines we have observed from the figures (7 to 9). power generation per day. In every month we have observed that maximum 200 plus units are generated per day and minimum 50 plus units are generated in few days this is because of the Environmental conditions in the Mining areas such as (solar radiation, temperature, dust, humidity etc.) Especially in few months we observed the days are cloudy, heavy rainfall, wind speed because of this generation unit is getting low.

7. Characterization of Collected Dust samples

Figure 10: Collected dust samples presently used in experimental study (a) iron ore (b) coal (c) limestone (d) sandstone

7.1 Surface Morphology of Dust Samples

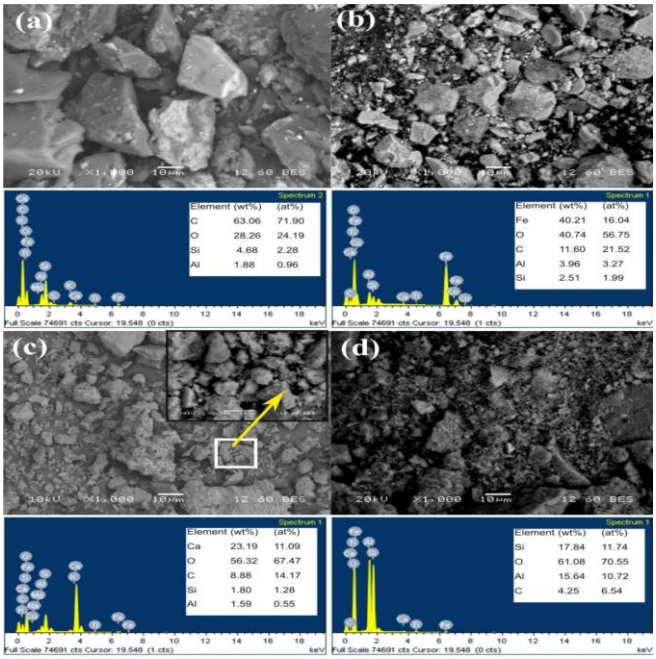

Figure 11: SEM images of the collected dust samples presently used in experimental study (a) iron ore (b) coal (c) limestone (d) sandstone

Scanning Electron Microscope was used to Examine the surface Morphology of collected dust from the mines. Figure:4 reveals the surface morphology of the collected dust particles from the SEM images it can be observed that the dust collected from the mines was dominated by very fine and silt particles.

7.2 Microstructure study of dust powders

Figure 11(a-d) shows the SEM micrographs and EDS spectra of coal, iron ore, limestone, and sandstone powders. It has been observed from the Figure (d) that the dust powder particles are irregular in shape and are in various sizes. This distribution of particle sizes and shapes influences the dust's shading effect on the PV module surface and the power output[83]. The coal and iron ore powders in Figure 11 (a) and (b) contain particles with an average length of 30.82µm, 13µm, respectively. The limestone and sandstone powders in Figure 4(c) and (d) contain very fine particles with agglomerations. It has been observed from the EDS analysis of the powders, the major constituents in coal, iron ore, limestone, and sandstone are carbon (71.90 weight %), iron (40.21 weight %), calcium (23.19 weight%), and silicon (17.84 weight %), respectively. The oxygen present in all powders in higher content with 20-60 w%, carbon, aluminum, and silicon are present nearly (2- 10) weight%.

8. Conclusion

In this experimental study, different mine dust samples of different weights are used at three irradiance values of 500, 700, 900 W/m^2 used to get the output of the Solar panel in terms of current (I), voltage(V), and power (W). In this study, dust samples are taken for the analysis of power output results. PV module outputs like voltage, current, and power are observed with four different mine dust samples.

According to the Data observation at Iron ore 80g weight sample, the maximum power loss of 68.50, 66.45 and 57.51% have been observed at three different irradiation levels of 500, 700, 900W/m^2 have been found. For Coal dust, 80g weight sample the maximum power loss of 97.75, 97.31, and 97.90% is observed at three different irradiation levels of 500, 700, 900W/m^2 have been found,

For the limestone 80g weight sample, the maximum power loss of 85.65, 85.53 and 87.74 % have been observed at three different irradiation levels of 500,700,900W/m^2 have found. For the Sandstone 80g weight sample, the maximum power loss of 80.72, 83.99 and 82.75% saw at three different irradiation levels of 500,700, 900W/m^2. The maximum power loss in percentage found in the Coal dust sample at three different irradiation levels of 500,700,900W/m^2. Due to the high density of coal dust power loss increased in the PV module.

In the observation of 20g of accumulated coal dust on the solar panel, it can reduce its power loss up to 66.29%, for 80g of accumulated coal dust on the solar panel. It can reduce its power loss up to 97.75%for 500W/m^2. For the same dust particle with different irradiance 700W/m^2 80gm of accumulated coal dust power loss up to 97.33% for the same coal dust particle with different irradiance 900W/m^2 for 80 gm of accumulated coal dust on PV module can reduce up to 97.90%.

In addition, from Images of SEM analysis, as shown in Fig (4), the coal dust sample is found with tiny particles in size of all samples taken in the experimental study. It indicates that finite dust particles are also going to affect the performance of the solar PV module. Different types of dust samples are collected from different Remote mining areas. In addition, it refers that the tiny dust sample size of the particle is inversely proportional to power loss in the solar PV module.

9. Acknowledgments

I wish to acknowledge my thanks to Mr. P. K. Panda, Sr. President ESSEL Mining company for providing me the necessary data for carrying out this study.

10. References

[1] A. A. Hegazy, “Effect of dust accumulation on solar transmittance through glass covers of plate-type collectors,” *Renew. energy*, vol. 22, no. 4, pp. 525–540, 2001, doi: 10.1016/S0960-1481(00)00093-8.

[2] H. Gunerhan, A. Hepbasli, and U. Giresunlu, “Environmentalimpacts from the solar energy systems,” *Energy Sources, Part A Recover. Util. Environ. Eff.*, vol. 31, no. 2, pp. 1131–1138, 2009, doi: 10.1080/15567030701512733.

[3] M. Luqman, S. R. Ahmad, S. Khan, U. Ahmad, A. Raza, and F. Akmal, "Estimation of Solar Energy Potential from Rooftop of Punjab Government Servants Cooperative Housing Society Lahore Using GIS," *Smart Grid Renew. Energy*, vol. 06, no. 05, pp. 128–139, 2015, doi: 10.4236/sgre.2015.65012.

[4] H. Jiang, L. Lu, and K. Sun, "Experimental investigation of the impact of airborne dust deposition on the performance of solar photovoltaic (PV) modules," *Atmos. Environ.*, vol. 45, no. 25, pp. 4299–4304, 2011, doi: 10.1016/j.atmosenv.2011.04.084.

[5] B. V Chikate and Y. Sadawarte Assistant Professor BDCOE Sewagram, "The Factors Affecting the Performance of Solar Cell," *Int. J. Comput. Appl. Sci. Technol.*, pp. 975–8887, 2015.

[6] M. Saidan, A. G. Albaali, E. Alasis, and J. K. Kaldellis, "Experimental study on the effect of dust deposition on solar photovoltaic panels in desert environment," *Renew. Energy*, vol. 92, pp. 499–505, 2016, doi: 10.1016/j.renene.2016.02.031.

[7] A. Hussain, A. Batra, and R. Pachauri, "An experimental study on effect of dust on power loss in solar photovoltaic module," *Renewables Wind. Water, Sol.*, vol. 4, no. 1, 2017, doi: 10.1186/s40807-017-0043-y.

[8] A. M. El-Nashar, "The effect of dust accumulation on the performance of evacuated tube collectors," *Sol. Energy*, vol. 53, no. 1, pp. 105–115, 1994, doi: 10.1016/S0038-092X(94)90610-6.

[9] V. M. Fthenakis, C. K. Hyung, and E. Alsema, "Emissions from photovoltaic life cycles," *Environ. Sci. Technol.*, vol. 42, no. 6, pp. 2168–2174, 2008, doi: 10.1021/es071763q.

[10] A. A. Allataifeh, K. Bataineh, and M. Al-Khedher, "Maximum Power Point Tracking Using Fuzzy Logic Controller under Partial Conditions," *Smart Grid Renew. Energy*, vol. 06, no. 01, pp. 1–13, 2015, doi: 10.4236/sgre.2015.61001.

[11] M. Mani and R. Pillai, "Impact of dust on solar photovoltaic (PV) performance: Research status, challenges and recommendations," *Renew. Sustain. Energy Rev.*, vol. 14, no. 9, pp. 3124–3131, 2010, doi: 10.1016/j.rser.2010.07.065.

[12] R. R. Hernandez *et al.*, "Environmental impacts of utility-scale solar energy," *Renew. Sustain. Energy Rev.*, vol. 29, no. November 2017, pp. 766–779, 2014, doi: 10.1016/j.rser.2013.08.041.

[13] M. S. El-Shobokshy and F. M. Hussein, "Effect of dust with different physical properties on the performance of photovoltaic cells," *Sol. Energy*, vol. 51, no. 6, pp. 505–511, 1993, doi: 10.1016/0038-092X(93)90135-B.

[14] Green, M. A. (1982). "Solar cells: operating principles, technology, and system applications." Englewood Cliffs, NJ, Prentice-Hall, Inc., 1982. 288 p.

Energy and environmental impact of banning the sale of traditional fossil fuel vehicles

Shouheng Sun
School of Economics and Management
University of Science and Technology Beijing
Beijing, China
shouhengsun@163.com

Qi Wu
School of Finance
Hebei University of Economics and Business
Shijiazhuang, China
kikimama8@163.com

Dafei Yang
School of Economics and Management
Beijing Institute of Petrochemical Technology
Beijing, China
dafeiyang@126.com

Abstract

This study investigates the energy and environmental impacts of banning the sale of traditional fossil fuel vehicles in China. By using the Logistic model, the dynamic evolution of China's vehicle market under different timing of banning the sale of traditional fuel vehicles was simulated. Based on this, the fossil energy saving and greenhouse gas emission reduction potential of promoting new energy vehicles under different energy development scenarios was further explored from the life cycle perspective. The results show that under China's current electricity mix, the life cycle GHG emissions intensity and fossil energy consumption intensity of battery electric vehicles are about 40.94% (120.04 g CO2-eq/km) and 45.90% (1.68 MJ/km) lower than those of gasoline-powered vehicles, respectively. As the proportion of renewable electricity generation continues to increase, by 2050, replacing traditional fuel vehicles with battery electric vehicles can reduce GHG emissions and fossil energy consumption by up to 58.26% and 53.03%, respectively. In addition, if China plans to ban the sale of traditional fuel vehicles between 2040 and 2060, the cumulative fossil energy savings and GHG emissions reductions during the period of 2020~2050 can reach approximately 32.54~129.10 million TJ and 2.70 ~ 9.32 billion tons of CO2-eq, respectively.

Keywords: Battery Electric Vehicle, Ban Sales of Fossil Fuel Vehicles, Fuel Life Cycle, Fossil Energy Consumption, Greenhouse Gas Emissions, Logistic Equation

I. INTRODUCTION

Traditional fossil fuel (e.g., diesel and gasoline) vehicle (TFV) have become the major source of GHG emissions and fossil energy consumption around the world[1–3]. As a promising way to promote the transition of the energy and environment to sustainability, the development and promotion of new energy vehicle (NEV) has become an irreversible global wave and trend [4–6]. However, the academic research on NEVs mainly focuses on relevant industrial policies, consumer behavior, vehicle and fuel technology, and their competitive advantages over TFVs in terms of energy and environmental sustainability [7–11], few studies discuss the energy and environmental impacts of the medium-and long-term development of NEVs for a country or region. In addition, the development of NEVs industry is not isolated, but closely linked with the coordinated development of other industries. The market evolution of NEVs and the corresponding energy and environmental impacts depend on regional energy planning and the level of development of vehicle and fuel technologies. In turn, promoting NEVs can also affect the development of these related aspects to a certain extent. Currently, many countries around the world have drawn up timetables for the withdrawal of traditional fossil fuel vehicles from the market (i.e., plans to ban the sales of TFVs), which will exert a complex and great impact on the energy, environment and the development of related industries. Therefore, it is of great significance to study the impact of medium and long-term development of NEVs on energy and the environment in the context of banning the sale of traditional fossil fuel vehicles, which can provide valuable insights for policy formulation and industrial planning to promote healthy and sustainable development in an all-round way. Taking China as an example, this paper systematically and deeply analyzes the energy and environmental impact of banning the sale of traditional fossil fuel vehicles on the basis of fully considering the energy development scenario, vehicle and fuel technology and market evolution. It attempts to provide a forward-looking reference for authorities to formulate reasonable and effective industrial planning, so as to better promote the coordinated and orderly development of energy, environment, automobile and other related industries.

II. MATERIALS AND METHODS

This study investigates the energy and environmental impacts of banning the sale of traditional fossil fuel vehicles in China from a life cycle perspective. Life cycle assessment (LCA) is a standardized method to measures the impact of products and services throughout its life cycle, covering the phases of resource extraction, manufacture, distribution, use, and disposal [12,13]. Considering that nearly 90% of cars in China are light-duty gasoline passenger cars, and battery electric vehicles (BEV) are the main direction of the development of the new energy vehicle industry, this study selects light duty passenger vehicles as the research object for comparative analysis.The system boundary of this study is shown in Figure1. The fuel types involved in the LCA analysis are gasoline

IEECP'22, July 21-22, 2022, Oxford, United Kingdom

and electricity. In this article, relevant data are derived from the statistical reports of China's transportation and energy industries, peer-reviewed journal articles, and other scientific and technical literature. The vehicle life cycle inventory data are mainly based on the Ecoinvent database.

The overall analysis framework of this study is as follows. Based on the energy planning and vehicle technology, it first compared and analyzed the fossil energy consumption intensity and the GHG emission intensity of BEV and TFV by using the life cycle assessment methods. Then, it uses Logistic equation to obtain the evolution of China automobile market under different scenarios of banning sale of TFV. Finally, combined with the fossil energy consumption intensity and the GHG emission intensity of BEV and TFV, and the market evolution of automobile in China under different scenarios of banning the sales of TFV, it investigates the energy and environment impacts of the medium-and long-term deployment of BEV.

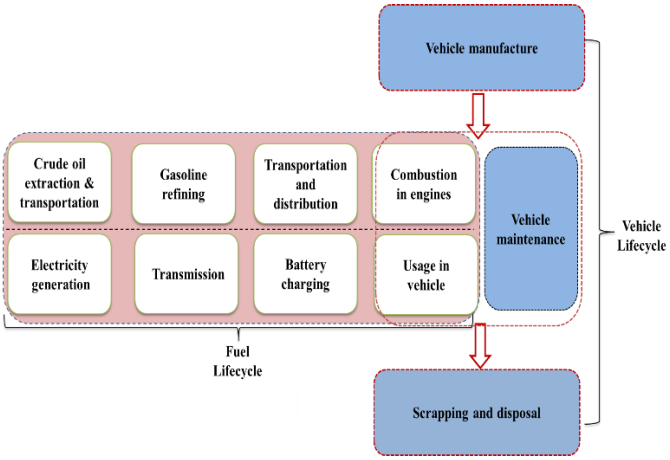

Figure 1. System boundary of the life cycle assessment

The Logistic equation was used to simulate and predict the growth trend of China's automobile market[14–16], as shown in Eq. (1).

$$M(t) = \frac{A}{1+Be^{-Ct}} \quad (1)$$

Where A refers to the maximum capacity of China's automobile market. $M(t)$ refers to the car ownership at time t. B and C are the two parameters of the logistic equation to be estimated.

In order to cooperate with the development of BEV industry, China has formulated relevant energy development plans to better ease the pressure on energy and environment. In this study, two energy scenarios were used to further explore the potential of BEV in energy saving and GHG emissions reduction: high-proportion thermal power scenario and low-proportion thermal power scenario, the details are shown in Figure 2 and Figure3.

For high-proportion thermal power scenario, the proportion of the coal-based thermal power generation is expected to drop to about 60% in 2030 and about 45% in 2050 [17,18]. As to the low-proportion thermal power scenario, the proportion of the coal-based thermal power generation is expected to drop to about 45% in 2030 and about 11% in 2050 [19,20] . At the same time, the fossil energy consumption of the coal-based thermal power generation is expected to drop to 8.50 MJ/kWh in2030, and 8.06 MJ /kWh in 2050[19,21]. In addition, the fuel economy of vehicles on road in China are presented in Figure 4.

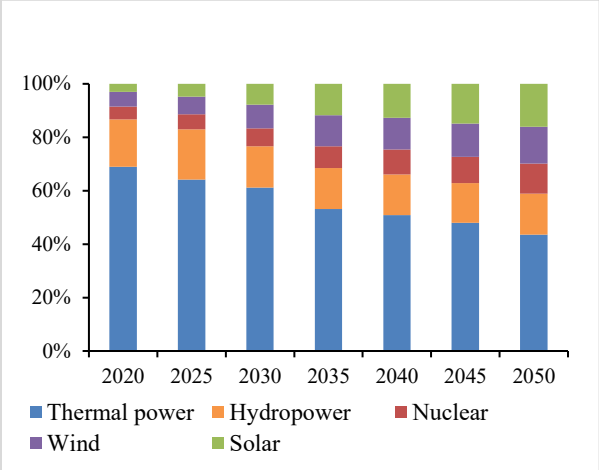

Figure2. High-proportion thermal power scenario in China

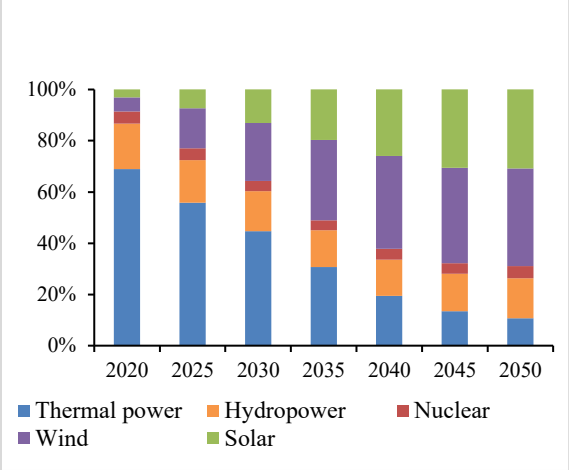

Figure 3. Low-proportion thermal power scenario in China

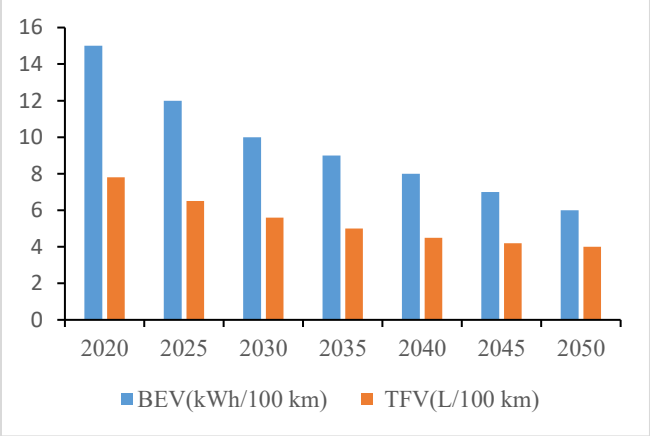

Figure 4. The fuel economy of vehicles on road in China [22–24]

III. RESULTS

A. Fossil Energy Consumption Intensity and GHG Emission Intensity of BEV and TFV

Based on the above energy planning and assumption, we compared and analyzed the fossil energy consumption intensity and the GHG emission intensity of BEV and TFV, as shown in Figure 5 and Figure 6.

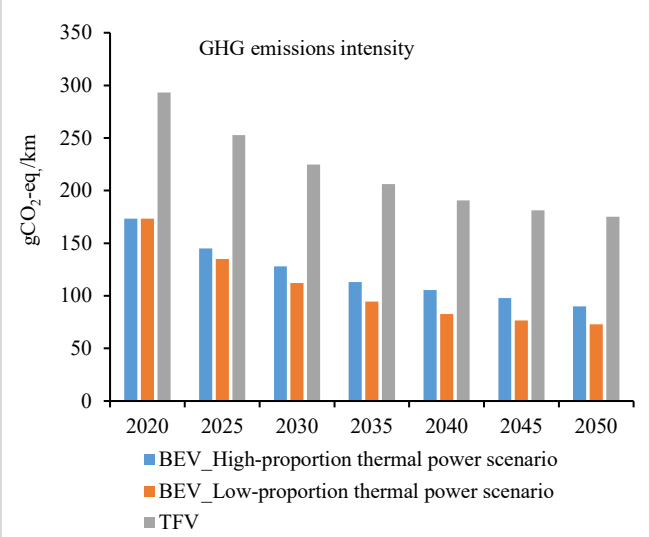

Figure 5. Comparison in GHG emissions intensity of TFV and BEV under different scenarios

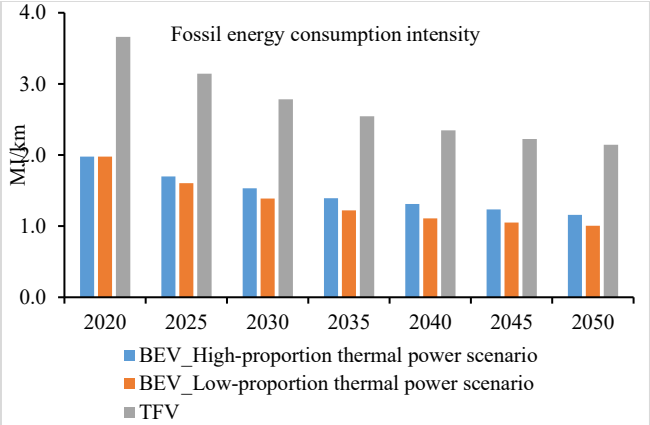

Figure 6. Comparison in fossil energy consumption intensity of TFV and BEV under different scenarios

As can be seen from Figure 5 and Figure 6, with the increase in the proportion of renewable electricity generation and the power generation efficiency of coal-fired thermal power stations, the advantages of BEV in energy conservation and emission reduction will become more and more significant. Under the high-proportion thermal power scenario, the GHG emission intensity of BEV will drop to 128.02 g CO2-eq/km in 2030 and 90.07 g CO2-eq/km in 2050, while the fossil energy consumption intensity of BEV could also be reduced to 1.53 MJ/km in 2030 and 1.16MJ/km in 2050. This means that replacing TFV with BEV can reduce GHG emissions and fossil energy consumption by up to 48.55% and 46.08%, respectively. If China's energy development follows the low-proportion thermal power scenario, the GHG emission intensity of BEV will drop to 112.11g CO2-eq/km in 2030 and 73.07 g CO2-eq/km in 2050, while the fossil energy consumption intensity of BEV could also be reduced to 1.39MJ/km in 2030 and 1.09MJ/km in 2050. Under this energy development scenario, replacing TFV with BEV can reduce GHG emissions and fossil energy consumption by up to 58.26% and 53.03%, respectively. Therefore, promoting BEV has great prospects in reducing fossil energy consumption and GHG emissions.

B. Dynamic evolution of China's auto market

This paper uses the Logistic equation to obtain the development trend of BEV and TFV under scenarios of banning the sale of TFV by 2040, 2050, and 2060 in China, respectively. The detailed results are shown in Figures 7–9. It can be seen that if China bans the sale of TFV from 2060, the market scale of BEV will exceed 100 million around 2042 and surpass the market scale of TFV by 2049. If China bans the sale of TFV from 2050, the number of BEV will reach 100 million around 2037 and then surpass the market scale of TFV around 2041. In particular, If China plans to ban the sale of TFV from 2040, the market scale of BEV will exceed that of TFV by around 2035.

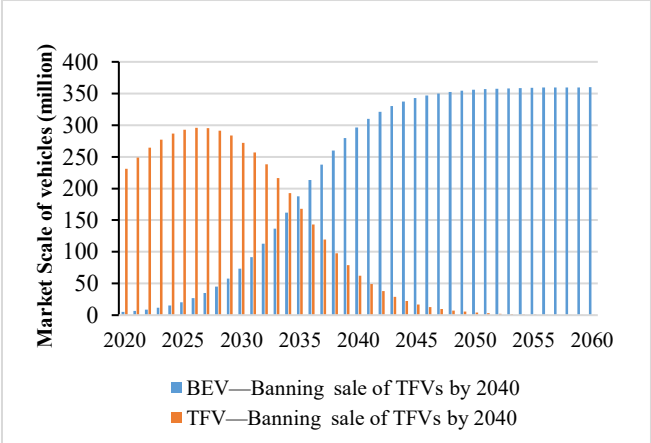

Figure 7. Market evolution under the scenario of banning the sale of TFV by 2040

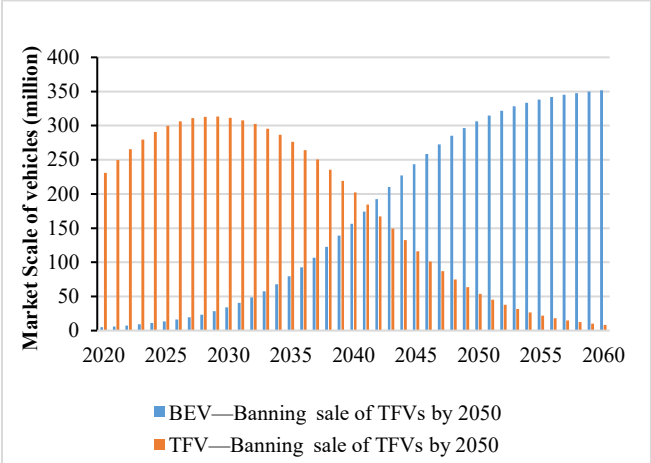

Figure 8. Market evolution under the scenario of banning the sale of TFV by 2050

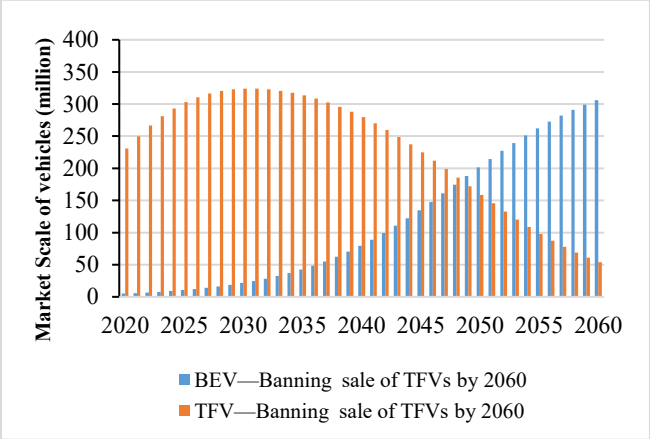

Figure 9. Market evolution under the scenario of banning the sale of TFV by 2060

C. The Energy and Environmental Impact of Banning the Sale of TFVs

In order to investigate the energy and environmental impacts of the medium-and long-term deployment of BEV, based on the BEV development trends and the energy planning scenario, we first calculated and compared the annual GHG emissions and energy consumption of the entire China automobile market with and without BEV, and then used 2020 as the starting point to calculate the cumulative fossil energy savings and GHG emission reductions brought about by the promotion of BEV during the period of 2020 ~ 2050. The detailed results are shown in Figure 10 and Figure11.

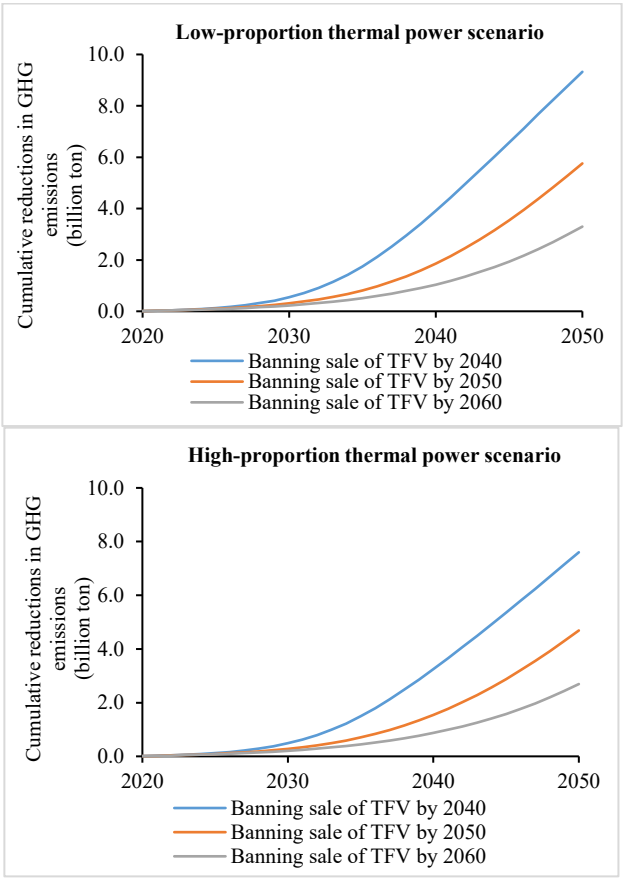

Figure 10. Cumulative GHG emissions reduction under different scenarios

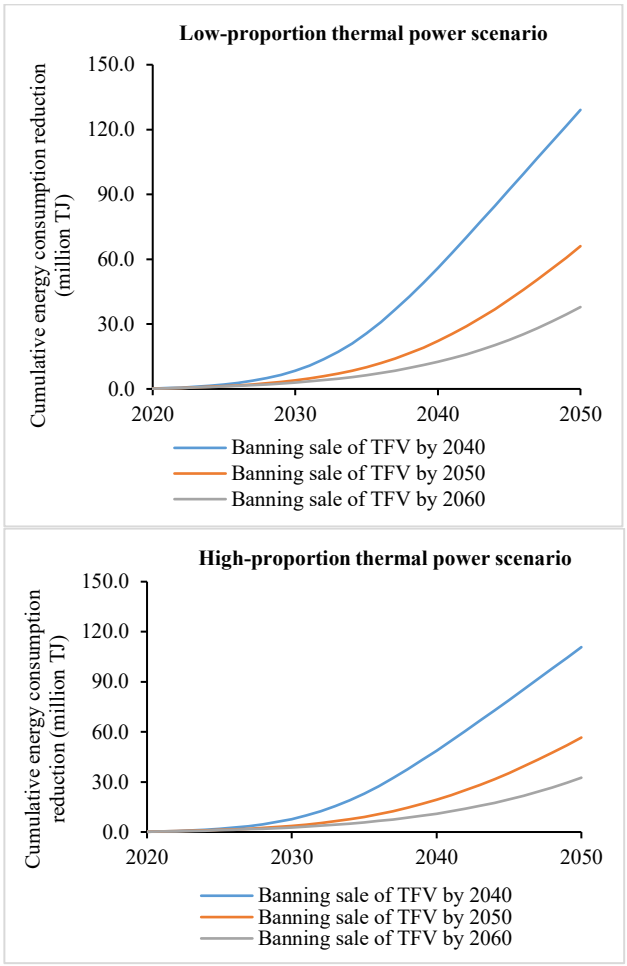

Figure 11. Cumulative energy consumption reduction under different scenarios

It can be seen from Figure 10 and Figure 11 that the promotion of BEV can significantly reduce the GHG emissions and fossil energy consumption of the automobiles market in China. If China plans to ban the sales of TFV from 2060, under the high-proportion thermal power scenario, a cumulative fossil energy savings of 2.74 million TJ and a cumulative GHG emissions reduction of 0.21 billion tons of CO2-eq can be achieved by 2030. By 2050, the cumulative energy-saving and GHG emissions reduction can reach 32.54 million TJ and 2.70 billion tons of CO2-eq, respectively. Furthermore, under the low-proportion thermal power scenario, the cumulative energy savings and GHG emissions reduction can reach 2.94 million TJ and 0.23 billion tons of CO2-eq by 2030 and 37.88 million TJ and 3.30 billion tons of CO2-eq by 2050. If the sale of TFV will be banned from 2050, with the continuous market diffusion of BEV, the cumulative energy savings by 2030 can reach 3.70 million TJ under high-proportion thermal power scenario and 3.99 million TJ under low-proportion thermal power scenario. In addition, the cumulative GHG emissions reduction by 2030 can also reach 0.28 billion tons of CO2-eq under high-proportion thermal power scenario and 0.31 billion tons of CO2-eq under low-proportion thermal power scenario. Furthermore, by 2050, the cumulative energy savings can reach 56.60 million TJ under high-proportion thermal power scenario and 66.05 million TJ under low-proportion thermal power scenario, and the cumulative GHG emissions reduction can also reach 4.69 billion tons of CO2-eq under high-proportion thermal power scenario and 5.76 billion tons of CO2-eq under low-proportion thermal power scenario.

In particular, if China plans to ban the sale of TFV by 2040, under the high-proportion thermal power scenario, the cumulative energy savings and GHG emissions reduction can reach 7.75 million TJ and 0.49 billion tons of CO2-eq by 2030. By 2050, the cumulative energy savings and GHG emissions reduction can reach 110.78 million TJ and 7.60 billion tons of CO2-eq, respectively. Furthermore, under the low-proportion thermal power scenario, the cumulative energy savings and GHG emissions reduction can reach 8.39 million TJ and 0.55 billion tons of CO2-eq by 2030 and 129.10 million TJ and 9.32 billion tons of CO2-eq by 2050.

IV. DISCUSSION AND CONCLUSIONS

This study investigates the energy and environmental impacts of banning the sale of traditional fossil fuel vehicles in China from a life cycle perspective. Combined with the development of China's energy sector and vehicle and fuel technology, the comparative advantages of BEV over the traditional gasoline-powered vehicle in terms of energy-saving and GHG emissions reduction was analyzed. In addition, the Logistic equation was used to simulate and predict the growth trend of BEV at different timing of banning the sale of TFV. Finally, on the basis of the market scale of BEV and TFV in China, the impact of the medium and long-term development of BEV on energy and the environment was further estimated. The main conclusions are shown as follows.

BEV has great potential in reducing fossil energy consumption and GHG emissions. Under China's current electricity mix, the life cycle GHG emissions intensity and fossil energy consumption intensity of BEV is about 40.94% (120.04 g CO2-eq/km) and 45.90% (1.68 MJ/km) lower than those of TFV, respectively. As the proportion of renewable electricity generation and the power generation efficiency of coal-fired thermal power stations continue to increase, the advantages of BEV in energy conservation and emission reduction will become more and more significant. By 2050, under the high-proportion thermal power scenario, replacing TFV with BEV can reduce GHG emissions and fossil energy consumption by up to 48.55% and 46.08%. In particular, if China's energy development follows the low-proportion thermal power scenario, replacing TFV with BEV can reduce GHG emissions and fossil energy consumption by up to 58.26% and 53.03%, respectively.

If China bans the sale of TFV from 2060, the market scale of BEV will exceed 100 million around 2042 and surpass the market scale of TFV by 2049. During 2020 ~ 2050, the cumulative fossil energy savings and GHG emissions reductions can reach 32.54~37.88 million TJ and 2.70 ~ 3.30 billion tons of CO2-eq, respectively. If China bans the sale of TFV from 2050, the number of BEV will reach 100 million around 2037 and then surpass the market scale of TFV around 2041. During the period of 2020~2050, a total of approximately 56.60~66.05 million TJ fossil energy savings and 4.69 ~ 5.76 billion tons of CO2-eq GHG emissions reductions can be obtained. In particular, if China plans to ban the sale of TFV from 2040, the market scale of BEV will exceed that of TFV by around 2035. During 2020 ~ 2050, the cumulative fossil energy savings and GHG emissions reduction can reach approximately 110.78~129.10 million TJ and 7.60 ~ 9.32 billion tons of CO2-eq, respectively.

Nowadays, China faces increasing pressure on energy and the environment in the process of economic development. Vigorously promoting new energy vehicles is one of the potential ways to effectively alleviate these problems. In order to better achieve sustainable and healthy development of China's new energy vehicle industry, authorities should formulate scientific and reasonable industrial strategies and policies, strengthen technological innovation, and accelerate the development of supporting industries. Since electricity production is the most important factor that can significantly affect the potential of BEV in reducing GHG emissions and fossil energy consumption in China, relevant national energy development plans such as increasing the proportion of green electricity, controlling the emission standards of the power plants, and continuously improving the generation efficiency of thermal power should be effectively implemented.

However, there also exist some limitations in the study. First, due to the lack of available data, this study selects passenger cars as the research object for comparative analysis and does not consider other components of the road transportation system such as transit buses, sanitation vehicles, and other types of heavy-duty vehicles. Furthermore, in terms of environmental impact, the LCA study only focuses on GHG emissions and does not include broader impacts on human health, ecosystems, and resource availability. All these need to be further supplemented and improved in the future.

V. REFERENCES

[1] Hulshof, D.; Mulder, M. Willingness to Pay for $$\hbox {CO} _2 $$ CO2 Emission Reductions in Passenger Car Transport. *Environ. Resour. Econ.* **2020**, *75*, 899–929.

[2] Matak, N.; Krajačić, G. Assessment of mitigation measures contribution to CO 2 reduction in sustainable energy action plan. *Clean Technol. Environ. Policy* **2020**, *22*, 2039–2052.

[3] Ramli, A.F.; Ab Muis, Z.; Ho, W.S.; Idris, A.M.; Mohtar, A. Carbon Emission Pinch Analysis: an application to the transportation sector in Iskandar Malaysia for 2025. *Clean Technol. Environ. Policy* **2019**, *21*, 1899–1911.

[4] Bicer, Y.; Dincer, I. Life cycle environmental impact assessments and comparisons of alternative fuels for clean vehicles. *Resour. Conserv. Recycl.* **2018**, *132*, 141–157.

[5] Hao, H.; Cheng, X.; Liu, Z.; Zhao, F. Electric vehicles for greenhouse gas reduction in China: A cost-effectiveness analysis. *Transp. Res. Part D Transp. Environ.* **2017**, *56*, 68–84, doi:10.1016/j.trd.2017.07.025.

[6] Shinde, A.M.; Dikshit, A.K.; Odlare, M.; Thorin, E.; Schwede, S. Life cycle assessment of bio-methane and biogas-based electricity production from organic waste for utilization as a vehicle fuel. *Clean Technol. Environ. Policy* **2021**, 1–11.

[7] Gnann, T.; Stephens, T.S.; Lin, Z.; Plötz, P.; Liu, C.; Brokate, J. What drives the market for plug-in electric vehicles?-A review of international PEV market diffusion models. *Renew. Sustain. Energy Rev.* **2018**, *93*, 158–164.

[8] Kene, R.; Olwal, T.; van Wyk, B.J. Sustainable Electric Vehicle Transportation. *Sustainability* **2021**, *13*, 12379.

[9] Kowalska-Pyzalska, A.; Kott, M.; Kott, J. How Much Polish Consumers Know about Alternative Fuel Vehicles? Impact of Knowledge on the Willingness to Buy. *Energies* **2021**, *14*, 1438.

[10] Lin, Y.; Wu, J.; Xiong, Y. Sensitivity of the Nonsubsidized Consumption Promotion Mechanisms of New Energy Vehicles to Potential Consumers' Purchase Intention. *Sustainability* **2021**, *13*, 4293.

[11] Sun, X.; Li, Z.; Wang, X.; Li, C. Technology development of electric vehicles: A review. *Energies* **2020**, *13*, 90.

[12] ISO *International Standard 14040. Environmental Management Life Cycle Assessment Requirements and Guidelines.*; 2006;

[13] ISO *International Standard 14040.Environmental Management Life Cycle Assessment Principles and Framework*; 2006;

[14] Morisita, M. The fitting of the logistic equation to the rate of increase of population density. *Popul. Ecol.* **1965**, *7*, 52–55.

[15] Nelder, J.A. 182. note: An alternative form of a generalized logistic equation. *Biometrics* **1962**, *18*, 614–616.

[16] Sun, S.; Wang, W. Analysis on the market evolution of new energy vehicle based on population competition model. *Transp. Res. Part D Transp. Environ.* **2018**, *65*, 36–50.

[17] Elshkaki, A. Material-energy-water-carbon nexus in China's electricity generation system up to 2050. *Energy* **2019**, *189*, 116355.

[18] National Development and Reform Commission *China 2050 high renewable energy penetration scenario and roadmap study*; Beijing, 2016;

[19] China Petroleum Economics and Technology Research Institute *World and China Energy Outlook*; Beijing, 2019;

[20] Zou, P.; Chen, Q.; Yu, Y.; Xia, Q.; Kang, C. Electricity markets evolution with the changing generation mix: An empirical analysis based on China 2050 High Renewable Energy Penetration Roadmap. *Appl. Energy* **2017**, *185*, 56–67.

[21] National Bureau of Statistics of China *China Energy Statistical Yearbook 2020*; China Statistics Press,Beijing, China., 2020;

[22] China Automotive Technology & Research Center *China Energy Saving and New Energy Vehicle Yearbook*; China Railway Publishing House: Beijing, 2020;

[23] Government of China *New Energy Vehicle Industry Development Plan (2021-2035)*; Beijing, 2020;

[24] China state information center *China's auto market outlook in 2021*; Publishing House of Electronics Industry: Beijing, 2021;

Whole-body Vibration Exposure of Opencast HEMM Operators –Development of a Conceptual Structural Equation Model

1st D. R. Grahacharya
Department of Mining Engineering,
National Institute of Technology,
Rourkela, India
email: 220mn1491@nitrkl.ac.in

2nd Falguni Sarkar
Department of Mining Engineering,
National Institute of Technology,
Rourkela, India
ORCID ID: 0000-0002-8254-4380
Email: sarkarf@nitrkl.ac.in

3rd Hrushikesh Naik
Department of Mining Engineering,
National Institute of Technology,
Rourkela, India
ORCID ID: 0000-0002-9605-7081
Email: hknaik@nitrkl.ac.in

Abstract

In the mining industry, HEMM (Heavy Earth Moving Machinery) operators usually suffer from Whole Body Vibration (WBV) exposure. The vibrations generated from machinery sources during operation are transmitted to the human body. There are several undesirable health hazards arises due to WBV exposure in opencast mines, which includes deterioration of 'nervous system', 'circulatory system', 'digestive system', and 'low back pain'. This paper is anticipated to examine how machine condition, haul road condition, operational culture and work time exposure affect vibration exposure of mine operators in an opencast mine. In this context, a conceptual model is developed by means of path-analysis through Structural Equation Modelling (SEM). As there are no statutory guidelines and standardized threshold limit available for WBV with Indian mine operators, relevant clauses of International Organization for Standardization are followed for monitoring WBV.

Keywords: Whole Body Vibration (WBV), opencast mines, conceptual model, SEM, ISO 2631-1(1997), ISO 2631-5(2004)

I. INTRODUCTION

Mining is an essential operation for sustainability of Indian power sector and economic environment. As mining is the backbone of Indian power sector and economy, we must continue mining uninterruptedly. It is very known fact that the mining operation involves many challenges with respect to safety of mine workers. Various agencies have been conducting a significant number of scientific investigations on the methodological and behavioral characteristics of mine safety, miner's health and mine based occupational diseases. However, the multifaceted mechanisms that lie beneath the contributory associations of safety perceptions and mine injuries are still not entirely explored [1]. "In recent years, researchers have been trying to comprehend the hidden structures, including environmental, organizational and socio-technical factors that potentially lead to accidents and fatalities in mining complexes" [1-4]. Although health hazards like dust, noise and noxious fumes etc. engrossed researchers' attention, health problems arise due to exposure of whole-body vibration remained dormant for several years. The human body parts most prone to have an effect due to WBV depend on the "magnitude of vibration, the frequency of vibration, distribution of the motion within the body, body postures, and, direction, and duration of vibration"[5]. There is physically powerful evidence that work-related exposure to WBV is allied with an augmented risk of "Low Back Pain (LBP), sciatic pain, and degenerative changes in the spinal system including lumbar inter-vertebral disc disorders and chronic pain etc."[6]. the diseases encountered due to WBV can increase sick leave, minor-disabilities, and man day's loss etc.

Operators of HEMM deployed in open cast mines viz. motor grader, dozer, crane, rock breaker, dumper, excavators, and large diameter drill are exposed to high level of WBV and if they are exposed to vibration more than threshold limits (As given in ISO) for long time, than they may start suffering from many diseases and physical problems which may turn into serious if not taken care of properly [7-12]. In Indian mining scenario, vibration is not considered as major aspect till date, therefore proper management actions should be introduced in Indian mines for fighting against vibration related diseases. Design and implementation of proactive WBV management plan are required, so that the effect of WBV can be assessed and diagnosed properly.

This paper is anticipated to examine how machine condition, haul road condition, operational culture and work time exposure affect vibration exposure of mine HEMM operators in an opencast mine. In this context, a conceptual model is developed by means of path-analysis through Structural Equation Modelling (SEM). Structural equation modelling (SEM) has been recurrently applied in mine accident analysis, safety management, and other fields [13]. Complex associations between exogenous latent variables and endogenous variables are generally investigated by using SEM [13]. SEM essentially comprises a measurement model and a latent variable model (path analysis) that demarcate the relations among latent variables [14].

IEECP'22, July 21-22, 2022, Oxford, United Kingdom

A. Whole-body Vibration Standards

ISO technical committee submitted the first draft proposal, "Classification of the Influence of Mechanical Vibration of Man", in June 1964 was tabled. After getting green signal and consent from 19 countries (UK and USSR not given consent) the finalized provisions of standard were enforced and made available. The standard was amended in 1978, 1982 and 1985 respectively.

a) ISO 2631-1(1997)

Comprehensive modification of ISO 2631 was commenced in 1979 and the new standard was finally published in 1997 in association with BS 6841. The appraisal methods comprise the fourth power VDV (Vibration Dose Value) and a running RMS (Root Mean Square) method with one-second time constant [15]. Indirect type of Health protection guidance is provided according to the VDV value. However, no guidance is provided for the running RMS method [15].

b) ISO 2631-5:2004

ISO 2631-5:2004 addresses "human exposures to mechanical multiple shocks measured at the seat pad when a person is seated". The adverse health effect in contrast to long vibration exposure with multiple shocks is related to dose measures. This version of the ISO standard towards WBV was concerned to show the adverse health effect in the lumbar spine [15]. WBV limits for the eight-hour working condition according to health guidance caution zone (HGCZ) are shown in Table1 **(As per ISO 2631-1 1997, Annex B)**.

Table1: (WBV limits for the eight-hour working condition according to health guidance caution zone (HGCZ) in (ISO 2631-1 1997, Annex B)

Parameter	Exposure action value (EAV)	Exposure limit value (ELV)	Units
RMS	0.45	0.90	m/s^2
VDV	8.5	17	$m/s^{1.75}$

II. ADVERSE IMPACT OF WBV ON HUMAN HEALTH

Mandal, 2006 [6] conducted detailed investigation on WBV exposure scenario of Indian mine workers and found that the vibration of frequencies between 0.5-80Hz is main reason for imposing detrimental effects on the human body parts and organs. The transmission of vibration through HEMMs to the body is dependent on body posture as well as other ergonomic factors. The effects of vibration are therefore complex. Exposure to WBV causes motions and influences on parts of the human body adversely, that may cause discomfort.

- Adversely affect performance.
- Aggravate pre-existing back injuries and
- Present a health and safety risk.
- Low-frequency vibration causes motion sickness

There are many adverse impacts related to WBV and some of the effects are shown in Figure 1.

Figure 1 Problems in lumbar spine due to WBV exposure (Source: Safety news alert, 2014)

III. CONCEPTUAL STRUCTURAL EQUATION MODEL FOR INVESTIGATING VIBRATION IMPACT ON HUMAN BODY

A. Theory and Hypothesis

a) Vehicle condition & maintenance

In opencast mines, the vehicle conditions play a vital role with respect to vibration exposure of operators. Vehicle condition refers to the vehicle age, break down proneness and frequency of maintenance of machine etc. Vehicle condition and maintenance effect on vibration can be measured by considering different manifest variable viz. machine age, frequency of maintenance, break down proneness and working hour of the vehicle.

b) Haulage Road condition

The haul road condition in Indian opencast mines is one of the main factors that affects human vibration exposure. If the road condition in mines is undulating and without proper dimension for transportation of ore/overburden to crusher plant or dump yard, then it leads high exposure of vibration. Blood et al. (2010) [16] concluded that "poor road conditions and maintenance of vehicles lead to an intermittent impact on operators in terms of spinal disorder and fatiguing of associated muscles". Impact of haulage road condition on vibration exposure can be measured by considering different manifest variables viz. frequency of road maintenance, feature of haul road, dimension of haul road and lead distance.

c) Operational culture

Operational culture refers to the working procedure and character of miner. If the mine operators are aware of the vibration problem and is a skilled person then the vibration

exposure will be less at that scenario. Mandal and Srivastava (2010) concluded that "poor environmental condition, habits of miners and posture relates to physical disorder in the form of back pain" [17]. Impact of Operational culture on vibration exposure can be measured by considering different manifest variable like training for operators, awareness of vibration, operators experience and overloading of machine.

d) Work time exposure

Working time directly affects the vibration exposure. It can be varied by different manifest variables i.e., production load, availability of skilled operators, haul road condition and over time. Kim et al. (2018) proposed that "Operators of HEMM's having a long duration of operating time for excavation of mineral may enhance the biomechanical loading in the vertebra and its associated muscles" [18]. Researchers found that "regular exposure for a high time duration to WBV will have the risk of musculoskeletal injuries by fatiguing or damaging the soft parts related to the spine and related associated muscles" [19].

B. In accordance with the above discussion on latent variables, we propose the following research hypothesis:

H-1. Machine condition and maintenance is inversely related to vibration exposure.
H-2. Haulage road condition (poor/good) is inversely related to vibration exposure.
H-3. Machine condition and maintenance is directly related to haul road condition.
H-4. Operational culture is inversely related to vibration exposure.
H-5. Work time exposure is directly related to vibration exposure.
H-6. Work time exposure is inversely related to haul road condition.
H-7. Machine condition and maintenance is directly related to operational culture.

C. The conceptual structural equation model:

The conceptual structural equation model is developed to investigate the vibration exposure of mine operators at opencast mines. The conceptual structural model can be divided into two parts: the measurement model and the structural model. The measurement model denotes how latent constructs are depending on the manifest variables.

A latent variable or construct is a hypothesized and unobserved concept that can only be approximated by observable or measurable variables. **Manifest variable** is the observed or derived value for a specific item or questions, obtained either from the respondent's responses to questions (as in questionnaires) or from observation by the researcher. Manifest variables are used as the indicators of latent constructs or variables.

The measurement model is established by 15 manifest variables such as machine age, frequency of maintenance, number of working hour per day, road maintenance, shape of road, distance of haul road, training, awareness, operators experience, overload condition, production load, availability of skilled operators, over time, haul road distance as indicator of five latent variables such as machine condition and maintenance, haul road distance, operational culture, work time exposure and vibration exposure. The five latent variables are correlated with each other.

The structural model equation represents the path relationship among the latent variables, explains the path effects, and allocates the explained variance. Path model is framed to scrutinize the strength and pattern of relationship amongst the machine condition and maintenance, haul road distance, operational culture, work time exposure and vibration exposure and their sequential relationship leading towards human body injury in mines.

In the path diagram, a straight line with a single arrowhead specifies that the manifest variable closest to the arrowhead is proposed to be caused by the latent variable from which the line emanates. The relationship between manifest variable (X) and latent variable (β) is denoted by lambda (λ). The conceptual Structural Equation Model (SEM) measurement (Figure 2) and structural model (Figure 3) are developed which are represented below schematically. The developed models will be tested for opencast mining industry in due course.

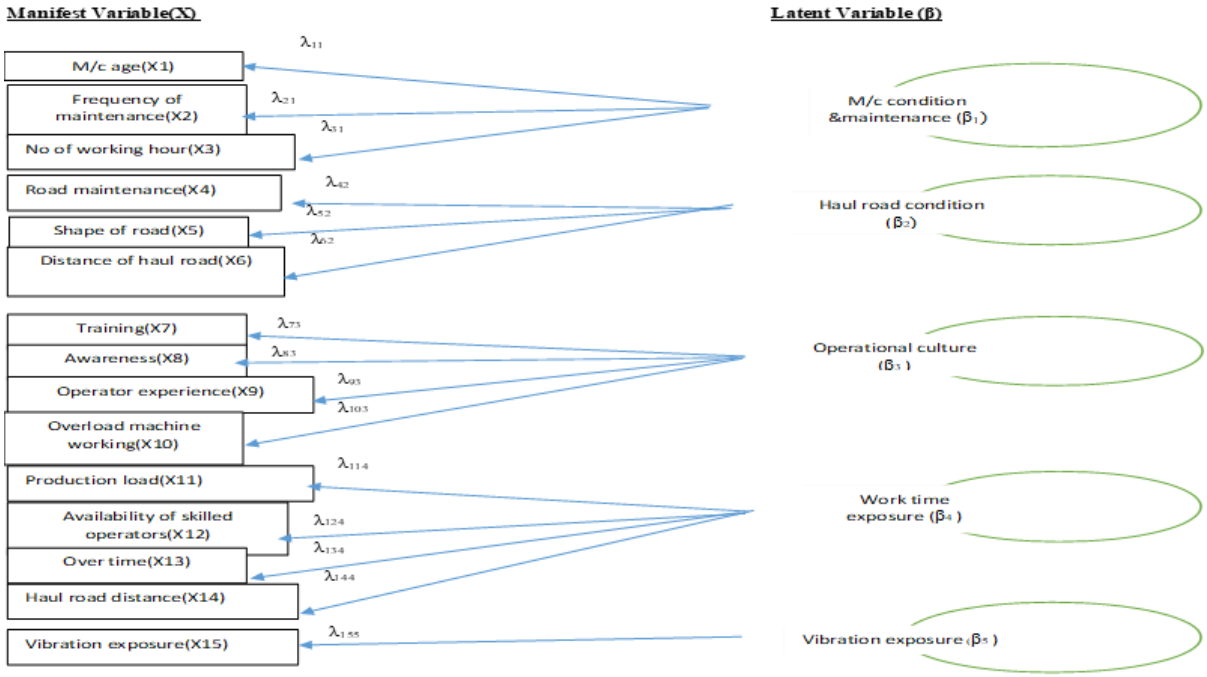

Figure 2 Path diagram of measurement model

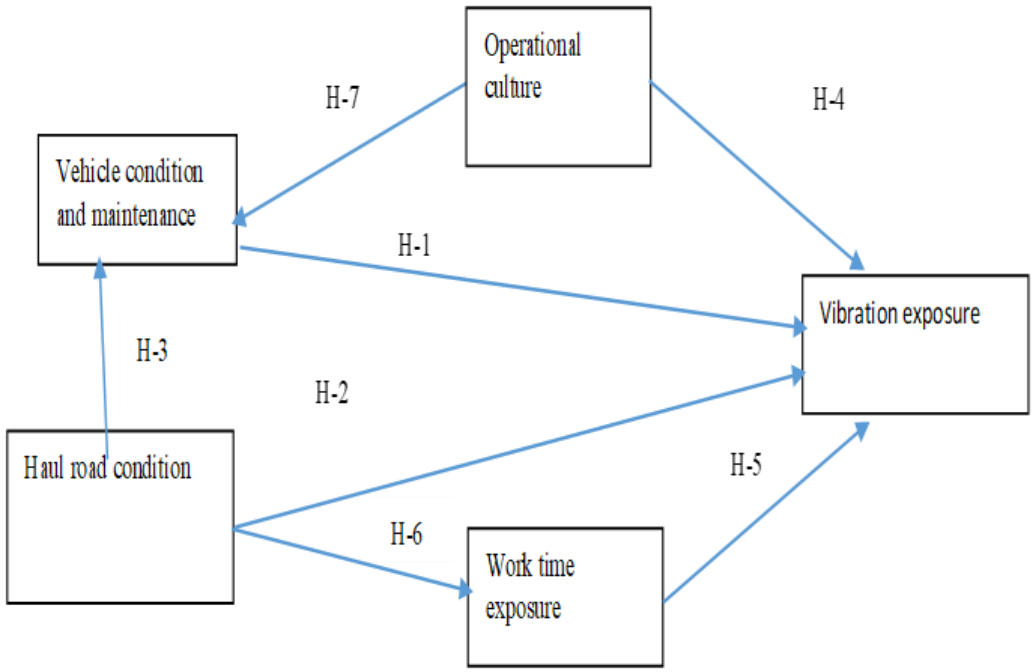

Figure 3 Hypothesized path Diagram among the vibration exposure, m/c condition and maintenance, haul road, operational culture, and work time exposure

IV. CONCLUSION

Study on Whole-body vibration exposure on Indian opencast mine HEMM operators may be considered as a prime issue to improve occupational health and safety scenario of mining industry. It is observed that the detrimental ill-effects (fatigue, insomnia, headaches, and shakiness) are mainly caused by high frequency and magnitudes of vibration faced by the operators during HEMM operation. A conceptual structural equation model (SEM) is developed to show how the vibration exposure in an opencast mine is related to different factors. The relation can be measured by questionnaire survey and by measurement data analysis. Thus, validation of the conceptual model requires extensive field investigation. It is expected that model outcomes will help the mining fraternity to reduce the effect of WBV and enhance OH&S awareness. To sum up the current study highlights machine condition & maintenance, haul road condition, operational culture, and work time exposure as antecedents to vibration exposure of mine operators in open cast mines.

V. ACKNOWLEDGMENTS

We extend our thanks to various authors given in the reference section for their quality research work to which we have referred and acknowledged thankfully.

VI. REFERENCES

[1] Li, S., Sari Y.A. and Kumral M., (2019) "New approaches to cognitive work analysis through latent variable modelling in mining operations", International Journal of Mining Science and Technology 29 (2019) 549–556.

[2] Komljenovic D, Loiselle G, Kumral M., (2017) Organization: a new focus on mine safety improvement in a complex operational and business environment. Int J Min Sci Technol 2017; 27 (4):617–25.

[3] Demir S, Abou-Jaoude E, Kumral M., (2017) Cognitive work analysis to comprehend operations and organizations in the mining industry. Int J Min Sci Techno 2017; 27 (4):605–9.

[4] Erdogan HH, Duzgun HS, Selcuk-Kestel AS., (2020) Quantitative hazard assessment for Zonguldak Coal Basin underground mines. Int J Min. Sci Technol 2020; 29 (3):453–67.

[5] Anand S. Sharma S. K. Mandal G. Suresh (2020) Whole body vibration exposure and its effects on heavy earthmoving machinery (HEMM) operators of opencast mines – a review. Journal of Mines, Metals and Fuels · September 2020.

[6] Mandal BB, Srivastava AK. (2006): Risk from On vibration in Indian mines in Indian Journal of Occupational and Environmental Medicine May 2006.

[7] Emkani, M., Nejad, N. H., Jalilian, H., Gholami, M., Sadeghi, N., and Rahimimoghadam, S. (2016). Exposure to whole-body vibration in heavy mine vehicle drivers and its association with upper limbs musculoskeletal disorders. Journal of Occupational Health and Epidemiology, Vol. 5(4), pp. 226-234.

[8] Erdem B, Dogan T, Duran Z (2020) Assessment of whole-body vibration exposure of mining truck drivers. J South Afr Inst Min Metall 120(9):547–559.

[9] International Organization for Standardization (ISO) (1997) Iso 2631-1:1997. Mechanical vibration and shock-evaluation of human exposure to whole-body vibration-part 1: General requirements. *Geneva* Switzerland: ISO.

[10] Mandal BB, Manwar VD (2017) Prevalence of musculoskeletal disorders among heavy earth moving machinery operators exposed to whole-body vibration in opencast mining. International Journal of Community Medicine and Public Health 4(2017):1566–1572.

[11] Mandal BB, Mansfield NJ (2016) Contribution of individual components of a job cycle on overall severity of whole-body vibration exposure: a study in Indian mines. Int J Occup Saf Ergon 22(1):142–151.

[12] Seidel H. (2005): On the relationship between whole-body vibration exposure and spinal health risk. *Industrial Health,* 43:361–77.

[13] Yingyu Zhang, Wei Shao, Mengjia Zhang, Hejun Li, Shijiu Yin and Yingjun Xu, (2016) "Analysis 320 coal mine accidents using structural equation modelling with unsafe conditions of the rules and regulations as exogenous variables" Accident Analysis and Prevention 92 (2016) 189–201.

[14] Bollen KA. (1989) Structural equations with latent variables. Oxford, England: John Wiley & Sons; 1989.

[15] Luz S. Marin, Andres C. Rodriguez, Estefany Rey-Becerra (2017) Assessment of Whole-Body Vibration Exposure in Mining Earth-moving Equipment and Other Vehicles Used in Surface Mining. Annals of Work Exposures and Health, 2017, Vol. 61, No. 6, 669–680.

[16] Blood RP, Ploger JD, Yost MG, Ching RP, Johnson PW. (2010): Whole body vibration exposures in metropolitan bus drivers: A comparison of three seats. Journal of Sound and Vibration, 329(1):109–20.

[17] Mandal BB, Srivastava AK. (2010): Musculoskeletal disorders in dumper operators exposed to whole body vibration at Indian mines. *Int J Mining, Reclam Environ,* 24(3):233–43.

[18] Kim JH, Marin LS, Dennerlein JT. (2018): Evaluation of commercially available seat suspensions to reduce whole body vibration exposures in mining heavy equipment vehicle operators. *Appl Ergon,* 71 (January):78–86.

[19] Smets MPH, Eger TR, Grenier SG. (2010): Whole-body vibration experienced by haulage truck operators in surface mining operations: A comparison of various analysis methods utilized in the prediction of health risks. Appl Ergon 2010; 41 (6):763–70.

Bioelectricity generation in microbial fuel cell by a membrane electrode assemble: Startup assessment

Ana Carla Sorgato
Department of Sanitary and Environmental Engineering
Federal University of Santa Catarina
Florianópolis, Brazil
ana.sorgato@posgrad.ufsc.br

Thamires C. Jeremias
Department of Sanitary and Environmental Engineering
Federal University of Santa Catarina
Florianópolis, Brazil
thamires.custodio@posgrad.ufsc.br

Fernanda Leite Lobo
Department of Hydraulic and Environmental Engineering
Federal University of Ceará
Fortaleza, Brazil
fernandalobo@ufc.br

Flávio R. Lapolli
Department of Sanitary and Environmental Engineering
Federal University of Santa Catarina
Florianópolis, Brazil
f.lapolli@ufsc.br

Abstract

For the last two decades, microbial fuel cell (MFC) has been studied to treat wastewater and simultaneously produce electricity. This innovative bioelectrochemical technology offers the possibility of generating electric current from wide a range of complex organic wastewater. From this perspective, the MFC requires knowledge of structural and material modification in electrodes aimed to enhance the overall performance. Therefore, membrane electrode assembly (MEA) was developed through a combination of electrodes and proton exchange membrane. The MEA provides maximized power generation and extended cell lifetime on the MFC system. In this study, the MFC-MEA was analyzed during the acclimation stage in scale-up aimed at chemical oxygen demand (COD) removal and energy generation from a growth medium rich in acetate. Electrochemical analysis and water quality measurements were assessed. We show that the selection and biofilm acclimatization procedure is a simplified process, starting from anaerobic sludge. The results showed the efficiencies of COD removal and maximum power density were 74.60% and 47.49 mWm^{-2}, respectively. Thus, this study indicates a successful startup and a promising reactor configuration for MFC technology.

Keywords: Acclimation; air cathode microbial fuel cell; COD removal; renewable energy; energy recovery

I. INTRODUCTION

In recent years, microbial fuel cell (MFC) technology has received increased attention. This technology consists of an bioelectrochemical reactor, which generates electricity directly from an organic fuel using electroactive microorganisms [1]. Wastewater can be used as the electron donor, solving two worldwide issues: energy supply and wastewater treatment [2], [3].
Unfortunately, the production of high power generation is still a challenge for practical applications [4]. Significant work has been done to overcome this issue, such as improvement in materials and structure [5]. A promising alternative to improve the MFC energy production is the employment of membrane electrode assembly (MEA) as an electrode [6], [7]. The MEA structure consists of the proton exchange membrane sandwiched between the anode (GDE – gas diffusion electrode) and cathode (GDL – gas diffusion layer). The benefits from this setup consist in electrode-membrane contact improvement and internal resistance reduction [8]. Moreover, the use of MEA dismisses the use of aeration and dissolved oxygen (DO) diffusion, improving energy production.
Despite the broad interest in many engineering aspects of the MFC, the electroactive bacteria play the most crucial aspect. Therefore, providing conditions that promote the development of electroactive bacteria contributes to the performance of the MFC system [9]. The bacteria present at the anode, builds a biofilm on the electrode surface, which is named electroactive biofilm [10]. The biofilm acts as a biocatalyst to oxidize the carbon source, produce electrons and protons, and generate electrical power from their metabolism [11]. Many of these abilities and potentials are expressed during the initial biofilm formation period and affect MFC performance thereafter. The startup time of MFC is directly related to the biofilm formation on the anode [12].
From this perspective, the aim of this work has been focused on the acclimation of a scaled-up MEA-MFC. In this research, an MEA was introduced as a high-performance air-cathode in MFC with the gowl to increase bioenergy generation and reduce the chemical oxygen demand (COD) using a growth medium rich in acetate

II. METHODOLOGY

A. MFC construction

The set-up used in this work consisted of a scaled-up single-chamber MFC. The MFC was fabricated using acryl sheets, with an anodic work volume of 2 L. The electrode consists of MEA, with a nominal area of 144 cm² (Figure 1). Air cathode was composed of an MEA. Each MEA was made up of a Nafion™ (212) membrane, which operated as the chamber separator. The membrane was sandwiched between a carbon felt anode (GDL) and a carbon cloth cathode (GDE) coated with a catalyst loading of 0.4 mg Pt cm^{-2} (Novo- cell, Americana, Brazil). The MEA also contain carbon nanoparticle (Vulcan XC 72R), which provides excellent electron conductivity, and polytetrafluoroethylene (PTFE) layer, to prevent the oxygen diffusion into the anode and water leak in the air-cathode. Stainless steel (SS) plates were used as electron collectors. A single copper wire connected the electrodes externally.

B. Inoculation and operation conditions

The inoculum source was sludge taken from an anaerobic tank installed at a municipal wastewater treatment plant (Florianopolis, Brazil). The sludge had a volatile suspended solids concentration of 20 g L^{-1}. MFC was inoculated with a mixture of anaerobic sludge (50 mL) and a growth medium. The medium contained 1 g L^{-1}

IEECP'22, July 21-22, 2022, Oxford, United Kingdom

sodium acetate, vitamins (5 ml L^{-1}), and minerals (12.5 ml L^{-1}), in 50mM phosphate buffer solution (PBS) (4.576 g Na_2HPO_4, 2.452 g $NaH_2PO_4 \cdot H_2O$, 0.31 g NH_4Cl, 0.13 g KCl) [13]. The acclimation was conducted by feeding the reactors with sludge and growth medium, each 24 h, until voltage generation. Thereafter, only sodium acetate (1 g L^{-1}) and PBS were fed to the reactor. In fed-batch operation, reactors were refilled each time when the voltage decreased to less than 50 mV, forming one complete cycle of operation. The experiment was conducted with an external resistance (R_{ext}) of 1000 Ω, in a constant temperature room of 30 ºC.

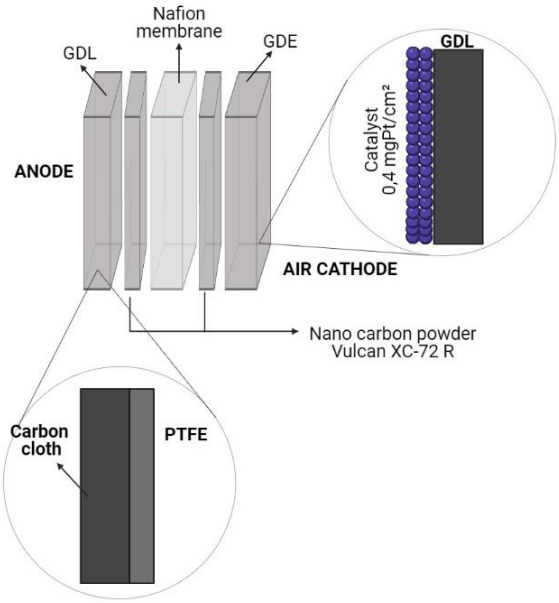

Figure 1. MEA electrode structure.

C. Calculations and measurements

The voltages across the resistor were measured every 3 min using a digital multimeter (ET-2615A, Minipa). Current, I [mA], was calculated according to Ohmic law, $I = E/R_{ext}$, where E is the voltage [mV] and R_{ext} is the external resistance [Ω]. Power, P [mW], was calculated according to P = I.E. Current density [mA cm^{-2}] and power density [mW m^{-2}] were determined by normalizing by area of the electrode. Polarization curves were generated by varying the external resistance, setting the MFC to open circuit for at least 30 min, or until a stable voltage was observed, and lowering the external resistance from 1000, 500, 200, 100, 50, 20, 10 Ω at 10 min intervals. Moreover, the MFC performance was evaluated in terms of COD. For this purpose, the MFC influent and effluent were collected at the start and end of each cycle. COD was measured by spectrophotometry (Hach DR5000) according to the adapted methodology from standard methods for the examination of water and wastewater, using the procedure of the analytic described in Hach 8000 (Hach Co., Loveland, CO). COD removal efficiency [%], was calculated based on the initial and final COD. pH and conductivity were obtained using a multiparametric probe (AKSO, AK88). Coulombic efficiency (CE), defined as the fractional recovery of electrons from the substrate, was calculated according to Eq 1:

$$CE = \frac{M \int_{t_0}^{t_1} Idt}{nvFv\Delta COD} \quad (1)$$

Where M is the molecular weight of oxygen (32 g mol^{-1}), I is the average current (mA), t is the hydraulic retention time (s), F is Faraday's constant (96,485 C mol^{-1}), n is the number of electrons exchanged per mole of oxygen (4 mol e^- mol^{-1}), v is the MFC volume (L), and ΔCOD is the change in COD over time t (g L^{-1}) [24].

III. RESULTS AND DISCUSSION

A. Voltage generation

Startup time was defined here as the time needed to produce repeatable current output over multiple cycles. Moreover, is related to biofilm development. According to voltage generation (measured over a 1000 Ω resistor), a latency phase was observed during the two first days, followed by an exponential increase up to day 3 to 5. After that, the voltage reached a plateau of around 650 mV. The MFC produced a maximum voltage of 795 mV. The start-up time took 15 days. This data can be seen in Fig. 2.

The development of an electroactive biofilm is responsible for MFC performance. In a typical startup of MFCs, the biofilm formation can be divided into three stages, such as reversible attachment, irreversible attachment, and biofilm generation [12], [14]. In stage 1, bacteria adapt to the new environment, flow around in the anode chamber, contact, and isolate with the anode reversibly. In this stage, typically no voltage can be generated, as can be seen on the first day. Stage 2 is characterized by the irreversible attachment of electroactive bacteria, and the increase in MFC voltage (Day 2-5). Subsequently, the microcolonies quickly grow to achieve stable voltage output. Following on, in stage 3, microcolonies turn to biofilm, generating continuous and stable power output (Day 6-15). These steps could be identified in Fig. 2.

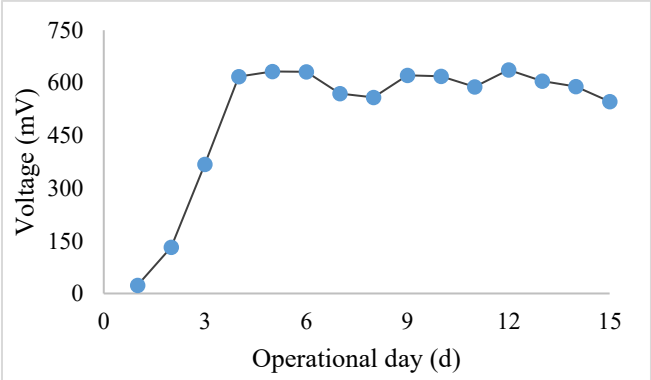

Figure 2 – Voltage measured across 1000 Ω resistor.

Similar results were found by Min et al. [15]. The authors pointed out that the MEA-MFC produced electric power after about a 50 h lag and stable operation with an average voltage was 519 ± 2 mV between 104 and 168 h after the start-up. In addition, the authors explain that a mixed culture obtained from domestic wastewater as inoculum, can easily within a short period immobilize on the anode electrode even though the anode was very close to the aerobic cathode chamber [15]. Moreover, in anaerobic sludge, the anaerobic environment is more selective and houses only species prone to reduce a terminal electron acceptor different from oxygen, which facilitates the adaptation [16]. MFCs inoculated with the mixed culture consistently produced more power than MFCs inoculated with the pure culture [17]. Vicari et al. [16]. compare the performance of different inoculum sources, anaerobic and anaerobic sludge. The authors noted that the MFC inoculated with the anaerobic sludge gave the best power density of 4.59 W m^{-2}, corresponding to 1.38 W m^{-3}.

In addition to the inoculum source, other factors such as external resistance [18], the electrode material [19], and appropriate methodology for inoculation [8], may have contributed positively to

the acclimatization period. Such benefits will reflect on the long-term performance.

In this present study, after MFC achieved 0.625 mV (Day 4), the sludge addition was suspended. Then, MFC was fed only with PBS, acetate, vitamin, and mineral solution. This procedure was repeated after the voltage drops to 50 mV, approximately. The voltage always increased immediately after the solution was replaced with a fresh medium, maintained a constant value for a period, and gradually decreased as the organic matter (e.g. COD) was consumed. This cycle took approximately 5 days (hydraulic retention time – HRT).

B. Power density and polarization test

In the start-up phase, the scaled-up MEA-MFC achieved a maximum current density of 60.11 mAm^{-2} and power density of 47.79 mWm^{-2}. This value is obtained at an open-circuit voltage (OCV) of 680 mV. The theoretical OCV value for an MFC fed with acetate is 805 mV [20]. This discrepancy could be attributed to high activation overpotentials, ohmic losses and concentration polarization, typical MFC disadvantages [21]. However, the current generation confirms the activity of electroactive bacteria. Nevertheless, analysis of inoculum and biofilm bacteria would be interesting to assess which electroactive species was present in MEA-MFC.

Table 1 shows the maximum power production obtained on different days during the acclimation stage. It is important to note the increase in value during the period. This performance could be attributed to the adaptation and growth of electroactive microorganisms and biofilm development.

Table 1. HRT, COD removal, coulombic efficiency, and power production from MEA-MFC

Operational day	HRT (d)	COD removal (%)	CE (%)	Max power density (mWm^{-2})
1	1	19.34	2.47	0.76
3	1	31.36	5.92	11.71
9	5	74.31	20.82	29.25
13	5	74.60	23.91	47.49

A polarization test was conducted on the last day of the start-up period, to characterize the overall performance of MFC and illustrate the potential losses. The maximum power density (P_{max}), i.e. the top of the parabola (Fig. 3), was 179.05 mWm^{-2} at a current density of 60.85 mAm^{-2} (R_{ext} = 500 Ω). Based on polarization data, decreasing the external load has increased the electrical current and decreased the cell voltage, which is typical fuel cell behavior [22]. According to Logan et al.[20], the polarization curve can be divided into three zones, which represent a kind of loss, such as activation, Ohmic, and mass transport. These three zones are observed, suggesting that the system is meeting the steady-state and showing a good performance [23].

At high current density, the polarization curve shows an overshoot phenomenon (Figure 3). Its presence could indicate that microbial biofilm has not matured to a sufficient level. However, Winfield et al. [24] explain that time favors this process. Then, more few days provide the establishment of a healthy biofilm and the disappearance of the overshoot. The assessment of electrode potentials could contribute to understanding this phenomenon in the MEA-MFC.

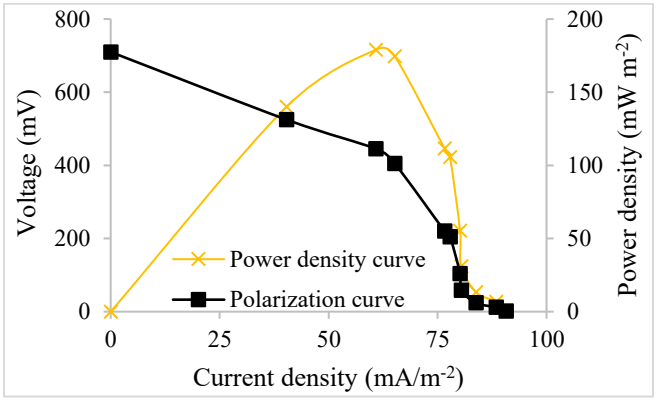

Figure 3. Polarization and power density curve.

C. COD removal

In evaluating an MFC as a bioelectrochemical device able to produce an electric current from the oxidation of organic matter, the COD concentration in the outlet of the MFC (effluent) is worth to be evaluated as one important parameter [16]. The acetate-fed medium has a COD concentration equal to 745 mg L^{-1}, pH 7, and 6.9 mS cm^{-1}. The depletion of COD remains in the current generation. However, in the biofilm, coexist the electroactive and no-electroactive microorganisms. Both groups are responsible for COD degradation.

It is important to note that over the days, the COD removal increased. In the first moment, the COD removal was not satisfactory, but expected, due to the adaptation period. After that, the operation condition changed, and the HRT became 5 days. The COD removal efficiency increased with the increase in time, which means, how much longer the influent spend inside the reactor, more available time for biodegradation [25].

This performance could be attributed to several factors. The composition of inoculum also severely influences the performance of COD removal efficiency, as the carbon source (glucose, acetate, sucrose) [26]. In addition, the external resistor also contributes to MFC performance. For a COD initial concentration of 840 mg L^{-1}, Zhang et al. [27] found rates equal to 0.030 h^{-1} with 100 Ω and 0.065 h^{-1} for 1000 Ω, then in lower resistance, COD removal rate increased.

The relation between COD removal and power production is expressed by CE (Table 1). The CE increased with COD removal, indicating microbial electroactive activity. Other studies reported similar values for the start-up phase [16], [17], [19].

Furthermore, despite the low percentage of COD removal in the first days, it can be inferred in Table 1 that a very efficient and robust bacterial community has grown in the anode as it is capable of converting 23,91% of the energy content of the medium into electricity.

IV. CONCLUSION

In this study, an air-cathode MEA-MFC equipped with the membrane electrode assembly (MEA) of 2 L was used for in situ power generation. Stable power generation could be obtained in 15 days. The inoculum source provides a rapid growth in voltage, resulting in a short inoculation period. After this acclimatization period. The scaled-up MEA-MFC can be applied for energy recovery from wastewater

V. ACKNOWLEDGMENTS

This study was financed in part by the Coordenação de Aperfeiçoamento de Pessoal de Nível Superior – Brasil (CAPES) – Finance Code 001. The authors received financial and technical support from the Federal University of Santa Catarina (UFSC)"

VI. REFERENCES

[1] J. Yu, Y. Park, E. Widyaningsih, S. Kim, Y. Kim, and T. Lee, "Microbial fuel cells: Devices for real wastewater treatment, rather than electricity production," *Sci. Total Environ.*, vol. 775, p. 145904, Jun. 2021, doi: 10.1016/j.scitotenv.2021.145904.

[2] H. Liu, R. Ramnarayanan, and B. E. Logan, "Production of Electricity during Wastewater Treatment Using a Single Chamber Microbial Fuel Cell," *Environ. Sci. Technol.*, vol. 38, no. 7, pp. 2281–2285, 2004, doi: 10.1021/es034923g.

[3] J. Vilas Boas, V. B. Oliveira, L. R. C. Marcon, M. Simões, and A. M. F. R. Pinto, "Optimization of a single chamber microbial fuel cell using Lactobacillus pentosus: Influence of design and operating parameters," *Sci. Total Environ.*, vol. 648, pp. 263–270, Jan. 2019, doi: 10.1016/j.scitotenv.2018.08.061.

[4] B. Fu, T. Xu, X. Guo, P. Liang, X. Huang, and X. Zhang, "Optimization and simulation of a carbon-based flow-through composite anode configuration to enhance power generation and improve effluent quality simultaneously for microbial fuel cells," *J. Clean. Prod.*, vol. 229, pp. 542–551, 2019, doi: 10.1016/j.jclepro.2019.04.308.

[5] H. Ni, K. Wang, S. Lv, X. Wang, L. Zhuo, and J. Zhang, "Effects of Concentration Variations on the Performance and Microbial Community in Microbial Fuel Cell Using Swine Wastewater," *Energies*, vol. 13, no. 9, p. 2231, May 2020, doi: 10.3390/en13092231.

[6] J. R. Kim, G. C. Premier, F. R. Hawkes, R. M. Dinsdale, and A. J. Guwy, "Development of a tubular microbial fuel cell (MFC) employing a membrane electrode assembly cathode," *J. Power Sources*, vol. 187, no. 2, pp. 393–399, Feb. 2009, doi: 10.1016/J.JPOWSOUR.2008.11.020.

[7] Y. Hubenova, G. Borisov, E. Slavcheva, and M. Mitov, "Gram-positive bacteria covered bioanode in a membrane-electrode assembly for use in bioelectrochemical systems," *Bioelectrochemistry*, vol. 144, p. 108011, Apr. 2022, doi: 10.1016/J.BIOELECHEM.2021.108011.

[8] G. K. S. Prakash, F. A. Viva, O. Bretschger, B. Yang, M. El-Naggar, and K. Nealson, "Inoculation procedures and characterization of membrane electrode assemblies for microbial fuel cells," *J. Power Sources*, vol. 195, no. 1, pp. 111–117, Jan. 2010, doi: 10.1016/J.JPOWSOUR.2009.06.081.

[9] K. L. Dinh *et al.*, "Lactate and acetate applied in dual-chamber microbial fuel cells with domestic wastewater," *Int. J. Energy Res.*, vol. 45, no. 7, pp. 10655–10666, Jun. 2021, doi: 10.1002/er.6550.

[10] M. J. Angelaalincy, R. Navanietha Krishnaraj, G. Shakambari, B. Ashokkumar, S. Kathiresan, and P. Varalakshmi, "Biofilm Engineering Approaches for Improving the Performance of Microbial Fuel Cells and Bioelectrochemical Systems," *Front. Energy Res.*, vol. 6, p. 63, Jul. 2018, doi: 10.3389/fenrg.2018.00063.

[11] B. E. Logan, R. Rossi, A. Ragab, and P. E. Saikaly, "Electroactive microorganisms in bioelectrochemical systems," *Nat. Rev. Microbiol.*, vol. 17, no. 5, pp. 307–319, 2019, doi: 10.1038/s41579-019-0173-x.

[12] P. Zhang *et al.*, "Accelerating the startup of microbial fuel cells by facile microbial acclimation," *Bioresour. Technol. Reports*, vol. 8, p. 100347, Dec. 2019, doi: 10.1016/J.BITEB.2019.100347.

[13] F. L. Lobo, X. Wang, and Z. J. Ren, "Energy harvesting influences electrochemical performance of microbial fuel cells," *J. Power Sources*, vol. 356, pp. 356–364, Jul. 2017, doi: 10.1016/J.JPOWSOUR.2017.03.067.

[14] M. Mukherjee, N. Zaiden, A. Teng, Y. Hu, and B. Cao, "Shewanella biofilm development and engineering for environmental and bioenergy applications," *Curr. Opin. Chem. Biol.*, vol. 59, pp. 84–92, Dec. 2020, doi: 10.1016/J.CBPA.2020.05.004.

[15] B. Min, F. W. Poulsen, A. Thygesen, and I. Angelidaki, "Electric power generation by a submersible microbial fuel cell equipped with a membrane electrode assembly," *Bioresour. Technol.*, vol. 118, pp. 412–417, Aug. 2012, doi: 10.1016/J.BIORTECH.2012.04.097.

[16] F. Vicari *et al.*, "Influence of the initial sludge characteristics and acclimation on the long-term performance of double-compartment acetate-fed microbial fuel cells," *J. Electroanal. Chem.*, vol. 825, pp. 1–7, Sep. 2018, doi: 10.1016/J.JELECHEM.2018.08.003.

[17] V. J. Watson and B. E. Logan, "Power Production in MFCs Inoculated With Shewanella oneidensis MR-1 or Mixed Cultures," *Biotechnol. Bioeng*, vol. 105, pp. 489–498, 2010, doi: 10.1002/bit.22556.

[18] G. Pasternak, J. Greenman, and I. Ieropoulos, "Dynamic evolution of anodic biofilm when maturing under different external resistive loads in microbial fuel cells. Electrochemical perspective," *J. Power Sources*, vol. 400, pp. 392–401, Oct. 2018, doi: 10.1016/J.JPOWSOUR.2018.08.031.

[19] S. Hays, F. Zhang, and B. E. Logan, "Performance of two different types of anodes in membrane electrode assembly microbial fuel cells for power generation from domestic wastewater," *J. Power Sources*, vol. 196, no. 20, pp. 8293–8300, Oct. 2011, doi: 10.1016/J.JPOWSOUR.2011.06.027.

[20] B. E. Logan *et al.*, "Microbial fuel cells: Methodology and technology," *Environ. Sci. Technol.*, vol. 40, no. 17, pp. 5181–5192, 2006, doi: 10.1021/es0605016.

[21] A. ElMekawy, H. M. Hegab, X. Dominguez-Benetton, and D. Pant, "Internal resistance of microfluidic microbial fuel cell: Challenges and potential opportunities," *Bioresour. Technol.*, vol. 142, pp. 672–682, Aug. 2013, doi: 10.1016/J.BIORTECH.2013.05.061.

[22] S. B. Pasupuleti, S. Srikanth, S. Venkata Mohan, and D. Pant, "Continuous mode operation of microbial fuel cell (MFC) stack with dual gas diffusion cathode design for the treatment of dark fermentation effluent," *Int. J. Hydrogen Energy*, vol. 40, no. 36, pp. 12424–12435, Sep. 2015, doi: 10.1016/J.IJHYDENE.2015.07.049.

[23] M. A. Rodrigo, P. Cañizares, H. García, J. J. Linares, and J. Lobato, "Study of the acclimation stage and of the effect of the biodegradability on the performance of a microbial fuel cell," *Bioresour. Technol.*, vol. 100, no. 20, pp. 4704–4710, Oct. 2009, doi: 10.1016/J.BIORTECH.2009.04.073.

[24] J. Winfield, I. Ieropoulos, J. Greenman, and J. Dennis, "The overshoot phenomenon as a function of internal resistance in microbial fuel cells," *Bioelectrochemistry*, vol. 81, no. 1, pp. 22–27, 2011, doi: 10.1016/j.bioelechem.2011.01.001.

[25] Y. Sharma and B. Li, "Optimizing energy harvest in wastewater treatment by combining anaerobic hydrogen producing biofermentor (HPB) and microbial fuel cell (MFC)," *Int. J. Hydrogen Energy*, vol. 35, no. 8, pp. 3789–3797, Apr. 2010, doi: 10.1016/J.IJHYDENE.2010.01.042.

[26] Z. Ullah and S. Zeshan, "Effect of substrate type and concentration on the performance of a double chamber microbial fuel cell," *Water Sci. Technol.*, vol. 81, no. 7, pp. 1336–1344, Apr. 2020, doi: 10.2166/wst.2019.387.

[27] X. Zhang, W. He, L. Ren, J. Stager, P. J. Evans, and B. E. Logan, "COD removal characteristics in air-cathode microbial fuel cells," *Bioresour. Technol.*, vol. 176, pp. 23–31, 2015, doi: 10.1016/j.biortech.2014.11.001.

Cr and Polycrystalline Diamond Coatings for Accident Tolerant Nuclear Fuel Tubes

Irena Kratochvilova*
Institute of Physics of the Czech Academy of Sciences,
Na Slovance 1999/2, 182 21, Prague 8,
Czech Republic
+420723814810
*corresponding author: krat@fzu.cz

Lucie Celbova
Institute of Physics of the Czech Academy of Sciences,
Na Slovance 1999/2, 182 21, Prague 8,
Czech Republic
+420723814810
celbova@fzu.cz

Radek Škoda
Czech Technical University in Prague,
Jugoslávských partyzánů 1580/3,
Prague 6, CZ-160 00,
Czech Republic
+420 224354158
Radek.Skoda@cvut.cz

Abstract

The essence of this work is to show a possibility to increase the safety of nuclear reactors and extend the life of nuclear fuel by reduction the corrosion of the zirconium fuel tubes by double layer coating consisting of polycrystalline diamond (PCD) and magnetron sputtered Cr. In double layer coating the water permeable 500 nm thick polycrystalline diamond layer consisted of hard diamond grains (<70%) and soft graphitic carbon phase. The Cr coating was 2-3 μm thick. We used Cr layer as bottom and PCD as top coating and also Cr layer as top and PCD as bottom coating of ZIRLO fuel tube. Coated and bare ZIRLO fuel cladding tubes were subjected to hot steam/water tests for 30 min at 900°C and for 40 min at 1000°C. The hot steam processed double layer coated ZIRLO oxidation was lower than uncoated hot steam processed ZIRLO. Surprisingly, the hot steam processed Cr coated ZIRLO oxidation was even lower than the double layer coated hot steam processed ZIRLO when PCD layer was bottom layer. On the contrary, when ZIRLO was coated by Cr layer as bottom and PCD layer as top layer then its accidental oxidation was lowest of all samples we have ever tested. Raman spectroscopy, scanning electron microscopy, X-ray diffraction and energy-dispersive spectroscopy were performed to study relevant processes and states affecting coated ZIRLO hot steam corrosion.

Keywords: nuclear fuel tubes corrosion, nanodiamond layer; chemical vapor deposition, Cr magnetron sputtering;

IEECP'22, July 21-22, 2022, Oxford, United Kingdom

A methodology for assesment of deep decarbonisation pathways for manufacturing industries in Ireland

Kirestena Saeed
Department of electrical and electonic engineering
Technological university of Shannon
limerick ,Ireland
kirestena.saeed@lit.ie

Dr.John Cosgrove
Department of electrical and electronic engineering
Technological universityof Shannon
Limerick, Ireland
John.Cosgrove@lit.ie

Dr.Frank Doyle
Department of electrical and electronic engineering
Technological university of Shannon
Limerick, Ireland
Frank.Doyle@lit.ie

Abstract

Industrial development has an important role in the economic growth, along with this development, industrial sector has been one of the fastest growing sources of greenhouse gas emissions this growth has been driven by the increase of intensive industry subsectors including cement, iron and steel, chemicals, and aluminum, and because of a socio-economic and population growth. industrial sector is accounts of 30% of greenhouse gas emissions and around 37% of global energy consumption. In agreement with the 2015 united nation conference of parties, (COP21) to reduce the global temperature to reach low than 2 ℃ by the year 2050 , 197 participating countries agreed to take measures to reduce greenhouse gas emissions .Achieving this target requires overall changes of the universal economy and may be possible if the level of carbon dioxide (CO_2) in the environment remains below 450 part per million , however the concentration of carbon dioxide$_2$ continue to increase which is need to a new policies and technologies to reduce the industrial emissions between 29%-41% by the year 2030. Rapid and deep decarbonisation of industry is needed to reduce emissions through many pathways, replacing fossil fuels with renewable technologies such as wind, solar, developing of new technologies and materials coupling with improving energy efficiency and electrification of high temperature heating. This research will investigate the existing information, scope, methodologies, and toolkit relating to deep decarbonisation and will intend a methodology to validate measures towards decarbonisation that are relevant to the Irish context. The research will focus on the greenhouse emissions from Irish manufacturing industries and will set an energy efficiency and energy reduction metric and will propose a methodology for the validation of deep decarbonisation pathways for manufacturing industries in Ireland.

Keywords: Industrial decarbonization, Renewable technology, Energy efficiency

IEECP'22, July 21-22, 2022, Oxford, United Kingdom

Strategy for institutional cook stoves promotion in the context of a behavioral change-A case study of Opoku Ware School and ST. Paul's Seminary, Accra, as the control in the research in Ghana.

Michael Kweku Commeh
Technology Consultancy Centre, College of Engineering, Kwame Nkrumah University Science & Technology
Kumasi, Ghana
Tel: (+233) 0200644968
mcommeh.tcc@knust.edu.gh

Christlove Opoku-Appiah
Logistics Comeph & Associates
Accra, Ghana
Tel: (+233) 0540413065
3kwesi60@gmail.com

Joseph Okine
(Rector)
St Paul's Seminary
Accra, Ghana
Tel:(+233)0208714609
jokineq@gmail.com

James Hawkins Ephraim
Director
Comeph & Associates Gh Ltd
Accra, Ghana
Tel: (+233) 0208716156
eygamkow@gmail.com

ABSTRACT

76% of households mainly cook using polluting fuels and inefficient cooking technologies or devices (Ghana Statistical Service [GSS] , 2017) [1]. As a result 13,000-16,000 people die from the aforementioned factors. Clean cook stoves borders on SDG 7 on clean energy and SDG 3 on health (Kumar et al., 2021) [2], SDG 2 on food security and sustainable agriculture, SDG 5 on gender, SDG 11 on cities, and SDG 13 on climate change, (Fenny et al., 2017) [3]. However, improved efficient cooking devices that eliminate the death associated with inefficient cooking stoves are not easily accepted, even when subsidized, (Ackah et al., 2021)[4] .What might be the underlying narratives to this resistance? This article tends to find out using OWASS as the first case study and using St. Paul's Seminary as a control. The research looked at the design of the institutional stove for both firewood and gas. The pot size is 210 litres stainless steel for 6 gas stoves and 6 firewood stoves.

The experiment from start to finish took exactly one year, from studying cooking dynamics including mental modelling mapping and some social philosophies. It also involved changing over from highly inefficient smoky stoves to efficient little or no indoor air pollution stoves.

Results indicated a relatively quick adoption of ICs within two months whilst St. Paul's Seminary took extra funds and a threatening approach to get cooks to adopt the technology over two months, even though incentives in the form of cash were given.
Three major narratives emerged as to the reason for the success toward the adoption or acceptance of the technology, namely; safety of the stove, efficiency or huge energy/cost saving, human centered design, power or control of the fire/flame and discipline in the supervision of management protocol by actors in the improved clean cooking devices value chain. Despite the huge success, work still needs to be done on the safety of the gas stove and continuous training on the management of the cooking devices, especially the gas stove.

Conclusively, acceptability was generally successful with OWASS while St. Paul was with difficulty despite the similarity in problems and solutions.

Keywords: Institutional cooking devices, actors, power play, safety & security and management protocol.

1. INTRODUCTION

76% of households mainly cook using polluting fuels and inefficient cooking technologies or devices (Ghana Statistical Service [GSS], 2017) [1]. As a result 13,000-16,000 people die from the aforementioned factors. Clean cook stoves borders on SDG 7 on clean energy and SDG 3 on health (Kumar et al., 2021) [2], SDG 2 on food security and sustainable agriculture, SDG 5 on gender, SDG 11 on cities, and SDG 13 on climate change, (Fenny et al., 2017). Ghana, like India, has 65% of its citizens cooking on inefficient biomass cooking devices. These biomass stoves produce smoke and greenhouse emissions (GHG) either in an enclosed area or an open area, (Nina , 2022) [3] ; Cooking in an enclosed area with inefficient biomass cooking devices leads to Indoor air pollution (IAP) and while cooking outside leads to localised pollution especially when attending to the smoldering firewood. It has been observed over the years that inefficient institutional cooking devices pollute more than household cookstoves using a cooking pot of fewer than 20 litres, (Venkataraman et al., 2010) [6]. A cooking device is termed as institutional when it is more than 20litres cooking pot. An efficient clean cooking device is a device that uses less fuel, 96%

IEECP'22, July 21-22, 2022, Oxford, United Kingdom

fewer emissions, uses more than 60% less fuel and no or 95% smoke. Normally institutional cooking devices which are found in big restaurants, hospitals, schools, street vendors etc. face a lot of resistance. Unfortunately, these institutional devices do massive damage to the environment, the climate as well as minimise income. Despite the negative results inefficient biomass institutional stoves give us, acceptability is at its rock bottom in Ghana. Funding by the United Nation Development programme under the Global Environmental Facility for large-scale intervention efforts to pilot 23 schools amounts to 46 stoves. In trying to address multiple methodological and sociocultural issues, each school had one flat bottom stainless steel pot and one stove fitting traditional round-bottom cooking pot, normally made of aluminum, in 2015. Despite its efficiency, speed and comfort during cooking, all the schools abandoned the new stoves and the question is WHY was the cook stoves abandoned?
This article tends to find out using OWASS as the first case study and St. Paul's Seminary as a control. The research looked at the design of the institutional stove for both firewood and gas. The pot size is 210l stainless steel for 6 gas stoves and 6 firewood stoves.

2. METHODOLOGY

This exploratory study provides preliminary data cook stove acceptability study between Opoku Ware Senior high School (OWASS) and St. Paul Catholic Seminary. The project at Opoku Ware was funded by alumni of the school, while St, Paul's Seminary was funded by School authorities. And the reason was to save money and have a clean hygienic kitchen.
Traditional cooking devices and practices were assessed through observations. Twenty vehicular metal tire rims were formerly used for 150-180 litres round bottom pots. The interventional stove is a sunken-in-stove, where the cylindrical stainless steel cooking pot is 210 litres figure 1.

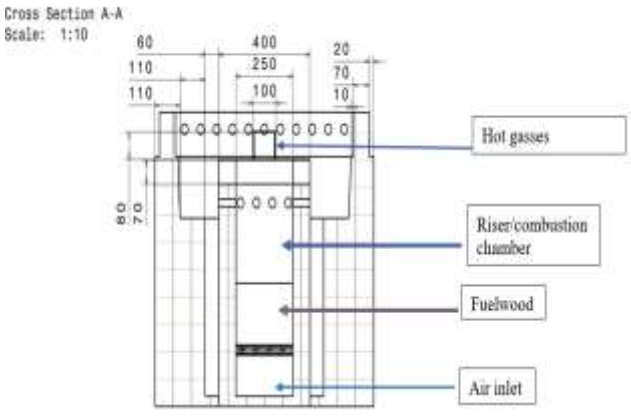

Figure 1. Sunken-in-stove

The thermal efficiency of the cooking device is above 60%, without any electrical power to add forced. In all 6 gas stoves and 6 advanced biomass stoves, one fish/meat smoker, maize and groundnut patching stove were installed as an intervention solution. The finished stove were artistically painted. GHc 20 was shared among the female cooks because they were the immediate users of the stoves after the management and maintenance training on both gas and biomass stoves at both OWASS and St. Paul Seminary. The Ghc 20 would be given every three months to the OWASS cooks for 12 months.
One also looked at the structuration theory Giddens, A., (1986) [7]; in which the concept of sociology offers perspectives on human behavior based on a synthesis of structure and agency effects known as the "duality of structure", where humans interact with meanings, standards, values, power and positing a dynamic relationship between these different facets of society. Behavioral science was used as a driver of change to identify and use in the intervention, taking seriously into consideration the "what is in it for me (WIIIFM)?" Questionnaires were administered to more than 70 actors in the value chain thus perception of Institutional cook stoves, perceptions about mission and strategy, external pressures and the environment, about stakeholders and concluding questions.

One looked at before and after of the concentrations of particulate matter (PM) with a diameter < 2.5 µm ($PM_{2.5}$), carbon monoxide (CO) and carbon dioxide (CO_2) related to traditional and advanced biomass cooking devices stove use were measured using indoor air pollution monitoring meter in real-time whilst cooking was going on in the kitchen and activities were been observed. Structured, but unconventional protocol of qualitative data on the acceptability of advanced stoves and objective measures of stove usage were also collected and observed.

3. RESULTS

90% of the stoves were indoors. All the actors in the value chain agreed 100% that the intervention was a success. Training for the cooks, both female and male was done. The males proved a little bit reluctant to use the new stove until money was shared among the female cooks. More so, the constant visit of the headmaster of the school and the Alumnus influenced the easy acceptability. Reminding the actors in the values chain of how costly the project was, also influenced the acceptance of the interventions. The assurance of safety and security of stoves played a big role in the acceptability. However, it took the rector, extra cost to train the cooks at St. Paul's Seminary and dismissal threats before the cooks reluctantly mastered the use of the new stoves.

The design (Pakravan, Mohammad H., 2021) [8] of the stove prevents smoke from being inhaled, it also prevents the heating and burning of the hands, body, etc. of the cooks. The easy control of both the firewood and gas stove influenced the quick acceptability and behavioral change rate. Initially, most women preferred firewood to the gas stove, but as peer competition intensified, humiliation from coworkers spurred everyone to improve their gas stove management skills through self-motivation. Both gas stoves and biomass stoves are now used without supervision since January 2022. The $PM_{2.5}$ concentrations averaged 2,468 g/m3 during the high peak cooking time, which is generally from 10 a.m. to 1 p.m., and 1,218 g/m3 during the low period.

The cooking devices, before the intervention, were 23 inefficient biomass stoves, hence the aforementioned results. There was no IAP recorded after the intervention due to the chimney included in all the stoves. All the smoke, if there was any, went out through the chimney. Cooks don't need to go to work in the dark where they are often met with arm robbers and rapists as the interventions allow them to cook breakfast within an hour rather than 6hours. The cooks sole problem was the non-visibility of the flame, which means they can't see it when it's on. Finally, we saw that the administration of the colorfully painted firewood stove was meticulous in order to minimize smoking on the frontage, but the single unpainted stove received less attention, resulting in black smoke staining the frontage, (Darrow, 2017).[9]. Color appears to have some impact on behavior modification in the maintenance and management of stoves, despite the lack of substantial study.

4. Conclusions

Acceptability at OWASS was quicker than that of St. Paul Seminary, even though the underlying were about the same. One reason for the quick acceptability of OWASS by the cooks was the fact that four biomass stoves were built six months before completing the rest. The high acceptance rate was largely due to the stove's design. The stove prevented heat, smoke and provided safety and security to the cooks who were mainly women. One can approach the stove and stock the firewood without inhaling smoke or emissions. The addition of a conduct through which the flame can be seen would be a further upgrade to the gas stove design. The low or no harmful gas emissions has influence over the acceptance rate in the two neighborhoods. Further understanding of how the introduction of an advanced stove influences patterns of institutions' energy use is needed. The intervention, however, with subsidies will go a long way to promote a speedy penetration rate of the project. Lesson(s) learnt here will help formulate policies to enhance the easy acceptability of new technology and feasibility and/or pilot studies aimed at the process of behavioral change efforts locally, nationally and maybe internationally.

Figure 2. Depicting before intervention

Figure 2. Depicting after intervention

5. ACKNOWLEDGMENTS

Our thanks to Enno formerly of SNV for introducing the original design of the institutional stove, U-Group 1967-74 Alumnus of OWASS for funding the project and Comeph & Associates for R&D, technology transfer and installation of the stoves and taking data.

REFERENCES

[1] 2017. Ghana: Ghana Statistical Service.

[2] Kumar, N., Phillip, E., Cooper, H., Davis, M., Langevin, J., Clifford, M. and Stanistreet, D., 2021. Do improved biomass cookstove interventions improve indoor air quality and blood pressure? A systematic review and meta-analysis. *Environmental Pollution*, 290, p.117997.

[3] Fenny, A. P., Crentsil, A. O., & Ackah, C. (2018). The health MDGs in Ghana: lessons and implications for the implementation of the sustainable development goals. Journal of Public Health, 26(2), 225-234.

[4] Ackah, I., Bukari, D., Banye, E. Z., & Bobio, C. (2021). Transitioning towards cleaner cooking fuels: an analysis of consumer preferences in Ghana's cookstoves market. Environmental Science and Pollution Research, 28(39), 54936-54949.

[5] Lakhani Nina . 2022. The world's forests do more than just store carbon, new research finds. (March 2022). Retrieved March 25,2022 from https://www.theguardian.com/environment/2022/mar/23/forests-climate-crisis-carbon-cooling-effect

[6] Venkataraman, C., Sagar, A. D., Habib, G., Lam, N., & Smith, K. R. (2010). The Indian national initiative for advanced biomass cook stoves: the benefits of clean combustion. Energy for sustainable development, 14(2), 63-72.

[7] Giddens A., (1986). The theory of structuration.

[8] Mohammad H. Pakravan and Nordica MacCarty. 2020. What motivates behavior change? analyzing user intentions to adopt clean technologies in low-resource settings using the theory of planned behavior. Energies 13, 11 (2020), 3021. DOI:http://dx.doi.org/10.3390/en13113021

[9] Alice-Ann Darrow. 2017. Meaningful collaboration in the inclusive music classroom: Students with severe intellectual disabilities. General Music Today 31, 1 (2017), 40–43. DOI:http://dx.doi.org/10.1177/1048371317716960

Production of synthesis gas obtained via alkaline water electrolysis and added biomass

João Gomes
Chemical Engineering Department
ISEL - Instituto Superior de Engenharia de Lisboa
Lisboa, Portugal
jgomes@deq.isel.ipl.pt

Jaime Puna
Chemical Engineering Department
ISEL - Instituto Superior de Engenharia de Lisboa
Lisboa, Portugal
jpuna@deq.isel.ipl.pt

Teresa Santos
Chemical Engineering Department
ISEL - Instituto Superior de Engenharia de Lisboa
Lisboa, Portugal
tsantos@deq.isel.ipl.pt

Abstract

This paper presents the results of the research currently being carried out at ISEL with the objective of developing new electrochemistry-based processes to obtain renewable synthetic fuels from alkaline water electrolysis using a carbon source. In the developed process, the gas mixture obtained from alkaline water electrolysis and a carbon source is not separated into their components but rather is introduced into a catalyzed reactor, in order to achieve conversion to synthetic 2nd generation biofuels, such as biomethane, biomethanol, bio-dimethyl ether, etc. Tests have been previously executed in a pilot electrolyzer and reactor of 1 kW, and are now being scaled up to a pilot electrolyzer and reactor of 5 kW, producing 250 l/h CH_4, as an intermediate step to a pilot of 100 kW.

Keywords: Water electrolysis; synthesis gas; biofuels

I. INTRODUCTION

It is well known that electricity cannot be stored in large quantities as such, but an alternative way of energy storage can be to convert electricity, particularly the one generated from renewable sources, like wind or solar, into chemical compounds. This procedure is a good solution to the currently existing problems of excess electricity in the grid. This paper describes a further new approach to new technology, previously reported by the authors [1] capable of producing syngas in a single step, without separation of the elementary gases, produced during the water alkaline electrolysis. It is called co-electrolysis of water, under the alkaline process, using a carbon source to directly produce the syngas mixture, at low temperatures and pressures, thus requiring significative fewer amounts of energy inputs [2-3]. This previous approach, uses graphite electrodes, as a source of carbon, that is further oxidized, during the electrolysis process, to carbon monoxide and carbon dioxide which are present in the generated gas mixture (syngas), and, efficiently converts electricity from renewable sources (mainly wind or solar, or when this electricity is in excess in the electrical grid, or in off-peak hours). Thus, this new technology is able to convert electricity into syngas, which is an intermediate for the generation of synthetic 2nd G biofuels, which was already demonstrated [4]. The main drawback is the (small) consumption of the graphite electrodes and its relatively high cost, which could be avoided if steel electrodes are used together with an additional carbon source, such as liquefied biomass, to be added to the electrolyzer. Concerning the use of liquefied biomass, some results from preliminary trials have been recently published elsewhere [5] and point out that, the process needs enhancement, such as the use of solid catalysts. In this new process, the gas obtained from electrolysis is not separated into its components and, it's introduced into a reactor together with a specific content of a previous mixture of cork/eucalyptus splinter liquefied biomass, at normal pressure and different temperatures. The gas is released upon contact with the biomass, thus resulting in a syngas, which is a mixture consisting essentially of carbon monoxide, hydrogen, carbon dioxide, and some remains of unreacted oxygen. In this work, the behavior of operational parameters such as biomass content, temperature, and the use of different amounts of acidified zeolite HY catalyst was investigated. In the performed tests, it was found that, in addition to the syngas, methane was also produced, with significant content.

The purpose of using samples of different kinds of liquified biomass of cork and/or eucalyptus bark, with and without the correspondent sugars solubilized in an aqueous solvent, was to investigate if, there was a significant influence on the output syngas/methane produced, at the methanation reactor, as well, the influence of temperature and catalyst content in this process. The temperature range chosen for this study must be significantly lower than the typical temperatures used in the gasification process (700–800 °C). The advantage of this technology is located, precisely, in the utilization of lower/medium temperatures, when compared with the

IEECP'22, July 21-22, 2022, Oxford, United Kingdom

coal/biomass gasification and steam reforming processes, which produces, also, syngas. The utilization of lower temperatures will lead to significant input energy savings to the process and, as consequence, lower operating costs. On the other hand, the influence of using lower catalyst contents in the methanation process in this study is to see if the methane concentration will increase in these temperatures, with and without catalyst [6].

II. MAIN RESULTS

Regarding the production of syngas, Table 1 shows the results obtained with complementary experiences in the methane glass reactor, where this gaseous mixture is produced, with the methane generation, through the reaction between the electrolysis gas and, the liquified biomass. The results achieved and calculated were: the volumetric yields production of solid, liquid, and gas phases, respectively, the remaining biomass collected in the reactor ($Yield_{(liq.biom.)}$) after the elapsed time of 60 minutes, at different temperatures, the condensate ($Yield_{(cond.)}$) and, also, the gas mixture produced ($Yield_{(gas)}$).

Table 1. Experimental results obtained with complementary experiences in the syngas/methane reactor.

(ºC)	$Vf_{(liq.biom.)}$ (mL)	$Yield_{(liq.biom.)}$ (%)	$Yield_{(cond.)}$ (%)	$Yield_{(gas)}$ (%) (*)
100	98	98.0	-	2.0
150	96	97.0	-	3.0
200	72	74.0	23.5	2.5

(*) – estimated considering the initial volume of 100 mL of liquified biomass minus the volumes of final liquified biomass and condensate produced.

Table 2 shows, at the end of 4 hours of experience, the correspondent final output values of the gas volumetric flow, as well, as the oxygen and methane volumetric contents in the produced gas mixture, for different reaction temperatures and different weight content (z. HY catalyst). To compare with another Y zeolite already prepared, ultra-stabilized with nickel (z. USY), it was also performed, two more experiments with this catalyst, which was supplied from another Portuguese university. The results achieved with USY zeolite do not show any significant improvement, mainly in the $\%CH_4$ content, when compared with the acidified HY zeolite catalyst.

III. CONCLUSIONS

From this research work, it can be concluded that it is possible to produce syngas and methane, using this electrolysis system (Electrofuel), together with a fixed bed catalytic reactor to produce methanation (Sabatier process), with significantly fewer energy inputs when compared with the conventional thermochemical processes of syngas/methane production, like pyrolysis and gasification. Comparing the combined electrochemical/Sabatier process (10.38 $kJ \cdot mol^{-1}$) with the pyrolysis one (14.29 $kJ \cdot mol^{-1}$) and considering the same syngas/methane flow and the same gas composition, an increase of 38% in the input energy was observed. By another hand, in the comparison between the same combined process (10.38 $kJ \cdot mol^{-1}$) with the gasification one (27.21 $kJ \cdot mol^{-1}$), an increase of 162% in the input energy was observed, both values applied for each mole of syngas/methane mixture.
With the utilization of these combined electrochemical/Sabatier reactors, it's possible to reduce input energy to the system and, as consequence, reduce energetic (operating) costs.

Table 2. Experimental results in the methanation reactor, for different reaction temperatures and different weight content catalyst.

% ($W_{cat.}/W_{liq.biom.}$)	T (°C)	F ($mL \cdot min^{-1}$)	$\%O_2$	$\%CH_4$
A2, no catalyst	150	142.9	33.5	0.19
	200	150.0	32.0	0.45
	250	138.5	33.3	0.45
	300	138.5	32.0	2.08
A2, z. HY, 2%	150	145.2	33.8	0.25
	200	134.2	32.5	1.84
	250	145.2	32.2	4.16
	300	157.9	30.2	12.8
A2, z. HY, 4%	150	145.2	33.9	0.28
	200	145.2	32.5	3.98
	250	134.2	30.0	5.02
	300	138.5	22.2	33.9
A2, z. USY, 1%	200	125.0	33.1	0.17
A2, z. USY, 2%	200	132.4	33.1	0.26
A3, no catalyst	200	145.2	32.3	0.16
A4, z. HY, 4%	200	133.6	32.2	3.81

Regarding the methane production in this reactor, the operating conditions obtained so far, which enhanced and maximized its production was, a temperature of 300 °C and a weight heterogeneous catalyst content of 4% of zeolite HY. However, it should be noticed that there are compounds, in the produced gas, that were measurable by the portable sensors. It was possible to conclude also, that, z. HY catalyst was progressively deactivated, through the visualization of carbon particles deposition on the surface catalyst. Nevertheless, the catalyst can be reactivated, by calcination, to be used again in the Sabatier reaction, so it's possible to conclude that, the use of z. HY catalyst was clearly suitable in the Sabatier reaction (methanation process), at normal pressure and temperatures between 200–300 °C.

Besides, the use of acidified zeolite HY catalyst and higher temperatures increases methane production, which points out for further research steps comprising the increase of catalyst mass, and, to study the increase of pressure and temperature in a new laboratory prototype. It will also be of interest to investigate the use of other heterogeneous catalysts which may be more active such as other zeolites, acid clays, or bimetallic catalysts, as well, as study the production of other biofuels, like biomethanol, bio-DME, etc., regarding this electrolytic system.

IV. ACKNOWLEDGMENTS

This work was partially funded by FCT - Fundação para a Ciência e Tecnologia, Portugal, through project reference PCIF/GVB/0167/2018.

V. REFERENCES

[1] Guerra, L.;Gomes, J.; Puna, J., Rodrigues, J. (2015) Preliminary study of synthesis gas production from water electrolysis, using the ELECTROFUEL concept. Energy, 89, 1050-1056.

[2] Chen, X.; Guan, C.; Xiao, G.;Du, X.; Wang, J. (2015) Syngas production by high temperature steam/CO2 co-electrolysis using solid oxide electrolysis cells. Faraday Discuss., 182, 341-351.

[3] Sapountzi, F.; Gracia, J.; Weststrate, C.; Friedriksson, H.; Niemantsverdriet, J. (2017) Electrocatalysts for the generation of hydrogen, oxygen and synthesis gas, Prog. Energy Combust. Sci., 58, 1-35.

[4] Guerra, L.; Rossi, S.; Rodrigues, J.; Gomes, J.; Puna, J., Santos, M. (2018) Methane production by a combined Sabatier reaction/water electrolysis process, J. Environ. Chem. Eng., 6, 671-676.

[5] Guerra, L.; Moura, K.; Rodrigues, J.; Gomes, J.; Puna, J.; Santos, M. (2018) Synthesis gas production from water electrolysis using the Electrocracking concept, J. Environ. Chem. Eng., 6, 604-609.

[6] Gonçalves, A., Puna, J., Guerra, L., Rodrigues, J., Gomes, J., Santos, M., Alves, D. (2019) Towards the development of syngas/biomethane electrolytic production, using liquefied biomass and heterogeneous catalyst, Energies, 12, 3787.

Multi-scale landscape visual impact assessment for onshore wind farms in rural area of China

1st Jinjin Guan 2nd Beining Li 3rd Yinan Lin

Faculty of Landscape Architecture
East China University of Science and Technology
Shanghai, China

jinjin.guan@rub.de lbn20003428@163.com lynmon@163.com

Abstract

Growing attention on global de-carbonization, energy security, and sustainable development has made wind energy one of the most popular renewable energy sources. With the trend of huge-size wind turbines and more distributed wind farms constructed in densely populated areas of China, the impact of wind turbines on landscape can't be ignored. This paper aims to assess landscape visual impact at different spatial scales caused by large-size wind turbines. Several wind farms with different topographic and spatial scales in the Yangtze River Delta of China were selected for viewshed analysis in GIS. Based on the theoretical research on visual perception mechanism and visual impact threshold, the indicators are collected by questionnaires and analyzed with linear regression analysis. The outcomes imply that dynamic components are highly related indicators within a close distance (＜ 1 km), landscape aesthetics are correlated within a middle distance (1-4 km), and ecological elements are significant at a large distance (＞ 4km). This paper explores correlated indicators of visual impact at different spatial scales that provide recommendations for wind farm site selection.

Keywords: Wind farm; landscape visual impact assessment; GIS; visual impact threshold

I. INTRODUCTION

The global demand for renewable energy is growing under the impact of climate change. Wind energy is one of the effective solutions to achieving the carbon-neutrality target for various countries. By 2021, over 100 countries have chosen wind energy as the substitute for fossil fuels. Based on the Global Wind Report, the cumulative capacity of wind energy has reached 837GW at the end of 2021 [1]. Among them, onshore wind is the mainstream with a 93% share. Onshore wind is favorable with comparatively low prices, mature technologies, and a broad market. However, the rapid expansion of wind facilities encountered various disturbances, including environmental, socio-cultural, political, economic, and community dimensions [2][3][4].

China ranks first as the leading country in both cumulative wind energy capacity and annual installation. Although the wind industry in China started later than in western countries, it currently occupies a large proportion of the global wind market in the last decade. By 2021, the total wind capacity achieved 338 GW, accounting for around 40% of the world [5]. The dramatic growth of wind capacity concentrates in the north and west provinces, causing the unbalancing spatial distribution of wind farms and serious wind curtailment [6][7]. As the annual yield of wind energy increases, the unbalanced spatial distribution of the supply side and the consumption side imposes a great burden on the grid connection of wind power and long-distance high-voltage transportation.

According to the 14th Five-Year Plan, low-speed, distributed wind farms are encouraged to be built in densely populated areas in southeast China to release burdens on grid connection and electricity transition [8]. The policy mitigates regional disparities, but it aggravates land-use conflicts and environmental impact in the locality, which causes fierce community resistance and puts challenges to spatial planning and wind project operation [9].

II. VISUAL IMPACT

The environmental impacts caused by wind energy are much fewer than by conventional energies. However, the installation of large-scale wind farms has gradually generated the conflicts between environment and wind energy development [10][11]. The landscape visual impact receives universal public attention as the number and height of WTs grow. Because it brings broad influences to people's daily life in an extensive spatial area. For areas with traditional and rural landscapes, the visual pollution is recognized as an impairment of local identity, and disturbing landscape aesthetics [12][13]. The extremely huge vertical scale of the wind turbines creates a huge contrast with the elements of the natural landscape. For a 20 to 25-year operation period, the

IEECP'22, July 21-22, 2022, Oxford, United Kingdom

visual impact and landscape degradation are considered an irreversible threat to the place identity.

As wind energy pioneers, Germany, the United Kingdom, and other European countries have developed various approaches to landscape visual impact assessment in wind farm planning.

Gerhards discusses the existing methods and classifies them into two paradigms: objective paradigm (or expert paradigm/spatial paradigm) and subjective paradigm (or psychophysical paradigm) according to whether the evaluators influence the evaluation results or not (Table 1) [14]. The objective methods are mainly developed by Nohl [15][16], Köppel et al. [17], Gerhards [14], and Roth [18][19], which advocate expert participation, standardized evaluation process, and quantitative analysis free from any influence from landscape viewers. The subjective paradigm emphasizes viewers' perception and emotion of the landscape. The analysis methodology can be flexible and individual without being limited by any structured framework or specific criteria and characterized by specific details.

In practice, objective and subjective paradigms are usually integrated into the Multi-Criteria Decision Making (MCDM) framework, Analytic Hierarchy Process (AHP), and Contingent Valuation Method (CVM) in site selection [27]. More specific methods, like the Fuzzy Analytic Hierarchy Process (FAHP), are applied to obtain the different weights of the criteria and evaluate the alternatives [28]. Sowińska-Świerkosz and Chmielewski discuss the methods of choosing reasonable indicators for landscape visual assessment [29]; Del Carmen Torres Sibille et al., approach the wind farm site selection and landscape protection by using a multi-criteria comprehensive assessment method [30]; the planning authorities in the United Kingdom have rich experiences in heritage and landscape protection, and have published specific guidelines dealing with landscape and wind farm planning [31]. The following are the three typical methods broadly used by various governments for assessing landscape visual impact in wind farm projects.

For protecting the visual landscape resource, a number of countries published guidelines to standardize the process of landscape visual impact assessment for wind farm planning [34][35][31]. The quantitative assessment methods put forward by Nohl, and improved by Paul et al. and Roth have been popularized for calculating the compensation area and fees [15][36][18]. Some multi-criteria, decision-making systems are set up for comprehensive planning targets, combining aesthetic knowledge, spatial analysis, and statistical methods to achieve more precise and reasonable conclusions of visual assessment and reasonable planning [37][38][11][39].

However, most landscape visual impact assessments for wind farms are result-oriented, deriving the results of wind turbines viewshed, instead of the reason causing visual impact. Indeed, the visual impact comes from wind facilities. But the mechanism of visual perception and visual impact can be researched to find out the influencing factors of visual impact. This paper attempts to investigate the visual impact and its correlated factors at different scales, which helps to explore definite solutions for visual impact mitigation.

III. METHODS

This research is based on the case study of Zhongying Wind Farm, located in the mountain area of Ningbo City, Zhejiang Province of East China (Fig.1). It is a typical rural wind farm surrounded by villages, farmland, forests, and tea gardens with a dense population nearby. A total of 18 WD103-2500T wind turbines have been installed on the ridge of Fuquan Mountain at altitudes of between 140 and 450 m, which causes serious visual impact, landscape deterioration, and influence on recreational visits. The visual intrusion, attached to other environmental impacts, arises the fierce social opposition and disapproval, especially from close-by villages. However, the landscape visual impacts are not explicitly the declining functions of distance, which change with various factors and their interaction relationship. This paper aims to explore the key factors influencing visual impact under different distance groups.

Through the pre-study of literature and field trip, a questionnaire sheet is designed based on the classification of distance from residents to the wind turbines to dig out the key factors in different distances. In the questionnaire, the degree of visual impact is asked to score as the dependent variable with an 11-point Likert-type scale (i.e., 0: serious impact, 10: no impact). Additionally, the related factors of visual impact collected from pre-investigation are listed in the questionnaire as independent variables as listed in Table 2. The data are processed by analysis of variance (ANOVA) and linear regression analysis through SPSS with four distance groups: 1) within 1 km; 2) 1 to 2 km; 3) 2 to 4 km; 4) above 4 km. Recommendations for landscape planning and visual impact mitigation solutions are put forward according to the statistical analysis in each distance group.

Classification	Objective methods	Subjective methods
Basic value	Aesthetic and ecological value of landscape	Public preference and landscape perception
Methodology	Multi-Criteria Decision Making (MCDM) framework AHP Contingent Valuation Method (CVM) Fuzzy Analytic Hierarchy Process (FAHP)	Preference model Scenic Beauty Estimation procedure (SBE) Law of Categorical Judgment (LCJ) SD
Paradigm	Expert paradigm	Psychophysical paradigm Cognitive paradigm Experimental paradigm
Representative literatures	(Lewis, 1964; Litton, 1968, 1974; Magill & Litton, 1986)	(Daniel & Boster, 1976； Buhyoff et al., 1978; Buhyoff et al., 1979)
Characteristics	Structural, practical, conscious,	Flexible ,individual, full of specific details
Relationship with viewers	Not including	Mainly including the perception and emotion of viewers
Classification	Objective methods	Subjective methods
Participants	Expert group consists of planners, ecologists, aesthetic experts, etc.	Expert group, community, the local planning authority, public

Table 1 Comparison of landscape visual assessment methods.

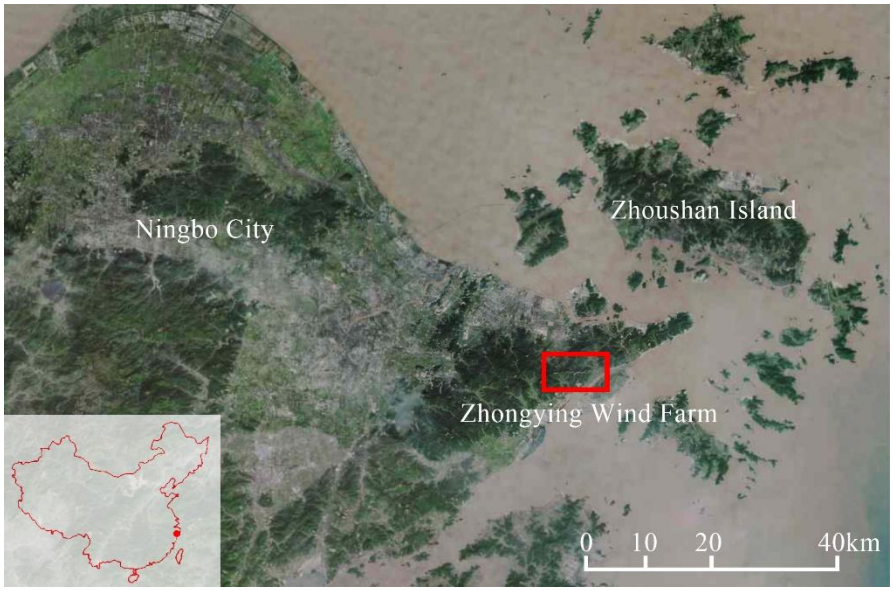

Figure 1. Location of Zhongying Wind Farm. (Source: ArcGIS Earth)

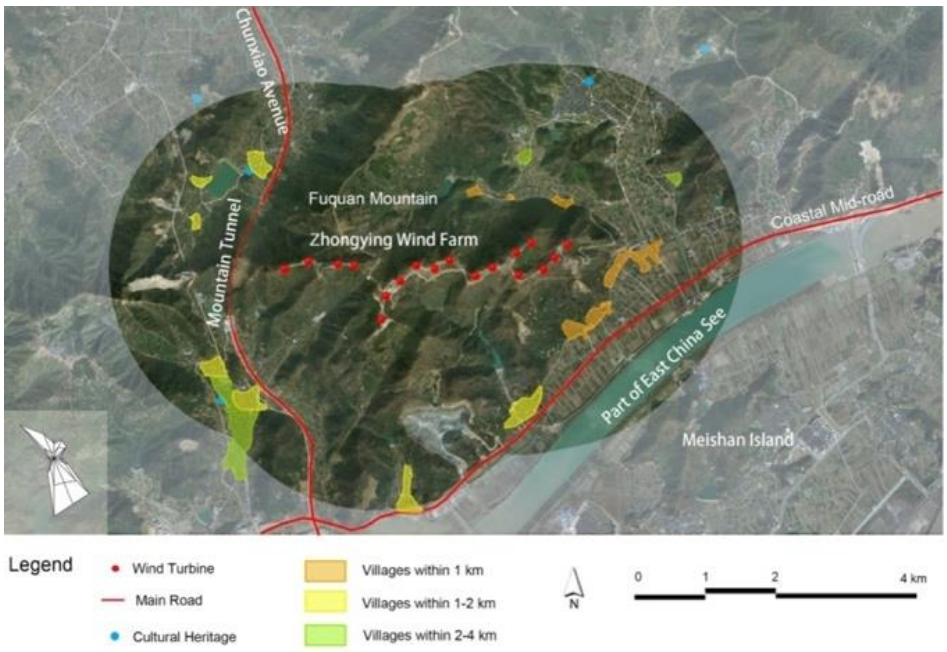

Figure 2. Distance groups category of Zhongying Wind Farm (Source: edited by authors)

IV. RESULTS

A. Data Collection and Preprocessing

The research team interviewed random sampling across 17 villages and rural areas around Zhongying Wind Farm of 180 respondents, with 169 valid samples returned. These samples were randomly selected across the research region to keep balancing samples between four distance groups.

B. One-Way Analysis of Variance

The data collected through questionnaires were processed in the following steps. Firstly, a total of 10 factors were divided into three categories according to their attributes and interaction with visual impact : WT-related variables, environment-related variables and respondent-related variables. The correlation between each independent variable (influencing factors) and dependent variable (visual impact) was detected by the one-way analysis of variance. In Table 2, it can be noted that among 10 variables, 7 variables were statistically significant. Dynamic rotation (F=97.728), aesthetic change (F=32.903), shadow flicker (F=29.121), visibility (F=27.331), and size of WTs (F=20.235) are statistically significant to the dependent variable, visual impact for wind turbines. Factors of ecological function degradation (F=15.975) and length of residence (F=9.757) are also significant with a lower F value. Factors of the number of WTs, original environment quality, and individual Eyesight are not correlated to visual impact from a statistical perspective since their P-values are over 0.05.

Table 2. Variance analysis of correlations between potential factors and visual impact

Variables	Categories	F (ANOVA)	P (Significance)
WT-related variables			
Dynamic rotation	1: quick; 2: medium; 3: slow	97.728**	0.000
Shadow flicker	1: very serious; 2: medium; 3: no feeling	29.121**	0.000
Size of WTs	1: too huge; 2: acceptable; 3: not huge	20.235**	0.000
Number of WTs	1: too many; 2: medium; 3: few	1.494	0.228
Environment-related variables			
Original environment quality	1: high; 2: medium; 3: low	0.112	0.894
Ecological function degradation	1: serious degradation; 2: acceptable degradation; 3: little/no degradation	15.975**	0.000
Visibility	0: invisible, 2: partly visible, 3: most visible, 4: totally visible.	27.331**	0.000
Aesthetic change	1: seriously changed; 2: acceptable change; 3: little or no change	32.903**	0.000
Respondent-related variables			
Individual Eyesight	1: good; 2: general; 3: poor	2.122	0.123
Length of residence	1:＜5, 2: 5-10, 3: 10-20, 4:＞20. (years)	9.757**	0.000

Note: * $p \leq 0.05$, ** $p \leq 0.01$.

C. Linear Regression Analysis

The second step is to introduce all the statistically significant variables into linear regression by distance category to tease further relative significance of each variable in each distance group and detect whether the correlation variables in each group change with the distance growth. The regression analysis is separately conducted by distance groups, with the same dependent variable, visual impact of wind turbines. The statistically significant variables (n=7) in the variance analysis are selected as independent variables. As Table 3 illustrates, four linear regression models were run with statistically significant variables.

In Group 1 (distance below 1 km), the score of visual impact is 2.39 within 0 to 10 scaling, referring to serious impact degree. Among the correlated variables, only the variable of dynamic rotation and length of residence were statistically significant ($P \leq 0.01$.). In Group 2 and Group 3 (distance from 1 to 4 km), the score of visual impact given by respondents is 5.39 and 5.78 respectively. The factor ecological function degradation ranks first as the most significant independent variable, which reveals that the respondents' attitude toward visual impact is highly influenced by local ecological service. In Group 4 (distance above 4 km), the visual impact score is 6.21. With the distance growing and less physically environmental impact, the focus of visual impact turns to the factor of aesthetic change.

V. DISCUSSION

A. Visual Perception and Visual Impact

Visual landscape refers to the visual expression of the elements, structure, and functions of landscape [40]. The connotation of "landscape" includes the visual perception of landscape, as well as other sensory and ecologic, economic, and functional aspects of landscape. Broadly speaking, landscape refers to all the characteristics of the earth's surface. Therefore, the influencing factors of landscape visual impact do not merely derive from the visual impairment from wind turbines, but also include the socio-demographic factors and surrounding environment. With three dimensions of factors involved in this research, the visual impact can be explained under the generalized visual landscape connotation.

Visual perception dominates the sensory with 87% of the sensory information, while the other 13% (e.g., auditory, olfactory, tactile) is assisted from other dimensions to confirm and reinforce the information [41]. Both in terms of information volume and spatial extent, visual perception is the most important sensory source for information, which also influences behavior, preference, and aesthetics in landscape research. It has also become an instrument in landscape protection, monitoring, and planning [42]. Visual perception is itself a complex information processing mechanism related to physiology, psychology and social attributes of human beings [43]. Notably, not all perceptional information has an impact, only if it exceeds a certain threshold that depends on the stimulus intensity of the object and the sensitivity of the observer. Viewers' responses can be classified into two types: visual perception threshold (whether people can see the object) and visual impact threshold (whether people feel themselves being influenced by the object). The visual perception threshold (detection and recognition) relies more on viewers' physiological perception capacities, which are measurable as above mentioned, rather than cognitive mechanism (psychological and social perception). The visual impact threshold is more challenging and subjective to obtain, which depends on viewers' subjective judgment criteria and differs largely from person to person, and from society to society [44].

Table 3. Results from linear regression of community acceptance for wind turbines

Independent variable	Group 1	Group 2	Group 3	Group 4
Dynamic rotation	1.914**	0.531	0.339	0.164
Shadow flicker	-0.129	0.030	0.163	-0.457
Size of WTs	-0.603	0.407	-0.105	-0.088
Ecological function degradation	0.250	1.655**	0.752**	0.490
Visibility	-0.598	-0.385	-0.437	-0.664
Aesthetic change	0.656	0.204	0.590**	1.220**
Length of residence	-1.093**	-0.116	-0.192	-0.169
Constant	4.804	0.974	3.761	5.079
R2	0.722	0.516	0.563	0.464
N	49	46	37	37

Note: [a] Constant values by model use unstandardized coefficients. All others use standardized coefficients.
* $p \leq 0.05$, ** $p \leq 0.01$.

B. Visual Impact and Distance

This paper attempts to explore the relationship between the correlation factors of visual impact and distance. According to the regression analysis, dynamic rotation speed of wind turbines' blades and length of residence for the respondents are both the key factors affecting the visual impact within a close distance. However, referencing the visual impact threshold theory, the former factor is more inclined to the physiological perception threshold, while the latter factor belongs to the category of cognitive mechanism (psychological and social perception). During the local investigation, the residents complained about the linkage effects caused by the huge blade rotation: noise, dizziness and the sense of insecurity. Shang and Bishop [44] point out that dynamic WTs are about 10 to 20% larger in their size in visual perception than the size of the static ones. As the distance grows, the viewshed area of wind turbines declines, and direct visual impact is not a dominant factor again. At medium and large spatial distances, ecological function degradation and aesthetic change are the main factors affecting the visual impact. The opponents concentrate on local ecological function disruption, especially harming the nearby flora and fauna, causing soil erosion and water pollution during the construction and operation process [45][46]. From the perspective of aesthetic, the huge size and technological impression spoil the original landscape character [47].

C. Recommendations

When the landscape suffers impairment, replacement is suggested on the same site or near the proposal project, to recover the whole environmental quality to some extent. Such compensation is not only possible through a similar restoration of the status quo, but also through a "landscaping-appropriate redesign". Landscape redesign is mandatory in the aesthetically significantly impaired space and the immediate vicinity of the intervention site. It is worth mentioning that a slight difference from the original landscape is allowed, as long as the essential features, elements, structure, and functions are guaranteed.

VI. CONCLUSION

In China, the growing demand for wind energy complies with the carbon neutrality strategy. While the rapid expansion of wind farms exacerbates environmental impacts, especially in dense population areas. Among all the negative impairments, visual impact is highly subjective and uncertain, making quantitative assessment difficult. This paper investigates the factors related to the visual impact of wind farms in rural areas in the eastern coastal area of China through the questionnaire, one-way analysis of variance and regression analysis. The results reveal that the visual impact does not decay with distance in a linear function. Further, the highly correlated factors of visual impact change with distance growth. In close-distance, dynamic elements are the key factor, followed by ecological function degradation in mid-distance, and aesthetic change in the long-distance. It is recommended to formulate compensation strategies under different buffer distances. The outcomes help to optimize the landscape planning and compensation implementation for wind farms. In the long run, this study seeks a feasible solution for balancing regional wind power development and environmental resource protection.

VII. REFERENCES

[1] J. Lee, F. Zhao, Global Wind Report 2021, 2021. http://www.gwec.net/global-figures/wind-energy-global-status/.

[2] N. Brennan, T.M. Van Rensburg, C. Morris, Public acceptance of large-scale wind energy generation for export from Ireland to the UK: evidence from Ireland, J. Environ. Plan. Manag. 60 (2017) 1967–1992. doi:10.1080/09640568.2016.1268109.

[3] M. Wolsink, Social acceptance revisited: gaps, questionable trends, and an auspicious perspective, Energy Res. Soc. Sci. 46 (2018) 287–295. doi:10.1016/j.erss.2018.07.034.

[4] J.R.F. Diógenes, J. Claro, J.C. Rodrigues, M.V. Loureiro, Barriers to onshore wind energy implementation: A systematic review, Energy Res. Soc. Sci. 60 (2020) 1–33. doi:10.1016/j.erss.2019.101337.

[5] J. Lee, F. Zhao, Global Wind Report 2022, 2022.

[6] J. Guan, Lessons from German On-shore wind farm planning, J. Phys. Conf. Ser. 1102 012029. (2018) 1–7. doi:10.1088/1742-6596/1102/1/012029.

[7] G.L. Luo, Y.L. Li, W.J. Tang, X. Wei, Wind curtailment of China's wind power operation: Evolution, causes and solutions, Renew. Sustain. Energy Rev. 53 (2016) 1190–1201. doi:10.1016/j.rser.2015.09.075.

[8] REN21, REN21 - 2019 Global Status Report, 2019. https://wedocs.unep.org/bitstream/handle/20.500.11822/28496/REN2019.pdf?sequence=1&isAllowed=y%0Ahttp://www.ren21.net/cities/wp-content/uploads/2019/05/REC-GSR-Low-Res.pdf.

[9] M. Eichhorn, F. Masurowski, R. Becker, D. Thrän, Wind energy expansion scenarios – A spatial sustainability assessment, Energy. 180 (2019) 367–375. doi:10.1016/j.energy.2019.05.054.

[10] J. Firestone, A. Bates, L.A. Knapp, See me, Feel me, Touch me, Heal me: Wind turbines, culture, landscapes, and sound impressions, Land Use Policy. 46 (2015) 241–249. doi:10.1016/j.landusepol.2015.02.015.

[11] P. Sklenicka, J. Zouhar, Predicting the visual impact of onshore wind farms via landscape indices: A method for objectivizing planning and decision processes, Appl. Energy. 209 (2018) 445–454. doi:10.1016/j.apenergy.2017.11.027.

[12] C. Hallan, A. González, Adaptive responses to landscape changes from onshore wind energy development in the Republic of Ireland, Land Use Policy. 97 (2020) 104751. doi:10.1016/j.landusepol.2020.104751.

[13] S. Linke, Ästhetik, Werte und Landschaft, in: O. Kühne, H. Megerle, F. Weber (Eds.), Landschaftsästhetik Und Landschaftswandel, Springer VS., Wiesbaden, 2017: pp. 23–40.

[14] I. Gerhards, Die Bedeutung der landschaftlichen Eigenart für die Landschaftsbildbewertung, Freiburg University, 2003.

[15] W. Nohl, Beeinträchtigung des Landschaftsbildes durch mastenartige Eingriffe: Materialien für die naturschutzfachliche Bewertung und Kompensationsermittlung, Ministeriums für Umwelt, Raumordnung und Landwirtschaft des Landes NordrheinßWestfahlen, München, Germany, 1993. https://www.landschaftswerkstatt.de/dokumente/Masten-Gutach-1993.pdf.

[16] W. Nohl, Ist das Landschaftsbild messbar und bewertbar? – Bestandsaufnahme und Ausblick, in: Presentation at the University of Natural Resources and Life Sciences Vienna, Wien, 2010: pp. 1–18. http://www.skiaudit.info/media/files/landschaftsbildtagung/nohl.pdf.

[17] J. Köppel, U. Feickert, L. Spandau, Praxis der Eingriffsregelung. Schadenersatz an Natur und Landschaft?, Ulmer, 1998.

[18] M. Roth, D. Gruehn, Visual Landscape Assessment for Large Areas - Using GIS, Internet Surveys and Statistical Methodologies, Proc. Latv. Acad. Sci. (2012) 129–142.

[19] M. Roth, E. Bruns, Landschaftsbildbewertung in Deutschland.Stand von Wissenschaft und Praxis.Landschaftsbildbewertung im Spannungsfeld von Wissenschaft und Praxis, Literaturdatenbank "DNL-online," Bonn, Germany, 2016. http://www.bfn.de/fileadmin/BfN/service/Dokumente/skripten/skript_439_Labi_fin.pdf.

[20] J.R. Lewis, British Rocky Shores Hormone Action, English Universities Press, London, UK, 1964. https://science.sciencemag.org/content/sci/147/3658/601.1.full.pdf.

[21] R.B. Litton, Forest landscape decription and inventories: A basis for land planning and design.U.S.D.A. Forest Service Research Paper PSW-49., Pacific Southwest Forest and Range Experiment Station Forest Service, U. S. Department of Agriculture, Berkeley, California, 1968.

[22] R.B. Litton, Visual Vulnerability of Forest Landscapes, J. For. 72 (1974) 392–397. doi:https://doi.org/10.1093/jof/72.7.392.

[23] A.W. Magill, R.B. Litton, A Color Measuring System for Landscape Assessment, Landsc. J. 5 (1986) 45–54. doi:10.3368/lj.5.1.45.

[24] T.C. Daniel, R.S. Boster, Measuring Landscape Aesthetics: The Scenic Beauty Estimation Method, USDA Forest Service Research Paper RM-167,Rocky Mountain Forest and Range Experiment Station, Fort Collins, CO., 1976. https://www.fs.fed.us/rm/pubs_rm/rm_rp167.pdf.

[25] G.J. Buhyoff, J.D. Wellman, H. Harvey, R.A. Fraser, Landscape architects' interpretations of people's landscape preferences, J. Environ. Manage. 6 (1978) 255–262.

[26] G.J. Buhyoff, W.A. Leuschner, J.D. Wellman, Aesthetic impacts of Southern Pine Beetle damage, J. Environ. Manage. 8 (1979) 261–267.

[27] IPCC, Summary for Policymakers. In: IPCC Special Report on Renewable Energy Sources and Climate Change Mitigation [O. Edenhofer, R. Pichs-Madruga, Y. Sokona, K. Seyboth, P. Matschoss, S. Kadner, T. Zwickel, P. Eickemeier, G. Hansen, S. Schlömer, C. von Stechow , Cambridge, United Kingdom and New York, NY, USA, 2011. http://www.uncclearn.org/sites/default/files/inventory/ipcc15.pdf.

[28] X. Tang, The theories, Methodology of Landscape Visual Environment Assessment and their Application: The case of the three Gorges of the Yantze River (Chongqing), Fudan University. [In Chinese], 2007.

[29] B.N. Sowińska-Świerkosz, T.J. Chmielewski, A new approach to the identification of Landscape Quality Objectives (LQOs) as a set of indicators, J. Environ. Manage. 184 (2016) 596–608. doi:10.1016/j.jenvman.2016.10.016.

[30] A. Del Carmen Torres Sibille, V.-A. Cloquell-Ballester, V.A. Cloquell-Ballester, R. Darton, Development and validation of a multicriteria indicator for the assessment of objective aesthetic impact of wind farms, Renew. Sustain. Energy Rev. 13 (2009) 40–66. doi:10.1016/j.rser.2007.05.002.

[31] Cornwall Council, An Assessment of the Landscape Sensitivity to On- shore Wind Energy and Large- scale Photovoltaic Development in Cornwall, 2013. www.landuse.co.uk.

[32] Cornwall Council, An Assessment of the Landscape Sensitivity to On- shore Wind Energy and Large- scale Photovoltaic Development in Cornwall, Cornwall, 2013. https://www.cornwall.gov.uk/environment-and-planning/cornwalls-landscape/landscape-character-assessment/?page=24874&page=24874.

[33] The Landscape Institute with the Institute of Environmental Management & Assessment of UK, Guidelines for Landscape and Visual Impact Assessment, 2nd ed., Spon Press, London & New York, 2005.

[34] R. Oligmüller, L. Ökol, A. Schäfers, A. Gers, Landschaftsbildbewertung.B-Plan Nr. 74n "Fernholte," Recklinghausen, 2017. http: // www.LuSRe.de.

[35] AILA (Australian Institute of Landscape Architects), Guidance Note for Landscape and Visual Assessment, Queensland State, Australia, 2018. https://www.aila.org.au/imis_prod/documents/AILA/QLD/2018/AILA_GNLVA_June_2018V2.pdf.

[36] V.H. Paul, D. Uther, M. Neuhoff, K. Winkler-hartenstein, H. Schmidtkunz, GIS-gestütztes Verfahren zur Bewertung visueller Eingriffe durch Hochspannungs- freileitungen.Herleitung von Kompensationsmaßnahmen für das Landschaftsbild, Naturschutz Und Landschaftsplan. 35 (2004) 139–144.

[37] J. Molina-Ruiz, M.J. Martínez-Sánchez, C. Pérez-Sirvent, M.L. Tudela-Serrano, M.L. García Lorenzo, Developing and applying a GIS-assisted approach to evaluate visual impact in wind farms, Renew. Energy. 36 (2011) 1125–1132. doi:10.1016/j.renene.2010.08.041.

[38] A. Minelli, I. Marchesini, F.E. Taylor, P. De Rosa, L. Casagrande, M. Cenci, An open source GIS tool to quantify the visual impact of wind turbines and photovoltaic panels, Environ. Impact Assess. Rev. 49 (2014) 70–78. doi:10.1016/j.eiar.2014.07.002.

[39] E.A. Virtanen, J. Lappalainen, M. Nurmi, M. Viitasalo, M. Tikanmäki, J. Heinonen, E. Atlaskin, M. Kallasvuo, H. Tikkanen, A. Moilanen, Balancing profitability of energy production, societal impacts and biodiversity in offshore wind farm design, Renew. Sustain. Energy Rev. 158 (2022). doi:10.1016/j.rser.2022.112087.

[40] S. Nijhuis, R. van Lammeren, M. Antrop, Exploring the Visual World, 2nd ed., IOS PRESS, 2011. doi:10.2307/j.ctt1xp3nmm.13.

[41] S. Bell, Landscape: Pattern, Perception and Process, 2nd ed., Routledge Taylor & Francis Group, USA and Canada, 2012. http://weekly.cnbnews.com/news/article.html?no=124000.

[42] D. Harris, D.F. Ruggles, Sites unseen: Landscape and Vision, University of Pittsburgh Press, Pittsburgh, 2007. doi:10.2307/j.ctt7zw9w9.

[43] D. Joly, T. Brossard, J. Cavailhès, M. Hilal, F.-P. Tourneux, C. Tritz, P. Wavresky, A Quantitative approach to the visual evaluation of landscape, Ann. Assoc. Am. Geogr. 99 (2009) 292–308. doi:10.1080/00045600802708473.

[44] H. Shang, I.D. Bishop, Visual Thresholds for Detection, Rrcognition and Visual Impact in Landscape Settings, J. Environ. Psychol. 20 (2000) 125–140. doi:10.1006/jevp.1999.0153.

[45] P. Roddis, S. Carver, M. Dallimer, P. Norman, G. Ziv, The role of community acceptance in planning outcomes for onshore wind and solar farms: An energy justice analysis, Appl. Energy. 226 (2018) 353–364. doi:10.1016/j.apenergy.2018.05.087.

[46] X. Guo, X. Zhang, S. Du, C. Li, Y.L. Siu, Y. Rong, H. Yang, The impact of onshore wind power projects on ecological corridors and landscape connectivity in Shanxi, China, J. Clean. Prod. 254 (2020). doi:10.1016/j.jclepro.2020.120075.

[47] W. Nohl, Landschaftsästhetisches Erleben: Grundformen und ihre nachhaltige Wirkung, Stadt+Grün. 59 (2010) 29–36.

An efficient model for induction motor fault detection using a deep transfer learning network

Alasmer Ibrahim
Wolfson Centre for Magnetics
Cardiff University
Cardiff CF24 3AA, UK
Ibrahima21@cardiff.ac.uk

Fatih Anayi
Wolfson Centre for Magnetics
Cardiff University
Cardiff CF24 3AA, UK
Anayi@cardiff.ac.uk

Michael Packianather
High-Value Manufacturing Group
Cardiff University
Cardiff CF24 3AA, UK
packianatherms@cardiff.ac.uk

Abstract

The reliability and availability of induction motors is significant which can be achieved by monitoring the performance of the motor regularly in the industry. Knowledge-based approaches can be able efficiently to deal with the sensor data for ensuring the reliability with high motor performance. Recently, deep learning networks based on machine learning structures have provided an accurate and faster framework for fault diagnosis by ignoring feature extraction process. However, training a deep convolutional neural network (CNN) is complex and time-consuming procedure. For this reason, this paper proposes a novel deep learning procedure for fault diagnosis using thermal images data of the induction motor applying residual neural network with 50 convolutional layers as feature extraction. The pre-trained deep convolutional (ResNet-50) of the transfer learning is trained on ImageNet based weight. This work includes the effect of data augmentation for enhancing the performance of the proposed model and ensuring its robustness for fault diagnosis. Firstly, the collected images are pre-processed resized as input datatype of Resnet-50 network. Next, transfer leaning model based on convolutional neural network (ResNet-50) structure is built to process the prepared images. Lastly, classifying the prepared images based on the related conditions of the induction motor. The experimental result shows that the proposed model has achieved an accuracy of 99.98%. The presented model has further compared with recent deep learning applications, and it has proved its robustness in fault diagnosis.

Keywords: Thermal mages, ResNet-50 model, pre-trained model, fault diagnosis.

I. INTRODUCTION

It is possible for several problems to arise unexpectedly in the induction motors and causing a failure during even the normal operation which can lead to production loss. However, by applying condition monitoring to check the behavior of the motor. So, the motor lifetime can be extended, and maintenance cost can be minimized [1]. Many types of defects may occur in an induction motor, which can be categorized under electrical and mechanical defects which are caused by abrasion, unbalanced loads, electrical stress. Mechanical failure such as the bearing fault is the most frequent fault in the induction motor which represents around 53% of the motor faults [2]. Electrical fault such as the rotor fault appears with 10% of the motor failure [3]. In addition, stator fault stator failure occurs typically at a rate of 38% of motor failure [4]. In recent years, many researchers have focused their attention on fault diagnostics in different science fields. As a common type of fault diagnosis, data-driven fault diagnostic technique which has attracted the researcher's attention may construct failure modes using the historical data of the application without the need of signal symptoms [5]. This can make it particularly adapted for complex systems with a large amount of data [6]. With the faster growth of smart manufacturing, the amount of data produced by machines and devices is further increased and easier to be collected. The ability to learn about huge amount of historical data is the most important aspect of the data-driven fault diagnostic technique [7]. A number of methods have applied in this field such as K-Nearest Neighbor (KNN), support vector machine (SVM), Random Forest algorithm (RF), Invasive Weed Optimization algorithm (IWO), and artificial neural networks (ANN). In [3] KNN was suggested to build a diagnostic system to detect the degradation of the bearing and the result was satisfactory based on the diagnostic performance. SVM is proposed in [8] to build a reliable fault diagnosis scheme for incipient low speed rolling elements bearing failure. The Experimental results reported that the proposed model has achieved a highest classification accuracy of 98.4%. In [9] RF was intended to achieve a novel hybrid approach for fault diagnosis of rolling bearings. The obtained results showed that the proposed method reached a classification accuracy rate of 88.23%. In [10] a new diagnostic model is proposed applying the current and the vibration signals. The model combines the invasive weed optimizer with three different machine learning algorithms. The results have confirmed that the performance of the proposed model is satisfactory. A novel model was proposed in [11] for diagnosing bearing faults. The experimental results showed that the proposed scheme is a successful framework. As the aforementioned machine learning methods are comprised of feature extraction and feature selection processes [12]. It is however difficult to extract discriminative features to build a robust classification model [13]. Therefore, Deep learning (DL) has developed as a new area of research in the machine-learning science in order to address the issues mentioned above which it is capable of autonomously learning the representation attributes from raw data [14]. The use of DL

IEECP'22, July 21-22, 2022, Oxford, United Kingdom

approaches in the field of fault diagnosis has become increasingly popular such as deep belief network (DBN) and convolutional neural network (CNN) [15]. The use of such DL network show great potential for fault diagnosis can achieve the reduction of the handcrafted features impact created by feature extraction algorithms. However, fault identification requires a minimal number of labelled samples which limit the final prediction accuracies. In addition, DL models can include up to 5 hidden layers [16]. So, it is difficult to train deep CNN models without a huge amount of training datasets to train deep CNN models. Several studies have built deep CNN models by combining transfer learning techniques (TL) on ImageNet [17], then applied these CNN models as feature extractors on a small dataset in another domain [18]. Hence, deep TL can offer promising approaches to the problem of fault diagnosis. TL model uses deep learning network (DL) to transfer high-level properties from source data to target data [19]. One of the advantages of deep transfer learning is to use a layer-by-layer learning pattern to extract attribute from the input data, which allows its deep architecture to produce high data representations with a potential enhancement of the diagnosis performance.

As a result of this, this work proposes an efficient fault diagnosis model using transfer convolutional neural network based on residual neural network as a feature extractor considering 50 layers. ResNet-50 can extract high-quality features from images on ImageNet. It is anticipated that the suggested (ResNet-50) would increase the final prediction accuracy on fault diagnosis. The proposed model is investigated using thermal images of the induction motor.

The rest of this paper is structured as follows: Section II defines the related work; Section III presents the proposed model; materials and methods are illustrated in section IV; Section V reports results; and the conclusion is drawn in section VI.

II.RELATED WORK

This study includes data-driven fault diagnosis utilizing deep CNN networks and feature transfer. Due to the rapid development of smart manufacturing, data-driven fault detection has emerged as a popular research topic in recent years[12]. In [20] a new fault diagnosis based on the use the transfer learning of sparse autoencoder method and the experimental result has achieved a high accuracy of 99.82 %. In [21] The use of recurrent neural networks and dynamic Bayesian modelling to detect faults in induction motors was investigated. The model has carried out the real-time experiments with three motors, estimating the probability distributions for the motor's conditions and the model achieved an efficient result. A new model based on a performance comparison of sparse autoencoder with SoftMax regression was proposed in [22], and the result was satisfactory. In [23] a new model was proposed for intelligent fault diagnosis applying normalized sparse autoencoder of air compressors. In [24] a fault diagnosis method was suggested using stacked sparse autoencoder with ensemble empirical mode decomposition and the result has proved the robustness of the extracted features. In [25] deep learning model based hierarchical diagnosis method to diagnose the rolling element bearing fault, the obtained result has investigated the reliability of the model. A new deep transfer learning model was suggested in [26] to diagnosis the industry application faults, and the achieved result has investigated several state-of-art transfer learning result considering the operating condition and fault severities. Recently, an adaptive deep CNN model was suggested in [27], and the result was effective and robust. In [28] a hierarchical adaptive CNN was investigated for weight updating by adding an adaptive learning rate and a momentum component. In [29] an intelligent fault diagnosis model using hierarchical CNN was proposed for diagnosing rolling bearing faults. The result has proved the effectiveness of the CNN model. A new fault diagnosis based on the use of CNN with empirical mode decomposition was proposed in [30] and its results have indicated that more accurate and reliable than previous approaches. In [31] a CNN model-based approach for fault diagnosis was suggested for rotating machinery. The model compared to traditional techniques that rely on manual feature extraction, the results have demonstrated that the suggested method provides superior diagnostic performance. As reported by the aforementioned methods, there are not any published studies using to ResNet-50 model-based CNN tested on thermal images data of the induction motor. Therefore, a novel intelligent model for fault diagnosis is proposed in this work applying the pre-trained ResNet-50 model with an adjusted densely connected classifier. The robustness of the proposed model was investigated using thermal images of different conditions of the induction motor.

III.PROPOSED TECHNIQUE

The presented work builds a novel application that uses a pre-trained (ResNet-50) model based on CNN as a feature extractor. The whole dataset is divided into train, validation, and test subsamples which each subsample continuously plays the role of validating dataset to achieve the reliable performance for fault diagnosis. This model is trained by applying the weight of the ImageNet dataset. The block diagram of proposed model is shown in figure 1. Images are pre-processed with class imbalance technique and data augmentation technique. This can affect the achieved results by controlling the image zoom, horizontal flip, rotation, translation, and image orientation. Then, the structure of resnet-50 network was initialized restoring the pre-trained weight in ResNet-50. Next, the images are taken as input to obtain the features and training the model for the classification purpose. SoftMax classifier layers were added with 128 hidden neurons and determined with seven label classes. Adam optimizer, ReLU activation function, L2 regulation, categorical cross-entropy (CE), and dropout layers.

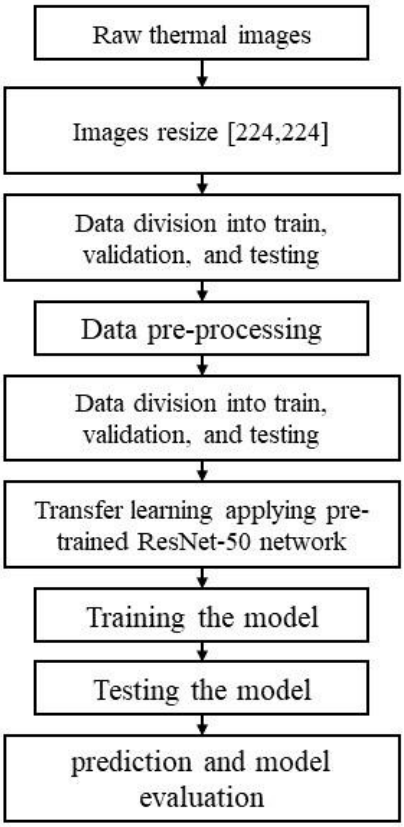

Figure1. Block diagram of the proposed network

The categorical cross-entropy

$$(CE) = -\sum_i^C t_i \log(f(s)_i) \quad (1)$$

Where t_i is the ground truth, and $f(s)i$ is the standard SoftMax.

$$f(s)_i = \frac{e^{s_i}}{\sum_i^C e^{s_j}} \quad (2)$$

Where s_i presents the given the class, s_j is the scores derived from the net for each class.

IV.MATERIALS AND METHODS

A. Deep ResNet-50 network architecture

CNN models' ability to accurately diagnose faults is constrained with the help of transfer learning that trained on ImageNet [17]. This work uses ResNet-50 that trained on ImageNet to classify different thermal images conditions of the induction motor. Resent-50 model has achieved an efficient performance in the field of images classification which extracts good quality features of images for building a strong fault diagnosis model.

The proposed ResNet-50 is consisted of 50-layers deep CNN[32] which includes one max- pooling layer, one average pool, and 48 convolutional layers. The basic structure of ResNet-50 is illustrated in figure 2 that used as feature extractor. The ResNet-50 is composed of five convolutional blocks of layers. The final convolutional block of a 50-layer deep residual network produces deep residual features that pre-trained on ImageNet. The convolutional blocks of a ResNet-50 are different from those of the traditional CNNs because of the introduction of a shortcut the connection between the input and output of each block. Using identity mappings as ResNet-50 shortcut connections can optimize the training process and minimise complexity[33]. That can lead to achieve a deeper model with fast training and less computational model if compared to i.e. VGG model [34].

The proposed work extracts the features from thermal images using last convolutional block of ResNet-50 (pre-trained model), and the output of the 5th Conv block is trained for fault classification. As a result, the output size of ReseNet-50 then is 2480.

B. Data Collection

The induction motor thermal images were captured in the Wolfson Magnetics Laboratory, School of Engineering Cardiff University, UK. The test rig is displayed in figure 3 which composes of the following components: induction motor, thermal camera (FLIR C2), and dynamometer, which serves as the load. The thermal camera was located approximately 60 cm from the motor housing center.

The thermal images have been captured with seven motor conditions considering the healthy and the faulty motor cases when the motor running at two speeds as described in Table1.

C. Data pre-processing

Due to the input size of the prosed ResNet-50 are 224 × 224 and the size of the collected images are 320×240, these images were resized to 224 × 224. Dataset was built which includes seven classes based on different motor conditions and each class has 350 images. The images are proposed with class imbalance technique and data augmentation technique to improve the model performance. This layer affects the achieved results by controlling the image zoom, horizontal flip, rotation, translation, and image orientation.

Table 1. Motor conditions

Fault mode	Motor load (rpm)	Images No.	Class label
Normal motor	1480/1450	350	0
IBF	1480/1450	350	1
OBF	1480/1450	350	2
8BRBF	1480/1450	350	3
IBF+1BRBF	1480/1450	350	4
OBF+5BRBF	1480/1450	350	5
BBF+8BRBF	1480/1450	350	6

D. Model evaluation

Some evaluation matrices have utilized to assess the performance of the proposed application such as the training accuracy and loss curves and the parameters given in the following equations:

$$\text{Overall accuracy} = \frac{TP+TN}{TP+FP+TN+FN} \quad (3)$$

$$\text{Precision} = \frac{TP}{TP+FP} \quad (4)$$

$$\text{Sensitivity} = \frac{TP}{TP+FN} \quad (5)$$

$$\text{F1\_score} = 2\times \frac{\text{Precision} \times \text{Sensitivity}}{\text{Precision} + \text{Sensitivity}} \quad (6)$$

Where TP is the true positive prediction, FP is false positive predictions, TN presents the true negative predictions, and the false negative predictions is stated by FN.

V. RESULT

The result of the pretrained model is presented for fault diagnosis in this section. Induction motor thermal images with different cases were employed as an input of the pre-trained ResNet model based on 50 layers network to extract the model features on ImageNet dataset. These features were trained on FC layer to predict the correct class. The classification result is presented in Table 2. The model has achieved classification accuracy of 99.98% with training error of 0.0015. In addition, the precision and F1-score have achieved great scores of 98.59, and 94.89; respectively. The overall trained accuracy and loss considering same epochs number are displayed in figure 4 and 5; respectively.

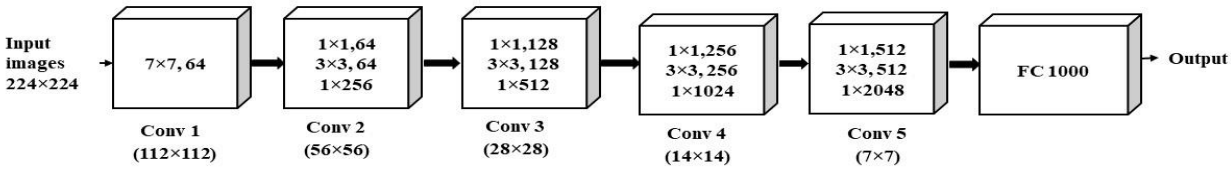

Figure 2. The architecture of the proposed ResNet-50 network

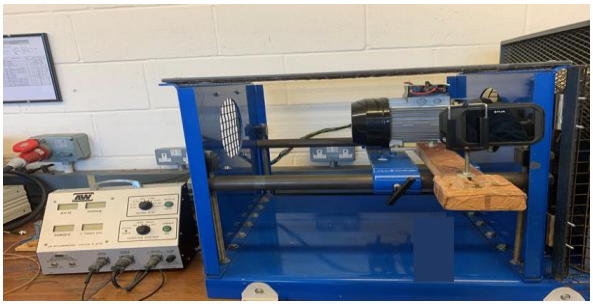

Figure 3. Test rig of the experiments

The classification accuracy of this model is further compared with recent published deep learning methos based (CNN). Normalized SAE was proposed by Jia in [23], stacked sparse autoencoder model was presented by Oi in [24], sparse filter (SF) proposed by Lei in [35], and deep belief network (DBN) presented by Gan [25].

Table 2. model classification result

Train ResNet-50 network with thermal images			
	score	Batch size	epochs
Accuracy (%)	99.98	64	100
Precision (%)	98.59	64	100
Sensitivity (%)	95.99	64	100
F1-score (%)	94.89	64	100

Table 3. accuracy comparison with other methods

Model	Accuracy
Proposed model	**99.98**
NSAE-LCN	99.92
SSAE	99.85
Sparse filter	99.66
DBN	99.03

It has been observed that the proposed ResNet-50 network achieves the best results and the accuracy compassion results are presented in Table 3. It can be concluded that the suggested pre-trained network ResNet-50 trained on ImageNet has successfully achieved a satisfactory application for diagnosing induction motor faults using motor thermal images.

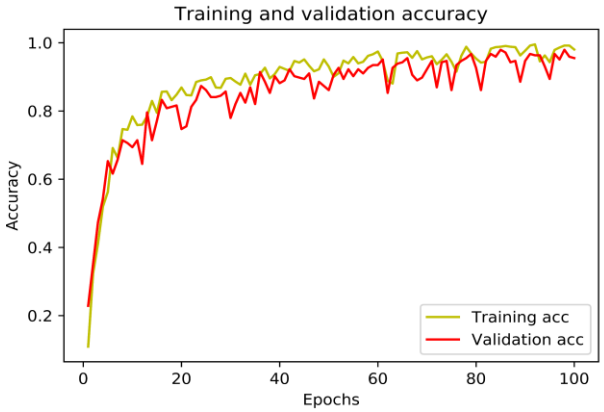

Figure 4. Training accuracy curve applying ReseNet-50

Figure 5. Training loss curve applying ReseNet-50

IV. CONCLUSION

This study develops a new fault diagnosis model applying a ResNet-50 CNN based transfer learning network. Thermal images were applied and pre-processed using data augmentation techniques for improving the final prediction accuracy, then provided as inputs to deeper feature extraction network based pretrained model of ReseNet-50. The combination of the proposed pre-trained network

with densely connected classifier has given a highest classification accuracy of 99.98%. in addition, the model has been compared with other deep learning model, and the results show that the proposed resent-50 is the best.

Concisely, the overall accuracy of the classification method is satisfactory, suggesting that this model has potential applicability in the identification of induction motor faults utilizing the thermal imaging data. In future work, detection time is also considered for implementing the model. Moreover, the proposed model is trained using cross-validation technique for further accuracy improvement. Furthermore, this model is implemented for online application that based on fault detection.

VII. ACKNOWLEDGMENTS

Alasmer Ibrahim acknowledges the sponsorship from the High Ministry of education in Libya.

VIII. REFERENCES:

[1] S. Ayas and M. S. Ayas, "A novel bearing fault diagnosis method using deep residual learning network," *Multimed. Tools Appl.*, no. 0123456789, 2022, doi: 10.1007/s11042-021-11617-1.

[2] Z. Gao, C. Cecati, and S. X. Ding, "A Survey of Fault Diagnosis and Fault-Tolerant Techniques—Part I: Fault Diagnosis With Model-Based and Signal-Based Approaches," *IEEE Trans. Ind. Electron.*, vol. 62, no. 6, pp. 3757–3767, 2015, doi: 10.1109/TIE.2015.2417501.

[3] P. Baraldi, F. Cannarile, F. Di Maio, and E. Zio, "Hierarchical k-nearest neighbours classification and binary differential evolution for fault diagnostics of automotive bearings operating under variable conditions," *Eng. Appl. Artif. Intell.*, vol. 56, pp. 1–13, 2016, doi: 10.1016/j.engappai.2016.08.011.

[4] K. Worden, W. J. Staszewski, and J. J. Hensman, "Natural computing for mechanical systems research: A tutorial overview," *Mech. Syst. Signal Process.*, vol. 25, no. 1, pp. 4–111, 2011, doi: 10.1016/j.ymssp.2010.07.013.

[5] L. Wen, X. Li, and L. Gao, "A New Two-Level Hierarchical Diagnosis Network Based on Convolutional Neural Network," *IEEE Trans. Instrum. Meas.*, vol. 69, no. 2, pp. 330–338, 2020, doi: 10.1109/TIM.2019.2896370.

[6] S. Yin, S. X. Ding, X. Xie, and H. Luo, "A review on basic data-driven approaches for industrial process monitoring," *IEEE Trans. Ind. Electron.*, vol. 61, no. 11, pp. 6418–6428, 2014, doi: 10.1109/TIE.2014.2301773.

[7] X. Li, L. Gao, Q. Pan, L. Wan, and K. M. Chao, "An Effective Hybrid Genetic Algorithm and Variable Neighborhood Search for Integrated Process Planning and Scheduling in a Packaging Machine Workshop," *IEEE Trans. Syst. Man, Cybern. Syst.*, vol. 49, no. 10, pp. 1933–1945, 2019, doi: 10.1109/TSMC.2018.2881686.

[8] M. Kang, J. Kim, and J. M. Kim, "Reliable fault diagnosis for incipient low-speed bearings using fault feature analysis based on a binary bat algorithm," *Inf. Sci. (Ny).*, vol. 294, pp. 423–438, 2015, doi: 10.1016/j.ins.2014.10.014.

[9] Z. Wang, Q. Zhang, J. Xiong, M. Xiao, G. Sun, and J. He, "New Hybrid Invasive Weed Optimization and Machine Learning Approach for Fault Detection," *IEEE Sens. J.*, vol. 17, no. 17, pp. 5581–5588, 2017, doi: 10.1109/JSEN.2017.2726011.

[10] A. Ibrahim, F. Anayi, M. Packianather, and O. Al-Omari, "New Hybrid Invasive Weed Optimization and Machine Learning Approach for Fault Detection," *2021 56th Int. Univ. Power Eng. Conf. Powering Net Zero Emiss. UPEC 2021 - Proc.*, no. Cm, 2021, doi: 10.1109/UPEC50034.2021.9548171.

[11] H. M. Ertunc, H. Ocak, and C. Aliustaoglu, "ANN- and ANFIS-based multi-staged decision algorithm for the detection and diagnosis of bearing faults," *Neural Comput. Appl.*, vol. 22, no. SUPPL.1, pp. 435–446, 2013, doi: 10.1007/s00521-012-0912-7.

[12] R. Liu, B. Yang, E. Zio, and X. Chen, "Artificial intelligence for fault diagnosis of rotating machinery: A review," *Mech. Syst. Signal Process.*, vol. 108, pp. 33–47, 2018, doi: 10.1016/j.ymssp.2018.02.016.

[13] J. Wang, Y. Ma, L. Zhang, R. X. Gao, and D. Wu, "Deep learning for smart manufacturing: Methods and applications," *J. Manuf. Syst.*, vol. 48, pp. 144–156, 2018, doi: 10.1016/j.jmsy.2018.01.003.

[14] Y. Lecun, Y. Bengio, and G. Hinton, "Deep learning," *Nature*, vol. 521, no. 7553, pp. 436–444, 2015, doi: 10.1038/nature14539.

[15] L. Wen, X. Li, and L. Gao, "A transfer convolutional neural network for fault diagnosis based on ResNet-50," *Neural Comput. Appl.*, vol. 32, no. 10, pp. 6111–6124, 2020, doi: 10.1007/s00521-019-04097-w.

[16] R. Zhao, R. Yan, Z. Chen, K. Mao, P. Wang, and R. X. Gao, "Deep learning and its applications to machine health monitoring," *Mech. Syst. Signal Process.*, vol. 115, pp. 213–237, 2019, doi: 10.1016/j.ymssp.2018.05.050.

[17] J. Yosinski, J. Clune, Y. Bengio, and H. Lipson, "How transferable are features in deep neural networks?," *Adv. Neural Inf. Process. Syst.*, vol. 4, no. January, pp. 3320–3328, 2014.

[18] T. D. Jeff Donahue∗, Yangqing Jia∗, Oriol Vinyals, Judy Hoffman, Ning Zhang, Eric Tzeng, "A Deep Convolutional Activation Feature.," vol. 32, 2014.

[19] L. Zuo, M. Jing, J. Li, L. Zhu, K. Lu, and Y. Yang, "Challenging tough samples in unsupervised domain adaptation," *Pattern Recognit.*, vol. 110, 2021, doi: 10.1016/j.patcog.2020.107540.

[20] L. Wen, X. Li, X. Li, and L. Gao, "A New Deep Transfer Learning Based on Sparse Auto-Encoder for Fault Diagnosis," *Proc. 2019 IEEE 23rd Int. Conf. Comput. Support. Coop. Work Des. CSCWD 2019*, vol. 49, no. 1, pp. 205–209, 2019, doi: 10.1109/CSCWD.2019.8791884.

[21] H. C. Cho, J. Knowles, M. S. Fadali, and K. S. Lee, "Fault detection and isolation of induction motors using recurrent neural networks and dynamic bayesian modeling," *IEEE Trans. Control Syst. Technol.*, vol. 18, no. 2, pp. 430–437, 2010, doi: 10.1109/TCST.2009.2020863.

[22] N. K. Verma, V. K. Gupta, M. Sharma, and R. K. Sevakula, "Intelligent condition based monitoring of rotating machines using sparse auto-encoders," *PHM 2013 - 2013 IEEE Int. Conf. Progn. Heal. Manag. Conf. Proc.*, pp. 1–7, 2013, doi: 10.1109/ICPHM.2013.6621447.

[23] F. Jia, Y. Lei, L. Guo, J. Lin, and S. Xing, "A neural network constructed by deep learning technique and its application to intelligent fault diagnosis of machines," *Neurocomputing*, vol. 272, pp. 619–628, 2018, doi: 10.1016/j.neucom.2017.07.032.

[24] Y. Qi, C. Shen, D. Wang, J. Shi, X. Jiang, and Z. Zhu, "Stacked Sparse Autoencoder-Based Deep Network for Fault Diagnosis of Rotating Machinery," *IEEE Access*, vol. 5, pp. 15066–15079, 2017, doi: 10.1109/ACCESS.2017.2728010.

[25] M. Gan, C. Wang, and C. Zhu, "Construction of hierarchical diagnosis network based on deep learning and its application in the fault pattern recognition of rolling element bearings," *Mech. Syst. Signal Process.*, vol. 72–73, pp. 92–104, 2016, doi: 10.1016/j.ymssp.2015.11.014.

[26] T. Han, C. Liu, W. Yang, and D. Jiang, "Deep transfer network with joint distribution adaptation: A new

intelligent fault diagnosis framework for industry application," *ISA Trans.*, vol. 97, pp. 269–281, 2020, doi: 10.1016/j.isatra.2019.08.012.

[27] W. Fuan, J. Hongkai, S. Haidong, D. Wenjing, and W. Shuaipeng, "An adaptive deep convolutional neural network for rolling bearing fault diagnosis," *Meas. Sci. Technol.*, vol. 28, no. 9, 2017, doi: 10.1088/1361-6501/aa6e22.

[28] X. Guo, L. Chen, and C. Shen, "Hierarchical adaptive deep convolution neural network and its application to bearing fault diagnosis," *Meas. J. Int. Meas. Confed.*, vol. 93, pp. 490–502, 2016, doi: 10.1016/j.measurement.2016.07.054.

[29] C. Lu, Z. Wang, and B. Zhou, "Intelligent fault diagnosis of rolling bearing using hierarchical convolutional network based health state classification," *Adv. Eng. Informatics*, vol. 32, pp. 139–151, 2017, doi: 10.1016/j.aei.2017.02.005.

[30] R. Chen and S. Shen, "Fault Diagnosis for Rotating Machinery Based on Convolutional Neural Network and Empirical Mode Decomposition," *Zhendong Ceshi Yu Zhenduan/Journal Vib. Meas. Diagnosis*, vol. 25, no. 3, pp. 233–235, 2005.

[31] H. Li, J. Huang, X. Yang, J. Luo, L. Zhang, and Y. Pang, "Fault Diagnosis for Rotating Machinery Using Multiple Sensors and Convolutional Neural Networks," *Entropy*, vol. 22, no. 8, pp. 101–110, 2020, doi: 10.3390/E22080851.

[32] A. Mahmood *et al.*, "Automatic hierarchical classification of kelps using deep residual features," *Sensors (Switzerland)*, vol. 20, no. 2, pp. 1–20, 2020, doi: 10.3390/s20020447.

[33] T. Gevers and A. Smeulders, "Identity Mappings in Deep Residual Networks," *Lect. Notes Comput. Sci. (including Subser. Lect. Notes Artif. Intell. Lect. Notes Bioinformatics)*, vol. 9909 LNCS, p. V, 2016, doi: 10.1007/978-3-319-46493-0.

[34] V. Sangeetha and K. J. R. Prasad, "Deep Residual Learning for Image Recognition Kaiming," *Indian J. Chem. - Sect. B Org. Med. Chem.*, vol. 45, no. 8, pp. 1951–1954, 2006, doi: 10.1002/chin.200650130.

[35] Y. Lei, F. Jia, J. Lin, S. Xing, and S. X. Ding, "An Intelligent Fault Diagnosis Method Using Unsupervised Feature Learning Towards Mechanical Big Data," *IEEE Trans. Ind. Electron.*, vol. 63, no. 5, pp. 3137–3147, 2016, doi: 10.1109/TIE.2016.2519325.

Parameters Extraction of Photovoltaic (PV) cells using a global optimizer inspired from the survival strategies of flying foxes (FFO)

Aalloul Radouane
Laboratory of Engineering and Materials (LIMAT), Faculty of Sciences Ben M'sik, Hassan II University of Casablanca, Morocco
radouane.aalloul-etu@etu.univh2c.ma

Adhiri Rahma
Laboratory of Engineering and Materials (LIMAT), Faculty of Sciences Ben M'sik, Hassan II University of Casablanca, Morocco
rahmadhiri@gmail.com

Benlattar Mourad
Matter Physics Laboratory (LPM)), Faculty of Sciences Ben M'sik, Hassan II University of Casablanca, Morocco
benlattar1975@gmail.com

El Aissaoui Abdellah
National Institute of Agricultural Research, Laboratory of Agricultural Engineering and Energy, Settat, Morocco
abdellah.elaissaoui@inra.ma

Abstract

Today the world is facing multiple challenges of energy security, economic recovery and the effect of the Global increase in temperature. Investing in new fossil fuel will only lock-in uneconomic practices, perpetuate existing risks and increase the threats of climate change. By contrast, renewable energies such as Photovoltaic is considered one of the sources of energy not emitting carbon dioxide and other greenhouse gases, contributing to global warming. Seen its simplicity and low maintenance costs, Solar cells are the most prominent alternative to deal with these issues. However, Standard Test Conditions (STC) of Photovoltaic (PV) modules are, in the most cases, not representative of the real working conditions of a solar module. For operating conditions in arid climate, temperature of PV modules considerably increases above the STC temperature and affects PV system performance. In order to effectively predict energy production for a given location, it is of great importance to develop a robust model to take into account the electrical and thermal behaviors of the PV module. Different models have been previously implemented using a single or double diode model. This work focuses on the latest one, which requires the determination of seven parameters .these parameters are : Iph, Rs, Rsh, n_1, n_2, I_{01} and I_{02}. By referring to the estimation methods proposed in the literature such as : Newton-Raphson, Gauss-Seidel and Metaheuristics algorithms. This work introduces a new method of global optimization algorithm based on the use of Flying Foxes Optimization (FFO) technique to estimate the PV cell/module parameters. The proposed population-based approach is inspired from the survival strategies of flying foxes during a heatwave. The two different ways flying foxes move in the search space as well as their replacement mechanism, constitute the main advantages of the proposed optimizer, as they enhance exploration. FFO's probability-based solution replacement assists its escape from local optima, and helps the optimizer avoid wasting time searching bad regions of the search space. The results demonstrate that the proposed FFO optimizer constitutes an attractive alternative optimization approach to the most successful metaheuristic optimizers, considering local and global search capabilities.

Results have been compared with those found by the methods of Newton-Raphson, Gauss-Seidel, Broyden , Genetic algorithm (GA), Particle Swarm Optimization (PSO) and Invasive Weeds Optimization (IWO) to show that the proposed algorithm (FFO) has a high fitting with the experimental data.

Keywords: *PV Model, Parameter Extraction, Double diode Model, Genetic Algorithm (GA), Flying Foxes Optimization (FFO)*

IEECP'22, July 21-22, 2022, Oxford, United Kingdom

Blackcurrant pomace as a biodegradable filler for rigid polyurethane foams

1st Patrycja Trestka
Department of Heat Engineering & Environment Protection
AGH University of Science and Technology
Krakow, Poland
0000-0003-4247-0046

2nd Beata Zygmunt-Kowalska
Department of Heat Engineering & Environment Protection
AGH University of Science and Technology
Krakow, Poland
0000-0001-7989-8682

3rd Monika Kuźnia
Department of Heat Engineering & Environment Protection
AGH University of Science and Technology
Krakow, Poland
0000-0002-2390-6070

4rd Mariusz Oleksy
Department of Polymer Composites
Rzeszow University of Technology
Rzeszow, Poland
molek@prz.edu.pl

Abstract

The dynamically rising costs of heating result in an increased interest in thermal insulation materials. The best thermal insulation material available on the market is a rigid polyurethane foam. The rise in mining prices of raw materials is disrupting the polyurethane industry, so it is imperative to reduce the amount of petrochemicals in foams. The aim of the article was to check the possibility of using blackcurrant pomace as a filler for polyurethane foams. First, rigid foam composites containing 10 wt.% of fruit processing waste were produced. The obtained materials were analyzed in terms of structure, basic parameters such as water absorption, dimensional stability, apparent density, mechanical properties and the impact of the aging process on the content of C, H, N elements. The conducted research showed that the pomace has antioxidant properties and has a positive effect on the mechanical properties. In addition, this type of filler has a positive effect on the delay in ignition of the foams.

Keywords: blackcurrant pomace, rigid polyurethane foam, biodegradable filler, fruit processing waste

I. INTRODUCTION

The price of heating and fuels in the European Union has risen sharply and has reached an unprecedented level. Therefore, it is necessary to perform thermal insulation for new buildings as well as for the existing ones. There are many products available on the building materials market, such as: mineral wool, polystyrene and polyurethane foams [1]. The main differences between these materials are the thermal conductivity coefficient (λ) and the price.

IEECP'22, July 21-22, 2022, Oxford, United Kingdom

Rigid polyurethane foam (RPUF) is the insulator most indicated due to the lowest heat conduction parameters. The λ value for commercial polyurethane foams ranges 0.02–0.04 $W \cdot m^{-1} \cdot K^{-1}$ [2]. RPUF is also popular for its other good properties: low density, biological and chemical inertness, as well as superior mechanical and hydrophobic properties [3][4]. In addition to insulating partitions of buildings, polyurethane foam is also used for pipes and refrigerators as an insulator [5], [6]. RPUFs are also used as light construction elements and in commercial refrigeration devices, but also in everyday objects, such as furniture and cars [7]–[11]. The biggest disadvantage of RPUF is its high price [12]. It is expensive due to fluctuations in the prices of the raw materials it is made of. Therefore, changes in the demand and supply of these raw materials can have a significant impact on the RPUF products. Therefore, many studies are conducted to reduce the amount of petrochemical products by partially replacing them with solid fillers. The use of fillers not only reduces the price of the polyurethane product, but also affects its properties and may increase the possibilities of its application. The use of waste as fillers is very popular. As a result, the by-product is additionally recycled. The used waste fillers can be divided according to their origin. An example of a filler of animal origin is feathers. Due to the issues of their disposal, they have been used in RPUF and have had a positive effect on the improvement of thermal and acoustic properties of the material [13], [14]. Fruit seeds and nut shells are also very popular fillers. Plant-based fillers are another group of fillers used in the RPUF industry. This type of filler includes fruit and vegetable pomace, fruit seeds[15] and nut shells [16], [17]. The above-mentioned natural fillers are characterized by the fact that their chemical composition often positively influences the mechanical, physical and thermal properties of foams [18]. Other fillers are those that come from the energy or steel industries. An example is fly ash from coal combustion, which has a positive effect on the reduction of flammability and reduces the rate of polymer degradation [19][20].

In this study, blackcurrant pomace was used as a filler. The evaluation of the application of this filler was based on the results showcased in the article. Namely - the results of research on the structure, physical properties, and strength properties of obtained composites. The novelties presented in the paper are the aging tests performed together with the determination of the elements C, H, N,

and O, which allowed to assess the influence of blackcurrant pomace on the oxidation process of polyurethane foams. It should be emphasized that the currant pomace is a rich source of polyphenolic compounds with confirmed antiradical properties [21]. In the literature, there are studies on the use of currant pomace in flexible polyurethane foams [22]. The authors observed that the discussed additive increased the foam growth time and the reduction of the temperature of the foaming process. The density of the material also increased. The pomace additionally accelerated the degradation of the rigid polyurethane segments and slowed down the degradation of the soft segments. No information has been found in the literature on the use of currant waste in rigid polyurethane. The experiment described in the article may expand the use of currant pomace not only in the food industry, but also in the material technology and have a positive effect on the properties and price of rigid polyurethane foams. Additionally, the addition of blackcurrant pomace to the PU foams may create a new method of utilizing this type of waste. This waste constitutes 20-35% of the weight of the processed raw material [23].

II. MATERIALS AND METHODS

A. Preparation of the filler and rigid polyurethane foams

This article uses blackcurrant pomace as a filler for RPUF. Before introducing it into the foams, it was processed by drying it to a constant mass at the temperature of 105°C and then, using a laboratory mill, the expeller was crushed to a powder form.

In order to analyze the filler used, the content of the elements (carbon, hydrogen, nitrogen) was examined, and is presented in Table 1.

Table 1. Elemental analysis of blackcurrant pomace

	C [%]	H [%]	N [%]
Blackcurrant pomace	49.20	6.94	2.26

The carbon content of blackcurrant pomace is over 49%, hydrogen is almost 7%, and nitrogen is just over 2%. These values do not differ from the chemical composition of agricultural and forest biomass. Blackcurrant pomace also contains a large amount of lignin, cellulose and hemicellulose.

Polyurethane foams were produced using the one-step method. A polyol masterbatch was mixed with an isocyanate to form a reference foam (PU_0), while a 10% foam (PU_10) with blackcurrant expeller was produced by introducing expeller into the polyol masterbatch and then adding the isocyanate. All ingredients were mixed with a mechanical agitator at a constant speed of 2000 rpm. RPUF were prepared using the two-component commercial system EKOPRODUR PM4032 (PCC Group, Poland).

The process of preparing the filler and foams is presented below (Figure 1).

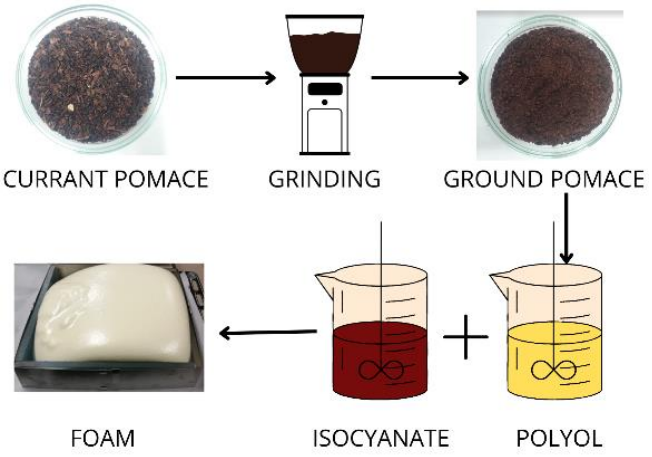

Figure 1. Scheme of preparation of the filler and RPUF

Polyurethane foam is produced by the intensive mixing of two main components: isocyanate and petroleum-derived polyol. During their mixing, additives such as catalysts and stabilizers are also added, which can create different properties of the polyurethane [24].

B. Methods

The microstructure of the obtained polyurethane composites was determined at a magnification of 6x using an optical microscope (Vision Engineering SX 45).

The apparent density of the material was tested on the basis of the EN ISO 845:2009 standard.

The water absorption of the foams was determined in accordance with the ASTM D570-98 standard by determining their starting weight, then after 5 minutes, 3 hours and 24 hours of a water bath.

The dimensional stability of polyurethane materials was determined in accordance with the PN-92/C89083 standard by testing the length change before the aging process, after 20 h and 40 h of the aging process, which was carried out at the temperature of 150°C.

The analysis of carbon, hydrogen, nitrogen and oxygen elements was carried out for the obtained materials in order to assess the aging process through the action of UV light and water spray as well as the actual weather conditions.

The brittleness of the obtained foams was analyzed according to the ASTM C 421-08 standard.

The compressive strength of the foam was determined in accordance with EN ISO 14125:198. In the test, the value of the given relative deformation was equal to 10%.

Flammability parameters were tested, such as: limit oxygen index (LOI) based on the PN-EN ISO 4589-2: 2006 standard, the UL 94V foam flammability test in accordance with the PN-EN 60695-11-10: 1999 standard and reaction to fire by determination of the grass calorific value (ISO 1716: 2018). Flammability tests were also carried out on a cone calorimeter, determining the characteristic parameters (average heat release rate (HRR), maximum heat release rate (PHRR), effective heat of combustion (EHC), time to ignition (TTI), percentage mass loss (PML)).

III. RESULTS

A. Physical properties of PU foams

The water absorption of the foam is summarized in Table 2. Based on the analysis of the results, it can be concluded that the water absorption increases most rapidly in the first minutes of immersion. The absorbency value increases with the passage of time. In both

cases, the foam soaks up water, however, for PU_10 foam, the increase in water absorption is significantly lower.

Table 2. Water absorption of rigid polyurethane foams

Sample	Water absorption [%]		
	5 min	3h	24h
PU_0	14.48	24.68	36.14
PU_10	12.63	15.32	34.55

The reduction in absorbency is most likely due to the cellulose in the filler, which disperses inside and over the edges of the cells, thus blocking the foam from absorbing moisture [15]. The changes in dimensions and mass of samples after 20 and 40 h of conditioning at 150 ° C are shown in Table 3.

Table 3. Dimensional stability and weight loss of rigid polyurethane foams

Sample	Dimensional stability		Loss in mass	
	(Δl, 20h, 150°C) [%]	(Δl, 40h, 150°C) [%]	(Δm, 20h, 150°C) [%]	(Δm, 40h, 150°C) [%]
PU_0	3.86	4.18	9.23	9.23
PU_10	1.33	1.79	11.36	11.36

Basically three times lower values of linear stability were obtained for the PU_10 sample as compared to the reference foam. This ratio was maintained after both 20 and 40 hours. The improved dimensional stability for cellulose-containing foams was also confirmed by M. Szpiłyk et al. [25]. The weight loss stabilized and remained unchanged after 40 h. The difference between the samples amounts to approx. 2% due to the moisture contained in the filler, which evaporated during the conditioning.

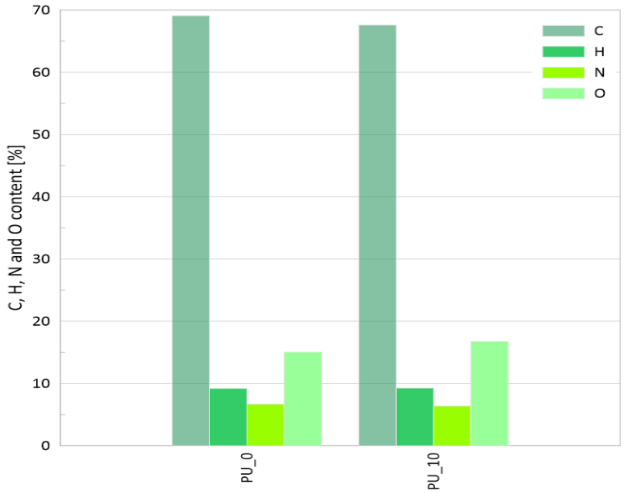

Figure 2 Elemental analysis of C, H, N and O of rigid polyurethane foams

Figure 2 shows the elemental analysis of basic foams. Compared to both foams, PU_0 has a higher carbon content and a lower oxygen content compared to PU-10. The other two elements, that is N and H, in both of the foams are at a comparable level.

Figure 3 shows the elemental analysis after an artificially created aging process. The foams were treated with UV light and water spray. Comparing with Figure 1, it can be seen that in both samples the carbon content remained at the same level, the hydrogen content in PU_0 decreased and the nitrogen and oxygen content increased slightly. At the same time, in the case of PU_10, the hydrogen content increased, the nitrogen content decreased, and the oxygen content decreased compared to the unmodified foam.

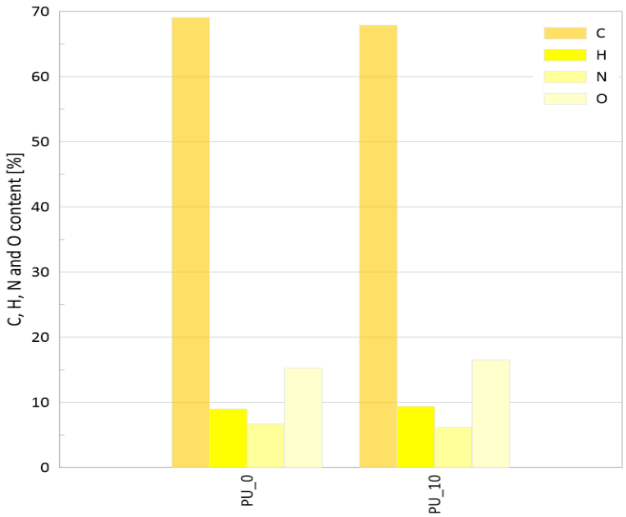

Figure 3 Elemental analysis of C, H, N and O of rigid polyurethane foams subjected to water spray and UV light

Figure 4 shows the results of the analysis for foams exposed to natural weather conditions. PU_0 has a lower carbon content, a higher hydrogen, nitrogen and oxygen content. In PU_10, the carbon content remains constant, the hydrogen and nitrogen content increases, but the oxygen content drops significantly from 16.77% for unmodified foam to 14.57% for the foam placed under the action of atmospheric conditions. Generally, foam modified with blackcurrant expeller filler is more resistant to artificial and real atmospheric conditions than PU_0. This is confirmed by the fact that such pomaces act as antioxidant substances.

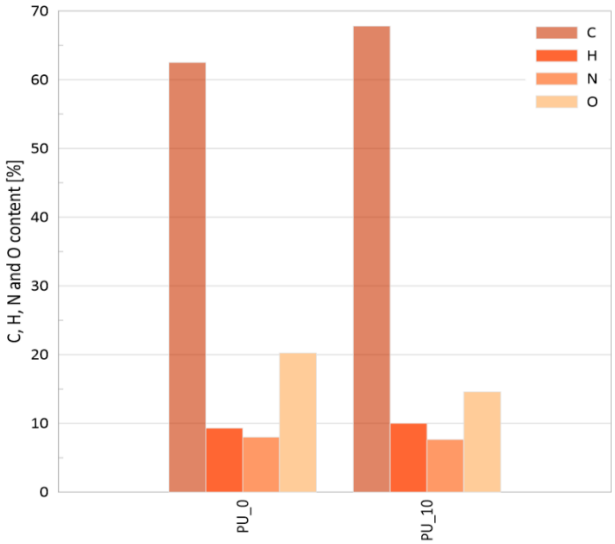

Figure 4 Elemental analysis of C, H, N and O of rigid polyurethane foams exposed to real atmospheric conditions

Such analyzes are very important from the point of using RPUF as insulating materials. In the literature, one of the main causes of aging of polyurethane insulations is the phenomenon of gas diffusion. As a result of oxygen and nitrogen entering the foam structure, cellular

gases such as carbon dioxide and cyclopentane are forced out, which results in an increase in heat conduction coefficient [26].

B. The structure of PU foams

a) b)

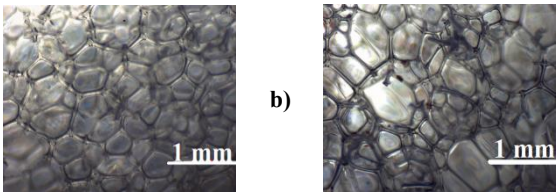

Figure 5. Structure of rigid polyurethane foams: a)PU_0, b)PU_10

The cellular structure of rigid polyurethane foam has a considerable impact on the mechanical properties. The photos from the optical microscope are summarized in Figure 2. PU_0 foam cells are characterized by similar dimensions, there is no large fluctuation in the values of the diameters. In the case of PU_10 foam, the morphology is more diversified, the cells are elongated and do not resemble spheres as for the reference foam. The presence of such a cell shape is related to the high reactivity of the polyurethane system. As a result, the currant pomace intensified the process of cell nucleation. This thesis is confirmed by examples from the literature in which the cellulosic filler caused the growth of the cells of the polyurethane composite [27], [28].

C. Mechanical properties of PU foams

Table 4. Apparent density and mechanical properties of rigid polyurethane foams

Sample	Apparent density [kg·m^{-3}]	Brittleness [%]	Compressive strength [MPa]	Young's modulus [MPa]
PU_0	36.09	16.98	0.04	6.70
PU_10	33.82	11.63	0.07	8.96

The literature shows that the apparent density of polyurethane foams is related to the mechanical properties. It is an important parameter therefore it has been determined that a typical RPUF should have a density in the range of 28-60 [kg·m^{-3}] [29]. PU_0 had an apparent density of about 36 [kg·m^{-3}], while the apparent density of PU_10 was almost 34 [kg·m^{-3}]. Both values fall within the defined range (Table 4). The literature also describes cases where the introduction of the filler resulted in a reduction of the apparent density in relation to the reference foam [30].

From the strength tests performed, a positive effect of this type of filler on the mechanical properties of RPUF can be observed. The maximum compressive strength increases (Table 4). The stress-strain diagram shows that the strength improved almost twice after introducing the filler at a load of 10%. From the presented graph, you can see three stages of degradation during compression [31].

Table 4 also shows the results of the brittleness testing of the foams obtained. They show that blackcurrant pomace has a positive effect on brittleness because it reduces it. The brittleness results are correlated with the apparent density of foams [32]. Other researchers received similar conclusions that introducing the filler to a specific concentration has a positive effect on the mechanical properties of polyurethane foams [33].

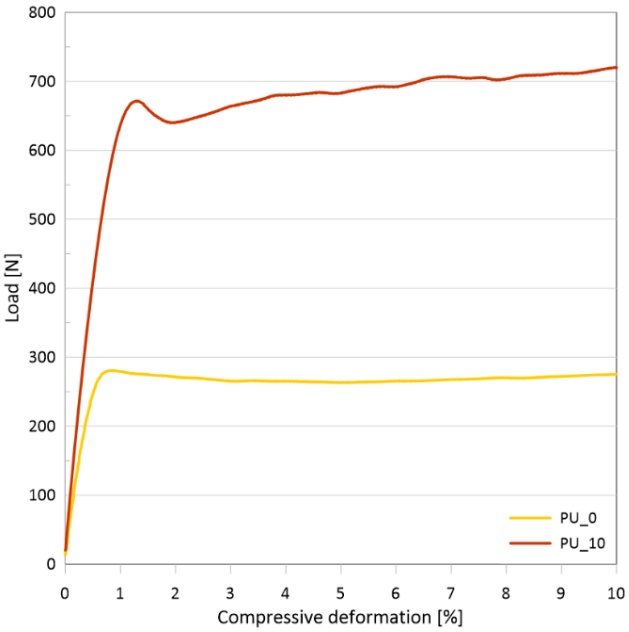

Figure 5. Compressive deformation of rigid polyurethane foams

D. Flammability of PU foams

The flammability of polyurethane foams is an important aspect because they are used as thermal insulation materials, so they should have a specific flammability class. Additionally, as RPUF burns down, many toxic gases are released into the atmosphere [34].

For the analyzed materials, the LOI was determined (Table 5), which for PU_0 was 21.4%, and for PU_10 - 20.7%, which is unfavorable in terms of planarity, because it means that the foam with a filler requires less amount of oxide to maintain the flame. Also, in the reaction to fire test, it was found that introducing the filler into the foam increases the heat value.

Table 5. Gross calorific value, LOI values, UL-94 vertical burning behaviors of rigid polyurethane foams

Sample	LOI [%]	Gross calorific value (MJ*kg^{-1})	UL94 V
PU_0	21.4	25.98	N.R
PU_10	20.7	26.02	N.R

The obtained results from the cone calorimeter show that PU_0 ignites faster compared to PU_10 (Table 6). In the context of the possibility of using polyurethane foams as thermal insulation materials, the HRR and PHRR parameters are very important. The first parameter was smaller for PU_10, while in the case of maximum heat release it was the other way round. Generally, the construction law stipulates that the RPUF should have a maximum PHRR of 300 [kW/m^2] [35], [36].

Table 6. Cone calorimeter results of rigid polyurethane foams

Sample	TTI [s]	EHC [MJ/kg]	HRR [kW/m^2]	PHRR [kW/m^2]	PML [%]
PU_0	4	7.98	63.88	77.70	85.7
PU_10	6	9.63	57.80	79.11	80.8

IV. Conclusions

The paper presents the results of research on a polyurethane foam and a polyurethane composite containing 10% of blackcurrant

pomace. The addition of a filler has many benefits in reducing the amount of petrochemicals in the foam, reducing production costs and improving some properties. The currant pomace acts as a blockage in the foam and hinders water absorption and increases the dimensional stability of the sample. Compared to the reference sample, the stability is three times higher after both 20 and 40 hours. Additionally, the simulations of the insulation aging process confirm the antioxidant effect of blackcurrant pomace. The foam modified with this filler degraded less as shown by the elements analysis. Moreover, the discussed filler intensified the process of nucleation of bubbles during foam growth. In the case of the reference foam, the foam structure consisted of spherical cells similar in size. In PU_10 foam, the bubbles are elongated and their diameters are more diversified. The filler lowers the apparent density of the foam, which is closely related to the mechanical parameters. The foams containing the filler also showed almost twice the compressive strength, but also lower brittleness, which confirms the positive effect of the filler on the mechanical properties. The differences in the gross calorific value and the LOI index between the samples are similar. The addition of the filler extended the ignition time of the foam and reduced the amount of average heat released.

V. ACKNOWLEDGMENTS

This research was funded by the Ministry of Science and Higher Education, Poland [grant AGH-UST no 16.16.110.663]

VI. REFERENCES

[1] A. M. Binyaseen, "Improving thermal performance of existing uninsulated R.C. domes through passive cooling measures using polyurethane foam in double skin layer in hot climate.," *Case Studies in Construction Materials*, vol. 16, p. e00866, Jun. 2022, doi: 10.1016/J.CSCM.2021.E00866.

[2] M. Krarti, "Advanced Building Energy Efficiency Systems," *Optimal Design and Retrofit of Energy Efficient Buildings, Communities, and Urban Centers*, pp. 45–115, Jan. 2018, doi: 10.1016/B978-0-12-849869-9.00002-8.

[3] S. Członka, M. F. Bertino, K. Strzelec, A. Strąkowska, and M. Masłowski, "Rigid polyurethane foams reinforced with solid waste generated in leather industry," *Polymer Testing*, vol. 69, 2018, doi: 10.1016/j.polymertesting.2018.05.013.

[4] D. Xu, K. Yu, and K. Qian, "Thermal degradation study of rigid polyurethane foams containing tris(1-chloro-2-propyl)phosphate and modified aramid fiber," *Polymer Testing*, vol. 67, pp. 159–168, May 2018, doi: 10.1016/J.POLYMERTESTING.2018.01.034.

[5] A. A. Mahmoud, E. A. A. Nasr, and A. A. H. Maamoun, "The Influence of Polyurethane Foam on the Insulation Characteristics of Mortar Pastes," *Journal of Minerals and Materials Characterization and Engineering*, vol. 05, no. 02, 2017, doi: 10.4236/jmmce.2017.52005.

[6] A. Strakowska, S. Członka, and K. Strzelec, "POSS compounds as modifiers for rigid polyurethane foams (Composites)," *Polymers (Basel)*, vol. 11, no. 7, 2019, doi: 10.3390/polym11071092.

[7] S. Członka, A. Strąkowska, K. Strzelec, A. Kairytė, and S. Vaitkus, "Composites of rigid polyurethane foams and silica powder filler enhanced with ionic liquid," *Polymer Testing*, vol. 75, pp. 12–25, May 2019, doi: 10.1016/j.polymertesting.2019.01.021.

[8] G. Bo *et al.*, "Synthesis and characterization of flame-retardant rigid polyurethane foams derived from gutter oil biodiesel," *European Polymer Journal*, vol. 147, Mar. 2021, doi: 10.1016/j.eurpolymj.2021.110329.

[9] L. Qian, L. Li, Y. Chen, B. Xu, and Y. Qiu, "Quickly self-extinguishing flame retardant behavior of rigid polyurethane foams linked with phosphaphenanthrene groups," *Composites Part B: Engineering*, vol. 175, Oct. 2019, doi: 10.1016/j.compositesb.2019.107186.

[10] S. Członka, M. F. Bertino, and K. Strzelec, "Rigid polyurethane foams reinforced with industrial potato protein," *Polymer Testing*, vol. 68, pp. 135–145, Jul. 2018, doi: 10.1016/j.polymertesting.2018.04.006.

[11] W. Xi, L. Qian, Z. Huang, Y. Cao, and L. Li, "Continuous flame-retardant actions of two phosphate esters with expandable graphite in rigid polyurethane foams," *Polymer Degradation and Stability*, vol. 130, pp. 97–102, Aug. 2016, doi: 10.1016/j.polymdegradstab.2016.06.003.

[12] M. Kurańska, A. Prociak, S. Michałowski, and K. Zawadzińska, "The influence of blowing agents type on foaming process and properties of rigid polyurethane foams," *Polimery/Polymers*, vol. 63, no. 10, 2018, doi: 10.14314/polimery.2018.10.2.

[13] M. Khaleel, U. Soykan, and S. Çetin, "Influences of turkey feather fiber loading on significant characteristics of rigid polyurethane foam: Thermal degradation, heat insulation, acoustic performance, air permeability and cellular structure," *Construction and Building Materials*, vol. 308, 2021, doi: 10.1016/j.conbuildmat.2021.125014.

[14] S. Członka, N. Sienkiewicz, A. Strąkowska, and K. Strzelec, "Keratin feathers as a filler for rigid polyurethane foams on the basis of soybean oil polyol," *Polymer Testing*, 2018, doi: 10.1016/j.polymertesting.2018.09.032.

[15] M. Leszczyńska *et al.*, "Vegetable fillers and rapeseed oil-based polyol as natural raw materials for the production of rigid polyurethane foams," *Materials*, vol. 14, no. 7, 2021, doi: 10.3390/ma14071772.

[16] Md. T. Islam *et al.*, "Effect of Coconut Shell Powder as Filler on the Mechanical Properties of Coir-polyester Composites," *Chemical and Materials Engineering*, vol. 5, no. 4, 2017, doi: 10.13189/cme.2017.050401.

[17] S. Członka, A. Strąkowska, and A. Kairytė, "Effect of walnut shells and silanized walnut shells on the mechanical and thermal properties of rigid polyurethane foams," *Polymer Testing*, vol. 87, 2020, doi: 10.1016/j.polymertesting.2020.106534.

[18] M. Leszczyńska, J. Ryszkowska, and L. Szczepkowski, "Rigid polyurethane foam composites with nut shells," in *Polimery/Polymers*, 2020, vol. 65, no. 10, pp. 728–737. doi: 10.14314/polimery.2020.10.8.

[19] B. Zygmunt-Kowalska, K. Pielichowska, P. Trestka, M. Ziąbka, and M. Kuźnia, "The Effect of Ash Silanization on the Selected Properties of Rigid Polyurethane Foam/Coal Fly Ash Composites," *Energies (Basel)*, vol. 15, no. 6, 2022, doi: 10.3390/en15062014.

[20] M. Kuźnia *et al.*, "Fluidized bed combustion fly ash as filler in composite polyurethane materials," *Waste Management*, 2019, doi: 10.1016/j.wasman.2019.05.012.

[21] A. Michalska, A. Wojdyło, G. P. Łysiak, K. Lech, and A. Figiel, "Functional relationships between phytochemicals and drying conditions during the processing of blackcurrant pomace into powders," *Advanced Powder Technology*, vol. 28, no. 5, 2017, doi: 10.1016/j.apt.2017.03.002.

[22] M. Auguścik-Królikowska *et al.*, "Composites of open-cell viscoelastic foams with blackcurrant pomace," *Materials*, vol. 14, no. 4, pp. 1–22, 2021, doi: 10.3390/ma14040934.

[23] L. Kawecka and S. Galus, "Wytłoki owocowe – charakterystyka i możliwości zagospodarowania".

[24] N. v. Gama, A. Ferreira, and A. Barros-Timmons, "Polyurethane foams: Past, present, and future," *Materials*, vol. 11, no. 10. MDPI AG, Sep. 27, 2018. doi: 10.3390/ma11101841.

[25] M. Szpiłyk, R. Lubczak, and J. Lubczak, "The biodegradable cellulose-derived polyol and polyurethane

foam," *Polymer Testing*, vol. 100, p. 107250, Aug. 2021, doi: 10.1016/J.POLYMERTESTING.2021.107250.

[26] Ewa Kręcielewska and Damien Mendard, "Współczynnik przewodzenia ciepła izolacji," *Ciepłownictwo*, vol. 11, pp. 14–20, 2014.

[27] K. Uram *et al.*, "Polyurethane composite foams synthesized using bio-polyols and cellulose filler," *Materials*, vol. 14, no. 13, 2021, doi: 10.3390/ma14133474.

[28] X. Zhou, M. M. Sain, and K. Oksman, "Semi-rigid biopolyurethane foams based on palm-oil polyol and reinforced with cellulose nanocrystals," *Composites Part A: Applied Science and Manufacturing*, vol. 83, pp. 56–62, Apr. 2016, doi: 10.1016/j.compositesa.2015.06.008.

[29] R. J. Prociak A., Rokicki G., *Materiały poliuretanowe*. PWN, 2016.

[30] M. Leszczyńska *et al.*, "Vegetable fillers and rapeseed oil-based polyol as natural raw materials for the production of rigid polyurethane foams," *Materials*, vol. 14, no. 7, Apr. 2021, doi: 10.3390/ma14071772.

[31] N. Sienkiewicz, S. Członka, A. Kairyte, and S. Vaitkus, "Curcumin as a natural compound in the synthesis of rigid polyurethane foams with enhanced mechanical, antibacterial and anti-ageing properties," *Polymer Testing*, vol. 79, Oct. 2019, doi:10.1016/j.polymertesting.2019.106046.

[32] F. Saint-Michel, L. Chazeau, J. Y. Cavaillé, and E. Chabert, "Mechanical properties of high density polyurethane foams: I. Effect of the density," *Composites Science and Technology*, vol. 66, no. 15, pp. 2700–2708, Dec. 2006, doi: 10.1016/j.compscitech.2006.03.009.

[33] M. Barczewski *et al.*, "Rigid polyurethane foams modified with thermoset polyester-glass fiber composite waste," *Polymer Testing*, vol. 81, Jan. 2020, doi: 10.1016/j.polymertesting.2019.106190.

[34] D. K. Chattopadhyay and D. C. Webster, "Thermal stability and flame retardancy of polyurethanes," *Progress in Polymer Science (Oxford)*, vol. 34, no. 10. pp. 1068–1133, Oct. 2009. doi: 10.1016/j.progpolymsci.2009.06.002.

[35] S. Członka, A. Strąkowska, K. Strzelec, A. Kairytė, and A. Kremensas, "Melamine, silica, and ionic liquid as a novel flame retardant for rigid polyurethane foams with enhanced flame retardancy and mechanical properties," *Polymer Testing*, vol. 87, Jul. 2020, doi: 10.1016/j.polymertesting.2020.106511.

[36] L. Qian, F. Feng, and S. Tang, "Bi-phase flame-retardant effect of hexa-phenoxy-cyclotriphosphazene on rigid polyurethane foams containing expandable graphite," *Polymer (Guildf)*, vol. 55, no. 1, pp. 95–101, Jan. 2014, doi: 10.1016/j.polymer.2013.12.015.

Theoretical performance study of $Cs_2AgBi(I_{(1-x)}Br_x)_6$: a promising lead-free perovskite for photovoltaic technology

Fatima Elfatouaki
LaMEE, Physics department,
FSSM, Cadi Ayyad University
Marrakech, Morocco
amitafelfa@gmail.com

Omar Farkad
LaMEE, Physics department,
FSSM, Cadi Ayyad University
Marrakech, Morocco
omarfarkad@gmail.com

Rabi Takassa
LaMEE, Physics department,
FSSM, Cadi Ayyad University
Marrakech, Morocco
rabitakassa@gmail.com

Sanae Hassine
LaMEE,Physics deaprtment
FSSM, Cadi Ayyad University
Marrakech, Morocco
Sanae88hassine@gmail.com

Oumaima Choukri
LaMEE,Physics deaprtment
FSSM, Cadi Ayyad University
Marrakech, Morocco
Oumaima.choukri14@gmail.com

El Alami Ibnouelghazi
LaMEE,Physics deaprtment
FSSM, Cadi Ayyad University
Marrakech, Morocco
ibnouelghazi@uca.ac.ma

Driss Abouelaoualim
LaMEE,Physics deaprtment
FSSM, Cadi Ayyad University
Marrakech, Morocco
dr.abouelaoualim@uca.ac.ma

Abdelkader Outzourhit
LaMEE,Physics deaprtment
FSSM, Cadi Ayyad University
Marrakech, Morocco
aoutzour@uca.ma

Abstract

In recent years, there has been a great interest in the development of lead-free, stable and high efficiency perovskite materials. In our work, we studied a lead-free, inorganic and non-toxic double perovskite solar cell (PSC) based on $Cs_2AgBi(I_{(1-x)}Br_x)_6$ using ab-initio calculations density function theory (DFT) study. The stability, electronic and optical properties are studied and the transport properties have been calculated. Thus, we have evaluated the band gap of the $Cs_2AgBi(I_{(1-x)}Br_x)_6$ absorber by two approximations GGA-PBE and TB-mbj. We found that the values of absorptivity and dielectric constant also increase with increasing Br doping. These mixed halide compounds show stronger absorption coefficients from 300 to 600 nm, the lowest light absorption capacity is observed between 600 and 800 nm.

The performance of the compounds is simulated via SLME. To improve the performance of the device, we analyzed and optimized different parameters of the PSC: optimal thickness, defect density and band gap of the absorber by the numerical simulation method of perovskite solar cell using SCAPS-1D (solar cell capacitance simulator) software. Thus, the optimized values of the doping density for the absorber layer, HTL and ETL were determined; the device achieved a good PCE. Bi-based double mixed halide perovskite materials have provided great scope for a broad range of applications cells with the same high performance as lead-based perovskite. They can be obtained experimentally in future.

Keywords: *$Cs_2AgBi(I_{(1-x)}Br_x)_6$ absorber, DFT study, perovskite solar cells, Photovoltaic technology*

IEECP'22, July 21-22, 2022, Oxford, United Kingdom

Removal of pollutants in wastewater treatment plants

Julita Šarko
Department of Environmental Protection and Water Engineering
Vilnius Gediminas Technical University
Vilnius, Lithuania
julita.sarko@vilniustech.lt

Aušra Mažeikienė
Department of Environmental Protection and Water Engineering
Vilnius Gediminas Technical University
Vilnius, Lithuania
ausra.mazeikiene@vilniustech.lt

Abstract

Wastewater treatment plants (WWTPs), which operate due to the vital activity of microorganisms, often do not achieve high nitrogen and phosphorus removal from wastewater. Nitrogen and phosphorus compounds in treated wastewater enter surface water bodies and cause their eutrophication. The effective treatment of wastewater is essential for creating a sustainable environment. Three WWTPs were selected with similar effluent discharges (10 m^3/d) and the removal of pollutants was analyzed. Chemical analysis data of wastewater samples of WWTPs effluent was collected and evaluated for each quarter for 5 years (2017-2021). The results showed that 76.67% of the residual total phosphorus concentration, 1.67% of biochemical oxygen demand (BOD_7), and 25% of total nitrogen from all analyzed samples did not meet the requirements for treated wastewater. In order to achieve a higher level of removal of nitrogen and phosphorus compounds, additional tertiary treatment is recommended.

Keywords: wastewater, pollutants, removal, efficiency

I. INTRODUCTION

Biological wastewater treatment, which operates due to the vital activity of microorganisms, is the main method of domestic wastewater treatment. Wastewater treatment plants (WWTPs) with conventional technology do not always meet the stricter requirements for the quality of treated wastewater [1]. The main wastewater treatment process can not completely remove nitrogen (N) and phosphorus (P) compounds. Often WWTPs with low flow of wastewater release the higher residual concentrations of these compounds in the treated wastewater. Untreated or insufficiently treated wastewater pollutes the natural environment: land, soil, lakes, rivers, or other bodies of water and groundwater [2]. Nitrogen and phosphorus compounds in treated wastewater enter surface water bodies and cause their eutrophication. The concentration of nitrogen and phosphorus compounds is higher than normal in surface water bodies [3, 4]. Eutrophication threatens the supply of drinking water, recreation, and fish and wildlife habitats [5, 6]. The condition of many European water bodies is poor due to eutrophication [7]. The European water policy aims to achieve good ecological status (defined as a small deviation from near-natural conditions) in all rivers, lakes, coastal and intermediate waters by 2027 at the latest [8].

Three WWTPs were selected with similar effluent discharges (10 m^3/d) in order to find out the efficiency of pollutants removal from wastewater and determine the need for tertiary treatment of wastewater.

II. METHODS

Three WWTPs with a flow rate of 10 m^3 per day but with a population equivalent (PE) less than 10000 were selected in Lithuania.

The data of wastewater quality before and after wastewater treatment from real wastewater treatment systems were collected and evaluated for each quarter for 5 years (2017-2021), with a total of 20 wastewater samples per WWTP.

Chemical analysis data of wastewater quality consisted of pH, total suspended solids (TSS), chemical oxygen demand (COD), biochemical oxygen demand (BOD_7), ammonium nitrogen (NH_4-N), nitrate nitrogen (NO_3-N), nitrite nitrogen (NO_2-N), total nitrogen (TN), ortho-phosphate phosphorus (PO_4-P) and total phosphorus (TP) concentrations. The standard analytical methods were applied to analyze the parameters listed above: EN ISO 10523:2012; EN 872:2005; ISO 6060:2003; EN 1899-1:2000; ISO 7150-1:1998; ISO 7890-3:1998; EN 26777:1999; EN 25663-2000; EN ISO 6878-2004; EN ISO 6878-2005. Selected data were processed statistically by applying a confidence interval of 95 % and values of arithmetical average, maximum, minimum, median, and standard deviation were calculated.

Wastewater chemical analysis results were compared to requirements for the quality of treated wastewater in Lithuania (DLK): an instantaneous maximum permitted concentration is 23 mg/L for BOD_7; an instantaneous maximum permitted concentration is 2 mg/L for TP; an instantaneous maximum permitted concentration is 20 mg/L for TN. BOD_7, TP and TN removal efficiency from wastewater must reach 70-90%, 80% and 70-80%, respectively [9]. An analysis has been carried out to evaluate how much requirements for the quality of treated wastewater are met.

IEECP'22, July 21-22, 2022, Oxford, United Kingdom

III. RESULTS

A. Removal efficiency

The results of BOD_7 in treated wastewater from the first WWTP (1), the second WWTP (2), and the third WWTP (3) are shown in Figure 1.

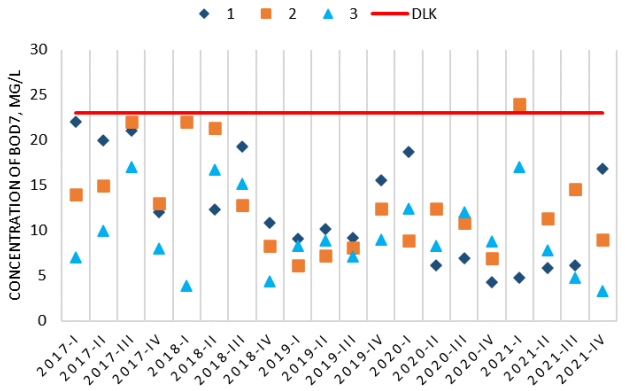

Figure 1. BOD_7 residual concentration compliance with the requirements (DLK)

The initial average concentration of BOD_7 before WWTPs was 400 mg/L.

The average concentration of BOD_7 in the treated wastewater in the first WWTP was 12.64 mg/L, the minimum - 4.26 mg/L, and the highest – 22 mg/L.

The average concentration of BOD_7 in the treated wastewater in the second WWTP was 13 mg/L, the minimum – 6.12 mg/L, and the highest – 24 mg/L.

The average concentration of BOD_7 in the treated wastewater in the third WWTP was 9.49 mg/L, the minimum – 3.32 mg/L, and the highest – 17 mg/L.

According to the BOD_7 indicator, all the WWTPs meet the requirements (Fig. 1). Only 1 unallowable concentration (24 mg/L) of BOD_7 was detected (1.67% of total samples).

The results of total nitrogen in treated wastewater from the first WWTP (1), the second WWTP (2), and the third WWTP (3) are shown in Figure 2.

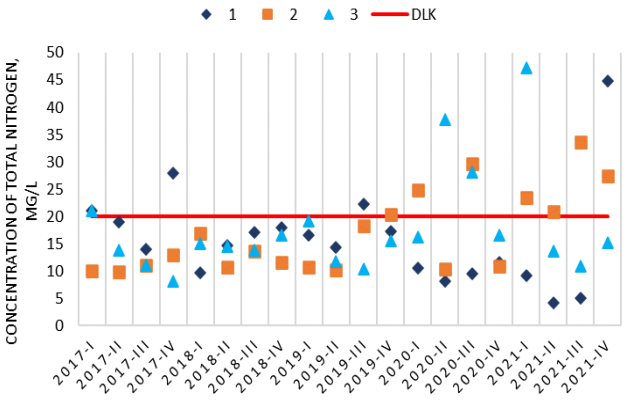

Figure 2. Total nitrogen residual concentration compliance with the requirements (DLK)

The initial average concentration of TN before WWTPs was 80 mg/L.

The average concentration of TN in the treated wastewater in the first WWTP was 15.73 mg/L, the minimum - 4.2 mg/L, and the highest – 44.8 mg/L.

The average concentration of TN in the treated wastewater in the second WWTP was 16.88 mg/L, the minimum – 9.9 mg/L, the highest –33.7 mg/L.

The average concentration of TN in the treated wastewater in the third WWTP was 17.81 mg/L, the minimum – 8.1 mg/L, the highest – 47.2 mg/L.

15 unallowable concentrations of TN were detected (25 % of total samples).

The results of total phosphorus in treated wastewater from the first WWTP (1), the second WWTP (2), and the third WWTP (3) are shown in Figure 3.

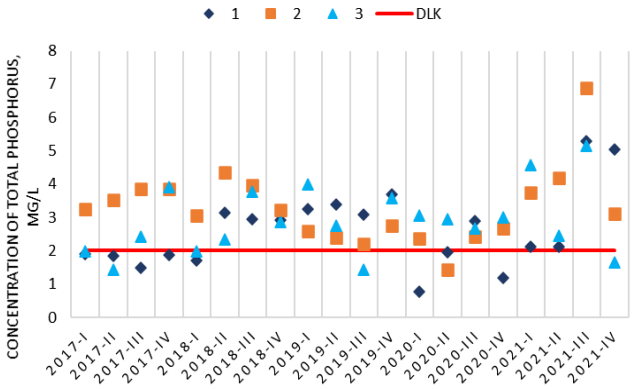

Figure 3. Total phosphorus residual concentration compliance with the requirements (DLK)

The initial average concentration of TP before WWTPs was 10 mg/L.

The average concentration of TP in the treated wastewater in the first WWTP was 2.63 mg/L, the minimum – 0.8 mg/L, and the highest – 5.29 mg/L.

The average concentration of TP in the treated wastewater in the second WWTP was 3.29 mg/L, the minimum – 1.43 mg/L, and the highest – 6.89 mg/L.

The average concentration of TP in the treated wastewater in the third WWTP was 2.9 mg/L, the minimum – 1.42 mg/L, and the highest – 5.15 mg/L.

46 unallowable concentrations of TP were detected (76.67 % of total samples).

The results of total phosphorus removal efficiency in the first WWTP (1), the second WWTP (2), and the third WWTP (3) are shown in Figure 4.

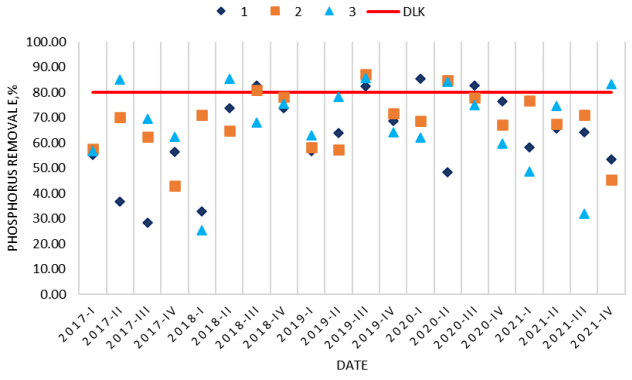

Figure 4. Total phosphorus removal efficiency compliance with the requirements (DLK)

The efficiency of TP removal was less likely to meet the requirements for the quality of treated wastewater: only 18.3 % met the requirements and 81.7 % did not.

It should be noted that the maximum permitted concentrations were exceeded by the quarterly average concentrations. Therefore, instantaneous concentrations could have been even higher.

B. Removal of nitrogen

Wastewater treated in conventional wastewater treatment plants with activated sludge has a low concentration of organic compounds, but high nitrate concentrations [10]. After biological wastewater treatment, nitrate nitrogen theoretically accounts for the majority of total nitrogen, because total nitrogen concentration in wastewater is reduced during biological treatment by nitrification (aerobic respiration: oxidation of ammonia to nitrates and nitrites) and denitrification (anoxic respiration: reduction of nitrates to gaseous nitrogen) [11].

Examining the data of wastewater treatment protocols for the selected period, the distribution of ammonium nitrogen and nitrate nitrogen in the concentration of total nitrogen was determined for each treatment plant.

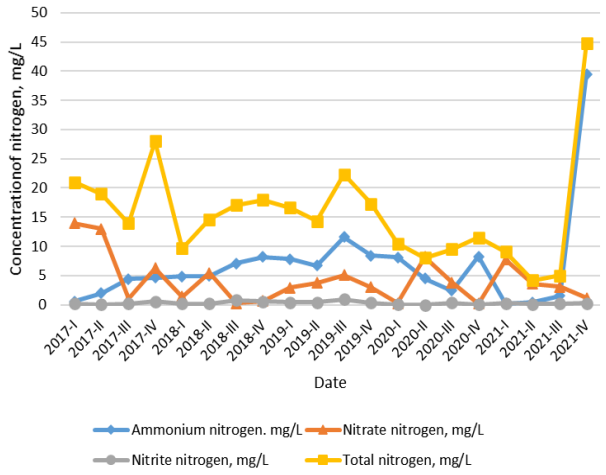

Figure 5. Distribution of ammonium nitrogen and nitrate nitrogen in the total nitrogen concentration in 1st WWTP

In Figure 5 can be seen, that in treated wastewater from the first WWTP ammonium nitrogen or nitrate nitrogen accounts for the majority of total nitrogen at a different quarter of the year. Also, the average percentage amount of ammonium nitrogen in the total nitrogen concentration was 43.4 % and the amount of nitrate nitrogen in the total nitrogen concentration was 27.1 %.

The average concentration of ammonium nitrogen in the treated wastewater in the first WWTP was 6.82 mg/L and the average concentration of nitrate nitrogen was 4.26 mg/L.

So, in most cases, the total nitrogen concentration consisted of ammonium nitrogen in the 1st WWTP.

In Figure 6 is shown, that in treated wastewater from the second WWTP ammonium nitrogen accounts for the majority of total nitrogen at a different quarter of the year. Also, the average percentage amount of ammonium nitrogen in the total nitrogen concentration was 68.2 % and the amount of nitrate nitrogen in the total nitrogen concentration was only 7.2 %.

The average concentration of ammonium nitrogen in the treated wastewater in the second WWTP was 11.52 mg/L and the average concentration of nitrate nitrogen was 1.21 mg/L.

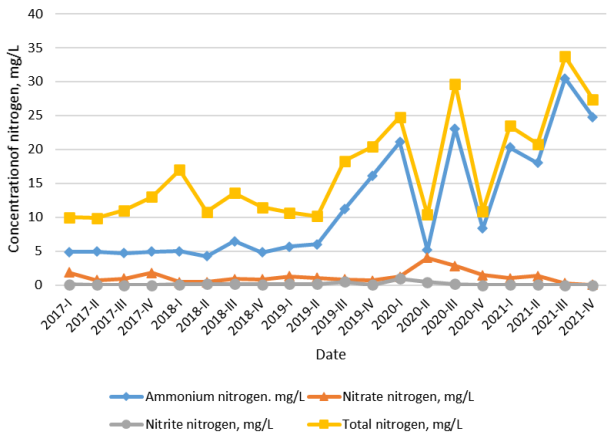

Figure 6. Distribution of ammonium nitrogen and nitrate nitrogen in the total nitrogen concentration in 2nd WWTP

So, in most cases, the total nitrogen concentration consisted of ammonium nitrogen in the 2nd WWTP.

In Figure 7 is shown, that in treated wastewater from the third WWTP ammonium nitrogen accounts for the majority of total nitrogen at a different quarter of the year. Also, the average percentage amount of ammonium nitrogen in the total nitrogen concentration was 59.6 % and the amount of nitrate nitrogen in the total nitrogen concentration was only 13.3%.

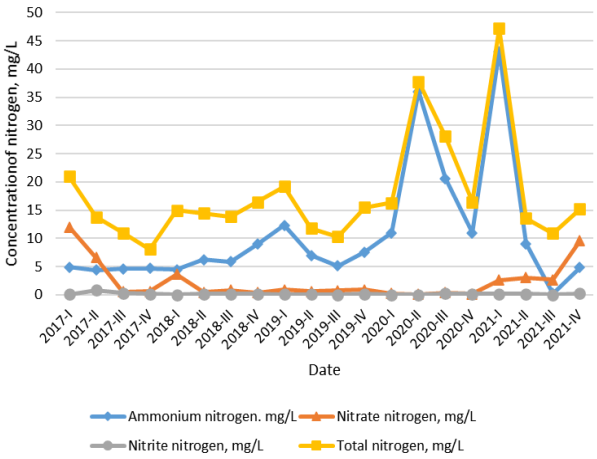

Figure 7. Distribution of ammonium nitrogen and nitrate nitrogen in the total nitrogen concentration in 3rd WWTP

The average concentration of ammonium nitrogen in the treated wastewater in the third WWTP was 10.61 mg/L and the average concentration of nitrate nitrogen was 2.37 mg/L.

So, in most cases, the total nitrogen concentration consisted of ammonium nitrogen in the 3rd WWTP.

Summarizing the nitrogen removal results, it can be said that a similar situation was found in three different WWTPs with the same flow rate - the concentration of ammonium nitrogen accounted for most of the total nitrogen concentration. These WWTPs have a problem with the nitrification process. It is important information for designing the tertiary wastewater treatment to achieve a higher level of removal of nitrogen compounds.

Obviously, before applying additional (tertiary) wastewater treatment, the composition of total nitrogen compounds in each treatment plant must be assessed.

C. Removal of phosphorus

When considering conventional phosphorus removal technologies, a few key factors must be taken into account. Firstly, there is the requirement to remove up to 80% of incoming TP load to meet the current discharge requirement of 2 mg/L. In conventional wastewater treatment plants, approximately 10% of total phosphorus can be removed during solids settling and 30% during the biological metabolism of microorganisms [12]. Consequently, phosphorus is removed inefficiently and an additional 40% removal of P is required.

The distribution of phosphate phosphorus in the concentration of total phosphorus was determined for each treatment plant.

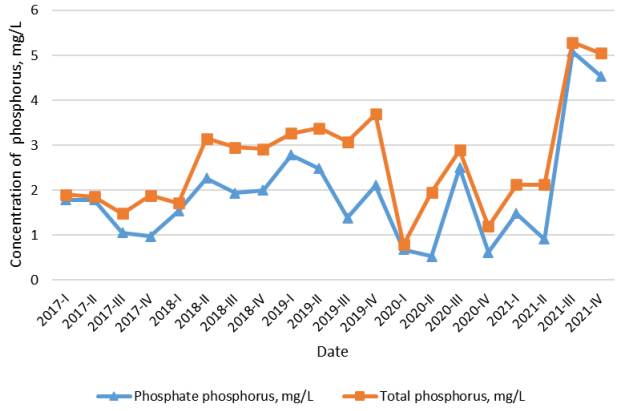

Figure 8. Distribution of phosphate phosphorus in the total phosphorus concentration in 1st WWTP

In Figure 8 can be seen, that in treated wastewater from the first WWTP the phosphate phosphorus accounts for the majority of the total phosphorus concentration. Also, the average percentage amount of phosphate phosphorus in the total phosphorus concentration was 72.9 %.

The average concentration of phosphate phosphorus in the treated wastewater in the first WWTP was 1.92 mg/L and the average concentration of total phosphorus was 2.63 mg/L.

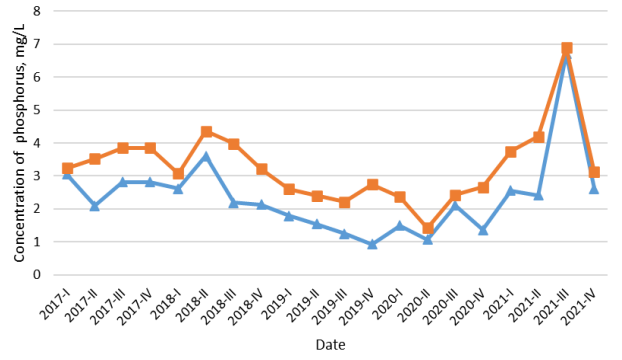

Figure 9. Distribution of phosphate phosphorus in the total phosphorus concentration in 2nd WWTP

In Figure 9 is shown, that in treated wastewater from the second WWTP the phosphate phosphorus accounts for the majority of the total phosphorus concentration. Also, the average percentage amount of phosphate phosphorus in the total phosphorus concentration was 71.6 %.

The average concentration of phosphate phosphorus in the treated wastewater in the second WWTP was 2.36 mg/L and the average concentration of total phosphorus was 3.29 mg/L.

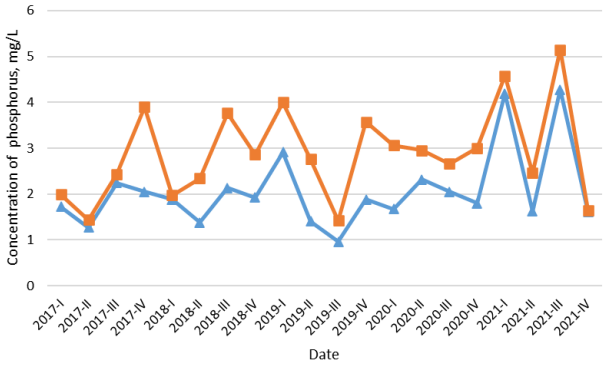

Figure 10. Distribution of phosphate phosphorus in the total phosphorus concentration in 3rd WWTP

In Figure 10 is shown, that in treated wastewater from the third WWTP the phosphate phosphorus accounts for the majority of the total phosphorus concentration. Also, the average percentage amount of phosphate phosphorus in the total phosphorus concentration was 71.2 %.

The average concentration of phosphate phosphorus in the treated wastewater in the third WWTP was 2.06 mg/L and the average concentration of total phosphorus was 2.90 mg/L.

It can be assumed, that the phosphate concentration of phosphates makes up the major part (about 70%) of total phosphorus. The orthophosphate (PO_4-P) is the most abundant form in domestic wastewater: it represents 60–85% of total phosphorus due to the hydrolysis of polyphosphates and organic phosphates [13].

In this study, it was found that the main pollutants in the wastewater, that cause eutrophication - nitrogen and phosphorus, were not removed effectively. In order to protect the environment around us, water resources, also to reduce eutrophication, it is necessary to install tertiary wastewater treatment plants, that will reduce residual concentrations of nitrogen and phosphorus compounds. It is recommended that tertiary wastewater treatment plants should not be expensive to install and operate, should be environmentally friendly, and be suitable for small and medium-sized wastewater treatment plants. Also, before applying tertiary wastewater treatment, the composition of wastewater pollutants in each treatment plant must be assessed.

IV. CONCLUSIONS

The results showed that 76.67% of the residual total phosphorus concentration, 1.67% of biochemical oxygen demand (BOD_7), and 25% of total nitrogen from all analyzed samples did not meet the requirements for treated wastewater. The efficiency of total phosphorus removal did not meet the requirements for the quality of treated wastewater in 81.7 % of cases. The results justified the need for tertiary treatment of wastewater in all three WWTP. In order to achieve a higher level of removal of nitrogen and phosphorus compounds, additional tertiary treatment is recommended.

REFERENCES

[1] Crini, G., & Lichtfouse, E. (2019, March 1). Advantages and disadvantages of techniques used for wastewater treatment. Environmental Chemistry Letters, Vol. 17, pp. 145–155. https://doi.org/10.1007/s10311-018-0785-9

[2] Farkas, K., Walker, D. I., Adriaenssens, E. M., McDonald, J. E., Hillary, L. S., Malham, S. K., & Jones, D. L. (2020, August 15). Viral indicators for tracking domestic wastewater contamination in the aquatic environment. Water Research, Vol. 181, p. 115926. https://doi.org/10.1016/j.watres.2020.115926

[3] Bali, M., & Gueddari, M. (2019). Removal of phosphorus from secondary effluents using infiltration–percolation process. Applied Water Science, 9(3), 3. https://doi.org/10.1007/s13201-019-0945-5

[4] Powley, H. R., Dürr, H. H., Lima, A. T., Krom, M. D., & Van Cappellen, P. (2016). Direct Discharges of Domestic Wastewater are a Major Source of Phosphorus and Nitrogen to the Mediterranean Sea. Environmental Science & Technology, 50(16), 8722–8730. https://doi.org/10.1021/acs.est.6b01742

[5] Culhane, F., Teixeira, H., Nogueira, A. J. A., Borgwardt, F., Trauner, D., Lillebø, A., … Robinson, L. A. (2019). Risk to the supply of ecosystem services across aquatic ecosystems. Science of the Total Environment, 660, 611–621. https://doi.org/10.1016/j.scitotenv.2018.12.346

[6] Lv, N., Li, T., Liu, H., Belarbi, Z., Daramola, D. A., & Trembly, J. P. (2020). Phosphate removal from wastewater using reinforced feed material at the tertiary treatment stage. IOP Conference Series: Materials Science and Engineering, 869(4), 042023. https://doi.org/10.1088/1757-899X/869/4/042023

[7] Renman, A., & Renman, G. (2022). Removal of Phosphorus from Hypolimnetic Lake Water by Reactive Filter Material in a Recirculating System—Laboratory Trial. Water 2022, Vol. 14, Page 819, 14(5), 819. https://doi.org/10.3390/W14050819

[8] Poikane, S., Kelly, M. G., Salas Herrero, F., Pitt, J. A., Jarvie, H. P., Claussen, U., … Phillips, G. (2019). Nutrient criteria for surface waters under the European Water Framework Directive: Current state-of-the-art, challenges and future outlook. Science of The Total Environment, 695, 133888. https://doi.org/10.1016/J.SCITOTENV.2019.133888

[9] Ministry of Environment of the Republic of Lithuania. Regulation on Wastewater Management of the Republic of Lithuania (In Lithuanian Language: LR Nuotekų Tvarkymo Reglamentas). (2006).

[10] Chang, J. J., Wu, S. Q., Dai, Y. R., Liang, W., & Wu, Z. Bin. (2013). Nitrogen removal from nitrate-laden wastewater by integrated vertical-flow constructed wetland systems. Ecological Engineering, 58, 192–201. https://doi.org/10.1016/j.ecoleng.2013.06.039

[11] Jaramillo, F., Orchard, M., Muñoz, C., Zamorano, M., & Antileo, C. (2018, July 15). Advanced strategies to improve nitrification process in sequencing batch reactors - A review. Journal of Environmental Management, Vol. 218, pp. 154–164. https://doi.org/10.1016/j.jenvman.2018.04.019

[12] Bunce, J. T., Ndam, E., Ofiteru, I. D., Moore, A., & Graham, D. W. (2018, February 22). A review of phosphorus removal technologies and their applicability to small-scale domestic wastewater treatment systems. Frontiers in Environmental Science, Vol. 6, p. 8. https://doi.org/10.3389/fenvs.2018.00008

[13] Bali, M., & Gueddari, M. (2019). Removal of phosphorus from secondary effluents using infiltration–percolation process. Applied Water Science, 9(3), 3. https://doi.org/10.1007/s13201-019-0945-5

Essential requirements for ecological and economic machining of steel

Egbert Schäpermeier
Alkoven, Austria
c.graf@graf-tech.de

Abstract

Dry processing within metal-cutting manufacture needs to be applied in order to reduce the adverse effects of cooling lubricants on the environment. In a study by Schäpermeier, the author indicates that during machining above a fixed temperature value, the contact area between the underside of the chip and the rake face (chip underside/rake face) experience boundary friction. As this process generates lubricants that are not harmful to the environment, the basic requirement for dry processing during chip formation with boundary friction is fulfilled.
In addition, the production of lubricants reduces the wear rate of the tool and eventually creates an economic incentive to achieve dry processing, by selecting the specifications to allow for boundary friction during the process of machining.

During the machine processing the highest temperatures occur in the contact area chip underside/rake face. In contrast to the assumption of FE modelling, the chip underside and the rake face are not smooth, but show a microscopic roughness. As a result, only parts of the contact area experience friction. This roughness on both surfaces leads to the formation of "cavities" that can be filled with cooling lubricants at low temperatures, and hence affects chip formation. With increasing temperature, the protrusions of the chip underside "soften" and the cavities' volume decreases. Following that, the protrusions are welded onto the rake face and form built-up edges. Eventually the temperature of the protrusions reaches the melting temperature of steel and the cavities are filled, thus the requirements for boundary friction are met. In this case only the protrusions of the rake face are in contact with the chip underside and the chip can transmit normal and transverse forces. The main characteristic of this process is that the total area of the protrusions represents the size of the machining surface. In spite of the melting temperatures, the protrusions at the chip underside do not melt due to the significantly short residence time and remain on the chip when it exits the contact area.
It is therefore crucial to achieve the required temperature within the contact area to allow for a machining process with boundary friction. This temperature range is solely dependent on the dimensions of the machining surfaces of both the work piece and the tool, as well as the cutting speed. The dimensions generally differ between roughing and finishing and further depend on the magnitude of the speed ratio. Merely the specifications of the feed and cutting speed determine whether the machining process can be achieved in an economically and ecologically advantageous way.

Keywords: *Similarity mechanics, thermal speed ratio, boundary friction, inherent lubricant, dry machining, stability, cutting data control calculator.*

Short biography

Studied mechanical engineering at the Duisburg Engineering School. Degree in engineering with university entrance qualification. Studied heat, power and work machines, RWTH Aachen. Degree Dipl.-Ing.. Practice, Head of Physics in contract research at the Battelle Institute Ffm. Promotion to Dr.-Ing. at the University of Karlsruhe. 1985 Lateral entry into machining, self-employment.

IEECP'22, July 21-22, 2022, Oxford, United Kingdom

Sustainable measures in heating application in a manufacturing system with multi-criteria decision analysis – A case study.

A Ameena
Department of Production Engineering,
National Institute of Tiruchirappalli,
Tamil Nadu, India
ameenashine2005@gmail.com

S Kumanan
Department of Production Engineering,
National Institute of Tiruchirappalli,
Tamil Nadu, India
kumanan@nitt.edu

Jatin Akhani
Department of Production Engineering,
National Institute of Tiruchirappalli,
Tamil Nadu, India
jatinthakkar97@gmail.com

Abstract

Natural resource conservation and environmental protection are essential due to the rapid depletion of natural resources and unfavorable environmental changes on a worldwide scale. Sustainable measures are targeted at decreasing ecological impacts, mainly through technical innovation in producing goods and processes, resulting in increased operational efficiency and higher natural resource management, lowering emissions and waste. Energy is a critical component in sustainable industrial measures to enhance overall production sustainability in pollution prevention and control.

Industrial process heating consumes more energy than any other type of energy in the manufacturing industry. Around the world, industrial heating systems are a significant energy consumer and CO2 (GHG) emitter. Most of the direct emissions within the company's organizational borders are caused by the combustion of the primary fuel used for plant heating, heat production, and other vehicle manufacturing operations. This motivated us to analyze and develop reliable sustainability measures for industrial heating systems.

A case study is conducted in the domain of industrial heating systems in an automobile manufacturing plant The study provides an intricate understanding to assess a heating system and its impacts. It will offer opportunities to opt for alternate possibilities of materials & methods to reduce the harmful effects. It also gives a brief idea of the application of the MCDM approach in energy decision making. Furthermore, finding heating applications procedures that use energy-efficient solar thermal systems is crucial for enabling industries with large solar energy potential to reduce their reliance on non - renewable and develop more environmentally friendly industrial systems in the future.

Keywords: Sustainability measures, Energy efficiency, MCDM, TOPSIS, Manufacturing system, Sustainable manufacturing.

I. INTRODUCTION

Nowadays, sustainable industrial systems are a must to reduce environmental and health concerns while preserving energy and natural resources. Industry must employ a variety of various implementations to improve processes and practices in the production system to attain sustainability [1]. Sustainable measures are targeted at decreasing environmental impacts mainly through technical innovation in the product-producing processes, which results in increased operational efficiency and higher natural resource management, lowering emissions and waste. Reduced energy consumption, minimizing waste, improved product durability, reduced environmental and health issues, improved product quality, and generation of renewable energy supplies are the key goals of establishing a sustainable manufacturing system [2]. A sizable portion of the world's overall energy consumption and CO2 emissions are caused by industrial activity [3]

Industrial process heating consumes more energy than any other type of energy in the manufacturing industry, accounting for more than 70% of total process energy end-use [4]. Around the world, reduction in energy consumption for industrial heating applications can be done by using various energy savings strategies [5]. The

IEECP'22, July 21-22, 2022, Oxford, United Kingdom

complexity of energy consumption sources, their variability, and the multiple levels of energy consumption in manufacturing systems are the focus of energy performance [6]. Reduced energy consumption and associated costs can result from investments in energy-efficient measures, which can offer a variety of benefits. Energy efficiency reduces reliance on fossil fuels, reduces harmful emissions, and has a positive influence on the environment [7].

Consequently, the broad adoption of energy-efficient technology and processes is a critical component in the manufacturing system for sustainable development [8]. The global decrease in carbon emissions is the primary force behind technological advances in energy efficiency and renewable energy. Several medium-energy-consuming enterprises are also encouraged to use energy-efficient technology due to the cost reductions associated with those technologies [9]. Employing renewable energy sources has several advantages, including reducing dependency on fossil fuel supplies and ecological damage from carbon emissions. [10,11]. The use of heat recovery and heat pumps lowers total costs while increasing system efficiency [12]. Khan et al discussed the impact to reduce the usage of fossil fuels, reduce the CO_2 emission level, and energy conservation [13].

To identify sustainability problems and suggest workable solutions in the specific application, the study is carried out systematically. A case study methodology is adopted in industrial heating systems in an auto manufacturing facility. MCDA TOPSIS approach is used to determine the viable solution in a conflicting condition in energy decision-making [14].

II. LITERATURE REVIEW

Measuring sustainability performance is essential for industrial firms that are also considering the wider impact of sustainability objectives on the economy and future policies [19]. More energy is used for industrial process heating than for any other purpose in the manufacturing sector, and it comes from several sources, including electricity, steam, and fuels [4]. Numerous process heating unit operations and related machinery are used to accomplish significant material transformations that are essential steps in the production of the majority of consumer and industrial goods [7].

How to lower energy consumption, production costs, and the environmental impact of the manufacturing systems is a key challenge for the industry's expansion [6]. Sustainability issues in manufacturing have motivated industries to focus more on suitable Industry focus has shifted to more appropriate operations and management methods because of manufacturing sustainability concerns, but there is no one proven strategy for successful adoption [23]. The first step in reducing dependence on fossil fuels is to use energy-saving programs designed to cut energy consumption and boost industrial energy efficiency [24]. Utilizing renewable energy sources is another method [5,12]. In a unique setting with a high-temperature heat pump system, energy use and greenhouse gas emissions can be decreased up to 90 percent and 40 percent, respectively [25].

Several studies have mentioned the advantages of solar heater water heating for domestic and industrial purposes and have stated the potential scope areas in order to use solar heat in industrial operations [26]. The majority of industrial solar thermal applications use solar water heating (SWH), which is the most affordable of all solar thermal technologies now in use [27]. The operations that require low temperatures, a constant amount of energy throughout the hours of sunlight, and high prices of conventional energy in the existing system are those that are most conducive to the integration of solar thermal energy in industrial applications [28]

Energy strategy can be effectively addressed by using MCDA, which is also increasingly used to resolve the conflicts that arise, by aggregating either performances or personal preferences, as it is a multidimensional problem [29]. Environmental, socio-economic, technical, and institutional constraints to energy planning are addressed using MCDM as an evaluation structure. In contrast to many other tools, MCDM tools are adaptable enough to address multi-criteria challenges linked to a variety of application [30].

III. PROBLEM DESCRIPTION

The present situation in the industrial sector is shifting in the direction of sustainability. A large global energy consumer and CO2 emitter are industrial heating systems. Even the slightest innovation or improvement in horizontal deployment can have a significant positive impact on sustainability. This motivated us to do research and develop credible sustainable heating system initiatives. The case study methodology is more dependable, they can deal with both tangible and intangible data, and they can calibrate outcomes. Many works successfully implemented case studies in Indian contexts using a variety of cutting-edge methodologies [31–33]. A case study methodology is utilized to analyze the best options for environmentally friendly heating applications in automobile manufacturing industry.

For the current study, gear component washing in an Engine shop was selected while reviewing the existing system. Presently Heating sources for washing gear components are catered with electric heaters will lead to high CO2 emissions, as fossil fuel (fuel-fired boilers) is the source of electricity generation. To enhance sustainability in the heating system there is potential scope for improvements in the factors like energy efficiency, energy conservation, and pollution reduction was reviewed. The major sustainability practices in the industrial heating system have been in two ways. First, modify the existing system to be better sustainable. Second, select and design alternate solutions from a sustainability point of view. Since selecting the best heating method involves complex decision variables. To develop a sustainable solution for the existing problem, two better sustainable heating systems were sized for the same application and their respective performance indicators were computed. The performance indicators of the existing electric heater system and alternatively sized systems were compared, and the appropriate system was selected as a sustainability measure.

IV. METHODOLOGY

The evaluation of heating systems is significant as they give information of its performance. The right data & information about are essential to deciding on appropriate improvement actions. The evaluation has four basic steps. First, examine the existing system, with detailed analysis of the energy use, energy demand, and energy losses in the existing system. This helps in reviewing possibilities to reduce the energy use or losses by suitable measures and identifies the parameters which are highly valued in terms of performance. This will give a basic understanding of the actual level of the performance performed by the present heating system, and it can be compared with the measures. Appropriate measures can be decided to achieve the desired level of performance numbers.

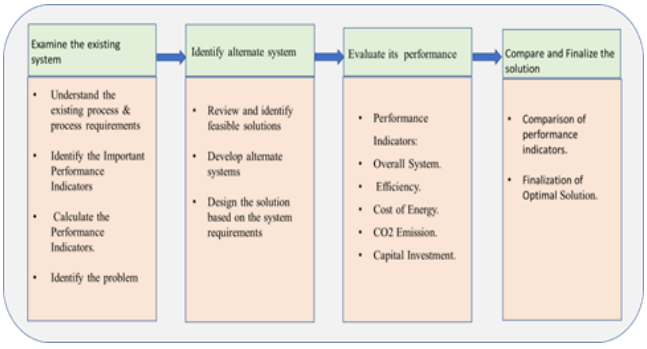

Figure 1. The methodology applied in this study

The goal of the present study is to select the best possible alternate energy-efficient heating system in sustainability. To achieve this goal, a methodology is proposed in this work. Figure 1. gives a brief overview of the used methods. The work is employed in a systematic way to analyze, develop, evaluate, and select the sustainable measure in an existing industrial system.

A. Analyze the performance measures of the existing system

First, we analyze the existing heating system and evaluate the performance measures. The evaluation of heating systems is important since it provides information about the system's performance. It's crucial to get the necessary data and information about a heating system's functioning before deciding on the best strategy [25]. Many factors contribute to the overall performance of the heating system & decision making of an industrial heating system, this framework has identified ten specific factors at two levels. These factors will add value to the evaluation and understanding of a particular system, and in turn, assists to select a suitable heating system for a specific application [34].

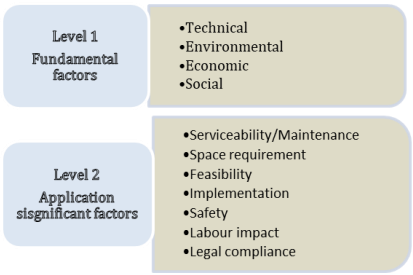

Figure 2. Performance indicators level

The fundamental factors in level 1 and application-specific factors in level 2 are described in Figure 2. The fundamental factors consist of technical, economic, environmental, and social factors. At the factory level, four significant performance indicators are considered for the systems' evaluation i.e System efficiency, Cost of energy, Impact on ecology (CO_2 emission), Capital investment & return of investment (ROI). Though various factors affect the net systems' performance in terms of System efficiency, Profitability & Impact on Ecology. The Level 2 factors are specific factors that demand unique requirements based on the specific application. These performance indicators can be used to assess an existing system, and compare an existing system with alternate systems, thereby guiding decision-making for energy conservation, energy efficiency improvements, and sustainability improvement activities. These indices will assist during the design stages of an

industrial heating system by providing an intricate understanding of the sustainability factors.

The actual energy usage must be determined in order to assess the performance indicators of the particular industrial heating system. The actual energy consumption was measured with an Energy meter & it was observed that 18.31 KW was consumed in 3.23 hrs. Implies of 6.80 kW / hr and a maximum of 7.2 kW / hr were recorded as the highest energy consumption at a single point in time. The process is a high energy-consuming process, energy conservation can be reviewed. The cost of energy is INR 7.1 / kWh, which can be reviewed for cost reduction. Reduction in CO2 emission and reduction in energy consumption will add value from a sustainability point of view. The existing sustainability problems associated with the electric heater system are clearly defined.

Table 1. Performance of the electric heating system

1.	Energy consumption calculation: 7.2kW/hr
2.	CO2 emission calculation :129.8 Kg / day
3.	Cost of Energy: The cost of 1KW of energy from TNEB is INR 7.1 Cost of energy / day = INR 1124.64 / day
4.	Energy Conversion Efficiency – 97-99%

B. Alternate measures for the existing system

Industrial heating systems are a major energy user and CO_2 polluter across the world. Even a minor innovation or improvement, on horizontal deployment, can contribute to a large extent towards sustainability. In recent solar energy, utilization has been an important area of sustainability. And in the last decade, Industrial heat pumps have gradually attained maturity in terms of performance and reliability. Hence a Solar thermal system and a Heat pump system can be considered an alternative to the existing electric heater [35,36] [37]. The basic categories of industrial heating systems are based on the source of heat generation [38]. In the existing system energy delivered by an electric heater is 100% sourced from electricity, whereas in a solar thermal & heat pump system, energy from nature is utilized which is renewable. Such systems will help for sustainability. So as an alternate method, heat pump, and solar thermal systems were selected. Performance evaluation of the alternate sources is done with the data's obtained from the plant's energy management department (utilities & services department) and a comparative study was carried out to find the alternate method (boiler heating systems, electric heater systems, heat pump systems, solar systems) for an energy-efficient heating system [39].

C. **Evaluate performance measures of an alternate system.**

1) Heat pump system

The heat pump system's benefit is, it extracts heat energy from the atmosphere and makes use of it for the initial heating of the refrigerant before it gets into the compressor. Hence, the required external power is considerably reduced as a benefit. Conservatively, the matured industrial heat pumps offer a co-efficient of performance of 2.3~3.0, based on the effectiveness of the heat transfer and the use of the heat pump equipment's cooling benefits [40]. Based on the heating requirements heat pump with a capacity of 14 kW was decided. If the cold load is used, energy due to chiller load consumption can be saved.

Table 2. Performance of heat pump heating system

1.	Operating hours /day -22 hrs
2.	Energy required for process / hr = 7.2 kW.h (HMT data)
3.	COP of Heat pump 2.3
4.	To deliver 7.2 kWh of energy, a Heat pump will require [(1/2.3) *7.2 of energy 7.2] of energy
5.	Energy consumption by heat pump / hr = 0.43 * 7.2 = 3.1 kWhr.
6.	Energy-saving / year through heat pump = 28169.8 kWhr. /Year
7.	CO2 emission / year = 13380.4 Kg / year
8.	The cost of 1KW of energy delivery through the heat pump is INR
9.	Cost of energy / day = INR 483.51 / day
10.	Cost saving / year through heat pump = INR 2,00,032 / year

COP (Coefficient of Performance) of a Heat pump is Considered conservatively 2.3 excluding the cooling load Electricity Price. Table 2. shows the performance evaluation of deploying a Heat pump as an alternate measure.

2) The solar thermal system

A solar thermal system with EVT (Evacuated Tube Collectors) is another alternate method of electrical heater system [13]. The solar thermal system can also be integrated into an already existing boiler or electrical heater system constituting a hybrid

system, which will primarily operate with the energy generated by the solar thermal system, and in case of poor sunlight or non-capability of the solar thermal to generate sufficient energy, the boiler or an electric heater operates as an auxiliary system. Based on the requirement of the application and geographical location parameters considered for the design of solar heating are:

Initial feed water temperature - 25˚C. The final temperature of the water/storage tank water temperature -65˚C. Sunshine hours in plant location (Chennai)- 6 hrs. Energy requirement / day-158.4 KW to be generated in 6hrs. Required Solar thermal capacity/sizing = 26.4 kWhr, M = Mass flow rate, liters per day 3405.6 liters (storage tank capacity, Mass flow rate, liters per day=3916.4litres (calculating with 15% buffer capacity).

Table 3. Performance of solar thermal heating system

1.	Investment Cost: Cost of investment / kWh, inclusive of piping & equipment = INR 45,000
2.	Total cost of investment = 26.4 x 45,000 = INR 11,88,000
3.	Total Cost = ETC equipment + Storage Tank + components (heat exchangers) + pump primary circuit & secondary circuit (Pumps & water lines) = INR 11,88,000
4.	Total energy used by the existing system per day = 158.4 kWh
5.	Total energy used by the present system per year = 49420.8 kWh
6.	Energy saved by deploying solar thermal system = 49420.8 kWh
7.	Cost-saving per year: Total energy saved / day = 158.4 KW
8.	Cost saved per day = 158.4 x 7.1 = 1124.64 INR
9.	Cost saved per year = 1124.64 x 312 = 3,50,888 INR

D. Comparison of Performance Indicators

The comparison of performance indicators of the different systems will provide an intricate understanding of the possibilities to reduce harmful effects, reduce energy consumption, optimize energy efficiency, reduce costs, etc. This understanding will be helpful in the design stage of an industrial heating system, to design the heating system in a sustainable manner. With respect to the case study, the performance indicators of alternate measures of heating systems with the existing system are compared.

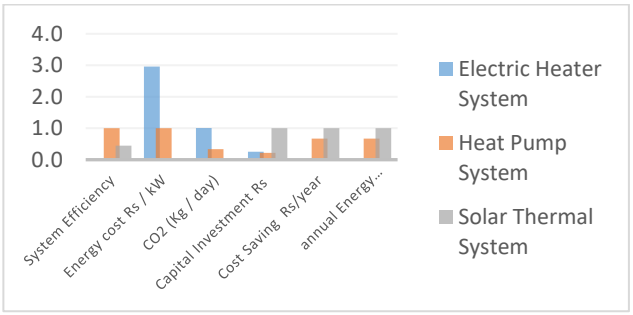

Figure 3. Comparison of heating system

A comparison of the performance of different heating systems is shown in Figure 3.

To summarize the comparison, calculations of system efficiency that the heat pump is more efficient compared to electric and solar heating. The advantage of the heat pump system is that it may heat up the refrigerant initially before it enters the compressor by using heat energy that is drawn from the atmosphere. As a result, energy use associated cost and CO_2 emission are significantly reduced. Solar thermal system heating systems reduced carbon footprint and energy cost. . Solar thermal systems have high capital investment costs & late Returns on Investment are disadvantageous. Practically, the Solar thermal system has less proven in large energy applications. It is not preferred due to its difficulty for system modification at times of process flexibility, the Heat pump can be considered energy-efficient but cost reduction and maintenance cost it's not recommended. A conflict arose between the sustainable performance and energy-efficient system. To choose the appropriate decision of the sustainable measure for the energy-efficient heating system.

The problem at hand will be tackled using a multicriteria approach that considers the requirement for sustainability as well as criteria for energy efficiency, cost-effectiveness, and technical viability. We should also confirm that the measures in the situation under co nsideration are financially viable. MCDA tool is the best option for finding a feasible solution in this scenario**.**

V. Sustainable performance evaluation with TOPSIS method

The MCDA tool is becoming more and more well-liked in the field of energy planning since it allows to make choices while simultaneously considering all the criteria and objectives [16]. MCDA is a tool that supports alternative energy technologies. The broad usage of MCDM techniques shows that they are effective at assisting decision-makers in addressing issues related to energy sustainability [17] [18]. MCDM TOPSIS is a preferred method in

the evaluation of optional energy source which allows direct comparison with the alternative solutions [16]. The methodological framework developed for ranking the alternatives is TOPSIS (Technique for Order Preference by Similarity to Ideal Solutions) approach is easily scalable to tackle diverse energy sustainability problems [41]. The TOPSIS method requires minimal input data and results are easy to understand and it is with shortest geometrical distance to ideal result [42].

The approach enables a comparative evaluation of different heating system with existing fuel fired heating to enhance sustainability in the selected automobile production unit. While considering the selection of criterions in sustainable dimension, performance in the social dimension such as legal compliance, workers safety and labour impact can't be considered as it is not an implemented system. The criteria selected in the two levels for applying the TOPSIS methodology are presented in a hierarchical form as in Figure 4.

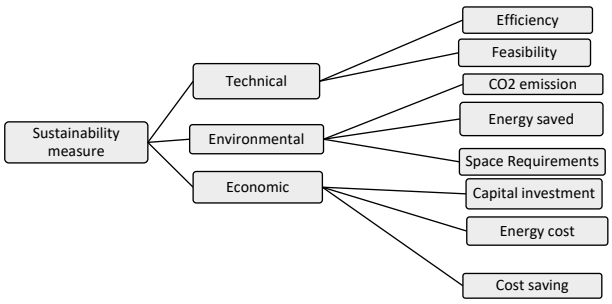

Figure 4. MCDA framework.

The TOPSIS approach uses distance measurements to calculate the relative strength of each alternative based on its positive ideal solution (PIS) and negative ideal solution (NIS). The given numbers are then ranked by evaluating a relative proximity degree for each option based on the values of their respective measures. The steps involved in TOPSIS methodology discussed as follows [15]:

Step 1: By placing criteria vertically and alternatives horizontally, an evaluation matrix is created.

$$Aij = \begin{bmatrix} a_{11} & a_{12} & \dots & a_{1n} \\ a_{21} & a_{22} & \dots & a_{2n} \\ : & : & \dots & : \\ : & : & \dots & : \\ a_{m1} & a_{m2}: & \dots & a_{mn} \end{bmatrix}$$

Step 2 – Evaluation matrix is converted to normalized decision matrix (R) with equation (1)

$$r_{ij} = \frac{a_{ij}}{\sqrt{\sum_{k=1}^{m} {a_{kj}}^2}}$$

$$\text{R matrix: } Rij = \begin{bmatrix} r_{11} & r_{12} & \dots & r_{1n} \\ r_{21} & r_{22} & \dots & r_{2n} \\ : & : & \dots & : \\ : & : & \dots & : \\ r_{m1} & r_{m2}: & \dots & r_{mn} \end{bmatrix} \quad \dots\dots\dots\dots\dots (1)$$

Step 3: Third step includes normalized matrix's values multiplied by weights of each criterion and establishing the weighted normalized matrix. $Vij = \begin{bmatrix} w_1r_{11} & w_2r_{12} & \dots & w_nr_{1n} \\ w_1r_{21} & w_2r_{22} & \dots & w_nr_{2n} \\ : & : & \dots & : \\ : & : & \dots & : \\ w_1r_{m1} & w_2r_{m2}: & \dots & w_nr_{mn} \end{bmatrix}$

Step 4: Finding the ideal best (A+) and ideal worst (A$^-$) for each criterion of each alternative from the above matrix: for beneficial criteria maximum value is the ideal best and minimum value is the ideal worst and vice versa for the non -beneficial criteria.

$$A^+ = \{(max_i v_{ij} \backslash j \epsilon J), (min_i v_{ij} \backslash j \epsilon J')\} \quad \dots\dots (2)$$

$$A^- = \{(min_i v_{ij} \backslash j \epsilon J), (max_i v_{ij} \backslash j \epsilon J)\} \quad \dots\dots\dots (3)$$

Step 5– Measures of separation are calculated using the Euclidian distance, which is used to quantify how far options stray from the ideal best and ideal worst solutions.

(S_i^*) denotes the Euclidian distance from the ideal best and calculated as in equation (4).

(S_i^-) denotes denotes the Euclidian distance from the ideal worst and calculated as in equation (5):

$$s_i^* = \sqrt{\sum_{j=1}^{n} (v_{ij} - v_j^*)^2} \quad (4)$$

$$s_i^- = \sqrt{\sum_{j=1}^{n} (v_{ij} - v_j^*)^2} \quad (5)$$

Step 6– Performance score is calculated as described by equation (6):

$$C_i^* = \frac{s_i^-}{s_i^* + s_i^-} \quad \dots \quad (6)$$

If Ci * values lies between 0 and 1. Value 1 representing the best ideal solution and zero denotes the ideal worst solution

Step 7- Based on the performance score, the alternatives can be ranked.

Table 4. TOPSIS method result and Rank

Heating Systems	Performance score(%) Pi	Rank
Fuel fired boiler	51.21	4
Electric heater	56.91	3
Heat pump system	62.95	1
Solar thermal system	61.62	2

Using the chosen alternatives and competing criteria, TOPSIS analysis was performed on the problem as stated above, and the results are shown in Table 4. A heat pump heating system is the most efficient option for the chosen system.

TOPSIS ranking hierarchy is Heat pump heating system< Solar thermal heating< Electric heating< Fuel fired heating.

VI. RESULTS

The performance indicators of heating systems are compared, and the result as shown in Figure 3. Analytical comparative study shows a conflict between the performances between system efficiency (Heat pump system) and energy consumption (Solar thermal system), thereby it's difficult to find a sustainable solution. If heat pump sourced with renewable energy source can be selected as an appropriate solution from this case study problem, but practically it is not feasible.

Under this uncertainty MCDA TOPSIS method is selected for finding the best feasible heating system. TOPSIS result with ranking of the alternatives are given in Table 4. With MCDA heat pump system secured the first, second is solar thermal system. Hence the heat pump system is the best feasible energy efficient heating system for heating washing liquid for engine component washing in plant to enhance sustainability in manufacturing industry.

With respect to the case study, it can be inferred that there is significant potential to reduce CO2 emission & to reduce energy consumption with an energy efficient system.

VII. CONCLUSIONS

This paper combines analytical method and MCDM methods to find sustainable measures in heating applications. A case study with a systematic framework is conducted in an automobile manufacturing plan. Steps involved are analyse, identify problem, suggestion sustainable measures, evaluation, and infer the result. The performance indicator values provide an intricate understanding about the effect of the overall systems' energy efficiency and sustainability.

Comparative study of the alternatives shows that integrated system with renewable energy source is the best technique for many applications based on the feasibility. In this specific case, a conflicting situation arise for the selection of energy efficient sustainable heating after analytical approach, so MCDA TOPSIS method is selected to rank the performance different heating system. It helps us to identify the best feasible measures within a set of predetermined criteria.

This framework will be helpful in reviewing the current procedure, comparing it to alternative methods, and clarifying opportunities for energy conservation, improving energy efficiency, and moving toward sustainability. This study helps to understand the application of MCDA in energy decision making. The result shows that there is a significant scope of improvements can be done to achieve the sustainability goal such as energy efficient system, energy saving thereby reduction in GHG (CO2) emission, energy cost, maintenance cost, capital investment etc. Also identifies in a feasible situation integration of renewable system with energy efficient system is the best sustainable measure. Renewable energy source with energy efficient that can be recommended as the best sustainable measure in low and moderate temperatures**.**

This study demonstrates that even minor improvements may lead the industrial system to advance to sustainability goals. Harmful impacts can be predicted & appropriate measures can be taken to prevent the adverse effects, thereby shifting towards industrial sustainability.

VIII. REFERENCES

[1] Trianni A, Cagno E, Neri A, Howard M. Measuring industrial sustainability performance: Empirical evidence from Italian and German manufacturing small and medium enterprises. Journal of Cleaner Production 2019;229:1355–76. https://doi.org/10.1016/j.jclepro.2019.05.076.

[2] Gupta S, Dangayach GS, Singh AK, Meena ML, Rao PN. Implementation of sustainable manufacturing practices in Indian manufacturing companies. Benchmarking 2018;25:2441–59. https://doi.org/10.1108/BIJ-12-2016-0186.

[3] Cagno E, Trianni A, Spallina G, Marchesani F. Drivers for energy efficiency and their effect on barriers: empirical evidence from Italian manufacturing enterprises. Energy Efficiency 2017;10:855–69. https://doi.org/10.1007/s12053-016-9488-x.

[4] Hasanuzzaman M, Rahim NA, Hosenuzzaman M, Saidur R, Mahbubul IM, Rashid MM. Energy savings in the

combustion based process heating in industrial sector. Renewable and Sustainable Energy Reviews 2012;16:4527–36. https://doi.org/10.1016/j.rser.2012.05.027.

[5] Abdelaziz EA, Saidur R, Mekhilef S. A review on energy saving strategies in industrial sector. Renewable and Sustainable Energy Reviews 2011;15:150–68. https://doi.org/10.1016/j.rser.2010.09.003.

[6] Cai W, Lai K hung. Sustainability assessment of mechanical manufacturing systems in the industrial sector. Renewable and Sustainable Energy Reviews 2021;135. https://doi.org/10.1016/j.rser.2020.110169.

[7] Apostolos F, Alexios P, Georgios P, Panagiotis S, George C. Energy efficiency of manufacturing processes: A critical review. Procedia CIRP, vol. 7, Elsevier B.V.; 2013, p. 628–33. https://doi.org/10.1016/j.procir.2013.06.044.

[8] Neofytou H, Sarafidis Y, Gkonis N, Mirasgedis S, Askounis D. Energy Efficiency contribution to sustainable development: A multi-criteria approach in Greece. Energy Sources, Part B: Economics, Planning and Policy 2020;15:572–604. https://doi.org/10.1080/15567249.2020.1849449.

[9] Pathirana S, Yarime M. Introducing energy efficient technologies in small- and medium-sized enterprises in the apparel industry: A case study of Sri Lanka. Journal of Cleaner Production 2018;178:247–57. https://doi.org/10.1016/j.jclepro.2017.12.274.

[10] Martiskainen M, Coburn J. The role of information and communication technologies (ICTs) in household energy consumption-prospects for the UK. Energy Efficiency 2011;4:209–21. https://doi.org/10.1007/s12053-010-9094-2.

[11] Reddi KR, Li W, Wang B, Moon Y. System dynamics modelling of hybrid renewable energy systems and combined heating and power generator. International Journal of Sustainable Engineering 2013;6:31–47. https://doi.org/10.1080/19397038.2012.689781.

[12] Wallerand AS, Kermani M, Voillat R, Kantor I, Maréchal F. Optimal design of solar-assisted industrial processes considering heat pumping: Case study of a dairy. Renewable Energy 2018;128:565–85. https://doi.org/10.1016/j.renene.2017.07.027.

[13] Khan MZH, Al-Mamun MR, Sikdar S, Halder PK, Hasan MR. Design, Fabrication, and Efficiency Study of a Novel Solar Thermal Water Heating System: Towards Sustainable Development. International Journal of Photoenergy 2016;2016. https://doi.org/10.1155/2016/9698328.

[14] Zlaugotne B, Zihare L, Balode L, Kalnbalkite A, Khabdullin A, Blumberga D. Multi-Criteria Decision Analysis Methods Comparison. Environmental and Climate Technologies 2020;24:454–71. https://doi.org/10.2478/rtuect-2020-0028.

[15] Cagno E, Neri A, Trianni A. Broadening to sustainability the perspective of industrial decision-makers on the energy efficiency measures adoption: some empirical evidence. Energy Efficiency 2018;11:1193–210. https://doi.org/10.1007/s12053-018-9621-0.

[16] Shankar KM, Kumar PU, Kannan D. Analyzing the drivers of advanced sustainable manufacturing system using AHP approach. Sustainability (Switzerland) 2016;8. https://doi.org/10.3390/su8080824.

[17] Ghofrani M, Hosseini NN. Optimizing Hybrid Renewable Energy Systems: A Review. Sustainable Energy - Technological Issues, Applications and Case Studies, InTech; 2016. https://doi.org/10.5772/65971.

[18] Ahrens MU, Foslie SS, Moen OM, Bantle M, Eikevik TM. Integrated high temperature heat pumps and thermal storage tanks for combined heating and cooling in the industry. Applied Thermal Engineering 2021;189. https://doi.org/10.1016/j.applthermaleng.2021.116731.

[19] Uppal A, Kesari JP, Zunaid M. Designing of Solar Process Heating System for Indian Automobile Industry. vol. 6. 2016.

[20] Farjana SH, Huda N, Mahmud MAP, Saidur R. Solar process heat in industrial systems – A global review. Renewable and Sustainable Energy Reviews 2018;82:2270–86. https://doi.org/10.1016/j.rser.2017.08.065.

[21] Kalogirou S. The potential of solar industrial process heat applications. Applied Energy 2003;76:337–61. https://doi.org/10.1016/S0306-2619(02)00176-9.

[22] Diakoulaki D, Karangelis F. Multi-criteria decision analysis and cost-benefit analysis of alternative scenarios for the power generation sector in Greece. Renewable and Sustainable Energy Reviews 2007;11:716–27. https://doi.org/10.1016/j.rser.2005.06.007.

[23] Jamwal A, Agrawal R, Sharma M, Kumar V. Review on multi-criteria decision analysis in sustainable manufacturing decision making. International Journal of Sustainable Engineering 2021;14:202–25. https://doi.org/10.1080/19397038.2020.1866708.

[24] Madan Shankar K, Kannan D, Udhaya Kumar P. Analyzing sustainable manufacturing practices – A case study in Indian context. Journal of Cleaner Production 2017;164:1332–43. https://doi.org/10.1016/j.jclepro.2017.05.097.

[25] Nallusamy S, Dinagaraj GB, Balakannan K, Satheesh S. Sustainable green lean manufacturing practices in small scale industries-A case study. 2015.

[26] Virmani N, Bera S, Kumar R. Identification and testing of barriers to sustainable manufacturing in the automobile industry: a focus on Indian MSMEs. Benchmarking 2021;28:857–80. https://doi.org/10.1108/BIJ-08-2020-0413.

[27] Cagno E, Neri A, Trianni A. Broadening to sustainability the perspective of industrial decision-makers on the energy efficiency measures adoption: some empirical evidence. Energy Efficiency 2018;11:1193–210. https://doi.org/10.1007/s12053-018-9621-0.

[28] Fawkes S, Oung K, Thorpe D, Reviewers XZ. Best Practices and Case Studies for Industrial Energy Efficiency Improvement-An Introduction for Policy Makers. 2016.

[29] Khan U, Zevenhoven R, Tveit TM. Evaluation of the environmental sustainability of a stirling cycle-based heat pump using LCA. Energies (Basel) 2020;13. https://doi.org/10.3390/en13174469.

[30] Organization. Advanced Heat Pump Water Heater Research Final Report Bonneville Power Administration Technology Innovation Project 292 The Energy Trust of Oregon Northwest Energy Efficiency Alliance Ravalli Electric Co-op Tacoma Public Utilities. 2015.

[31] IEEE Power & Energy Society. 2010 Asia-Pacific Power and Energy Engineering Conference : proceedings : March 28-31, 2010, Chengdu, China. IEEE; 2010.

[32] Li T, Li A, Guo X. The sustainable development-oriented development and utilization of renewable energy industry——A comprehensive analysis of MCDM

methods. Energy 2020;212. https://doi.org/10.1016/j.energy.2020.118694.

[33] Neksfit P, Rekstad H, Zakeri GR, Schiefloe PA. CO2-heat pump water heater: characteristics, system design and experimental results*. vol. 21. n.d.

Ambitious but deficient: Technology innovation route of China's energy industry

1st Weibin Peng
School of Economics,Hangzhou Normal University
Hangzhou, People's Republic of China
pwb7129@hznu.edu.cn

2nd Xiaohui Chen
School of Economics,Hangzhou Normal University
Hangzhou, People's Republic of China
20020150@hznu.edu.cn

2nd Wang Yizhuo
School of Economics,Hangzhou Normal University Hangzhou, People's Republic of China
wangyizhuo@stu.hznu.edu.cn

Abstract

Energy industry is a vital area related to the security and economic development of a sovereign country, and the green and low carbon development is becoming the main development direction of global energy technology innovation (ETI). Driven by the energy revolution and the digital revolution, a new round of global technological revolution and industrial transformation is in the ascendant. China is constantly promoting ETI and actively exploring the factors affecting energy innovation efficiency in order to achieve the commitment of "carbon peak" and "carbon neutral". China's ETI still has shortcomings that are expected to break through. Using the province-level data of key variables in the field of ETI from 2008 to 2019, we found the stock of human capital, income level, carbon emission, industrial structure and the financial expenditure on science and technology may influence the energy innovation efficiency. The main reason of the energy innovation efficiency is the stock of human capital. And China is catching up with developed countries in the scale of its talent team with its consistently efforts. The increase of carbon emissions has a significant positive correlation with energy innovation efficiency at the national level while there is a negative correlation between carbon emissions and energy innovation efficiency in eastern China. Although China has formulated an ambitious five-year plan in the field of ETI, the basic research and human capital required to improve the efficiency of energy innovation are still shortcomings. Furthermore, state-owned enterprises and private enterprises cannot jointly build an innovation consortium has significantly restricted the efficiency of China's ETI. Due to the lack of unified coordination at the national level, there is vicious competition and prominent industry similarities in new energy between provinces The road to progress in China's energy technology innovation is still quite long.

Keywords: energy industry; ETI; human capital stock; "carbon peak" and "carbon neutral"

IEECP'22, July 21-22, 2022, Oxford, United Kingdom

I. INTRODUCTION

A healthy planet is an essential requirement and key enabler for sustainable development in which environmental, economic, and social objectives are addressed in a balanced manner through an integrated approach. According to the Medium Term Strategy for UNEP 2022-2025 entitled "For people and planet: the United Nations Environment Programme strategy for 2022–2025 to tackle climate change, loss of nature and pollution", the COVID-19 pandemic is more than a health crisis: it is also a humanitarian and socioeconomic crisis. It has exposed and aggravated vulnerabilities and inequalities and it is exacerbating already existing challenges in meeting the Sustainable Development Goals (SDGs) worldwide. The demand for economic growth and the growing global population have tripled the extraction of natural resources worldwide to destructive levels [1]. Climate warming, over-exploitation of resources, and loss of biodiversity have made energy a key area of concern for the security and development of a sovereign country. Since the outbreak of the Russian-Ukrainian war, global energy prices have continued to rise, posing a huge threat to global economic growth. The stability, diversity and low cost of energy supply have become an important political issue that have to reconsider by government. Green and low-carbon development has attracted more attention around the world. Renewable energy alternative technologies, electric vehicle technologies, natural gas hydrogen production technologies, and new power systems, safe and efficient nuclear energy technology is becoming the main development direction of global energy technology innovation.

Driven by the energy revolution and the digital revolution, a new round of global technology revolution and industry transformation is in the ascendant. So far, more than 130 countries/regions around the world have proposed zero emission targets [2]. ETI is considered one of the best pathways to transition to a global clean energy system and can play a vital facilitation role in global action to reduce carbon emissions. In 2021, the European Union, the United Kingdom, the United States, Russia, Japan, South Korea, and China have successively issued action policies for carbon peaking and carbon neutrality. On January 29, 2022, China's National Development and Reform Commission (CNDRC) and National Energy Administration (NEA) jointly issued the "14th Five-Year Plan for Modern Energy System". China is about to lead energy development based on technology innovation and insist on taking innovation as the primary driving force for development. The "14th Five-Year Plan" emphasizes that ETI will be developed around five aspects: advanced renewable energy, new power systems, safe and efficient nuclear energy, green and efficient fossil energy development and utilization, and energy digitalization and intelligence. China has

formulated an ambitious technology innovation roadmap for this purpose. It aims to anchor carbon peaking and carbon neutrality, accelerate the transformation of the energy structure, improve the efficiency of the energy system, achieve a high-quality jump in energy, achieve an innovation-driven development strategy, improve the level of innovative human capital, and promote the digitalization and intelligence of the energy industry and energy The modernization of the industrial chain has continuously injected new momentum into promoting high-quality economic development and building a modern country.

Although ETI has been emphasized by many countries, it is not easy to achieve. Since persistent investment of R&D does not necessarily bring about great progress in the field of ETI, the efficiency of energy innovation must be considered. Energy innovation efficiency (EIE) is a performance measurement of energy innovation. In recent years, research on EIE and its influencing factors has become a research hotspot in academia. A basic premise is how to measure it. Judging from the literature review, the academic community has not reached a consensus standard. At present, the mainstream measurement methods mainly include nonparametric methods including Data Envelopment Analysis (DEA) [3][4][5][6]. The number of patents applied and granted to measure innovation input and output efficiency [7][8]. When trying to measure green EIE by building a model, it is considered feasible to build a DEA model through a two-stage innovation value chain, which has been applied in a study of technology innovation efficiency of industry enterprises in 31 provinces in China [9]. DEA has been used to evaluate the effect of innovation-driven policies in related research of new energy vehicles, such as measuring the innovation efficiency of Chinese new energy vehicle listed companies from 2015 to 2017.

The number of national patent applications can also be used as a measure of the efficiency of technology innovation. The number of green patents as a measure of the field of energy innovation has a great fit. For example, the results of an empirical study on 79 countries' panel data from 1995 to 2017 show that renewable energy and energy efficiency boost innovation performance at aggregate and disaggregated levels [10]. Deng and Liao (2009) believe that the measure of technology innovation can also be replaced by the number of patents applied or granted [11]. For example, the innovation of renewable energy can be replaced by the number of patents applied or granted by using the negative binomial distribution. Based on this, it is a meaningful exploration that green patents can be used to measure the efficiency of energy innovation.

It is well known that human capital is an indispensable factor in driving a country to achieve innovation. The empirical analysis based on the Heterogeneous Stochastic Frontier Model (HSFM) shows that human capital stock has a significant role in promoting regional innovation efficiency, and the improvement of human capital level can enhance the stability of regional innovation efficiency [12], high school, undergraduate and graduate students, etc. The increase of human capital at the educational level can promote the improvement of regional innovation efficiency [13]. Of course, the factors affecting ETI are extremely complex. The positive impact of per capita income level on ETI is a prominent example. Fagerberg & Srholec's (2007) empirical analysis of 115 countries during the period 1992-2004 shows that the innovation efficiency system is highly positively correlated with per capita income levels[14]. Yang and Yao (2018) believe that if the income of an industry is increased, the enthusiasm of laborers to innovate can be ignited, thereby improving the innovation efficiency of the industry[15]. Based on the above analysis, it is believable that the higher the per capita income of the region, the higher the enthusiasm of the laborers, and the higher the efficiency of ETI. Another factor affecting ETI is closely related to carbon emission constraints. An analysis of the correlation between energy consumption carbon emissions and green innovation efficiency in China's equipment manufacturing industry found that coal and crude oil carbon emissions have a positive impact on green innovation efficiency [16].

The existing research mainly focus on measuring energy innovation efficiency with DEA model, and there are few literatures on energy innovation performance with green energy patent application as the measurement criterion; Scholars have paid attention to the inhibitory effect of income distribution gap on innovation efficiency [17]. However, there are still deficiencies in the research on improving the income level of the whole industry and improving the efficiency of energy innovation with the help of economic growth and labor productivity. At the same time, although many studies have focused on the impact of technological innovation on carbon emission reduction, there are relatively few related studies on how carbon emissions affect energy technological innovation. At present, technological innovation has become the main battlefield in the game of great powers, and the scale of innovative human capital has a profound impact on the improvement of national innovation efficiency. If a country wants to expand the scale of innovative human capital, it must strive to improve the quality of innovative human capital and create more world-class scientific and technological leaders and innovative teams. Only in this way can it be possible to achieve key energy innovation results, improve the efficiency of energy innovation, and obtain long-term competitive advantages.

This paper takes the number of green patent applications by residents of 31 provinces in China from 2008 to 2019 as the core explanatory variable to measure the efficiency of energy technology innovation. In order to discuss the development prospects of China's ETI efficiency, the article measured the human capital stock, income level and carbon emission reduction level respectively, and verified the impact of human capital stock, income level and carbon emission on the efficiency of China's ETI by constructing an empirical analysis.

II. CHINA AMBITIOUSLY BUILDS ROADMAP FOR FUTURE ENERGY TECHNOLOGY INNOVATION

China is a country that lacks oil and gas among the world's major powers. Its dependence on foreign oil is as high as 70 percent, and there is limited room for increasing production in the future. Developing renewable energy and attaching importance to energy technology innovation is an indispensable development direction to resolve China's energy security. After the outbreak of the Russian-Ukrainian war, China had to formulate more aggressive new energy development goals, vigorously promote the large-scale, high-proportion, high-quality, and market-oriented development of renewable energy, try to improve new energy consumption and storage capabilities, and actively build renewable energy. A new power system with new energy as the main body, improve the institutional mechanism and policy system that is conducive to the joint development and utilization of renewable energy by the whole society, and provide a strong guarantee for the construction of a clean, low-carbon, safe and efficient energy system. And based on the clean energy system, guide the industry to develop in the direction of low energy consumption and high technology, and gradually reduce the proportion of oil in the industrial economy [18].

$755 billion has been spent on deploying low-carbon energy technologies around the world since 2021, with nearly half of that investment taking place in Asia. China has invested US$266 billion in energy transition, accounting for 35 percent of the total global investment in the first place [19]. Since 2008, China's investment in traditional energy supply industries such as electricity, heat and gas has gradually slowed down. The output of clean resources such as natural gas, nuclear power, and wind energy continues to rise, and

the proportion of clean energy in the energy structure continues to increase. For example, the proportion of raw coal production has dropped by 9.2 percent in ten years, and the proportion of total crude oil production has dropped by 2.5 percent in ten years[20]. These are all China's efforts to continue to adhere to the energy demand-oriented, give full play to the advantages of the domestic large-scale market, focus on solving the core technical problems of energy, and speed up energy conservation and emission reduction. It is hoped to achieve carbon peak by 2030 and carbon neutrality by 2060, which reflects China's ambitious strategic deployment on the road of ETI.

According to World Energy Investment 2021 by IEA, under the influence of the COVID-19 pandemic, enterprises in 2020 reduced their expenditure on energy research and development in the private sector due to the reduction of budgets. But annual global energy investment rises to US$1.9 trillion by 2021, rebounding nearly 10 percent from 2020, bringing total investment back to pre-pandemic levels. Meanwhile, its investment structure has shifted towards the power and end-use sectors, rather than traditional fuel production [21]. Therefore, the background of the times has put forward higher requirements for the functions of the government - the government should play the role of formulating policies and regulations, emphasize the innovative role of the economy, and continue to promote the zero-emission policy. For example, in terms of traditional fuel energy, CNDRC issued the "Guiding Opinions on Accelerating the Intelligent Development of Coal Mine “on February 25, 2020. Demonstrate coal mines, give priority support in terms of capacity replacement and mine capacity increase, and introduce relevant industrial support policies to encourage financial institutions to increase support for intelligent coal mines. The Ministry of Finance has also issued relevant inclusive preferential policies. In addition to the tax reduction and exemption policies for general high-tech enterprises, such as levying corporate income tax at a reduced rate of 15 percent for recognized high-tech enterprises, there are also tax reduction and exemption policies for enterprises that meet the requirements for environmental protection and energy conservation. 10 percent of the investment in special equipment such as water saving and safe production can be deducted from the tax payable in the current year; these preferential policies are available to qualified coal enterprises, aiming to encourage coal enterprises to speed up intelligent mining.

Therefore, China has also made breakthrough achievements in energy conservation and emission reduction in recent years. In terms of scale, in 2022, the annual power generation of China's new energy facilities will exceed 1 trillion kWh for the first time, the total annual power generation of China's photovoltaic power generation will reach 350 billion kWh, and the annual total power generation of wind power will exceed 400 billion kWh. It ranks first in the world at present; it has also made great achievements in new energy facility technology, such as independent development, including the strongest offshore wind turbine in Asia-Pacific with a single installed capacity of 10 megawatts, and Baihe, whose installed capacity ranks second in the world. Tan Hydropower Station and other advanced new energy power generation equipment. China will continue to promote green and low-carbon development, while strengthening cooperation with overseas countries, aiming to jointly build a community with a shared future for mankind.

At the same time, with the transformation and upgrading of China's energy structure, the global energy supply and demand structure has changed. Higher requirements are put forward for the improvement of energy innovation efficiency. China needs to identify the paths that affect the efficiency of energy innovation, continuously improve its comprehensive strength, broaden the channels for improving the overall efficiency of energy innovation, absorb funds from various aspects, and encourage domestic and foreign companies to invest in clean energy. investment, and actively absorb international capital and private capital. According to Sohu.com, we used web crawler technology to extract 297 pieces of text information about "energy technology innovation", with a total of about 118,000 words. We used R (4.2.0) software to perform word segmentation and word frequency statistics to extract keywords with a word frequency greater than 50. A total of 113, draw a word cloud map (Figure 1). It can be seen that “technology”, “innovation”, “development” and “greenness” have not only become the hotspots of China's large-scale Internet portals, but also the hotspots of capital investment. China has successfully created a fabulous landscape in the whole society that attaches importance to technology innovation and to promote the transformation of energy utilization.

III. RESEARCH METHODS AND RESEARCH DATA

A. Research Methods

Considering that many scholars usually use a two-way fixed effect analysis model when analyzing green ecological efficiency and green economic efficiency[22], this research method is also used to eliminate the estimation error in traditional statistical models. To ensure the availability and comparability of research data, panel data of 31 provinces from 2008 to 2019 is used to measure the influencing factors of China's energy innovation efficiency in this paper. The relevant data come from the China Statistical Yearbook and the State Intellectual Property Office.

Figure 1. A word cloud map of China's ETI

To explore the effect of human capital on the efficiency of energy innovation, we select the number of green patent applications in each province as a proxy variable to measure the level of energy innovation. Gross wages measure human capital stock and provincial per capita income, respectively.

The industry upgrading coefficient mentioned by (Xu and Jiang (2015) is used to measure the industrial structure upgrading level of each province[23]:

$$IS = \sum_{i=1}^{3} q_i \times i = q_1 \times 1 + q_2 \times 2 + q_3 \times 3$$

Among them, q_i is the proportion of the output value of the i-th industry, and the data comes from the China Statistical Yearbook (CSY).

Fiscal science and technology expenditures are the expenditures made by the government and its related departments to support technology activities. It refers to the scientific research expenditures arranged in the national financial budget. The data comes from the CSY. In view of the large number of green patent applications, the average number of students in colleges and universities, and the salary of the employed population, this study carried out a regression empirical study after logarithmic operation. The calculation model is as follows:

$$lngreenpatent = \beta_0 + \beta_1 lnhc + \beta_2 wage + \beta_3 carbon + \beta_4 lnd + \beta_5 fin + \lambda_t + \mu_i + \varepsilon_{it}$$

Among them, β_0 is the intercept term, β_i（$i = 1,2\ldots5$）represents the coefficient parameter corresponding to each explanatory variable, λ_t is the time effect that does not change with the individual, μ_i is the individual effect that does not change with time, and ε_{it} represents random error term..

B. RESEARCH RESULTS

B.1 Descriptive Statistical Analysis

As shown in Table 1, the main variable names, mean, standard deviation, minimum and maximum values are listed. Tibet was excluded from the study due to missing data on Tibet. Through descriptive statistical analysis, the number of energy green patent applications in China and the level of wages fluctuate greatly, indicating that there is a large gap from energy patent applications to income in provincial level (Figure 2). China's industry upgrading coefficient has little difference between 30 provinces.

Table 1. Descriptive Statistics for Primary Variables

VARIABLES	N	Mean	Sd	Min	Max
Gp	360	6,180	9,836	31	67,258
Hc	360	2,518	888.1	969	6,750
Wage	360	3,068	2,960	140.4	20,510
Fin	360	0.438	0.257	0.153	1.368
Carbon	360	162.3	119.3	2.208	628.6
Ind	360	2.369	0.127	2.132	2.834

B.2 Regression Analysis

A multicollinearity test was performed before regression analysis of the study data. If the VIF index is less than 10, there is no need to eliminate the corresponding explanatory variables, and the model fits well.

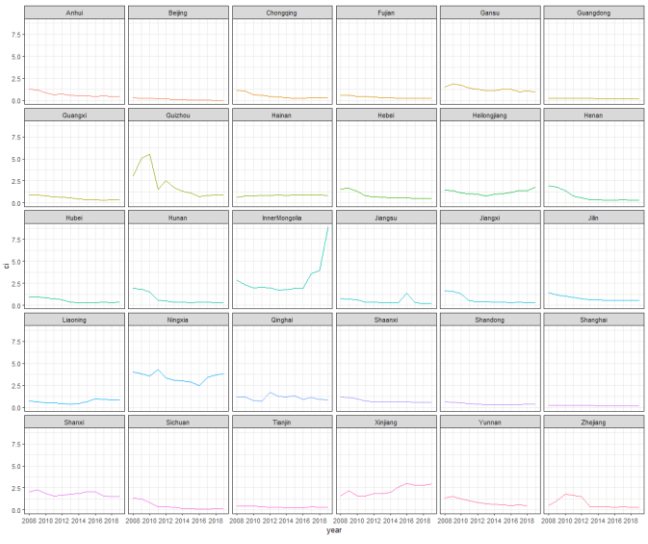

Figure 2. Inter-provincial differences in the number of green energy patent applications

Panel data supported fixed effects by Hausman test. Table 2 reports the regression results for the mixed regression model, the fixed-effects model, and the two-way fixed-effects model. With the addition of individual fixed effects and two-way fixed effects, the goodness of fit R^2 of the model increased from 92.2 percent to 96.2 percent, indicating that the two-way fixed-effects model had a good fitting effect.

Table 2. Test for Multicollinearity

Variable	VIF	1/VIF
lnd	3.810	0.262
Fin	2.860	0.349
Hc	2.140	0.468
Wage	1.910	0.523
Carbon	1.440	0.697
Mean VIF	2.430	—

Firstly, EIE and human capital stock are regressed. As shown in Figure 3, there is a significant positive correlation between energy innovation efficiency and human capital stock. Secondly, Table 3 reports the results of influencing factors. For human capital stock and national financial investment in science and technology, first, an individual fixed effect model is introduced into the regression of human capital stock, and the coefficient increases from 0.563 to 1.028, indicating that OLS underestimates the impact of human capital stock on green energy innovation efficiency. influence. However, after the introduction of the two-way fixed effect, its coefficient has dropped to a certain extent, indicating that the individual fixed effect overestimates the impact of human capital stock on the efficiency of green energy innovation. But overall, whether it is an OLS or a two-way fixed-effect model, the human capital stock has a positive impact on the efficiency of green energy innovation; secondly, the more the state finances invest in science and technology education, the higher the country's energy innovation efficiency. The side shows that the increase of investment in science and technology education and the growth of human capital stock also complement each other. Since the 19th National Congress of the Communist Party of China, China's talent team expansion scale has continued to catch up with developed countries, and it is at the breaking point of qualitative change in the cultivation of world-class talents and the creation of output. The strategy of strengthening the country with talents is the source of living water for China's energy innovation efficiency.

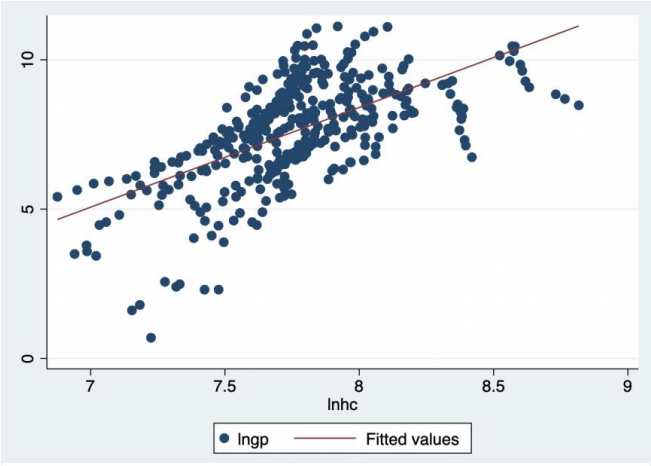

Figure 3. Scatter plot of green innovation efficiency and human capital stock

Regarding the income of Chinese residents, based on the same sample, its significance weakens with the gradual introduction of individual fixed effects and two-way fixed effects, indicating that the impact of wage levels on innovation efficiency is overestimated. It also shows that income is less important to the efficiency of energy innovation than the stock of human capital. However, it is undeniable that the level of income does affect the level of domestic ETI. When residents' income continues to increase, their knowledge-based investment in themselves increases, and the quality of workers continues to improve. Then, under the guidance

of the country's active innovation, residents are more willing to participate in innovation work, and the stronger the innovation capability in the region, which will improve the efficiency of energy innovation. To a certain extent, raising the national wage level by the state has a certain positive effect on energy innovation, but its effect is not as large as the stock of human capital. Therefore, when formulating national policies, China focuses on guiding and cultivating more innovative talents.

Table 3. Influencing Factor Regression Results

	(1)	(2)	(3)
VARIABLES	lngp	lngp	lngp
Lnhc	0.563***	1.028***	0.921***
	(5.72)	(6.65)	(7.88)
Lnwage	1.445***	1.002***	0.203*
	(40.79)	(16.62)	(1.78)
Fin	0.204	0.641***	0.667***
	(1.41)	(4.70)	(6.48)
Crbon	-0.000	0.002***	0.001***
	(-1.08)	(3.82)	(3.00)
lnd	-0.053	4.051***	-0.830*
	(-0.16)	(9.56)	(-1.87)
Constant	-7.559***	-18.036***	-0.487
	(-9.79)	(-14.73)	(-0.32)
Observations	360	360	360
R-squared	0.922	0.928	0.962
Province FE	YES	YES	YES
Year FE	NO	NO	YES
Number of id		30	30

What deserves attention is the amount of carbon emissions and the level of industrial structure upgrading. The fundamental reason for China's high carbon emissions is that energy and its related industrial systems are largely dependent on fossil resources. China's power industry and high-energy-consuming industries (steel, petrochemical, cement, non-ferrous metals, etc.) carbon dioxide emissions account for about 80 percent of the country's total carbon dioxide emissions and are industries that need to be focused on. This study combines the economic theory hypothesis "Environmental Kuznets Curve" to illustrate. In terms of carbon emissions, carbon emissions and energy innovation efficiency first increase with the growth of per capita GDP. After the inflection point, carbon emissions and energy innovation efficiency decrease with the growth of per capita GDP. The empirical results show that, at the Chinese level, the increase in carbon emissions has a significant positive correlation with the improvement of energy innovation efficiency, indicating that China is actively promoting the green transformation of its economic structure and improving its energy innovation capabilities. China is constantly conducting comprehensive and revolutionary explorations and adjustments, aiming to make China's high-quality development goals compatible with global climate governance goals.

In descriptive statistics, China has almost kept pace in upgrading its industrial structure across regions, so it is unreliable to only do individual fixed-effect results. For decades, China has continuously promoted the optimization and upgrading of the energy industry structure, promoted the green and low-carbon transformation of traditional high-energy-consuming industries, and vigorously developed green and low-carbon industries. However, empirical results show that energy innovation efficiency is negatively correlated with industrial upgrading. Based on this, this research tentatively believes that although China's energy technology has made great progress, the way of upgrading the industrial structure is still unscientific and the driving force for innovation efficiency is insufficient. Therefore, to achieve the "dual carbon" goal, China It is not only necessary to break through many key technologies in various fields, but also to break the barriers between various energy types and energy-related industries, to break through the key bottlenecks and core technologies of multi-energy integration and complementarity and industrial process reengineering in related key industries, especially to overcome related industries. Difficulties in industrial transformation and upgrading. For example, while adjusting the industrial structure and carrying out industrial transfer, scientifically plan the direction of industrial transfer and adjustment, take the market and products as the guide, eliminate backward and energy-intensive enterprises without blindly expanding the scale, so as to continuously strengthen the innovation of energy technology system and drive Efficient energy saving and emission reduction.

In order to further explore the influence factors of various factors on the efficiency of energy innovation, this study conducted a regional heterogeneity regression on the eastern, central and western regions of China (Table 4). Among them, according to the level of economic development classification. The eastern region of China includes 11 provinces including Beijing, Tianjin, Hebei, Shanghai, Jiangsu, Zhejiang, Fujian, Shandong, Guangdong, Hainan and Liaoning; the central region includes Shanxi, Anhui, Jiangxi, Henan, Hubei, Hunan, Jilin and Heilongjiang in 8 provinces in China; 12 provinces in the west, including Inner Mongolia, Guangxi, Chongqing, Sichuan, Guizhou, Yunnan, Tibet, Shaanxi, Gansu, Qinghai, Ningxia and Xinjiang(Because there is no data of Tibet, only 11 provinces were considered).

From the regression results shown in Table 4, the human capital stock in the eastern, central, and western regions of China, significantly affects the efficiency of energy innovation at the level of 1 percent, which indicates that the reserve of innovative talents has a decisive impact on energy innovation. Therefore, China needs to make greater breakthroughs in cultivating outstanding scientists and technology talents. Significantly improve the ability of independent innovation, promote the continuous improvement of energy efficiency, and realize the "dual carbon" goal as soon as possible.

Table 4. Regional Heterogeneity Regression Results

	(1)	(2)	(3)
	lngpEast	lngpMiddle	lngpWest
Lnhc	0.943***	1.548***	0.971***
	(4.67)	(4.34)	(3.50)
Lnwage	0.201	0.636**	-1.342***
	(1.54)	(2.59)	(-3.84)
Fin	0.568***	0.895***	0.088
	(4.37)	(3.86)	(0.34)
Carbon	-0.002*	0.001	-0.000
	(-1.83)	(1.27)	(-0.59)
Lnd	0.578	-2.214**	-1.083
	(0.77)	(-2.22)	(-1.39)
Constant	-2.954	-5.189*	9.177***
	(-1.20)	(-1.90)	(2.92)
Observations	132	96	132
R-squared	0.974	0.975	0.964
Number of id	11	8	11
Province FE	Yes	Yes	Yes
Year FE	Yes	Yes	Yes

Some scholars have studied the efficiency of green innovation among regions in China, and the empirical results show that there is

a downward trend in the efficiency of green innovation in western China from 2006 to 2016[23][24]. The results of this study show that the income level in the western region has a negative impact on innovation efficiency at the 1% significance level. Therefore, the current energy problem in the economic development of western China is not only to ensure the sustainable income increase of low-income groups. While nominal wages across the country are rising steadily, the income distribution mechanism will be reformed, efforts will be made to narrow the income gap, and steady progress will be achieved in improving income and energy efficiency. The correlation between carbon emissions and EIE in eastern China is significantly negative. According to the Environmental Kuznets Curve, it can be speculated that the inflection point has already appeared first in eastern China. This shows that in order to realize the international commitment of carbon emission reduction, Chinese government has achieved optimistic achievements in the exploration of green and low-carbon transformation through continuous technology innovation.

IV. DEFICIENCIES THAT CHINA'S ENERGY TECHNOLOGY INNOVATION NEEDS TO BREAK THROUGH

Under the dual pressures of global warming and shortage of fossil fuels, reducing carbon emissions is not only required for China to fulfill its national commitment to reducing greenhouse gas emissions, but also a strategic choice for China's low-carbon and green development transition. It is worth noting that China's energy consumption is still very large, and it is urgent to break through the inherent deficiencies that restrict the efficiency of energy technology innovation to achieve the goal of carbon emissions. AS we all know, the indicator of carbon intensity is mainly used to measure the relationship between the national economy and carbon emissions. If a country's economic growth is accompanied by a decline in carbon dioxide emissions per unit of GDP, it means that the country has achieved a transition to low-carbon development. From the three-dimensional map of carbon intensity in China's provinces from 2008 to 2019 depicted in Figure 4, China has made continuous efforts for "carbon peaking" and "carbon neutrality". As an important goal of China's "14th Five-Year Plan" pollution prevention and control battle, the carbon emission intensity of China's provinces has shown a long-term downward trend for more than ten years. Therefore, China's carbon emission intensity has made positive progress.

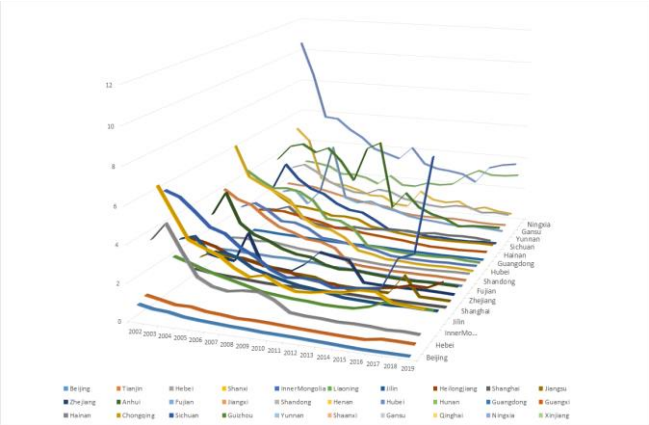

Figure 4. Carbon intensity map by province in China:2008-2019

Nonetheless, the empirical results of this study significantly suggest that energy technology innovation is driven by talent stock. due to the lack of unified coordination at the national level, there is vicious competition and prominent industrial similarities in the development of new energy between provinces, insufficient investment in basic research, lack of agglomeration effect and scale effect for talents of ETI, and state-owned enterprises and private enterprises cannot jointly build an innovation consortium has significantly restricted the efficiency of China's ETI.

In order to realize its ambitious energy technology innovation plan, it is necessary to take effective measures to overcome the shortcomings of development. Firsly, to improve the efficiency of energy innovation, under the ambitious energy innovation plan, it is still indispensable that China must continuously increase the importance of talents from the demand side and increased the intensity of investment promotion. Secondly, although China's industrial structure is not very different, for some provinces with large energy supply, China is constantly strengthening energy supply and demand adjustment, improving energy supply security capabilities, continuously promoting the optimization, and upgrading of industrial structure, and increasing a series of policies such as forest carbon sinks. Measures to improve green total factor productivity; Thirdly, since China has promoted the carbon peaking action, it has continuously promoted the implementation of the carbon peaking and carbon neutral "1N" policy system and promoted the construction of an economic system with green, low-carbon and circular development.

V. REFERENCES

[1] United Nations Environment Assembly (UNEA). https://sustainable development.un.org/index.php?page=view&type=30022&nr=2802& menu=3170.

[2] Altnta, H., & Kassouri, Y. "The impact of energy technology innovations on cleaner energy supply and carbon footprints in europe: a linear versus nonlinear approach". Journal of Cleaner Production, 2020, pp.276

[3] Furman J. L. Hayes R. "Catching Up or Standing Still?National Innovative Productiv-ity among"Follower Countries"", 1978~1999. Research Policy, 2004,33 (9),pp.1329~1354.

[4] Wei Chu, Shen Manhong. "Energy Efficiency and Its Influencing Factors: An Empirical Analysis Based on DEA". Management World, 2007(08):66-76.DOI:10.19744/j.cnki.11-1235/f. 2007.08.009.

[5] Li Shuangjie, Li Chunqi. "Modified Design and Application of Total Factor Energy Efficiency Measurement Method ". Research on Quantitative Economy, Technology and Economics, 2018, 35,(9): 110-125. DOI: 10.13653/j.cnki.jqte.2018.09 .007.

[6] Li Jinkai, Ma Jingjing, Wei Wei. "Research on regional differences in energy and carbon emission efficiency of China's eight comprehensive economic zones ". Research on Quantitative Economics and Technical Economics,2020,37,(6) ,pp.109-129.

[7] Ma Limei, Wang Junjie. "Energy Transition and Renewable Energy Innovation: An Empirical Study Based on Transnational Data". Zhejiang Social Sciences, 2021,(4) ,pp.21-30.

[8] Rkpa, B. , Abjac, D. , & Tl, D. "Linking scientific research and energy innovation: A comparison of clean and dirty technologies.

[9] Luo Liangwen, Liang Shengrong. "Green technology innovation efficiency and factor decomposition of Chinese regional industrial enterprises". Chinese Population, Resources and Environment, 2016, 26,(9) ,pp.149-157.

[10] Wen, J. , Okolo, C. V. , Ugwuoke, I. C. , & Kolani, K. "Research on influencing factors of renewable energy". energy efficiency, on technological innovation. does trade, investment and human capital development. 2022.

[11] Deng Haibin, Liao Jinzhong. "nstitutional Arrangement and Technological Innovation: Research Based on Negative Binomial Model ". Research in Science, 2009,27(7) ,pp.1101-1109.

[12] Shao Qinglong, Rao Lei. "Analysis of Influencing Factors of Renewable Energy Innovation——Based on the Empirical Test of OECD Countries ".Soft Science Xue, 2016, 30(01):71-75.DOI:10.13956/j.ss.1001-8409.2016.01.16.

[13] Liang Wenqun, Niu Chonghuai, Yang Chunyan. "Research on Human Capital Innovation Effect Based on Heterogeneous Stochastic Frontier Model ". Science and Technology Progress and Countermeasures, 2016,33(15) ,pp.145-150.

[14] Fagerberg, J. , & Srholec, M. . (2017). "National innovation systems, capabilities and economic development ". Martin Srholec.

[15] Wei Chu, Shen Manhong. “Energy Efficiency and Its Influencing Factors: An Empirical Analysis Based on DEA". Management World, 2007(08):66-76.DOI:10.19744/j.cnki.11-1235/f.2007.08.009 .

[16] Yang Lanpin, Yao Guoqing. "The Influence of Factor Income Distribution on Innovation Efficiency: From the Perspective of Comparison of Different Types of Industries". Jianghan Forum, 2018,(7) ,pp.21-29.

[17] Xu Jianzhong, Wang Manman, Guan Jun. "Research on the mechanism of energy consumption carbon emissions and green innovation efficiency from the perspective of dynamic endogenous: Based on the empirical analysis of China's equipment manufacturing industry" Management Review, 2019, 31(09):81-93.DOI:10.14120/j.cnki.cn11-5057/f.2019.09.007.

[18] Wang Yichen. "What does it mean for oil prices to exceed 10 yuan per liter".Economic Daily.2022-06-23.https://www.163.com/dy/article/HAH1SEQJ0519AKBM.html# fr=email.

[19] BNEF. "Energy Transition Investment Trends 2022." from https://assets.bbhub.io/professional/sites/24/Energy-Transition-Investment-Trends-Exec-Summary-2022.pdf.

[20] CLP Media Intelligence Research Center. "China Energy Big Data Report".Energy Micro-Observation.2021-06-08. https://baijiahao.baidu. com/s?id=1701960324247634405&wfr=spider&for=pc.

[21] BNEF."World Energy Investment 2021".from https://www.iea.org /reports/world-energy-investment-2021.In Energy Tran sition Investment Trends 2022.from https://assets.bbhub.io/pr ofessional/sites/24/Energy-Transition-Investment-Trends -Exe c-Summary-2022.pdf.

[22] He Weida, Wen Jialong, Zhang Manyin. "Research on the Impact of Digital Economy Development on China's Green Ecological Efficiency: Based on Two-Way Fixed Effects Model". Economic Issues, 2022(01):1-8+30.DOI:10.16011/ j.cnki.jjwt.2022.01.002.

[23] Xu Min, Jiang Yong. "Can the upgrading of China's industrial structure narrow the consumption gap between urban and rural areas? ". Research on Quantitative Economics and Technical Economics, 2015, 32(3) ,pp. 3-2

[24] Lv Yanwei, Xie Yanxiang, Lou Xianjun. "Research on the Convergence of Regional Green Innovation Efficiency in China ". Science and Technology Progress and Countermeasures, 2019, 36,(15) ,pp.37-42.

A Systemic and Multi-disciplinary Diagnosis Model for Microgrids Sustainability Studies

Antoine Boche
LAAS-CNRS, Université de Toulouse, CNRS, UPS
Toulouse, France
antoine.boche@laas.fr

Clément Foucher
LAAS-CNRS, Université de Toulouse, CNRS, UPS
Toulouse, France
clement.foucher@laas.fr

Luiz Fernando Lavado Villa
LAAS-CNRS, Université de Toulouse, CNRS, UPS
Toulouse, France
lflavado@laas.fr

Abstract

There is a growing research interest in studying microgrids in rural areas as a means to promote energy access. These microgrids could be the key to energy access on a global scale because of their many advantages compared to classic grid expansion. Despite all these qualities, feedback from microgrids in rural areas shows that most fail to reach sustainability, but the reasons for their long-term failure are still not a consensus in the literature. This work intends to contribute to understanding microgrids' sustainability and their expansion by modelling them using a systemic vision approach. For this purpose, we propose a diagnosis tool that includes energy, financial, information and social aspects. A series of study cases are analyzed through this approach, showing it as a possible diagnostic tool for microgrids in the short and long term.

Keywords: Energy Modeling & Design, Grid System, Diagnosis, Rural Electrification, Sustainable Development, Systemic Approach

I.INTRODUCTION

According to the United Nations, 789 million people live with no access to electricity [1]. Without a more engaged action, 650 million people will remain without energy access by 2030 [2]. The investment required for universal energy access through grid expansion by 2030 will cost more than $48 billion each year. In contrast, the technologies providing safe and clean electricity are now cheaper and more accessible than ever to the population [3], but rural electrification programs remain challenging endeavours. Because of the limited resources of its target users, rural electrification is well suited for a bottom-up approach where the grid starts small and expands over time together with its community resources and energy needs [4].

Microgrid expansion can take many forms, such as an increase in the number of users, increased energy production capacity, and increased subsidies from local authorities, among many possibilities.

IEECP'22, July 21-22, 2022, Oxford, United Kingdom

This work uses a systemic approach to study these expansions and their impact on the microgrid.

Systemic approaches, such as the one proposed in the Macroscope [5], allow a complex system to be represented by simple interactions among base fields. It calls for the study of the system and its thorough description through a multi-disciplinary canvas that yields its base fields.

This work proposes a novel microgrid modelling method based on a systemic approach, identifies its main fields and studies their interactions. This new microgrid representation adds value to how it links together different fields. These cross-field links are expected to bring a more general understanding of the microgrid, its operation, and its failures and be a more versatile tool for its study.

Many other models have been presented in the literature to consider a maximum of parameters for an interdisciplinary study of microgrids with different goals in mind. Carpintero-Renteria [6] makes a clear and complete state of the art of the operation of the microgrid with its model. Sachs [7] brings a sustainable business model solution for developing a microgrid. Akinyele [8] shows all the difficulties which can appear in various fields of microgrid development and sustainable solutions to counter them. Hicks [9] ultimately criticises the limits of microgrids. All these models have in common the systemic approach but failed to consider the possible exchanges between the fields in their analysis.

Section II provides an overview of the proposed meta-model. Section III introduces the fields represented in the meta-model. Section IV presents the diagnosis tool using the meta-model. Section V exposes an example of a real microgrid use case. Section VI finally, explore possible future works. ds its base fields.

II.Meta-model Overview

In rural electrification microgrid literature, the two most important definitions of microgrids are the "energy microgrid" and the "community microgrid".

The European Microgrids project [10] defines *microgrids* as "Low Voltage distribution networks comprising various distributed generators, storage devices and controllable loads that can operate either interconnected or isolated from the main distribution grid as a controlled entity". Three base fields can be derived from this definition, namely electrical, control, and communication.

A definition of community microgrids is given by Gui [11] as the following: "A community microgrid is connected with its community through physical placement and can be partially or fully owned by said community. [...] Considering the social dimension, a 'community microgrid' can be viewed as a microgrid with the key

objectives of achieving economic, social and environmental benefits in community electricity supply and distribution". Two extra base fields can be identified from this definition, namely social and financial.

In this work, four base fields will be used to represent the microgrid system: energy, information, financial and social aspects. Control and communication are merged into a single field as they handle the same type of object, information.

These four base fields define the challenges surrounding microgrid implementation. Such as the overall quality of the power grid equipment and operation, the value extraction of the data processed, the sustainable operation of the business model as well as the acceptance of the community during microgrid implantation.

Table 1. Description of the exchange between fields

To \ From	Energy	Information	Financial	Social
Energy	Energy flows	The data sent to the power grid for its control	All the investment that is brought for the good functioning of the power grid	The involvement of the users for the good usage of the microgrid
Information	All the data retrieved from the electrical grid in order to be processed by the different algorithms for the control or monitoring of the grid	Information flows	Investment for the improvement or maintenance for the good operation of the data and command processing equipment	Community's establishment and compliance with rules relating to the use of data generated within the microgrid
Financial	The economic productions linked to the operation of the microgrid and the energy consumption itself	All the data processed to provide a clear view of the health and operation of the microgrid for its management	Financial flows	Community's establishment of and compliance with rules relating to the use of power grid and its pricing system
Social	Represents the impact of the electricity grid on the community through the consumption of energy	All the data processed in order to be able to provide a diagnosis of microgrid usage to the grid users	Follow-up and training of the community by the microgrid manager to ensure compliance with the established rules	Social interactions

The proposed meta-model links together the four base fields and is based on a series of definitions described as follows:

- **Field:** a fundamental block which composes the microgrid. They are bounded by four fundamental fields of expertise, namely energy, information, financial and social.
- **Flow:** A flow is an interaction between one or several elements of the same field.
- **Exchange:** An exchange is an interaction between one or more elements of two different fields.

We define an exchange that goes from one field to another as unilateral: it takes from one field to provide to another field.

III.Meta-Model in-depth description

The fields are made of different elements that share the same unit in their flow: these elements produce, consume or transform the same unit.

The energy field of the meta-model makes it possible to represent the fundamental element of microgrids, which is the energy flow or power flow. It represents all the energy exchanges within the microgrid and illustrates the amount of energy available [12]. Its unit is the Watt.

The information field of the meta-model represents all the data processed by the microgrid and the control of the microgrid. However, in a so-called "intelligent"; microgrid, this field becomes central for grid management, whether it be for the control or the monitoring and maintenance [13]. Its unit is the bit.

The financial field of the meta-model makes it possible to represent all the financial exchanges of the microgrid. As this field is often a limiting factor for the development of microgrids (especially in rural areas), it is essential to be able to represent it for its study [14]. Its unit is the local currency.

The social field, which is often forgotten or neglected in the study of microgrids, is fundamental to represent the microgrid in a systemic way, thus understanding its functioning and state of health in depth. Its unit is social acceptance [15].

The fields presented above, based on isolated microgrids' meta-models, can be assembled into a single systemic meta-model. This assembly is done through what is called exchanges in this work. These exchanges are essential to understanding a microgrid as they may couple variables that are not necessarily studied together. There are twelve exchanges in the proposed systemic microgrid meta-model, as detailed in Table 1.

IV.Microgrid equilibrium

The notion of sustainability is fundamental in the design and operation of microgrids. It provides a clear vision and framework for developing a microgrid, which remains a somewhat fragile system [16]. Indeed, many microgrids have fallen into disrepair or function extremely poorly, particularly in rural areas with more limited resources, because certain limiting factors were not considered in the system's design [17]. The notion of systemic sustainability of a microgrid has already been partially addressed, but the presented meta-model provides a way to represent the grid's sustainability through the equilibrium of all the fields: the microgrid equilibrium.

With all its fields in excellent shape, this model will represent a microgrid that reaches energy sustainability, financial resilience, data value, and complete social acceptance. And overall, the microgrid will reach perennial operation.

The equilibrium of the entire microgrid is governed by the inner flows and the exchanges between the different fields. Dynamically speaking, these exchanges and flows can lead to failure or success. This section defines these two types of equilibrium and the means to evaluate them. To enter into what is called a virtuous circle, all fields must give as much as they receive. Since all microgrids are highly different in their architecture, sources, governance, population and many other factors, it is impossible to give a single solution for their

sustainability, but the meta-model allows to represent every microgrid in its entirety. For a short-term scale, the essential characteristic to identify the health level of the fields flows detailed in Table 2. A microgrid with an excellent operation in its fields will have increased resilience (at least for a short period of time) no matter the quality of the microgrid exchanges. Indeed, the high quality of its fields represents inertia and stability to the microgrid.

However, for a more extended period of time, the exchanges of the microgrid will have a much more significant impact because if they are not efficient, they will gradually deplete the stocks of the different fields. Therefore, each exchange has associated indicators with being able to judge its good or bad functioning in Table 2.

To summarize this, it can be said that the flows of the fields represent the static sustainability of the microgrid and the exchanges represent the dynamic sustainability of the microgrid.

Table 2 details the notation for the flows and exchanges of the proposed diagnostic model. The ratings range from the worst possible scenario (rated as "--") to the best possible scenario (rated as "++"). The diagnostic tool that is presented uses this rating scale to rate each flow and exchange with a range of 1 to 4 according to the information collected on the microgrid to be diagnosed.

V. Use case

To benchmark the proposed meta-model, a study of six microgrids whose data is available in a United Nations report [18].

A colour code (red, orange, green, dark green) represents the quality of an exchange or a flow. These different indicators provide a general view of the sustainability of the microgrid but also the possibility to accurately anticipate weak points in the system and correct them before it is too late. The equation used for this calculation was:

$$Field_{Score} = Mean\,(3 \cdot Field_{flow} + \sum Field_{Exchanges})$$

Where $Field_{score}$ is the total score of any given field, $Field_{flow}$ is the value given to the quality of the inner flow of the field and $Field_{Exchanges}$ is the score given to all the outward exchanges of a given field. The threefold importance factor was given to the flows to emphasize their inertia role in the fields.

The results are shown in Table 3. An average score and a variance are calculated for each microgrid on the bottom. The average and variance are calculated on the right-hand side for each type of exchange or flow. The rating used for the fluxes and exchanges varies from 1 for poor to 4 for excellent.

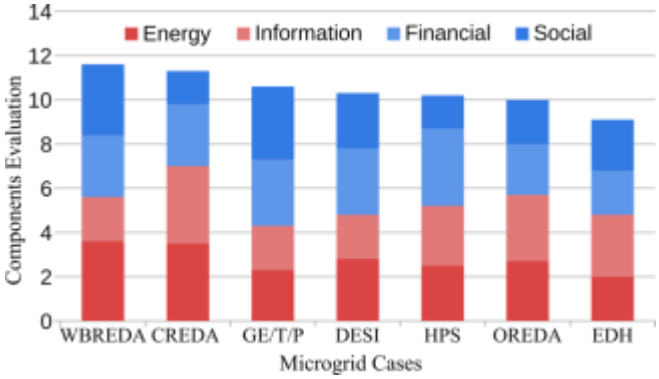

Figure. 1. Microgrid use case evaluation

Figure 1 illustrates the results for each field. The blue fields are related to the community microgrid, and the red fields are related to the energy microgrid. The microgrids are lined from the highest score on the left to the lowest on the right.

Figure 2 compares the average and variance of the flows and exchanges for the seven study cases. It highlights how the social and information fields are the most neglected, with missing scores and no information available.

Following the UN report, the proposed diagnosis tool shows that microgrids that put resources into financial and social have a higher probability of success. This is the case for the first and third best-rated microgrids.

Figure 2 also shows that social-related exchanges are generally less accounted for in these study cases yielding a high variance.

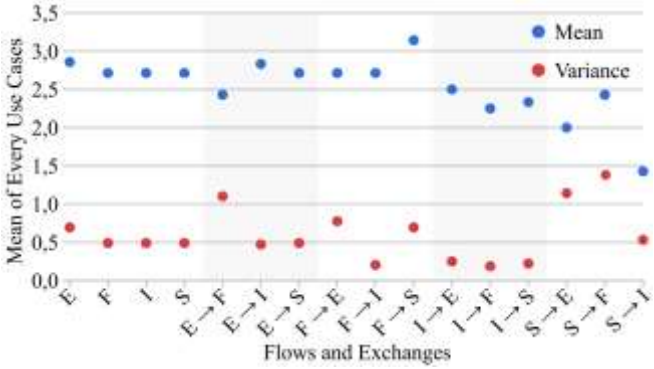

Figure. 2. Microgrid flows and exchanges comparison

Moreover, we can also notice that the internal flows of the four fields all have a relatively good score, those being more visible in the functioning of a microgrid than the exchanges and are less often forgotten or neglected. On the other hand, the disparities are even more significant within the different exchanges, which shows the need for a comprehensible and systemic model for microgrids, particularly for rural electrification.

Indeed, although information flows are often well-considered and established, the exchanges that start from this domain seem to be very often neglected in the studied examples. Moreover, the social exchanges are very disparate depending on the case studies, supporting the fact that the social domain lacks consideration in the development of microgrids. These evaluations tend to support the conclusions of the UN report, which shows difficulties in the overall functioning of the microgrids as well as in the social consideration of the population, which can be compensated by information and social exchanges.

VI. Future Work

It is essential to understand that this diagnostic tool is still to be developed and refined. The various UN cases have shown the value of this microgrid vision by providing predictions similar to the report's conclusions. This approach centralizes all microgrid information into a multi-criteria assessment that is much simpler to understand while maintaining a high level of detail.

Work remains to be done in refining the way we model the content of the four fields to allow for the simulation of a microgrid model so that its evolution over time can be studied.

The detailed modelling of the elements of the fields still has to be formally defined. This would allow simulation of the model to study various expansion scenarios and bring a much more detailed evaluation of the microgrid operation.

The development of a meta-model with a lower level of abstraction could better represent and understand the exchanges and flows between the elements. Instead of making a global link between the fields, this meta-model would represent the flows and exchanges between the elements themselves. While keeping certain simplifications in the representation of the microgrid, this meta-model will allow, in addition to the diagnosis of the microgrid, a systemic simulation of its functioning.

The final aim would be to identify how expansion scenarios of different fields affect the long-term sustainability of a microgrid.

Table 2. Evaluation of the Different Flows and Exchanges.

To \ From	Energy	Information	Financial	Social
Energy	From energy sustainability with all objectives fulfilled (++) to no sustainability objectives validated (- -)	microgrid control is very accurate and stable (++) to microgrid control is poor and unstable (- -)	Funds are re-invested into power hardware with high maintenance (++) to no re-investment with poor maintenance (- -)	Community uses the power grid perfectly well (++) to community uses the power grid poorly (- -)
Information	Many precise measurements of the energy production are available (++) to no automated and imprecise measurement is available (- -)	From high data value and consummate control (++) to no objective validated for the data and control (- -)	Funds are re-invested into information hard-ware and software (++) to no funds are re-invested (- -)	The community fully respects the rules established for data collection (++) to community does not respect the rules at all (- -)
Financial	Energy enables productive uses (++) to energy has no productive uses (- -)	High quality data is available for planning and operation (++) to no data is available (- -)	From financial resilience (++) to no resiliency objectives validated (- -)	Payment collection is highly efficient (++) to payment collection is not reliable (- -)
Social	All energy needs of the community are satisfied (++) to not even the basic needs are satisfied (- -)	High quality data is available for the users to follow consumption (++) to no data is available (- -)	Funds are re-invested into the community (++) to no funds are re-invested into the community (- -)	From high social acceptance (++) complete rejection by the community (- -)

Table 3. Evaluation of the Different UN Use Cases

		CREDA	DESI	GE/T/P	EDH	OREDA	WBREDA	HPS	Mean	Variance
Internal Flows	Energy	4	3	2	2	3	4	2	2,86	0,69
	Financial	3	3	3	2	2	2	4	2,71	0,49
	Information	4	2	2	3	3	2	3	2,71	0,49
	Social	2	3	3	2	3	4	2	2,71	0,49
External Exchanges	Energy → Finance	3	4	3	1	1	3	2	2,43	1,10
	Energy → Information	4	2	3	2	3	N/A	3	2,83	0,47
	Energy → Social	2	2	2	3	3	3	4	2,71	0,49
	Finance → Energy	3	3	3	2	1	4	3	2,71	0,78
	Finance → Information	3	3	2	2	3	3	3	2,71	0,20
	Finance → Social	2	3	4	2	4	4	3	3,14	0,69
	Information → Energy	3	2	2	2	3	N/A	3	2,50	0,25
	Information → Finance	3	2	N/A	N/A	N/A	2	2	2,25	0,19
	Information → Social	3	2	N/A	N/A	N/A	N/A	2	2,33	0,22
	Social → Energy	1	2	4	2	1	3	1	2,00	1,14
	Social → Finance	1	3	4	4	1	3	1	2,43	1,67
	Social → Information	1	1	3	2	1	1	1	1,43	0,53
Results	Mean	2,63	2,50	2,86	2,21	2,29	2,92	2,44		
	Variance	1,05	0,53	0,59	0,49	1,14	0,91	0,93		

VII. Conclusion

This short paper reviewed the evaluation of different areas of microgrids to extract a more systemic meta-model. A meta-model was proposed to provide a clear view of all aspects of a microgrid to provide a diagnostic and planning tool for its sustainability.

Contrary to the visions that can be found in the literature, the representation of microgrids proposed in this short paper provides a complete tool that allows both to represent the microgrid in a systemic way, to be able to identify the different exchanges that exist between them but also to diagnose the overall health of the microgrid and to be able to estimate the future impacts of its internal problems. This is an essential vision to understand the different extensions of a microgrid.

VIII. References

[1] Nations, U. Sustainable UN. Development Goal 7, 2019.

[2] Bank, W. More People Have Access to Electricity Than Ever Before, but World Is Falling Short of Sustainable Energy Goals, 2019.

[3] The Evolution of Distributed Energy Resources. Microgrid Knowledge 2020.

[4] Narayan, N.; Vega-Garita, V.; Qin, Z.; Popovic-Gerber, J.; Bauer, P.; Zeman, M. The Long Road to Universal Electrification: A Critical Look at Present Pathways and Challenges. Energies 2020, 13, 508.

[5] De Rosnay, J. Le macroscope, vers une vision globale.Paris: Éditions du Seuil 1975.

[6] Carpintero-Rentería, M.; Santos-Martín, D.; Guerrero, J.M. Microgrids Literature Review through a Layers Structure. Energies 2019, 12, 4381.

[7] Sachs, T.; Gründler, A.; Rusic, M.; Fridgen, G. Framing Microgrid Design from a Business and Information Systems Engineering Perspective.Business & Information Systems Engineering 2019, 61, 729–744.

[8] Akinyele, D.; Belikov, J.; Levron, Y. Challenges of Microgrids in Remote Communities: A STEEP Model Application. Energies 2018, 11, 432.

[9] Hicks, J.; Ison, N. An exploration of the boundaries of 'community' in community renewable energy projects: Navigating between motivations and context. Energy Policy 2018, 113, 523–534.

[10] Tsikalakis, A.G.; Hatziargyriou, N.D. Centralized control for optimizing microgrids operation. 2011 IEEE Power and Energy Society General Meeting, 2011, pp. 1–8. ISSN: 1944-9925,

[11] Gui, E.M.; Diesendorf, M.; MacGill, I. Distributed energy infrastructure paradigm: Community microgrids in a new institutional economics context. Renewable and Sustainable Energy Reviews 2017, 72, 1355–1365.

[12] Mariam, L.; Basu, M.; Conlon, M.F. Microgrid: Architecture, policy and future trends. Renewable and Sustainable Energy Reviews 2016, 64, 477–489.

[13] Sirviö, K.H.; Laaksonen, H.; Kauhaniemi, K.; Hatziargyriou, N. Evolution of the Electricity Distribution Networks—Active Management Architecture Schemes and Microgrid Control Functionalities. Applied Sciences 2021, 11, 2793.

[14] Piterou, A.; Coles, A.M. A review of business models for decentralised renewable energy projects. Business Strategy and the Environment 2021, 30, 1468–1480.

[15] Wolsink, M. The research agenda on social acceptance of distributed generation in smart grids: Renewable as common pool resources. Renewable and Sustainable Energy Reviews 2012, 16, 822–835.

[16] Gunnarsdottir, I.; Davidsdottir, B.; Worrell, E.; Sigurgeirsdottir, S. Sustainable energy development: History of the concept and emerging themes. Renewable and Sustainable Energy Reviews 2021, 141, 110770.

[17] Danish, M.S.S.; Matayoshi, H.; Howlader, H.R.; Chakraborty, S.; Mandal, P.; Senjyu, T. Microgrid Planning and Design: Resilience to Sustainability. 2019 IEEE PES GTD Grand International Conference and Exposition Asia (GTD Asia), 2019, pp. 253–258.

[18] Schnitzer, D.; Lounsbury, D.S.; Carvallo, J.P.; Deshmukh, R.; Apt, J.; Kammen, D.M. Microgrids for Rural Electrification: A critical review of best practices based on seven case studies. United Nations Foundation 2014.

Green Hydrogen as a Balancing Option in an Intelligent Power Grid

Anna Kolmykova, Prof., Dr.
Egineering Department
University of Economy and Management
Bremen, Germany
anna.kolmykova@fom.de

Abstract

Green hydrogen provides an opportunity for long-term energy storage in order to balance the difference between supply and demand. The goal of this paper is to investigate the feasibility of a balancing role of green hydrogen in a future intelligent power grid. The paper compares different options to balance an intelligent power grid. These options are described by their value chains - beginning with renewable energy production, through conversion into storage medium till reconversion (Power to X to Power). The energy supply chains are tested in regard of various characteristics for an intelligent power grid. The obtained results confirmed the possibility of integration of green hydrogen into intelligent power grid, although the transportation was identified as a bottleneck in the supply chain. However, the use of green hydrogen as a single balance option is not sufficient. The combination of various balancing options in an intelligent power grid has been proposed**.**

Keywords: *Green hydrogen, intelligent power grid, energy supply chain*

IEECP'22, July 21-22, 2022, Oxford, United Kingdom